KOPRI ABSTRACTS

Volume 13 (2021)

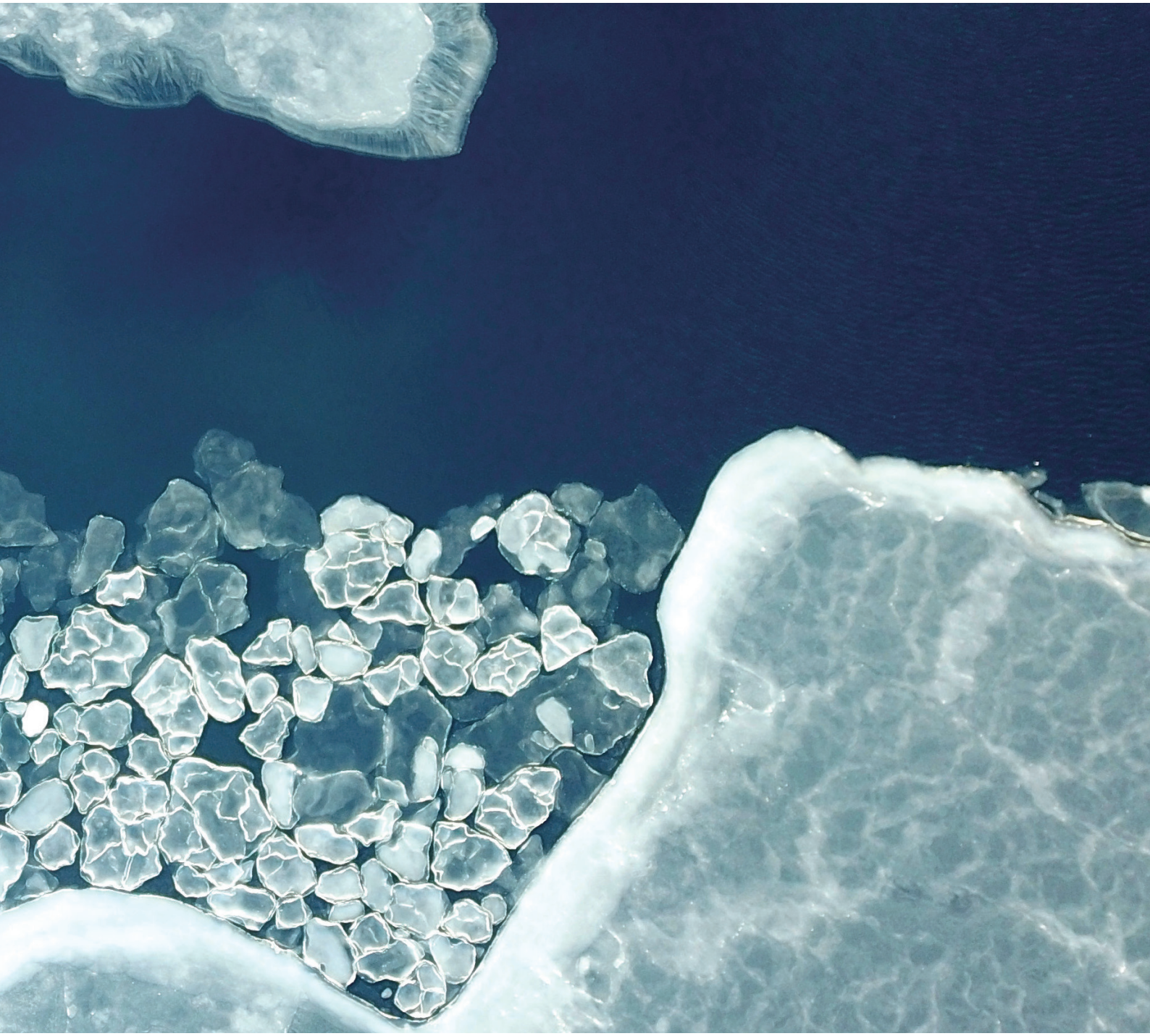

KOPRI 극지연구소
Korea Polar Research Institute

KOPRI ABSTRACTS

Volume 13 (2021)

CONTENTS

KOPRI ABSTRACTS

Volume 13 (2021)

KOPRI ABSTRACTS contains journal articles written by KOPRI researchers and other researchers funded by KOPRI. It is published once a year and has distributed worldwide by KOPRI since launching in 2014. In 2004, KOPRI was established as an autonomous institute in KORDI (current, KIOST). Volume 1 (1984-2003) contains KORDI's research activities in the arctic and the antarctic.

Published on 16 September 2022
Published by Korea Polar Research Institute

Editorial office KOPRI Library
26 Songdomirae-ro, Yeonsu-gu, Incheon, 21990, Korea

Cover Photo Noh, Younho
Design partstudio

ISSN 2289-0734

Compiled by Library of Korea Polar Research Institute.

Summary of 2021 Research Paper Achievement

We examined three years of research activities by the Korea Polar Research Institute (KOPRI), including research paper publications, domestic and international collaborative researches, and the outlook for its subject fields of research and major journals registered. KOPRI's SCI/SCI(E)-level papers are analyzed based on indices and data in Web of Science, a database of Clarivate Analytics (former Thomson Reuters).

01. Research papers in recent 3 years

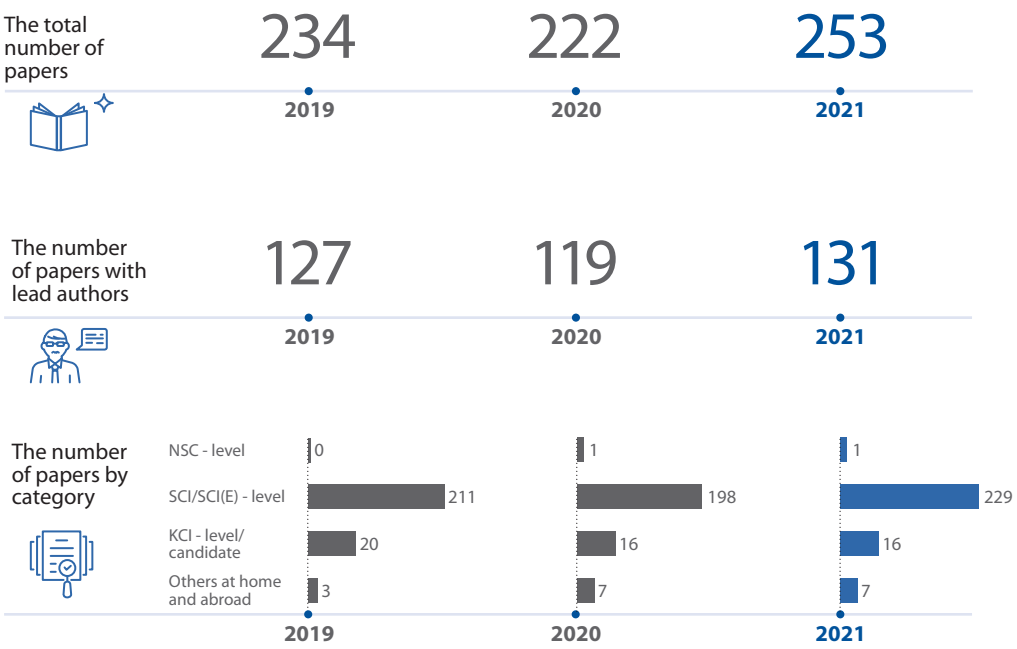

02. Collaborative research results at home and abroad

The analysis of papers published in 2021 found that KOPRI conducted collaborative research with individuals or institutions from a total number of **490** institutes and **34** countries.

Top 5 countries and number of research papers

Country	Number of records	% of 225
SOUTH KOREA	225	100%
USA	50	21.9%
GERMANY	25	10.9%
CHINA	24	10.5%
ENGLAND	18	7.8%
ITALY	17	7.4%

Top 5 institutes and number of research papers

Institution	Number of records	% of 228
KOREA POLAR RESEARCH INSTITUTE (KOPRI)	220	96.4%
UNIVERSITY OF SCIENCE TECHNOLOGY (UST)	32	14%
SEOUL NATIONAL UNIVERSITY (SNU)	25	10.9%
KOREA UNIVERSITY	23	10%
HELMHOLTZ ASSOCIATION	19	8.3%
KOREA INSTITUTE OF OCEAN SCIENCE TECHNOLOGY (KIOST)	17	7.4%

03. Subject fields of research

Research topics in 2021 KOPRI Abstracts are categorized into Climate Sciences, Life Sciences, Geosciences, Marine Sciences, and Policy & Technology. ***Climate Sciences*** cover paleoclimate, atmosphere sciences, glaciology, remote sensing, and space sciences; ***Life Sciences*** include ecology and biodiversity, genomic & biotechnology; ***Geosciences*** include geology, geophysics, and underwater acoustics; and ***Marine Sciences*** cover oceanography(physical, chemical, biological and geological) as well as subjects in ecology and technological developments with marine environments.

Subject fields of research in 2021 KOPRI Abstracts

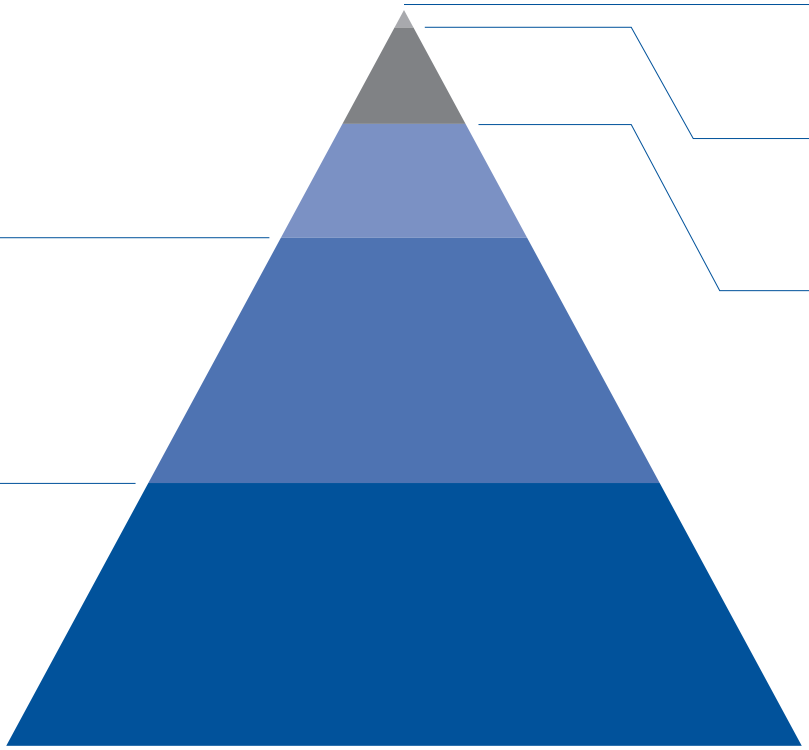

Top 25 Subject fields of research

· Source: Web of Science, Clarivate Analytics

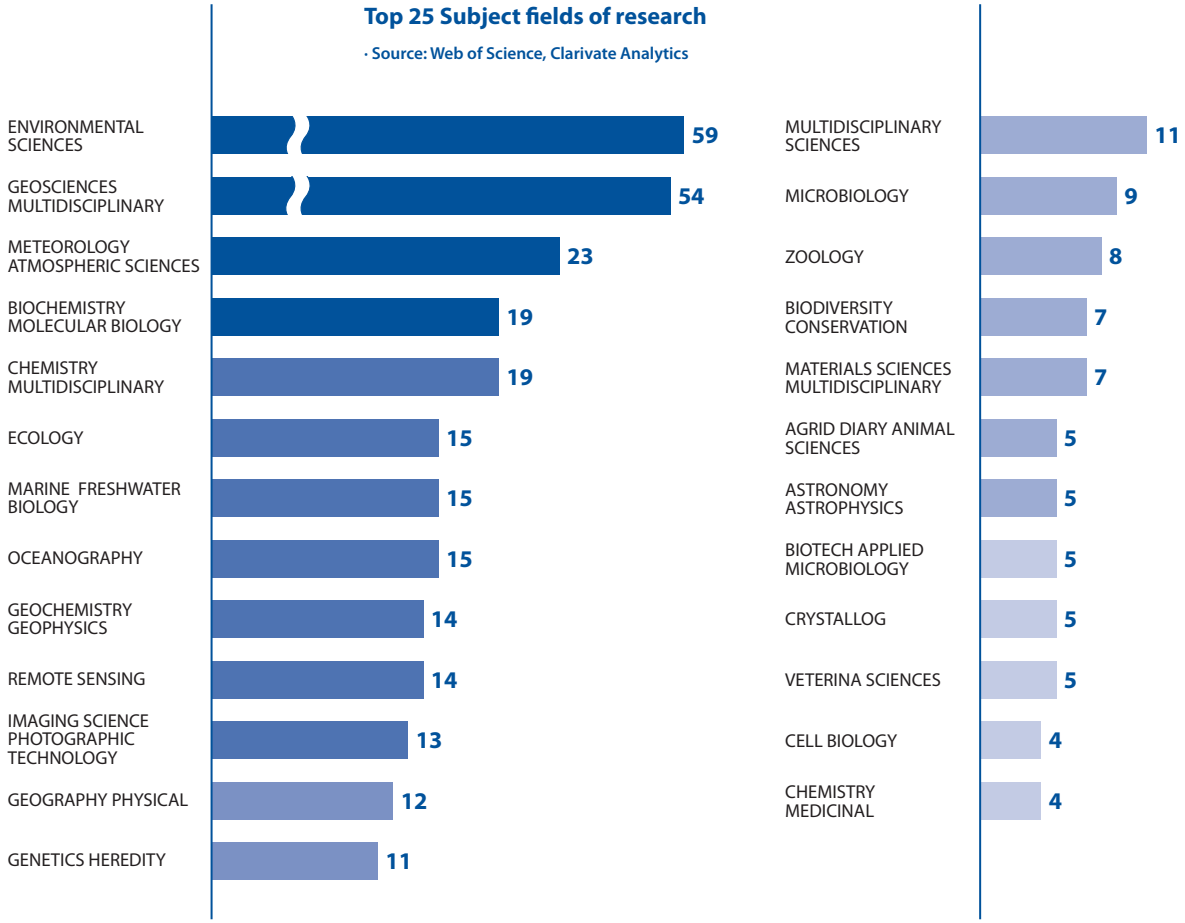

04. Major journals published

Journals and the number of papers where more than 3 papers were published

· Source: Web of Science, Clarivate Analytics

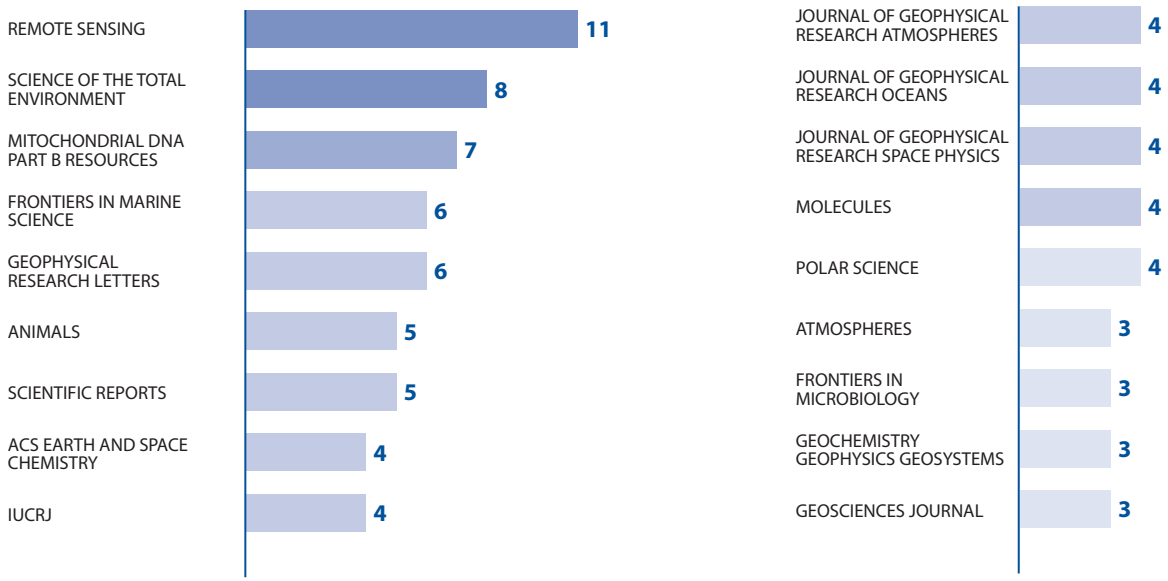

2021년 연구논문 성과 요약

최근 3년간 연구소의 연구논문 성과와 국내외 공동연구성과, 연구주제 분야 및 주요 등재 저널 동향을 살펴보았다. Clarivate Analytics(구 톰슨로이터)의 데이터베이스인 Web of Science 지표와 데이터를 기준으로, 본 연구소의 SCI/SCI(E)급 논문을 대상으로 분석하였다.

01. 최근 3년간 연구논문 성과

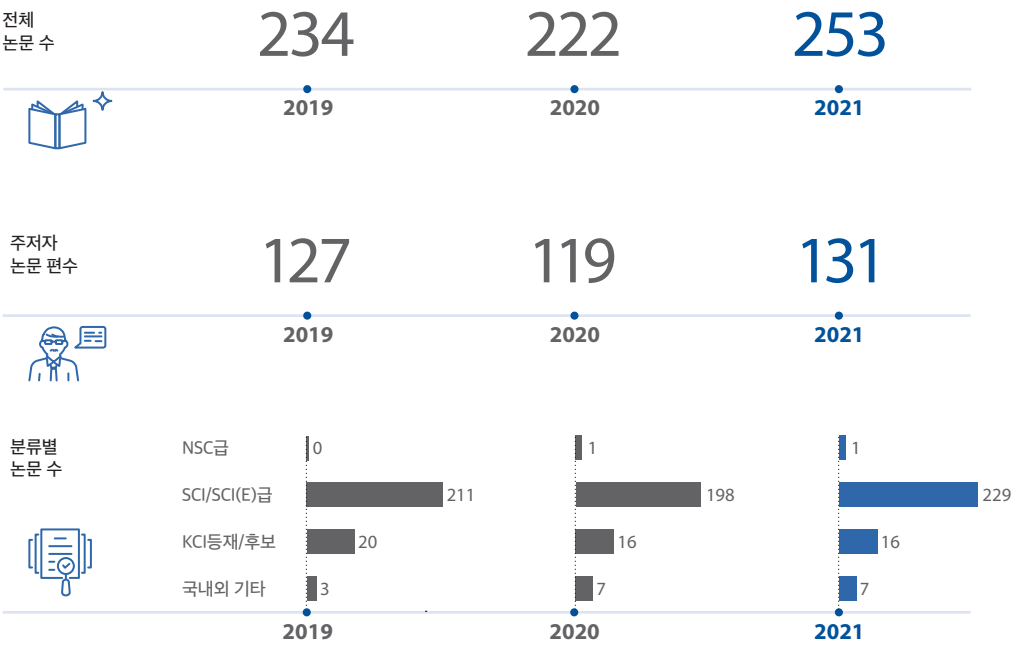

02. 국내외 공동 연구성과

2021년 WOS에 등재된 SCI/SCI(E)급 논문 229편의 논문 분석 결과, 극지연구소는 국내외 **490**개 기관, **34**개 국가와 공동연구를 수행하였다.

공동연구 수행 국가 TOP 5 및 논문 수

국가	논문 수	%(225 기준)
대한민국	225	100%
미국	50	21.9%
독일	25	10.9%
중국	24	10.5%
영국	18	7.8%
이탈리아	17	7.4%

공동연구 수행 기관 TOP 5 및 논문 수

기관	논문 수	%(228 기준)
극지연구소(KOPRI)	220	96.4%
과학기술연합대학원대학교(UST)	32	14%
서울대학교	25	10.9%
고려대학교	23	10%
HELMHOLTZ ASSOCIATION	19	8.3%
한국해양과학기술원(KIOST)	17	7.4%

03. 연구 주제 분야

2021 KOPRI Abstracts 연구 주제는 기후과학, 생명과학, 지구시스템, 해양과학, 정책&기술 분야로 분류하였다. **기후과학**은 대기, 고층대기, 빙하, 고기후, 고환경, 원격탐사 등을 포함하며, **생명과학**은 유전학·유전체학, 생리·생화학, 생물다양성·생태·진화, 생물공학을, **지구과학**은 지질, 지구물리, 수중음향을, **해양과학**은 해양학(물리, 화학, 생물학, 지질학)뿐만 아니라 해양환경에 따른 생태학 및 기술개발 등의 주제를 포함하였다.

2021 KOPRI Abstracts의 연구주제 분야

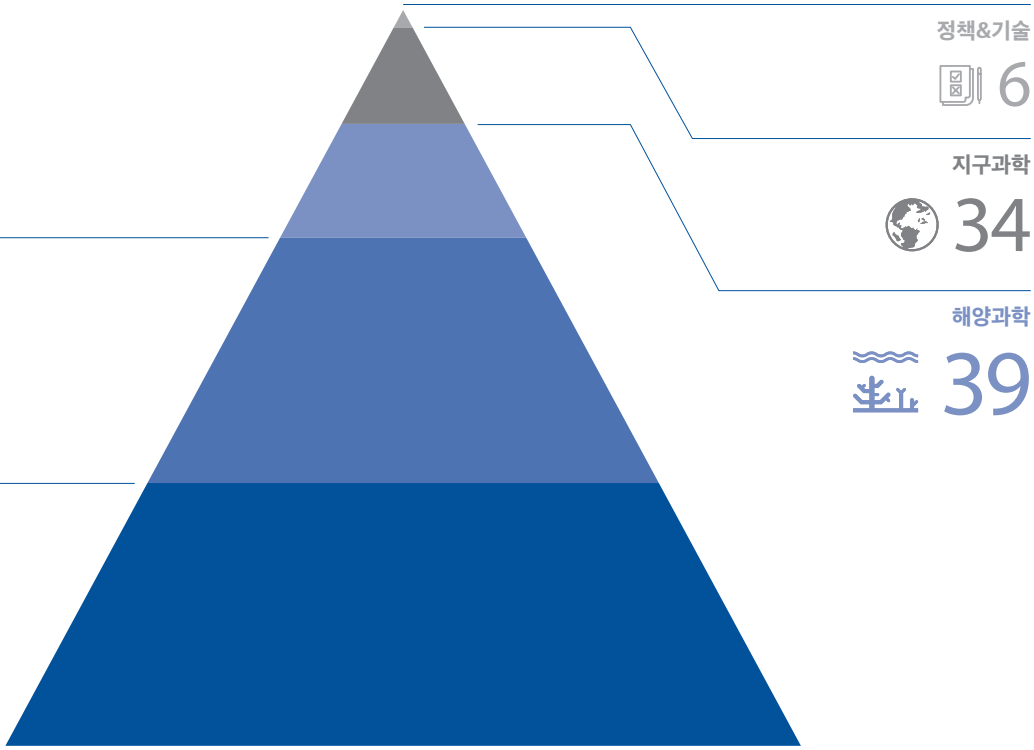

연구 분야 TOP 25

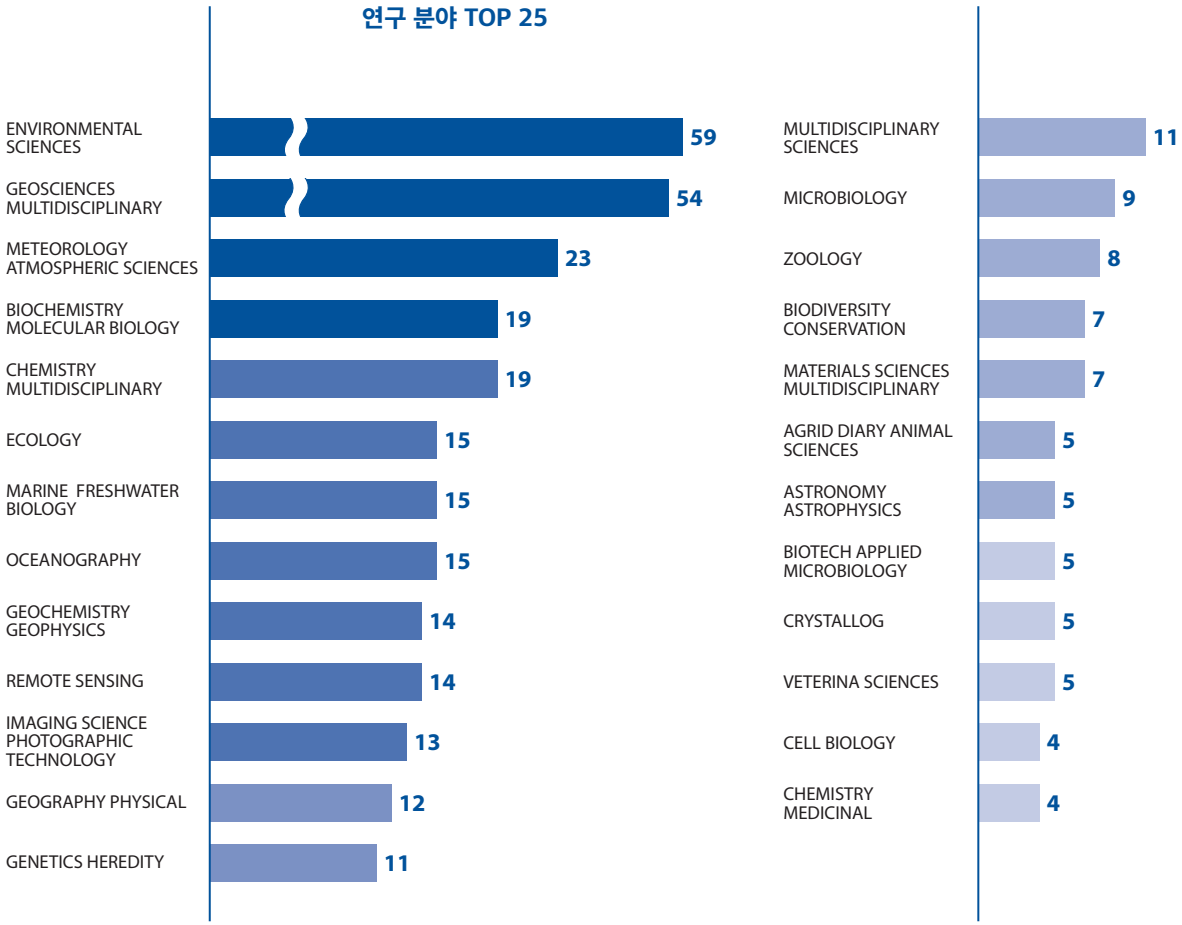

04. 주요 등재 저널

3편 이상 등재된 저널과 논문 수

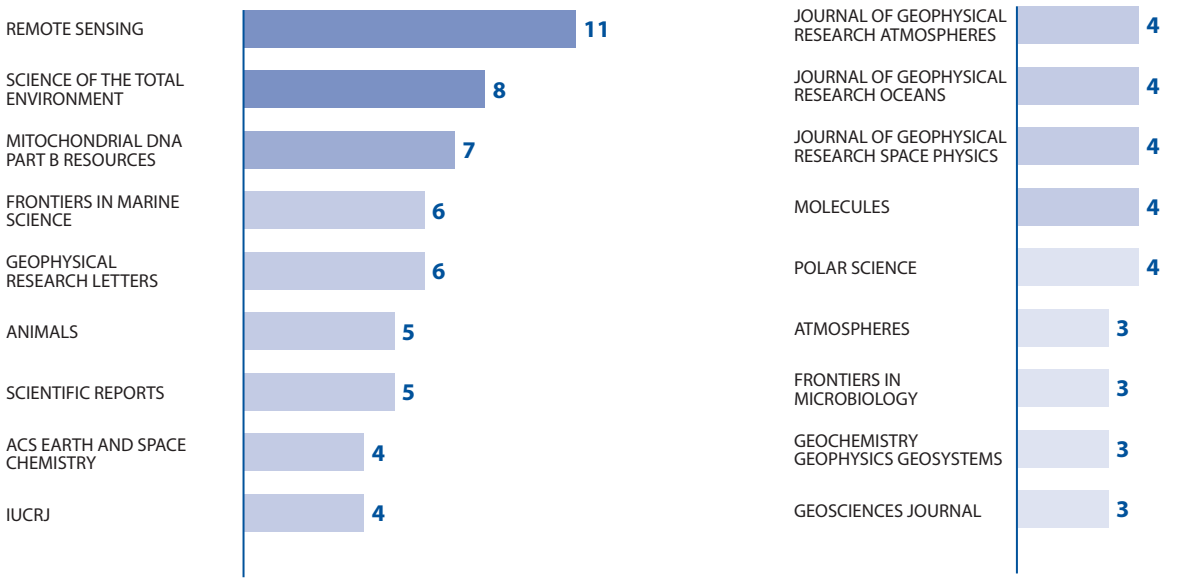

KOPRI ABSTRACTS

Volume 13 (2021)

NOTICE

1-1 *Geology*

^{10}Be and ^{10}Be/^{9}Be in glaciomarine sediments of Ross Sea, Antarctica: implications for mid-late Quaternary paleoenvironmental changes

Dash, Chinmay., **Lee, Min Kyung**., Seong, Yeong Bae., **Rhee, Hyun Hee**., **Lee, Jae Il**. and **Yoo, Kyu-Cheul**.

Journal of the Geological Society of Korea. 2021. 57(5): 691-705.

doi: 10.14770/jgsk.2021.57.5.691.

Web of Science Subject
*If there is no Web of Science Subject in this bibliography, this article is a journal not registered in Web of Science.

Reference
*The following KOPRI authors can be seen as highlighted in bold text

This study documents the variation of *Be* isotopes (^{10}Be and ^{9}Be) and their ratio (^{10}Be/^{9}Be) from a Ross Sea sediment core (LC42) with relation to mid to late Pleistocene geomagnetic and paleoclimatic changes. Significant changes in *Be* isotope concentration are observed during pre and post-Mid-Pleistocene Transition (MPT) periods. The ^{10}Be concentration and ^{10}Be/^{9}Be ratio show a gradual decrease during the late Matuyama Chron, suggesting a relative increase in geomagnetic intensity. The overproduction episode associated with the Matuyama-Brunhes Boundary (MBB) does not show any pre- MBB precursor event. The progressively decreasing trend observed in ^{10}Be and ^{10}Be/^{9}Be ratio records from 1 to 0.8 Ma, with minimum values at around 0.8 Ma, suggests a relatively open sea condition during the early part of MPT and an extended glacial condition around MIS 22.The ^{10}Be and ^{10}Be/^{9}Be ratios are approximately constant during the pre-Mid Bruhnes Event (MBE) period and show a gradual increase after the MBE, indicating a climatic transition from colder (pre-MBE) to relatively warmer (post-MBE) conditions.

Abstract

keywords: *Be* isotope; Pleistocene; Antarctica; Ross Sea; glacier

Keywords

PART1.

Climate Sciences

1-1 *Geology*

^{10}Be and ^{10}Be/^{9}Be in glaciomarine sediments of Ross Sea, Antarctica: implications for mid-late Quaternary paleoenvironmental changes

Dash, Chinmay., **Lee, Min Kyung**., Seong, Yeong Bae., **Rhee, Hyun Hee**., **Lee, Jae Il**. and **Yoo, Kyu-Cheul**.

Journal of the Geological Society of Korea. 2021. 57(5): 691-705.
doi: 10.14770/jgsk.2021.57.5.691.

This study documents the variation of *Be* isotopes (^{10}Be and ^{9}Be) and their ratio (^{10}Be/^{9}Be) from a Ross Sea sediment core (LC42) with relation to mid to late Pleistocene geomagnetic and paleoclimatic changes. Significant changes in *Be* isotope concentration are observed during pre and post-Mid-Pleistocene Transition (MPT) periods. The ^{10}Be concentration and ^{10}Be/^{9}Be ratio show a gradual decrease during the late Matuyama Chron, suggesting a relative increase in geomagnetic intensity. The overproduction episode associated with the Matuyama-Brunhes Boundary (MBB) does not show any pre- MBB precursor event. The progressively decreasing trend observed in ^{10}Be and ^{10}Be/^{9}Be ratio records from 1 to 0.8 Ma, with minimum values at around 0.8 Ma, suggests a relatively open sea condition during the early part of MPT and an extended glacial condition around MIS 22.The ^{10}Be and ^{10}Be/^{9}Be ratios are approximately constant during the pre-Mid Bruhnes Event (MBE) period and show a gradual increase after the MBE, indicating a climatic transition from colder (pre-MBE) to relatively warmer (post-MBE) conditions.

keywords: *Be* isotope; Pleistocene; Antarctica; Ross Sea; glacier

1-2 *Physical Geography; Geology*

A 350-year multiproxy record of climate-driven environmental shifts in the Amundsen Sea Polynya, Antarctica

Kim, So-Young., Lim, Dhongil., Rebolledo, Lorena., **Park, Taewook.**, Esper, Oliver., Munoz, Praxedes., **La, Hyoung Sul.**, **Kim, Tae Wan.** and **Lee, SangHoon.**

Global and Planetary Change. 2021. 205.
doi: 10.1016/j.gloplacha.2021.103589.

With a growing concern over rapid Antarctic ice loss in recent years, the Amundsen Sea, one of the fastestmelting areas in Antarctica, currently becomes a hotspot for the Earth sciences in the context of its linkage to global climate. As a center of strong physical and biological coupling processes, polynyas of the Amundsen Sea could act as sentinels of changes in atmosphere–ice–ocean interactions, offering a unique perspective into its sensitivity to climate variability. Here, we present a new, multiproxy-based high-resolution sedimentary record from the Amundsen Sea polynya, which provides new insights into environmental conditions of the region over the last 350 years and their linkages to climatic factors. Our results show that the polynya witnessed step-wise environmental shifts in parallel with the phases and strength of large-scale climate patterns, i.e., the Southern Annular Mode (SAM) and El Niño–Southern Oscillation (ENSO). Notably, intersite correlation of on-shelf Circumpolar Deep Water (CDW) intrusion signals at different locals suggests that the CDW may have gained increased access to the shelves at the time of a strong coupling of positive SAM and El Niño states. We tentatively speculate that anomalous large-scale atmospheric and oceanic circulation patterns over the Southern Hemisphere, forced by increasing greenhouse gas levels, were strongly involved in the mid-20th century CDW invigoration, which may be greater in scale that goes well beyond the Amundsen Sea region. This result is relevant to the current debate on spatial heterogeneity in the timing and phasing of major climatic events in Antarctica, underscoring an unambiguous connection of the Antarctic climate state to the large-scale ocean-atmosphere reorganizations. Our study also extends a growing evidence that today's global warming trend is expected to have a severe effect on future configuration of Antarctic continental ice-shelf environment.

keywords: Amundsen Sea Polynya; Sediment; Circumpolar Deep Water; Atmospheric circulation

1-3 *Meteorology & Atmospheric Sciences*

Activities of Small-Scale Gravity Waves in the Upper Mesosphere Observed From Meteor Radar at King Sejong Station, Antarctica (62.22°S, 58.78°W) and Their Potential Sources

Song, Byeong-Gwon., Song, In-Sun., Chun, Hye-Young., **Lee, Changsup.** and 5 others.
Journal of Geophysical Research-Atmospheres. 2021. 126(10).
doi: 10.1029/2021jd034528.

Gravity wave (GW) activities in the upper mesosphere (80–100 km) and their potential sources are investigated using meteor radar observations at King Sejong Station, Antarctica (KSS; 62.22°S, 58.78°W) during recent 14 years (2007–2020). GW activities are estimated by horizontal wind variances of small-scale GWs (periods <2 h, horizontal wavelength <400 km, or vertical wavelength <3–5 km). The wind variances show clear semiannual variations with maxima at solstices, and annual variations are also seen above z = 90 km. The deseasonalized wind variances at z = 96.8 km have a statistically significant periodicity of ~11 years that can be associated with solar cycle variations. Three major potential GW sources in the lower atmosphere are examined. Orography is a potential source of GWs in winter and autumn, when the basic-state wind is westerly from the surface up to the mesosphere. The residual of the nonlinear balance equation (RNBE) at 5 hPa, a diagnostic of the GWs associated with jet stream, is the largest in winter and has a secondary maximum in spring. The correlation between the observed GWs and RNBE is significant in equinoxes, while correlation is low in winter. Deep convection in storm tracks is a potential source in autumn and winter. Secondary GWs generated in the mesosphere can also be observed in the upper mesosphere. Ray-tracing analysis for airglow images observed at KSS indicates that secondary GWs are mostly generated in winter mesosphere, which may be associated with the breaking of orographic GWs.

keywords: Antarctica; gravity waves; meteor radar; MLT; upper mesosphere

1-4 *Science & Technology*

Antarctic ozone hole modifies iodine geochemistry on the Antarctic Plateau

Spolaor, Andrea., Burgay, Francois., Fernandez, Rafael P., Turetta, Clara., Cuevas, Carlos A., **Kim, Kitae.** and 9 others.
Nature Communications. 2021. 12(1).
doi: 10.1038/s41467-021-26109-x.

Polar stratospheric ozone has decreased since the 1970s due to anthropogenic emissions of chlorofluorocarbons and halons, resulting in the formation of an ozone hole over Antarctica. The effects of the ozone hole and the associated increase in incoming UV radiation on terrestrial and marine ecosystems are well established; however, the impact on geochemical cycles of ice photoactive elements, such as iodine, remains mostly unexplored. Here, we present the first iodine record from the inner Antarctic Plateau (Dome C) that covers approximately the last 212 years (1800-2012 CE). Our results show that the iodine concentration in ice remained constant during the pre-ozone hole period (1800-1974 CE) but has declined twofold since the onset of the ozone hole era (~1975 CE), closely tracking the total ozone evolution over Antarctica. Based on ice core observations, laboratory measurements and chemistry-climate model simulations, we propose that the iodine decrease since ~1975 is caused by enhanced iodine re-emission from snowpack due to the ozone hole-driven increase in UV radiation reaching the Antarctic Plateau. These findings suggest the potential for ice core iodine records from the inner Antarctic Plateau to be as an archive for past stratospheric ozone trends.

1-5 *Engineering; Environmental Sciences & Ecology; Meteorology & Atmospheric Sciences*

Approximated expression of the hygroscopic growth factor for polydispersed aerosols

Jung, Chang H., **Yoon, Young Jun.** and 6 others.
Journal of Aerosol Science. 2021. 151.
doi: 10.1016/j.jaerosci.2020.105670.

Hygroscopic growth of aerosols plays an important role in the characterization of atmospheric aerosols. Physico-chemical and optical properties of aerosols are dependent on relative humidity (RH) as well as on

their size and composition. In this study, scattering enhancement factors, f (RH), for polydispersed aerosols were approximated. f(RH) of ammonium sulfate and ammonium nitrate (AS) and NaCl aerosols (ss) were considered under the assumption of externally mixed aerosols. f(RH) was calculated using the Mie theory for polydispersed aerosols at a given RH and corresponding water uptake (denoted as $f_{Mie}(RH)$). f(RH) was approximated as a quadratic function of RH (denoted as $f_{app}(RH)$). The obtained approximated f(RH) or $f_{app}(RH)$) values were compared with the values based on the Mie theory and showed a reasonable agreement between them. To the best of our knowledge, this is the first study that parametrizes the size dependency of f(RH) for log normally distributed aerosols.

keywords: Analytical approximated expression; Polydispersed aerosol; Hygroscopic growth factor; Aerosol size distribution; Scattering enhancement factor

1-6 *Environmental Sciences & Ecology*

Atmospheric deposition of inorganic nutrients to the Western North Pacific Ocean

Seok, Min-Woo., Kim, Dongseon., Park, Geun-Ha., Lee, Ki-tack., Kim, Tae-Hoon., **Jung, Jinyoung.**, **Kim, Kitae.**, **Park, Ki-Tae.** and 7 others.

Science of the Total Environment. 2021. 793.
doi: 10.1016/j.scitotenv.2021.148401.

We evaluated the potential impacts of atmospheric deposition on marine productivity and inorganic carbon chemistry in the northwestern Pacific Ocean (8–39°N, 125–157°E). The nutrient concentration in atmospheric total suspended particles decreased exponentially with increasing distance from the closest land-mass (Asia), clearly revealing anthropogenic and terrestrial contributions. The predicted mean depositional fluxes of inorganic nitrogen were approximately 34 and 15 μmol m^{-2} d^{-1} to the west and east of 140°E, respectively, which were at least two orders of magnitude greater than the inorganic phosphorus flux. On average, atmospheric particulate deposition would support 3–4% of the net primary production along the surveyed tracks, which is equivalent to ~2% of the dissolved carbon increment caused by the penetration of anthropogenic CO_2. Our observations generally fell within the ranges observed over the past 18 years, despite an increasing trend of atmospheric pollution in the source regions during the same period, which implies high temporal and spatial variabilities of atmospheric nutrient concentration in the study area. Continued atmospheric anthropogenic nitrogen deposition may alter the relative abundances of nitrogen and phosphorus.

keywords: Marine productivity; Dry deposition; Air-mass backward trajectory; Total suspended particles

1-7 *Environmental Sciences & Ecology; Geology*

Biological productivity and glaciomarine sedimentation in the Central Basin of the northwestern Ross Sea since the last glacial maximum

Khim, Boo-Keun., Colizza, Ester., **Lee, Jae Il.** and 3 others.

Polar Science. 2021. 28.
doi: 10.1016/j.polar.2021.100682.

This study documents multi-proxy data representing surface water productivity and AMS ^{14}C dates of box (BC3) and gravity (GC2) cores in the Central Basin of the northwestern Ross Sea. Based on AMS ^{14}C dates, a comparison of sediment properties between BC3 and GC2 reveals that BC3 records the complete Holocene (i.e., interglacial) history, which is correlated to the uppermost part of GC2. The lithostratigraphic succession of GC2 consists of the repetition of contrasting layers distinguished by the productivity proxies. In contrast to the uppermost sediment layer (i.e., interglacial), the subsurface sediment layer (i.e., deglacial) is distinctly characterized by very high biogenic components. Such pronounced biogenic remnants in the deglacial sediments are not explained exclusively by *in situ* enhanced productivity in the surface water. Our results, thus, suggest that eroded and reworked shelf sediments from a previous interglacial period enriched in biogenic components by the advancing ice sheet might be transported through the melt-water plumes from the grounding line to the Central Basin, to provide high geochemical properties of deglacial sediments. Thus, growth and retreat of the grounded ice sheet played an important role in glaciomarine sedimentation change in the Central Basin of the northwestern Ross Sea.

keywords: Glaciomarine; Geochemistry; Productivity; Ice sheet; Continental margin; Antarctica

1-8 *Oceanography*

Bottom current control on sediment deposition between the Iselin Bank and the Hillary Canyon (Antarctica) since the late Miocene: An integrated seismic-oceanographic approach

Conte, R., Rebesco, M., De Santis, L., Colleoni, F., Bensi, M., Bergamasco, A., Kovacevic, V., Gales, J., Zgur, F., Accettella, D., De Steur, L., Ursella, L., McKay, R., Kim, S., Lucchi, R. G. and **Kim, Sunghan.**

Deep-Sea Research Part I-Oceanographic Research Papers. 2021. 176.

doi: 10.1016/j.dsr.2021.103606.

In this paper we analyze how oceanic circulation affects sediment deposition along a sector of the Ross Sea continental margin, between the Iselin Bank and the Hillary Canyon, and how these processes evolved since the Late Miocene. The Hillary Canyon is one of the few places around the Antarctic continental margin where the dense waters produced onto the continental shelf, mainly through brine rejection related to sea ice production, flow down the continental slope and reach the deep oceanic bottom layer. At the same time the Hillary Canyon represents a pathway for relatively warm waters, normally flowing along the continental slope within the Antarctic Slope Current, to reach the continental shelf. The intrusion of warm waters onto the continental shelf produces basal melting of the ice shelves, reduces their buttressing effect and triggers instabilities of the ice sheet that represent one of the main uncertainties in future sea level projections. For this study we use seismic, morpho-bathymetric and oceanographic data acquired in 2017 by the R/V OGS Explora. Seismic profiles and multibeam bathymetry are interpreted together with age models from two drilling sites (U1523 and U1524) of the International Ocean Discovery Program (IODP) Expedition 374. Oceanographic data, together with a regional oceanographic model, are used to support our reconstruction by showing the present-day oceanographic influence on sediment deposition. Regional correlation of the main seismic unconformities allows us to identify eight seismic sequences. Seismic profiles and multibeam bathymetry show a strong influence of bottom current activity on sediment deposition since the Early Miocene and a reduction in their intensity during the mid-Pliocene Warm Period. Oceanographic data and modelling provide evidence that the bottom currents are related to the dense waters produced on the Ross Sea continental shelf and flowing out through the Hillary Canyon. The presence of extensive mass transport deposits and detachment scarps indicate that also mass wasting participates in sediment transport. Through this integrated approach we regard the area between the Iselin Bank and the Hillary Canyon as a Contourite Depositional System (ODYSSEA CDS) that offers a record of oceanographic and sedimentary conditions in a unique setting. The hypotheses presented in this work are intended to serve as a framework for future reconstructions based on detailed integration of lithological, paleontological, geochemical and petrophysical data.

keywords: Contourite drift; Seismics; Oceanography; Ross Sea Bottom Water; Antarctic Slope Current; International Ocean Discovery Program; Expedition 374

1-9 *Science & Technology*

Carbon response of tundra ecosystems to advancing greenup and snowmelt in Alaska

Kim, JiHyun, Kim, Yeonjoo, Zona, Donatella, Oechel, Walter, **Park, Sang-Jong**, **Lee, Bang Yong.** and 3 others.

Nature Communications. 2021. 12(1).

doi: 10.1038/s41467-021-26876-7.

The ongoing disproportionate increases in temperature and precipitation over the Arctic region may greatly alter the latitudinal gradients in greenup and snowmelt timings as well as associated carbon dynamics of tundra ecosystems. Here we use remotely-sensed and ground-based datasets and model results embedding snowmelt timing in phenology at seven tundra flux tower sites in Alaska during 2001-2018, showing that the carbon response to early greenup or delayed snowmelt varies greatly depending upon local climatic limits. Increases in net ecosystem productivity (NEP) due to early greenup were amplified at the higher latitudes where temperature and water strongly colimit vegetation growth, while NEP decreases due to delayed snowmelt were alleviated by a relief of water stress. Given the high likelihood of more frequent delayed snowmelt at higher latitudes, this study highlights the importance of understanding the role of snowmelt timing in vegetation growth and terrestrial carbon cycles across warming Arctic ecosystems.

1-10 *Astronomy & Astrophysics*

A Case Study of Transversely Heated Low-Energy Helium Ions by EMIC Waves in the Plasmasphere

Kim, Khan-Hyuk., **Kwon, Hyuck-Jin.** and 3 others.

Journal of Geophysical Research-Space Physics. 2021. 126(2).

doi: 10.1029/2020ja028560.

The Van Allen Probe A spacecraft observed strong ~0.5-Hz helium (He^+) band and weak ~0.8-Hz hydrogen (H^+) band EMIC waves on April 17, 2018, at L = ~4.5–5.2, in the dawn sector, near the magnetic equator, and close to the plasmapause. We examined low-energy ion fluxes observed by the Helium Oxygen Proton and Electron (HOPE) instrument onboard Van Allen Probe A during the wave interval and found that low-energy He^+ flux (<10 eV) enhancements occur nearly simultaneously with He-band and H-band EMIC wave power enhancements in a direction mostly perpendicular to the background magnetic field without significant low-energy H^+ and O^+ flux variations. We suggest that cold He^+ ions (<1 eV) are preferentially and transversely heated up 10 eV through the interaction with EM IC waves inside the plasmasphere. The low-Earth orbit spacecraft observed localized precipitations of energetic protons in the upper ionosphere at subauroral latitudes near the magnetic field footprint of Van Allen Probe A. Our observations provide a clear evidence that EMIC waves play an important role in the overall dynamics in the inner magnetosphere, contributing to the high-energy particle loss and low-energy particle energization.

1-11 *Physical Geography*

Change in the Impacts of Teleconnection Patterns on December Temperature in Korea during the Period before and after Regime Shift

Kim, Ye Jin., Woo, Chan Mi., Jin, Seon Min., **Kim, Jeong-Hun.** and 3 others.

Journal of Climate Research. 2021. 16(2): 133-146.

doi: 10.14383/cri.2021.16.2.133.

This study analyzed how the impacts of major teleconnection patterns on December mean temperature in Korea have been changed during the period before and after the regime shift of 1986 for the last 61 years from 1958 to 2018. During the period before the regime shift, the teleconnection patterns originating from the North Atlantic mainly affected the temperature variability in Korea, but its influence almost disappeared after the regime shift. On the other hand, the Arctic Oscillation (AO) and warm Arctic and cold Eurasia (WACE) patterns played a more important role in the temperature variability in Korea after the regime shift. Regression analysis showed that the AO could explain about 12% of the total temperature variability before the regime shift, but about 22% after the regime shift. WACE pattern also explained about 4% before the regime shift, but after the regime shift, the importance increased by about 4.5 times to 18%. On the other hand, East Atlantic pattern (EA) and North Atlantic Oscillation (NAO), which are east-west teleconnection patterns, explained 27% and 11%, respectively, before the regime shift, but had little influence within 3% after the regime shift. This means that the influence of east-west teleconnection patterns disappeared after the regime shift, and teleconnection patterns by the Arctic Circle became more important.

keywords: regime shift; AO; EA; WACE; december temperature

1-12 *Environmental Sciences & Ecology; Geology*

Characteristics of stem respiration in black spruce (*Picea mariana*) stand, interior Alaska

Kim, Yongwon., **Lee, Bang Yong.** and 2 others.

Polar Science. 2021. 29.

doi: 10.1016/j.polar.2021.100693.

Boreal forests account for roughly one third of the carbon sequestered in terrestrial ecosystems, and the high latitude boreal ecosystem they make up has been consequently vulnerable to recent climate change. This study investigated stem respiration of Alaska dominant black spruce trees in interior Alaska during the growing season of 2007. The continuous measurement of stem respiration was conducted in black spruce trees of four different ages (4.3, 7.2, 9.8, and 13.5 cm in diameter at breast height (DBH)) in interior Alaska, using a CO_2 analyzer, a 12-V pump, chambers, and a data-logger. Mean stem respiration is 0.014 ± 0.006 mg CO_2 m^{-2} s^{-1} (range 0.003–0.039 mg CO_2 m^{-2} s^{-1}) in different aged four black spruce

trees, indicating remarkably temporal variations in stem respiration with temperatures in air and stem. We found that metabolism is 1.5-fold higher in the younger black spruce tree than in the older. Temperatures in air and stem are significant regulators in regulating stem respiration. The stand-level annual stem respiration simulated by Q_{10} value based on air temperature is 73.9 g CO_2 m^{-2}, corresponding to 5.0% of the ecosystem respiration (Re) estimated by eddy covariance tower in 2007. Our findings demonstrate that stem respiration is a significant component in the scaleup of the regional carbon budget in a black spruce forest of interior Alaska.

keywords: Stem respiration; Temperature of air and stem; Black spruce forest; Alaska

1-13 *Chemistry; Geochemistry & Geophysics*

Climate-Associated Changes in Mercury Sources in the Arctic Fjord Sediments

Lee, Ju Hyeon., Kwon, Sae Yun., Lee, Hoin., **Nam, Seung-Il., Kim, Jung-Hyun.,** Joo, Young Ji., **Jang, Kwangc-hul.** and 2 others.

Acs Earth and Space Chemistry. 2021. 5(9): 2398-2407.
doi: 10.1021/acsearthspacechem.1c00095.

Despite the large climatic fluctuations in the Arctic over the Holocene, the dominant mercury (Hg) sources and the potential changes in Hg sources associated with the climate remain unclear. Here, we use Hg isotopes to reconstruct changes in Hg sources and processes in two Svalbard fjord sediment cores spanning the Holocene. The Hg isotope ratios of the fjord sediment cores are similar to bedrock and Hg bound to terrestrial total organic carbon (TOC) but different from other sediment cores influenced by atmospheric Hg drawdowns via the sinking of marine particulate organic matter. The absence of significant Hg and TOC relationships indicates that bedrock erosion caused by glacier dynamics is the major Hg source to the fjord sediment rather than those bound to marine and terrestrial TOC. Measurable shifts in Hg sources are observed at regional cooling (4.3 ka) and during the Medieval Warm Period in the late Holocene. The negative shift in δ^{202}Hg (by −0.5‰) at 4.3 ka from baseline (~10 ka) is consistent with the rapid increase in glacier-mediated physical and chemical erosions of bedrock. The significant positive shifts in δ^{202}Hg (by 0.5‰) in the late Holocene are explained by enhanced input of atmospheric Hg and its drawdown via the sinking of marine particulate organic matter and some anthropogenic influence, which suppressed the positive Δ^{199}Hg and Δ^{200}Hg shifts. This study suggests that Hg isotope ratios measured in sedimentary archives can be used to decipher climate and other local to global changes modifying Hg sources in the Arctic.

keywords: stable isotope; Holocene; climate change; sediment core; proxy; reconstruction; Svalbard; Dicksonfjorden; Woodfjorden

1-14 *Environmental Sciences & Ecology; Geology; Meteorology & Atmospheric Sciences*

Cold-Season Arctic Amplification Driven by Arctic Ocean-Mediated Seasonal Energy Transfer

Chung, Eui-Seok. and 5 others.

Earths Future. 2021. 9(2).
doi: 10.1029/2020ef001898.

The Arctic warming response to greenhouse gas forcing is substantially greater than the rest of the globe. It has been suggested that this phenomenon, commonly referred to as Arctic amplification, and its peak in boreal fall and winter result primarily from the lapse-rate feedback, which is associated with the vertical structure of tropospheric warming, rather than from the sea-ice albedo feedback, which operates mainly in summer. However, future climate model projections show consistently that an overall reduction of sea-ice in the Arctic region leads to a gradual weakening of Arctic amplification, thereby implying a key role for sea-ice albedo feedback. To resolve this apparent contradiction, we conduct a comprehensive analysis using atmosphere/ocean reanalysis data sets and a variety of climate model simulations. We show that the Arctic Ocean acts as a heat capacitor, storing anomalous heat resulting from the sea-ice loss during summer, which then gets released back into the atmosphere during fall and winter. Strong air-sea heat fluxes in fall/winter in sea-ice retreat regions in conjunction with a stably stratified lower troposphere lead to a surface-intensified warming/moistening, augmenting longwave feedback processes to further enhance the warming. The cold-season surface-intensified warming/moistening is found to virtually disappear if ocean-atmosphere-sea ice interactions

are suppressed, demonstrating the importance of ice insulation effect and ocean heat uptake/release. These results strongly suggest that the warm-season ocean heat recharge and cold-season heat discharge link and integrate the warm and cold season feedbacks, and thereby effectively explain the predominance of the Arctic amplification in fall and winter.

keywords: Arctic amplification; lapse-rate feedback; ocean heat recharge; discharge; sea-ice albedo feedback; seasonal evolution

1-15 *Astronomy & Astrophysics*

A Comparison of Fabry–Perot Interferometer and Meteor Radar Wind Measurements Near the Polar Mesopause Region

Lee, Changsup., **Jee, Geonhwa.**, Kam, Hosik., Wu, Qian., **Ham, Young-Bae.**, Kim, Yong Ha. and **Kim, Jeong-Han.**

Journal of Geophysical Research-Space Physics. 2021. 126(4).

doi: 10.1029/2020ja028802.

The neutral winds in the Mesosphere and Lower Thermosphere (MLT) region have been observed at King Sejong Station, Antarctica using a meteor radar (MR) and a Fabry–Perot interferometer (FPI) simultaneously. These two independent MLT wind measurements are compared to each other to identify the characteristics of FPI measurement. Instead of using a fixed emission height for FPI winds, for the first time, we consider the temporal variations of airglow emission layer in association with corresponding meteor height distributions for more accurate comparison between the FPI and MR winds. The temporal variations of the airglow emission layers are examined from the inverse relationship between the height integrated emission rate and the peak emission height derived from the TIMED/SABER observations. It is found that FPI winds are consistently smaller than MR winds and the discrepancy becomes larger for OI emission at higher altitude, which may be related to large wind shear in the MLT region and variabilities of the emission layers. Finally, we found that the FPI can provide reliable height-averaged winds in the MLT region where existing a strong wind shear from this simultaneous MR wind measurements.

keywords: Fabry–Perot interferometer; meteor radar; airglow; neutral wind; mesopause

1-16 *Meteorology & Atmospheric Sciences*

Comparison of Regional Climate Model Performances for Different Types of Heat Waves over South Korea

Yoon, Donghyuck., Cha, Dong-Hyun., Lee, Myong-In., Min, Ki-Hong., **Jun, Sang-Yoon.** and **Choi, Yonghan.**

Journal of Climate. 2021. 34(6): 2157-2174.

doi: 10.1175/jcli-d-20-0422.1.

South Korea's heat wave events over 39 years (1980–2018) were defined by spatiotemporal criteria, and their quantitative characteristics were analyzed. The duration and intensity of these events ranked highest in 2016 and 2018. An examination of synoptic conditions of heat wave events in 2016 and 2018 based on a reanalysis dataset revealed a positive anomaly of 500-hPa geopotential height, which could have induced warm conditions over the Korean Peninsula in both years. However, a difference prevailed in that there was a blocking high over the Kamchatka Peninsula and a continental thermal high over northern China in 2016, while the expansion of the western North Pacific subtropical high was mainly associated with 2018 heat wave events. Numerical experiments using the Weather Research and Forecasting (WRF) Model were conducted to 1) evaluate how distinct meteorological characteristics of heat wave events in 2016 and 2018 were reproduced by the model, and 2) investigate how they affect extreme temperature events. Typical synoptic features of the 2016 heat wave events (i.e., Kamchatka blocking and continental thermal high) were not captured well by the WRF Model, while those of 2018 were reasonably reproduced. On the contrary, the heat wave event during late August 2016 related to the Kamchatka blocking high was realistically simulated when the blocking was artificially sustained by applying spectral nudging. In conclusion, the existence of a blocking high over the Kamchatka region (i.e., northern Pacific region) is an important feature to accurately predict long-lasting heat waves in East Asia.

keywords: Asia; Extreme events; Numerical analysis/modeling; Regional models; Blocking

1-17 *Chemistry; Engineering; Materials Science; Physics*

Data Assimilation of AOD and Estimation of Surface Particulate Matters over the Arctic

Han, Kyung M., Jung, Chang H., Park, Rae-Seol., Park, Soon-Young., Lee, Sojin., Kulmala, Markku., Petaja, Tuukka., Karasinski, Grzegorz., Sobolewski, Piotr., **Yoon, Young Jun., Lee, Bang Yong.** and 2 others.

Applied Sciences-Basel. 2021. 11(4).
doi: 10.3390/app11041959.

In this study, more accurate information on the levels of aerosol optical depth (AOD) was calculated from the assimilation of the modeled AOD based on the optimal interpolation method. Additionally, more realistic levels of surface particulate matters over the Arctic were estimated using the assimilated AOD based on the linear relationship between the particulate matters and AODs. In comparison to the MODIS observation, the assimilated AOD was much improved compared with the modeled AOD (e.g., increase in correlation coefficients from −0.15−0.26 to 0.17−0.76 over the Arctic). The newly inferred monthly averages of PM_{10} and $PM_{2.5}$ for April−September 2008 were 2.18−3.70 μg m^{-3} and 0.85−1.68 μg m^{-3} over the Arctic, respectively. These corresponded to an increase of 140−180%, compared with the modeled PMs. In comparison to in-situ observation, the inferred PMs showed better performances than those from the simulations, particularly at Hyytiala station. Therefore, combining the model simulation and data assimilation provided more accurate concentrations of AOD, PM_{10}, and $PM_{2.5}$ than those only calculated from the model simulations.

keywords: CMAQ model; MODIS; AERONET; aerosol optical depth (τ); optimal interpolation; Arctic; data assimilation; PMs

1-18 *Geology; Meteorology & Atmospheric Sciences*

Dating of the GV7 East Antarctic ice core by high-resolution chemical records and focus on the accumulation rate variability in the last millennium

Nardin, Raffaello., Severi, Mirko., Amore, Alessandra., Becagli, Silvia., Burgay, Francois., Caiazzo, Laura., Ciardini, Virginia., Dreossi, Giuliano., Frezzotti, Massimo., **Hong, Sang-Bum.** and 8 others.

Climate of the Past. 2021. 17(5): 2073-2089.
doi: 10.5194/cp-17-2073-2021.

Ice core dating is the first step for a correct interpretation of climatic and environmental changes. In this work, we release the dating of the uppermost 197m of the 250m deep GV7(B) ice core (drill site, 70°41′S, 158°52′E; 1950ma.s.l. in Oates Land, East Antarctica) with a sub-annual resolution. Chemical records of NO_3^-, MSA (methanesulfonic acid), non-sea-salt SO_4^{2-} ($nssSO_4^{2-}$), seasalt ions and water stable isotopes ($\delta^{18}O$) were studied as candidates for dating due to their seasonal pattern. Different procedures were tested but the $nssSO_4^{2-}$) record proved to be the most reliable on the short- and long-term scales, so it was chosen for annual layer counting along the whole ice core. The dating was constrained by using volcanic signatures from historically known events as tie points, thus providing an accurate age–depth relationship for the period 1179–2009 CE. The achievement of the complete age scale allowed us to calculate the annual mean accumulation rate throughout the analyzed 197m of the core, yielding an annually resolved history of the snow accumulation on site in the last millennium. A small yet consistent rise in accumulation rate (Tr = 1.6, p<0:001) was found for the last 830 years starting around mid-18th century.

1-19 *Meteorology & Atmospheric Sciences*

Delayed Impacts of Arctic Sea-Ice Loss on Eurasian Severe Cold Winters

Jang, Yeon-Soo., **Jun, Sang-Yoon.** and 3 others.

Journal of Geophysical Research-Atmospheres. 2021. 126(23).
doi: 10.1029/2021jd035286.

This study suggests a possible mechanism of how the Arctic sea-ice loss can influence the mid-latitude climate in the Eurasian continent. It is shown that the low sea-ice concentration over the Barents-Kara-Laptev Seas in autumn typically leads to cold Eurasian in winters. It is demonstrated that the Arctic-to-midlatitude connection depends on the state of late autumn atmospheric circulation. When the autumn sea-ice reduction is accompanied by anticyclonic circulation over northern Eurasia, Eurasia becomes anomalously cold in the early winter. However, when cyclonic circulation is dominant, Eurasian cold anomalies appear in the late winter. This seasonally delayed response is further found to be related to the wind-driven sea-ice drift that causes warm anomalies

over the Barents-Kara Seas in the following winter. These observational results are confirmed by model simulations, indicating that the recent Eurasian cold winters could be linked to their forced response to the Arctic sea-ice loss.

keywords: sea-ice; warm Arctic-cold continent; Arctic warming; cold winter

1-20 *Science & Technology*

Detection of Arctic Summer Melt Ponds Using ICESat-2 Altimetry Data

Han, Daehyeon., Kim, Young Jun., Jung, Sihun., Sim, Seongmun., Kim, Woohyeok., Jang, Eunna., Im, Jungho. and **Kim, Hyun-Cheol.**

Korean Journal of Remote Sensing. 2021. 37(5): 1177-1186.
doi: 10.7780/kjrs.2021.37.5.1.27.

As the Arctic melt ponds play an important role in determining the interannual variation of the sea ice extent and changes in the Arctic environment, it is crucial to monitor the Arctic melt ponds with high accuracy. Ice, Cloud, and Land Elevation Satellite-2 (ICESat-2), which is the NASA's latest altimeter satellite based on the green laser (532 nm), observes the global surface elevation. When compared to the CryoSat-2 altimetry satellite whose along-track resolution is 250 m, ICESat-2 is highly expected to provide much more detailed information about Arctic melt ponds thanks to its high along-track resolution of 70 cm. The basic products of ICESat-2 are the surface height and the number of reflected photons. To aggregate the neighboring information of a specific ICESat-2 photon, the segments of photons with 10 m length were used. The standard deviation of the height and the total number of photons were calculated for each segment. As the melt ponds have the smoother surface than the sea ice, the lower variation of the height over melt ponds can make the melt ponds distinguished from the sea ice. When the melt ponds were extracted, the number of photons per segment was used to classify the melt ponds covered with open-water and specular ice. As photons are much more absorbed in the water-covered melt ponds than the melt ponds with the specular ice, the number of photons per segment can distinguish the water- and ice-covered ponds. As a result, the suggested melt pond detection method was able to classify the sea ice, water-covered melt ponds, and ice-covered melt ponds. A qualitative analysis was conducted using the Sentinel-2 optical imagery. The suggested method successfully classified the water- and ice-covered ponds which were difficult to distinguish with Sentinel-2 optical images. Lastly, the pros and cons of the melt pond detection using satellite altimetry and optical images were discussed.

keywords: ICESat-2; Sea ice; Melt pond; Altimetry; Photon height; Photon count

1-21 *Astronomy & Astrophysics; Physics*

Detection of Low-Energy X-rays Using YSO Scintillation Crystal Arrays for GRB Experiments

Kim, Minbin., Ripa, Jakub., Park, Il H., Bogomolov, Vitaly., Brandt, Soren., Budtz-Jorgensen, Carl., Castro-Tirado, Alberto J., Chang, Sheng-Hsiung., Chang, Yenyun., Chen, Chia Ray., Chen, C-W., Chen, Pisin., Connell, Paul., Eyles, Chris., Gaikov, Georgii., Hong, Gihan., Huang, Jian Jung., Huang, Ming-Huey Alfred., Jeong, Soomin., **Kim, Jieun.** and 13 others.

Universe. 2021. 7(11).
doi: 10.3390/universe7110396.

We developed an X-ray detector using 36 arrays, each consisting of a 64-pixellated yttrium oxyorthosilicate (YSO) scintillation crystal and a 64-channel multi-anode photomultiplier tube. The X-ray detector was designed to detect X-rays with energies lower than 10 keV, primarily with the aim of localizing gamma-ray bursts (GRBs). YSO crystals have no intrinsic background, which is advantageous for increasing low-energy sensitivity. The fabricated detector was integrated into UBAT, the payload of the Ultra-Fast Flash Observatory (UFFO)/*Lomonosov* for GRB observation. The UFFO was successfully operated in space in a low-Earth orbit. In this paper, we present the responses of the X-ray detector of the UBAT engineering model identical to the flight model, using ^{241}Am and ^{55}Fe radioactive sources and an Amptek X-ray tube. We found that the X-ray detector can measure energies lower than 5 keV. As such, we expect YSO crystals to be good candidates for the X-ray detector materials for future GRB missions.

keywords: gamma-ray burst; YSO; UBAT; UFFO

1-22 *Physical Geography; Geology; Remote Sensing; Imaging Science & Photographic Technology*

Digital surface model generation for drifting Arctic sea ice with low-textured surfaces based on drone images

Kim, Jae-In., Hyun, Chang-Uk., Han, Hyangsun. and **Kim, Hyun-Cheol.**

Isprs Journal of Photogrammetry and Remote Sensing. 2021. 172: 147-159.

doi: 10.1016/j.isprsjprs.2020.12.008.

Arctic sea ice is constantly moving and covered with low-textured surfaces, making it difficult to generate reliable digital surface models (DSMs) from drone images. The movement of sea ice makes georeferencing of DSMs difficult, and the low-textured surfaces of sea ice cause the uncertainty of image matching. This paper proposes a robust method to generate high-quality DSMs for drifting sea ice. To overcome the challenges, the proposed method introduces four improvements to the object-space-based image-matching pipeline: relative georeferencing to recover the horizontality and scale of sea-ice DSMs using a terrestrial light detection and ranging (LiDAR) dataset, match inspection to verify the matched points using several matching constraints, adaptive search-window adjustment to ensure distinct texture information through simple texture analysis, and robust vertical positioning to reduce the matching uncertainty via matching-indicator modeling. Performance evaluations were conducted with drone and LiDAR datasets obtained from a sea-ice campaign using the Korean Icebreaker Research Vessel (IBRV) Araon in the summer of 2017. The experimental results indicated that the proposed method can achieve significant quality enhancements compared with the existing matching method and that all the considerations contributed significantly to the enhancements.

keywords: Sea ice; Digital surface model; Unmanned aerial vehicle; Image matching; Georeferencing; Low-textured surface

1-23 *Environmental Sciences & Ecology; Geology; Meteorology & Atmospheric Sciences*

Dimethyl Sulfide-Induced Increase in Cloud Condensation Nuclei in the Arctic Atmosphere

Park, Ki-Tae., **Yoon, Young Jun.**, Lee, Kitack., Tunved, Peter., Krejci, Radovan., Strom, Johan., **Jang, Eunho.**, **Kang, Hyo Jin.**, Jang, Sehyun., **Park, Jiyeon.**, **Lee, Bang Yong.** and 3 others.

Global Biogeochemical Cycles. 2021. 35(7).

doi: 10.1029/2021gb006969.

Oceanic dimethyl sulfide (DMS) emissions have been recognized as a biological regulator of climate by contributing to cloud formation. Despite decades of research, the climatic role of DMS remains ambiguous largely because of limited observational evidence for DMS-induced cloud condensation nuclei (CCN) enhancement. Here, we report concurrent measurement of DMS, physiochemical properties of aerosol particles, and CCN in the Arctic atmosphere during the phytoplankton bloom period of 2010. We encountered multiple episodes of new particle formation (NPF) and particle growth when DMS mixing ratios were both low and high. The growth of particles to sizes at which they can act as CCN accelerated in response to an increase in atmospheric DMS. Explicitly, the sequential increase in all relevant parameters (including the source rate of condensable vapor, the growth rate of particles, Aitken mode particles, hygroscopicity, and CCN) was pronounced at the DMS-derived NPF and particle growth events. This field study unequivocally demonstrates the previously unconfirmed roles of DMS in the growth of particles into climate-relevant size and eventual CCN activation.

keywords: Aerosols; Arctic atmosphere; cloud condensation nuclei; dimethyl sulfide; phytoplankton

1-24 *Chemistry; Environmental Sciences & Ecology*

DMS sea-to-air fluxes and their influence on sulfate aerosols over the Southern Ocean, south-east Indian Ocean and north-west Pacific Ocean

Zhang, Miming., Marandino, Christa A., Yan, Jinpei., Lin, Qi., **Park, Keyhong.** and Xu, Guojie.

Environmental Chemistry. 2021. 18(5-6): 193-201.

doi: 10.1071/en21003.

Oceanic dimethyl sulfide (DMS) is the most abundant biogenic sulfur compound emitted into the atmosphere and could indirectly regulate the global climate by impacting end product sulfate aerosols. DMS emissions and their influence on sulfate aerosols, i.e. methanesulfonic acid (MSA) and non-sea-salt

sulfate (nss-SO_4^{2-}), were investigated over the Atlantic Ocean and Indian Ocean sectors of the Southern Ocean (SO), the south-east Indian Ocean, and the north-west Pacific Ocean from February to April 2014 during the 30th Chinese National Antarctic Research Expedition. We found a strong large-scale DMS source in the marginal sea ice zone from 34°W to 14°E of the SO (south of 60°S), in which the mean flux was 49.0 ± 65.6 μmol m^{-2} d^{-1} (0.6–308.3 μmol m^{-2} d^{-1}, n = 424). We also found a second large-scale DMS source in the South Subtropical Front (~40°S, up to 50.8 μmol m^{-2} d^{-1}). An inconsistency between concentrations of atmospheric sulfate compounds and DMS emissions along the cruise track was observed. The horizontal advection of air masses was likely the main reason for this discrepancy. Finally, the biological exposure calculation results also indicated that it is very difficult to observe a straightforward relationship between oceanic biomass and atmospheric MSA.

keywords: dimethyl sulfide; DMS; sulfate aerosol; DMS sea-to-air fluxes; the Southern Ocean; Indian Ocean; Pacific Ocean; relationships

1-25 *Geology*

Early and middle Miocene ice sheet dynamics in the Ross Sea: Results from integrated core-log-seismic interpretation

Perez, Lara F., De Santis, Laura., McKay, Robert M., Larter, Robert D., Ash, Jeanine., Bart, Phil J., Bohm, Gualtiero., Brancatelli, Giuseppe., Browne, Imogen., Colleoni, Florence., Dodd, Justin P., Geletti, Riccardo., Harwood, David M., Kuhn, Gerhard., Laberg, Jan Sverre., Leckie, R. Mark., Levy, Richard H., Marschalek, James., Mateo, Zenon., Naish, Timothy R., Sangiorgi, Francesca., Shevenell, Amelia E., Sorlien, Christopher C., van de Flierdt, Tina. and **Kim, Sunghan.**

Geological Society of America Bulletin. 2022. 134(1-2): 348-370.
doi: 10.1130/b35814.1.

Oscillations in ice sheet extent during early and middle Miocene are intermittently preserved in the sedimentary record from the Antarctic continental shelf, with widespread erosion occurring during major ice sheet advances, and open marine deposition during times of ice sheet retreat. Data from seismic reflection surveys and drill sites from Deep Sea Drilling Project Leg 28 and International Ocean Discovery Program Expedition 374, located across the present-day middle continental shelf of the central Ross Sea (Antarctica), indicate the presence of expanded early to middle Miocene sedimentary sections. These include the Miocene climate optimum (MCO ca. 17–14.6 Ma) and the middle Miocene climate transition (MMCT ca. 14.6–13.9 Ma). Here, we correlate drill core records, wireline logs and reflection seismic data to elucidate the depositional architecture of the continental shelf and reconstruct the evolution and variability of dynamic ice sheets in the Ross Sea during the Miocene. Drill-site data are used to constrain seismic isopach maps that document the evolution of different ice sheets and ice caps which influenced sedimentary processes in the Ross Sea through the early to middle Miocene. In the early Miocene, periods of localized advance of the ice margin are revealed by the formation of thick sediment wedges prograding into the basins. At this time, morainal bank complexes are distinguished along the basin margins suggesting sediment supply derived from marine-terminating glaciers. During the MCO, biosiliceous-bearing sediments are regionally mapped within the depocenters of the major sedimentary basin across the Ross Sea, indicative of widespread open marine deposition with reduced glacimarine influence. At the MMCT, a distinct erosive surface is interpreted as representing large-scale marine-based ice sheet advance over most of the Ross Sea paleo-continental shelf. The regional mapping of the seismic stratigraphic architecture and its correlation to drilling data indicate a regional transition through the Miocene from growth of ice caps and inland ice sheets with marine-terminating margins, to widespread marine-based ice sheets extending across the outer continental shelf in the Ross Sea.

1-26 *Science & Technology*

East Asian climate response to COVID-19 lockdown measures in China

Lee, Sun-Seon., Chu, Jung-Eun., Timmermann, Axel., **Chung, Eui-Seok.** and Lee, June-Yi.

Scientific Reports. 2021. 11(1).
doi: 10.1038/s41598-021-96007-1.

The COVID-19 pandemic caused disruptions of public life and imposed lockdown measures in 2020 resulted in considerable reductions of anthropogenic aerosol emissions. It still remains unclear how the associated short-term changes in atmospheric

chemistry influenced weather and climate on regional scales. To understand the underlying physical mechanisms, we conduct ensemble aerosol perturbation experiments with the Community Earth System Model, version 2. In the simulations reduced anthropogenic aerosol emissions in February generate anomalous surface warming and warm-moist air advection which promotes low-level cloud formation over China. Although the simulated response is weak, it is detectable in some areas, in qualitative agreement with the observations. The negative dynamical cloud feedback offsets the effect from reduced cloud condensation nuclei. Additional perturbation experiments with strongly amplified air pollution over China reveal a nonlinear sensitivity of regional atmospheric conditions to chemical/radiative perturbations. COVID-19-related changes in anthropogenic aerosol emissions provide an excellent testbed to elucidate the interaction between air pollution and climate.

1-27

Enhanced climate variability during the last millennium recorded in alkenone sea surface temperatures of the northwest Pacific margin

Lee, Kyung Eun., Park, Wonsun., Yeh, Sang-Wook., Bae, Si Woong., Ko, Tae Wook., Lohmann, Gerrit. and **Nam, Seung-Il.**

Global and Planetary Change. 2021. 204.
doi: 10.1016/j.gloplacha.2021.103558.

Previous studies on surface temperature reconstructions for the last 2000 years (2 k) revealed a long-term cooling trend for the last millennium in comparison to the previous millennium. However, knowledge on the decadal- to centennial-scale variability in sea surface temperature and the underlying governing mechanisms throughout the period is limited. We reconstructed high-resolution continuous sea surface temperature changes over the last 2 k in the northwest Pacific margin based on the alkenone unsaturation index. Our alkenone temperature record revealed enhanced and more rapidly changing climate variability during the last millennium (approximately 1200–1850 Common Era) than during the previous millennium. Cold and hot extremes also occurred more frequently during the last millennium. The enhanced and rapidly changing climate variability appears to be associated with frequent volcanic eruptions and grand solar minima. The reconstructed surface temperature variability tends to be associated with variations in the East Asia summer monsoon and the Pacific Decadal Oscillation, implying that these variations are also enhanced in the last millennium than in the previous millennium.

keywords: Last millennium; Common Era; Past sea surface temperature; Volcanic forcing; East Asian summer monsoon; North Pacific

1-28 *Environmental Sciences & Ecology; Geology; Remote Sensing; Imaging Science & Photographic Technology*

Evaluation of Total Ozone Column from Multiple Satellite Measurements in the Antarctic Using the Brewer Spectrophotometer

Kim, Songkang., **Park, Sang-Jong.**, Lee, Hana., Ahn, Dha Hyun., Jung, Yeonjin., **Choi, Taejin.**, **Lee, Bang Yong.**, **Kim, Seong-Joong.** and Koo, Ja-Ho.

Remote Sensing. 2021. 13(8).
doi: 10.3390/rs13081594.

The ground-based ozone observation instrument, Brewer spectrophotometer (Brewer), was used to evaluate the quality of the total ozone column (TOC) produced by multiple polar-orbit satellite measurements at three stations in Antarctica (King Sejong, Jang Bogo, and Zhongshan stations). While all satellite TOCs showed high correlations with Brewer TOCs (R = ~0.8 to 0.9), there are some TOC differences among satellite data in austral spring, which is mainly attributed to the bias of Atmospheric Infrared Sounder (AIRS) TOC. The quality of satellite TOCs is consistent between Level 2 and 3 data, implying that "which satellite TOC is used" can induce larger uncertainty than "which spatial resolution is used" for the investigation of the Antarctic TOC pattern. Additionally, the quality of satellite TOC is regionally different (e.g., OMI TOC is a little higher at the King Sejong station, but lower at the Zhongshan station than the Brewer TOC). Thus, it seems necessary to consider the difference of multiple satellite data for better assessing the spatiotemporal pattern of Antarctic TOC.

keywords: ozone; Antarctica; Brewer spectrophotometer; satellite

1-29 *Environmental Sciences & Ecology; Geology; Remote Sensing; Imaging Science & Photographic Technology*

Feasibility Study on Estimation of Sea Ice Drift from KOMPSAT-5 and COSMO-SkyMed SAR Images

Park, Jeong-Won., **Kim, Hyun-Cheol.**, Korosov, Anton., Demchev, Denis., Zecchetto, Stefano., **Kim, Seung Hee.**, **Kwon, Young-Joo.** and 2 others.

Remote Sensing. 2021. 13(20).

doi: 10.3390/rs13204038.

Estimating the sea ice drift field is of importance in both scientific study and activities in the polar ocean. Ice motion is being tracked at large scale (10 km and larger) on a daily basis; however, a higher resolution product is desirable for more reliable monitoring of rapid changes in sea ice. The use of wide-swath SAR has been extensively studied; yet, recent high-resolution X-band SAR sensors have not been tested enough. We examine the feasibility of KOMPSAT-5 and COSMO-SkyMed for retrieving sea ice motion by using the dataset of the MOSAiC expedition. The ice drift match-ups extracted from consecutive SAR image pairs and buoys for more than seven months in the central Arctic were used for a performance evaluation and validation. In addition to individual tests for KOMPSAT-5 and COSMO-SkyMed, a cross-sensor combination of two sensors was tested to overcome the drawback, a relatively long revisit time of high-resolution SAR. The experimental results show that higher accuracies are achievable from both single- and cross-sensor configurations of high-resolution X-band SARs compared to wide-swath C-band SARs, and that sub-daily monitoring is feasible from the cross-sensor approach.

keywords: KOMPSAT-5; COSMO-SkyMed; sea ice drift; synthetic aperture radar; cross-sensor

1-30 *Physical Geography; Geology*

Glacial and environmental changes in northern Svalbard over the last 16.3 ka inferred from neodymium isotopes

Jang, Kwangchul., **Ahn, Youngkyu.**, **Joe, Young Jin.**, Braun, Carmen A., Joo, Young Ji., **Kim, Jung-Hyun.**, Bayon, Germain., Forwick, Matthias., Vogt, Christoph. and **Nam, Seung-Il.**

Global and Planetary Change. 2021. 201.

doi: 10.1016/j.gloplacha.2021.103483.

The reconstruction of past ice sheet extents and dynamics in polar regions is essential for understanding the global climate system and obtaining more reliable predictions of future climate change. Here, we present a multiproxy dataset integrating the Nd isotopic compositions (ε_{Nd}) of paired detrital and authigenic Fe oxide fractions, grain size distributions, organic geochemistry, and mineral assemblages in a glacimarine sediment core (core HH17–1085-GC) retrieved from the continental shelf off northern Svalbard. Our results indicate variability in sediment provenance and chemical weathering patterns since the last deglaciation, allowing us to distinguish a succession of distinct paleoclimate events: 1) a general retreat of the Svalbard-Barents Sea Ice Sheet (SBIS) from the continental shelf before ca. 16.3 ka BP; 2) an intense episode of meltwater discharge related to massive glacier loss between ca. 12.1–9.9 ka BP; and 3) a period of reduced meltwater input between ca. 9.9 and 2.7 ka BP followed by 4) a phase of glacier re-advance over the last two millennia. Evidence for the prolonged supply of radiogenic detrital ε_{Nd} and dolomite at the site of core HH17–1085-GC indicates that the onset of deglaciation offshore northeastern Svalbard may have occurred at least 1 ka later than that at the northwestern shelf, which can be further evaluated by obtaining a more precise end-member determination for the northeastern source with a quantitative ε_{Nd} dataset from Nordaustlandet. In the context where both polar sea-ice and oceanic circulation are expected to have played minor roles in determining the sedimentary ε_{Nd} compositions, the evidence for pronounced Nd isotopic decoupling between paired authigenic and detrital signatures ($\Delta\varepsilon_{Nd}$) at ca. 15.2 and 14.1 ka BP is interpreted as reflecting chemical weathering changes following the retreat of the SBIS on northern Svalbard, probably corresponding to punctual episodes of glacial re-advances. Our findings provide a better understanding of the deglacial history of northern Svalbard during and after the last deglaciation and highlight the utility of Nd isotopes as a proxy for reconstructing paleo-cryosphere changes.

keywords: Neodymium isotopes; Svalbard-Barents Sea Ice Sheet; Hinlopen strait; Svalbard; Glacial activity

1-31 *Meteorology & Atmospheric Sciences*

Historical fidelity and future change of Amundsen Sea Low under 1.5°C–4 °C global warming in CMIP6

Gao, Miaoni., **Kim, Seong-Joong.** and 6 others.

Atmospheric Research. 2021. 255.
doi: 10.1016/j.atmosres.2021.105533.

The realistic simulation and projection of the Amundsen Sea Low (ASL) are essential for understanding the Antarctic climate and global climate change. Using 14 models that participated in phase 6 of the Coupled Model Intercomparison Project (CMIP6), this study evaluates the climatological characteristics of ASL with comparison to the ERA5 reanalysis and their CMIP5 versions and assesses the future change of ASL under 1.5°C–4 °C global warming. The climatological spatial distribution of ASL is captured reasonably but with underestimated intensity by CMIP6 multi-model ensemble (MME). Among the CMIP6 models, EC-Earth3 has most accurate representation of ASL according to the pattern correlation and biases. The seasonal variation of the ASL depth and location are found to be reasonably reproduced by the CMIP6 models. CMIP6 MME has higher skills in simulating the seasonal cycle of absolute depth and zonal migration of the ASL center. The relative central pressure of ASL is underestimated in all seasons and there is a 4-degree northward shift bias of the ASL center in austral winter, which were also evident in the CMIP5. The semiannual cycle of ASL absolute depth with two deepest pressure in April and October is also captured by CMIP6 MME. However, the observed peak of pressure between the two months occurs in June, while it delays one month and appears until July in CMIP6 MME. Compared with CMIP5, CMIP6 MME exhibit evident reduced uncertainties and overall improvement in simulating absolute depth and location of the ASL center, which might be attributed to models' capability of representing the location of Southern Hemisphere westerlies, while the biases in relative depth become even large in CMIP6 MME. In response to future warming from 1.5 °C to 4 °C above pre-industrial levels, the absolute depth of ASL will very likely deepen with larger amplitude in all seasons, while the relative depth might enhance only under high-level warmer world in austral autumn to winter. The CMIP6 MME also projects that the ASL will shift poleward constantly in austral summer and migrate southwestward during austral autumn with the rising global mean temperature. Among all the seasons, the most prominent future changes in intensity and location of ASL are found in autumn. The enhancement and poleward movement of ASL could also be identified during the Ross Sea ice advance season under 1.5 °C–4 °C global warming. The results reveal the potential of CMIP6 models in the ASL study and the impact of ASL on Antarctic climate under different global warming levels.

keywords: Amundsen Sea Low; CMIP6; Historical Fidelity; Future Projection; Global Warming Levels

1-32 *Physical Geography; Geology*

Holocene sedimentation in the Hupo Trough of the southwestern East Sea (Japan Sea) and development of the East Korea Warm Current

Khim, Boo-Keun., **Kim, Sunghan.**, Park, Yu-Hyeon., Lee, Jongmin., Ha, Sangbeom. and **Yoo, Kyu-Cheul.**

Holocene. 2021. 31(7): 1148-1157.
doi: 10.1177/09596836211003238.

Various sediment properties, such as mean grain size, total organic carbon, total nitrogen, C/N ratio, $CaCO_3$, and biogenic opal content, were analyzed for a box core (BC02; 45 cm long) and a gravity core (GC02; 628 cm long), which were collected from the western margin of the Hupo Trough located off the eastern coast of Korea. The study area has been affected by the East Korea Warm Current (EKWC), a branch of the Tsushima Warm Current (TWC). The analytical results obtained for BC02 and the upper part of GC02 were in agreement, affirming the core-top preservation of GC02. Based on the corrected calibrated AMS ^{14}C dates, the sedimentation rate of GC02 changed abruptly at ~8.2 ka from ~4.0–10.2 cm/kyr in the lower part to ~56.6–91.0 cm/kyr in the middle to upper part. This corresponds to the lithologic change from sandy mud to mud sediments showing the mean grain size change from 6.9 to 46.0 μm. Diverse paleoceanographic proxies representing the surface water condition exhibited varying degree of change at ~8.2 ka, after which all the properties remain almost unchanged, implying stable and continuous depositional conditions following the complete development of the EKWC. Furthermore, it indicated that the sediment depositional conditions in the Hupo

Trough in response to the EKWC might have stabilized at ~8.2 ka since the opening of the Korea Strait during the Holocene sea level rise. Moreover, microfossil data from previous studies on the establishment of the TWC in the East Sea (Japan Sea) support our interpretation that the sediment properties revealed the Holocene development of the EKWC in the Hupo Trough.

keywords: geochemical properties; paleoceanography; sea level; sediment deposition; Tsushima Warm Current

1-33 *Environmental Sciences & Ecology; Meteorology & Atmospheric Sciences*

How do intermittency and simultaneous processes obfuscate the Arctic influence on midlatitude winter extreme weather events?

Overland, J. E., Ballinger, T. J., Cohen, J., Francis, J. A., Hanna, E., Jaiser, R., Kim, B. -M., **Kim, Seong-Joong.** and 4 others.

Environmental Research Letters. 2021. 16(4).
doi: 10.1088/1748-9326/abdb5d.

Pronounced changes in the Arctic environment add a new potential driver of anomalous weather patterns in midlatitudes that affect billions of people. Recent studies of these Arctic/midlatitude weather linkages, however, state inconsistent conclusions. A source of uncertainty arises from the chaotic nature of the atmosphere. Thermodynamic forcing by a rapidly warming Arctic contributes to weather events through changing surface heat fluxes and large-scale temperature and pressure gradients. But internal shifts in atmospheric dynamics —the variability of the location, strength, and character of the jet stream, blocking, and stratospheric polar vortex (SPV)—obscure the direct causes and effects. It is important to understand these associated processes to differentiate Arctic-forced variability from natural variability. For example in early winter, reduced Barents/Kara Seas sea-ice coverage may reinforce existing atmospheric teleconnections between the North Atlantic/Arctic and central Asia, and affect downstream weather in East Asia. Reduced sea ice in the Chukchi Sea can amplify atmospheric ridging of high pressure near Alaska, influencing downstream weather across North America. In late winter southward displacement of the SPV, coupled to the troposphere, leads to weather extremes in Eurasia and North America. Combined tropical and sea ice conditions can modulate the variability of the SPV. Observational evidence for Arctic/midlatitude weather linkages continues to accumulate, along with understanding of connections with pre-existing climate states. Relative to natural atmospheric variability, sea-ice loss alone has played a secondary role in Arctic/midlatitude weather linkages; the full influence of Arctic amplification remains uncertain.

keywords: Arctic; jet stream; polar vortex; climate change; extreme weather; sea ice; Arctic amplification

1-34 *Environmental Sciences & Ecology*

Impact of North Atlantic-East Asian teleconnections on extremely high January PM_{10} cases in Korea☆

Kim, Jeong-Hun., **Kim, Seong-Joong.**, Youn, Daeok., Kim, Maeng-Ki., **Kim, Joo-Hong.** and 2 others.

Environmental Pollution. 2021. 290.
doi: 10.1016/j.envpol.2021.118051.

In this study, we investigated the daily variability of PM_{10} concentrations in January in Korea during the past 19 years (2001–2019), as well as the associated atmospheric circulation patterns. The daily PM_{10} concentrations were classified into three cases: low (L; < 50 μg/m³), high (H; 50–100 μg/m³), and extremely high (EH; ≥ 100 μg/m³). We found that the strength of the East Asian winter monsoon influenced the PM_{10} variability in the L and H cases. However, the EH cases were strongly influenced by the rapid growth of barotropic warming (anticyclonic anomaly) over the eastern North Atlantic and Northern Europe (ENE), and the stationary Rossby waves grew rapidly over Eurasia within only four days. Analysis of the quasi-geostrophic geopotential tendency budget revealed that the anticyclonic anomaly over the ENE was enhanced by vorticity advection. Linear baroclinic model experiments confirmed that vorticity forcing over the ENE induces favorable atmospheric conditions for the occurrence of EH PM_{10} events in East Asia. As a result, the PM_{10} concentration sharply increased sharply by approximately three times over four days. This study suggests that understanding atmospheric teleconnections between the ENE and East Asia can effectively predict the occurrence of EH PM_{10} events in Korea, helping to reduce the human health risks from atmospheric pollution.

keywords: PM_{10} concentration; East asia winter monsoon; Wave propagation; Atmospheric teleconnection

1-35 *Meteorology & Atmospheric Sciences*

Impacts of Saharan Mineral Dust on Air-Sea Interaction over North Atlantic Ocean Using a Fully Coupled Regional Model

Chen, Shu-Hua., Huang, Chu-Chun., Kuo, Yi-Chun., Tseng, Yu-Heng., Gu, Yu., Earl, Kenneth., Chen, Chih-Ying., **Choi, Yonghan.** and Liou, Kuo-Nan.

Journal of Geophysical Research-Atmospheres. 2021. 126(4).
doi: 10.1029/2020jd033586.

This study examines the modifications of air-sea coupling processes by dust-radiation-cloud interactions over the North Atlantic Ocean using a high-resolution coupled atmosphere-wave-ocean-dust (AWOD) regional model. The dust-induced mechanisms that are responsible for changes of sea surface temperature (SST) and latent and sensible heat fluxes (LHF/SHF) are also examined. Two 3-month numerical experiments are conducted, and they differ only in the activation and deactivation of dust-radiation-cloud interactions. Model results show that the dust significantly reduces surface downward radiation fluxes (SDRF) over the ocean with the maximum change of 20–30 W m–2. Over the dust plume region, the dust effect creates a low-pressure anomaly and a cyclonic circulation anomaly, which drives a positive wind stress curl anomaly, thereby reducing sea surface height and mixed layer depth. However, the SST change by dust, ranging from –0.5 to 0.5 K, has a great spatial variation which differs from the dust plume shape. Dust cools SST around the West African coast, except under the maximum dust plume ridge, and extends westward asymmetrically along the northern and southern edges of the dust plume. Dust unexpectedly warms SST over a large area of the western tropical North Atlantic and north of the dust plume. These SST changes are controlled by different mechanisms. Unlike the SST change pattern, the LHF and SHF changes are mostly reduced underneath the dust plume region, though they are different in detail due to different dominant factors, and increased south of the dust plume over the tropic.

keywords: African dust; air-sea interaction; COAWST; dust-cloud-radiation interaction; mixed layer depth; sea surface temperature; surface heat fluxes; wind stress curl

1-36 *Geology*

Increasing Difference in Interannual Summertime Surface Air Temperature Between Interior East Antarctica and the Antarctic Peninsula Under Future Climate Scenarios

Mao, Rui., **Kim, Seong-Joong.**, Gong, Dao-Yi., Liu, Xiao-hong., Wen, Xinyu., Zhang, Liping., Tang, Feng., Zong, Qi., Xiao, Cunde., Ding, Minghu. and **Park, Sang-Jong.**

Geophysical Research Letters. 2021. 48(16).
doi: 10.1029/2020gl092031.

In this study, using the Climate Model Intercomparison Project 5 (CMIP5) simulations and by empirical orthogonal function (EOF) analysis, the first mode of variability in interannual surface air temperature (SAT) in Antarctica (EOF1) was examined for the period between 1979–2004 and 2051–2099 during the austral summer. The ensemble mean of EOF1 of the CMIP5 models shows a positive SAT anomaly over the northern Antarctic Peninsula (AP) and a negative SAT anomaly over Eastern Antarctica (EA) in both periods. A poleward expansion of the AP positive anomaly and an increase in the negative anomaly over interior EA are expected in 2051–2099, resulting in a larger difference of interannual SAT between interior EA and the AP in 2051–2099 than in 1979–2004. The increasing difference in the interannual SAT is consistent with a larger magnitude of the SAM-related circulation anomalies in the future.

keywords: Temperature difference; Future climate; CMIP5; the Southern Hemisphere Annular Mode

1-37 *Environmental Sciences & Ecology; Geology; Meteorology & Atmospheric Sciences*

Increasing ENSO-rainfall variability due to changes in future tropical temperature-rainfall relationship

Yun, Kyung-Sook., Lee, June-Yi., Timmermann, Axel., Stein, Karl., Stuecker, Malte F., Fyfe, John C. and **Chung, Eui-Seok.**

Communications Earth & Environment. 2021. 2(1).
doi: 10.1038/s43247-021-00108-8.

Intensification of El Niño-Southern Oscillation (ENSO)-rainfall variability in response to global warming is a robust feature across Coupled Model Intercomparison Project (CMIP) iterations, regardless of a lack of robust

projected changes in ENSO-sea-surface temperature (SST) variability. Previous studies attributed this intensification to an increase in mean SST and moisture convergence over the central-to-eastern Pacific, without explicitly considering underlying nonlinear SST–rainfall relationship changes. Here, by analyzing changes of the tropical SST–rainfall relationship of CMIP6 models, we present a mechanism linking the mean SST rise to amplifying ENSO–rainfall variability. We show that the slope of the SST–rainfall function over Niño3 region becomes steeper in a warmer climate, ~42.1% increase in 2050–2099 relative to 1950–1999, due to the increase in Clausius-Clapeyron-driven moisture sensitivity, ~16.2%, and dynamic contributions, ~25.9%. A theoretical reconstruction of ENSO-rainfall variability further supports this mechanism. Our results imply ENSO's hydrological impacts increase nonlinearly in response to global warming.

1-38 *Environmental Sciences & Ecology*

Increasing spring dust storms in the future over the Taklimakan Desert, Northwest China: implications from changes in circulation pattern frequency in CMIP6

Mao, Rui., Gong, Dao-Yi., **Kim, Seong-Joong.** and 3 others.
Environmental Research Communications. 2021. 3(11).
doi: 10.1088/2515-7620/ac37ee.

Dust storms over the Taklimakan Desert (TD), Northwest China, not only influence human health but also affect regional climate through direct effects of dust aerosols on solar and longwave radiation. The Coupled Model Intercomparisons Project Phase 5 (CMIP5) models project a decrease in dust storms because of a decrease in dust emissions over the TD in the future under warming scenarios. However, inaccurate simulations of dust emissions cause the CMIP5 models to simulate dust storms poorly. Here we analyzed typical circulation patterns that initiate dust storms over the TD and examined changes in the frequency of typical circulation patterns derived from the CMIP6 models in an extreme warming scenario. The results show that there will be an increase in typical circulation pattern frequency in the latter half of the 21st century compared with 1958–2014, implying an increase in dust storms over the TD in the future under the extreme warming scenario. The increase in dust storms over the TD may be related to an increase in synoptic activities in the future from the Middle Asia to the TD, which is caused by a southern movement of subtropical westerly jet stream under the extreme warming scenario.

keywords: dust storms; CMIP6; Taklimakan Desert; subtropical westerly jet stream; circulation pattern frequency

---

1-39

Introduction of PMIP4 Experimental Design for Simulating Quaternary Climates

Jun, Sang-Yoon. and **Kim, Seong-Joong.**
THE KOREAN JOURNAL OF QUATERNARY RESEARCH. 2021.33(1-2): 49-58.

In the Paleoclimate Modeling Intercomparison Project phase 4 (PMIP4), various experiments for quaternary climatic change are being carried out along with the Coupled Model Intercomparison Project phase 6 (CMIP6). With the CMIP6 preindustrial climate experiment (*piControl*), the equilibrium climate simulations of 6 ka Holocene experiment (*midHolocene*), 21 ka Last Glacial Maximum experiment (*lgm*), and 127 ka Last Interglacial experiment (*lig127k*) experiment, and transient climate simulations of 850–1849 Common Era Last Millennium experiment (*past1000*), 21–9 ka last deglaciation, and 140–127 ka penultimate deglaciation experiment have been carried out under PMIP4 protocols by several modeling groups. In this technical note, important physical parameters and boundary conditions of these Tier 1 experiments and a list of additional Tier 2 and 3 experiments are summarized.

keywords: PMIP4; Quaternary simulation; CMIP6

1-40 *Environmental Sciences & Ecology; Geology; Remote Sensing; Imaging Science & Photographic Technology*

Investigating Wintertime Cloud Microphysical Properties and Their Relationship to Air Mass Advection at Ny-Alesund, Svalbard Using the Synergy of a Cloud Radar-Ceilometer-Microwave Radiometer

Cho, Yeonsoo., **Park, Sang-Jong.**, **Kim, Joo-Hong.**, Yeo, Huidong., Nam, Jihyun., **Jun, Sang-Yoon.** and 2 others.

Remote Sensing. 2021. 13(13).
doi: 10.3390/rs13132529.

This study investigates the relationship of cloud properties and radiative effects with air mass origin during the winter (November–February, 2016–2020) at Ny-Ålesund, Svalbard, through a combination of cloud radar, ceilometer, and microwave radiometer measurements. The liquid cloud fraction (CF) was less than 2%, whereas the ice CF predominantly exceeded 10% below 6 km. The liquid water content (LWC) of mixed-phase clouds (LWC_{mix}), which predominantly exist in the boundary layer (CF_{mix}: 10–30%), was approximately four times higher than that of liquid clouds (LWC_{liq}). Warm air mass advection ($warm_{adv}$) cases were closely linked with strong southerly/southwesterly winds, whereas northerly winds brought cold and dry air masses ($cold_{adv}$) to the study area. Elevated values of LWC and ice water content (IWC) during $warm_{adv}$ cases can be explained by the presence of mixed-phase clouds in the boundary layer and ice clouds in the middle troposphere. Consistently, the r_e of ice particles in $warm_{adv}$ cases was approximately 5–10 μm larger than that in $cold_{adv}$ cases at all altitudes. A high CF and cloud water content in $warm_{adv}$ cases contributed to a 33% (69 W m^{-2}) increase in downward longwave (LW) fluxes compared to cloud-free conditions.

keywords: Arctic clouds; cloud microphysical properties; air mass advection; cloud radar; Ny-Ålesund

1-41 *Geology*

Isolated Proton Aurora Driven by EMIC Pc1 Wave: PWING, Swarm, and NOAA POES Multi-Instrument Observations

Kim, Hyangpyo., Shiokawa, Kazuo., Park, Jaeheung., Miyoshi, Yoshizumi., Miyashita, Yukinaga., Stolle, Claudia., Connor, Hyunju Kim., Hwang, Junga., Buchert, Stephan., **Kwon, Hyuck-Jin.** and 6 others.

Geophysical Research Letters. 2021. 48(18).
doi: 10.1029/2021gl095090.

We report the concurrent observations of F-region plasma changes and field-aligned currents (FACs) above isolated proton auroras (IPAs) associated with electromagnetic ion cyclotron Pc1 waves. Key events on March 19, 2020 and September 12, 2018 show that ground magnetometers and all-sky imagers detected concurrent Pc1 wave and IPA, during which NOAA POES observed precipitating energetic protons. In the ionospheric F-layer above the IPA zone, the Swarm satellites observed transverse Pc1 waves, which span wider latitudes than IPA. Around IPA, Swarm also detected the bipolar FAC and localized plasma density enhancement, which is occasionally surrounded by wide/shallow depletion. This indicates that wave-induced proton precipitation contributes to the energy transfer from the magnetosphere to the ionosphere.

keywords: EMIC wave; field-aligned current; isolated proton aurora; Pc1 wave; proton precipitation; Swarm satellite

1-42 *Environmental Sciences & Ecology; Meteorology & Atmospheric Sciences*

Large seasonal and interannual variations of biogenic sulfur compounds in the Arctic atmosphere (Svalbard; 78.9°N, 11.9°E)

Jang, Sehyun., **Park, Ki-Tae.**, Lee, Kitack., **Yoon, Young Jun.**, **Kim, Kitae.**, **Chung, Hyun Young.**, **Jang, Eunho.**, Becagli, Silvia., **Lee, Bang Yong.** and 4 others.

Atmospheric Chemistry and Physics. 2021. 21(12): 9761-9777.
doi: 10.5194/acp-21-9761-2021.

Seasonal to interannual variations in the concentrations of sulfur aerosols (< 2.5 μm in diameter; non sea-salt sulfate: NSS-SO_4^{2-}; anthropogenic sulfate: Anth-SO_4^{2-}; biogenic sulfate: Bio-SO_4^{2-}; methanesulfonic acid: MSA) in the Arctic atmosphere were investigated using measurements of the chemical composition of aerosols collected at Ny-Ålesund, Svalbard (78.9° N, 11.9° E) from 2015 to 2019. In all measurement years the concentration of NSS-SO_4^{2-} was highest during the pre-bloom period and rapidly decreas0ed towards summer. During the pre-bloom period we found a strong correlation between NSS-SO_4^{2-} (sum of Anth-SO_4^{2-} and Bio-SO_4^{2-}) and Anth-SO_4^{2-}. This was because more than 50 % of the NSS-SO_4^{2-} measured during this period was Anth-SO_4^{2-}, which originated in northern Europe and was subsequently transported to the Arctic in Arctic haze. Unexpected increases in the concentration of Bio-SO_4^{2-} aerosols (an oxidation product of dimethylsulfide: DMS) were occasionally found during the pre-bloom period. These probably originated in regions to the south (the North Atlantic Ocean and the Norwegian Sea) rather than in ocean areas in the proximity of Ny-Ålesund. Another

oxidation product of DMS is MSA, and the ratio of MSA to Bio-SO_4^{2-} is extensively used to estimate the total amount of DMS-derived aerosol particles in remote marine environments. The concentration of MSA during the pre-bloom period remained low, primarily because of the greater loss of MSA relative to Bio-SO_4^{2-} and the suppression of condensation of gaseous MSA onto particles already present in air masses being transported northwards from distant ocean source regions (existing particles). In addition, the low light intensity during the pre-bloom period resulted in a low concentration of photo-chemically activated oxidant species including OH radicals and BrO; these conditions favored the oxidation pathway of DMS to Bio-SO_4^{2-} rather than to MSA, which acted to lower the MSA concentration at Ny-Ålesund. The concentration of MSA peaked in May or June and was positively correlated with phytoplankton biomass in the Greenland and Barents seas around Svalbard. As a result, the mean ratio of MSA to the DMS-derived aerosols was low (0.09 ± 0.07) in the pre-bloom period but high (0.32 ± 0.15) in the bloom and post-bloom periods. There was large interannual variability in the ratio of MSA to Bio-SO_4^{2-} (i.e., 0.24 ± 0.11 in 2017, 0.40 ± 0.14 in 2018, and 0.36 ± 0.14 in 2019) during the bloom and post-bloom periods. This was probably associated with changes in the chemical properties of existing particles, biological activities surrounding the observation site, and air mass transport patterns. Our results indicate that MSA is not a conservative tracer for predicting DMS-derived particles, and the contribution of MSA to the growth of newly formed particles may be much larger during the bloom and post-bloom periods than during the pre-bloom period.

1-43 *Science & Technology*

A large West Antarctic Ice Sheet explains early Neogene sea-level amplitude

Marschalek, J. W., Zurli, L., Talarico, F., van de Flierdt, T., Vermeesch, P., Carter, A., Beny, F., Bout-Roumazeilles, V., Sangiorgi, F., Hemming, S. R., Perez, L. F., Colleoni, F., Prebble, J. G., van Peer, T. E., Perotti, M., Shevenell, A. E., Browne, I., Kulhanek, D. K., Levy, R., Harwood, D., Sullivan, N. B., Meyers, S. R., Griffith, E. M., Hillenbrand, C-D., Gasson, E., Siegert, M. J., Keisling, B., Licht, K. J., Kuhn, G., Dodd, J. P., Boshuis, C., De Santis, L., McKay, R. M. and **Kim, Sunghan.**

Nature. 2021. 600(7889): 450-455.

doi: 10.1038/s41586-021-04148-0.

Early to Middle Miocene sea-level oscillations of approximately 40–60 m estimated from far-field records[1-3] are interpreted to reflect the loss of virtually all East Antarctic ice during peak warmth[2]. This contrasts with ice-sheet model experiments suggesting most terrestrial ice in East Antarctica was retained even during the warmest intervals of the Middle Miocene[4,5]. Data and model outputs can be reconciled if a large West Antarctic Ice Sheet (WAIS) existed and expanded across most of the outer continental shelf during the Early Miocene, accounting for maximum ice-sheet volumes. Here weprovide the earliest geological evidence proving large WAIS expansions occurred during the Early Miocene (~17.72–17.40 Ma). Geochemical and petrographic data show glacimarine sediments recovered at International Ocean Discovery Program (IODP) Site U1521 in the central Ross Sea derive from West Antarctica, requiring the presence of a WAIS covering most of the Ross Sea continental shelf. Seismic, lithological and palynological data reveal the intermittent proximity of grounded ice to Site U1521. The erosion rate calculated from this sediment package greatly exceeds the long-term mean, implying rapid erosion of West Antarctica. This interval therefore captures akey step in the genesis of a marine-based WAIS and a tipping point in Antarctic ice-sheet evolution.

1-44 *Environmental Sciences & Ecology; Geology; Remote Sensing; Imaging Science & Photographic Technology*

Mapping Potential Plant Species Richness over Large Areas with Deep Learning, MODIS, and Species Distribution Models

Choe, Hyeyeong., **Chi, Junhwa.** and Thorne, James H.

Remote Sensing. 2021. 13(13).

doi: 10.3390/rs13132490.

The spatial patterns of species richness can be used as indicators for conservation and restoration, but data problems, including the lack of species surveys and geographical data gaps, are obstacles to mapping species richness across large areas. Lack of species data can be overcome with remote sensing because it covers extended geographic areas and generates recurring data. We developed a Deep Learning (DL) framework using Moderate Resolution Imaging Spectroradiometer (MODIS) products and modeled

potential species richness by stacking species distribution models (S-SDMs) to ask, "What are the spatial patterns of potential plant species richness across the Korean Peninsula, including inaccessible North Korea, where survey data are limited?" First, we estimated plant species richness in South Korea by combining the probability-based SDM results of 1574 species and used independent plant surveys to validate our potential species richness maps. Next, DL-based species richness models were fitted to the species richness results in South Korea, and a time-series of the normalized difference vegetation index (NDVI) and leaf area index (LAI) from MODIS. The individually developed models from South Korea were statistically tested using datasets that were not used in model training and obtained high accuracy outcomes (0.98, Pearson correlation). Finally, the proposed models were combined to estimate the richness patterns across the Korean Peninsula at a higher spatial resolution than the species survey data. From the statistical feature importance tests overall, growing season NDVI-related features were more important than LAI features for quantifying biodiversity from remote sensing time-series data.

keywords: biodiversity; data fusion; deep learning; LAI; MODIS; multilayer perceptron (MLP); NDVI; remote sensing; species richness; S-SDMs

1-45 *Meteorology & Atmospheric Sciences*

Mesospheric Short-Period Gravity Waves in the Antarctic Peninsula Observed in All-Sky Airglow Images and Their Possible Source Locations

Kam, Hosik., Song, In-Sun., **Kim, Jeong-Han.** and 9 others.

Journal of Geophysical Research-Atmospheres. 2021. 126(24).
doi: 10.1029/2021jd035842.

This study presents an analysis of OH airglow images observed from an all-sky camera (ASC) at King Sejong Station (KSS), Antarctic for the 2012–2016 period. The two-dimensional power spectra of short-period gravity waves (<1 hr) as a function of phase velocities are obtained using the M-transform method that employs the time sequence of ASC images. The amplitudes of the power spectral densities show that the mesospheric wave activity is the largest during winter (May, June, and July) and is the smallest in fall (February, March, and April). Wind-blocking diagrams are constructed on the same two-dimensional domain as in the two-dimensional spectra using horizontal winds obtained from MERRA-2 reanalysis at z = 0–80 km and from KSS meteor radar data at z = 80–90 km. Climatologically, the spectral regions of slowly propagating gravity waves (<30 m s^{-1}) are overlaid by the wind-blocking areas, which suggests the filtering of gravity waves with small phase speeds by winds below the upper stratosphere. Eastward propagating gravity waves in winter and intense south-eastward waves in spring (October) are found to be unfiltered by the stratospheric winds. It is also found from the spectral analysis that these unfiltered gravity waves can originate from the upper stratosphere or the lower mesosphere, and not from the troposphere, which suggests the possibility of ASC observation of the secondary gravity waves generated near the stratopause.

keywords: mesospheric short-period gravity wave; Antarctic Peninsula; wind filtering effect

1-46 *Physical Geography; Geology*

Mid-Holocene thinning of David Glacier, Antarctica: chronology and controls

Stutz, Jamey., Mackintosh, Andrew., Norton, Kevin., Whitmore, Ross., Baroni, Carlo., Jamieson, Stewart S. R., Jones, Richard S., Balco, Greg., Salvatore, Maria Cristina., Casale, Stefano., **Lee, Jae Il.** and 11 others.

Cryosphere. 2021. 15(12): 5447-5471.
doi: 10.5194/tc-15-5447-2021.

Quantitative satellite observations only provide an assessment of ice sheet mass loss over the last four decades. To assess long-term drivers of ice sheet change, geological records are needed. Here we present the first millennial-scale reconstruction of David Glacier, the largest East Antarctic outlet glacier in Victoria Land. To reconstruct changes in ice thickness, we use surface exposure ages of glacial erratics deposited on nunataks adjacent to fast-flowing sections of David Glacier. We then use numerical modelling experiments to determine the drivers of glacial thinning. Thinning profiles derived from 45 ^{10}Be and ^{3}He surface exposure ages show David Glacier experienced rapid thinning of up to 2 m/yr during the mid-Holocene (~6.5 ka). Thinning slowed at 6 ka, suggesting the initial formation of the Drygalski Ice Tongue at this time. Our work, along with ice thinning

records from adjacent glaciers, shows simultaneous glacier thinning in this sector of the Transantarctic Mountains occurred 4–7 kyr after the peak period of ice thinning indicated in a suite of published ice sheet models. The timing and rapidity of the reconstructed thinning at David Glacier is similar to reconstructions in the Amundsen and Weddell embayments. To identify the drivers of glacier thinning along the David Glacier, we use a glacier flowline model designed for calving glaciers and compare modelled results against our geological data. We show that glacier thinning and marine-based grounding-line retreat are controlled by either enhanced sub-ice-shelf melting, reduced lateral buttressing or a combination of the two, leading to marine ice sheet instability. Such rapid glacier thinning events during the mid-Holocene are not fully captured in continental- or catchment-scale numerical modelling reconstructions. Together, our chronology and modelling identify and constrain the drivers of a ~2000-year period of dynamic glacier thinning in the recent geological past.

1-47 *Chemistry; Geochemistry & Geophysics*

Molecular Mechanism of Gas Diffusion in Ice-Ih

Yi, Yoo Soo., **Han, Yeongcheol.**, Kwon, Kideok D., Lee, Sung Keun. and **Hur, Soon Do.**

Acs Earth and Space Chemistry. 2021. 5(11): 3258-3267.

doi: 10.1021/acsearthspacechem.1c00308.

Atmospheric gases trapped in polar ice have been used to reconstruct polar and global climate changes, providing better time resolution when less diffused. Experiments have shown that gas diffusion in ice is negligible on a laboratory time scale, but its cumulative impact on old glacial ice (>1 Myr remains unclear. Here, we employ density functional theory calculations to investigate the diffusion mechanism of gases trapped in ice-Ih from the atomistic level. The results suggest that the diffusion energy barrier between interstitial sites is primarily dependent on the atomic size and charge distribution of hopping gases. The diffusion of noble gases (He, Ne, Ar, Kr, and Xe) primarily occurs via the interstitial mechanism, consistent with previous results of classical molecular dynamics simulations. In contrast, the precisely determined diffusion paths and energy barriers for CO_2, O_2, and N_2 suggest that these molecular gases prefer to hop along the hexagonal channel also via the interstitial mechanism, and the bond-breaking mechanism proposed previously to explain the diffusion of those molecular gases as fast as Ne may be unnecessary.

keywords: ice core; noble gases; gas diffusion mechanism; interstitial mechanism; paleorecord smoothing; density functional theory

1-48 *Geochemistry & Geophysics; Mineralogy; Mining & Mineral Processing*

Multibeam Bathymetry and Distribution of Clay Minerals on Surface Sediments of a Small Bay in Terra Nova Bay, Antarctica

Jung, Jaewoo., Ko, Youngtak., **Lee, Joohan.**, Yang, Kiho., Park, Young Kyu., **Kim, Sunghan.**, **Moon, Heung-soo.**, **Kim, Hyoung Jun.** and **Yoo, Kyu-Cheul.**

Minerals. 2021. 11(1).

doi: 10.3390/min11010072.

The second Antarctic station of South Korea was constructed at Terra Nova Bay, East Antarctica, but local seafloor morphology and clay mineralogical characteristics are still not fully understood. Its small bay is connected to a modern Campbell Glacier, cliffs, and raised beaches along the coastline. Fourteen sampling sites to collect surface sediments were chosen in the small bay for grain size and clay mineral analyses to study the sediment source and sediment-transport process with multibeam bathymetry and sub-bottom profiles. Under the dominant erosional features (streamlined feature and meltwater channel), icebergs are the major geological agent for transport and deposition of coarse-sized sediments along the edge of glaciers in summer, and thus the study area can reveal the trajectory of transport by icebergs. Glacier meltwater is an important agent to deposit the clay-sized detritus and it results from the dominance of the illite content occurring along the edge of Campbell Glacier Tongue. The high smectite content compared to Antarctic sediments may be a result of the source of the surrounding volcanic rocks around within the Melbourne Volcanic Province.

keywords: Antarctica; Ross Sea; Terra Nova Bay; multibeam bathymetry; surface sediments;clay mineralogy

1-49 *Astronomy & Astrophysics*

The Observation and SD-WACCM Simulation of Planetary Wave Activity in the Middle Atmosphere During the 2019 Southern Hemispheric Sudden Stratospheric Warming

Lee, Wonseok., Song, In-Sun., **Kim, Jeong-Han.** and 4 others.

Journal of Geophysical Research-Space Physics. 2021. 126(6).
doi: 10.1029/2020ja029094.

A sudden stratospheric warming (SSW) is an extremely rare event in the Southern Hemisphere (SH), but occurred in early September 2019. From the Antarctic meteor radar (MR) stations, Davis (68.6°S, 77.9°E) and King Sejong Station (62.2°S, 58.8°W), quasi 10-day oscillations were clearly observed in the zonal mesospheric winds before the central date (DOY 253) of the SSW. From the northern low-latitude Tirupati (13.6°N, 79.4°E) MR, a strong wave activity with a period of ~6 days was detected in the zonal winds right after the central date. This oscillation is also seen in the geopotential height measurements from the Microwave Limb Sounder (MLS) on board the Aura satellite near the Tirupati region. To elucidate the possible source of the quasi 6-day wave (Q6DW), we use a specified dynamics version of the Whole Atmosphere Community Climate Model (SD-WACCM) constrained by the reanalysis data from the surface to 50 km. The simulation results show that the amplitude of the westward and equatorward propagating Q6DW was enhanced after the SSW central date in the MLT region, and the Q6DW can be attributed to the baroclinic/barotropic instability in the SH high-latitude mesosphere where the divergence of Eliassen-Palm flux occurred. Thus, we suggest that the Q6DW activity observed by the Tirupati MR and MLS originated from the SH high-latitude mesospheric region. Both the observation and the simulation results clearly demonstrate that the 2019 SH SSW affected not only the high-latitude MLT region but also the low-latitude MLT region.

keywords: lower thermosphere; mesosphere; meteor radar; planetary waves; SD-WACCM; sudden stratospheric warming

1-50 *Geology*

Observational Evidence of Distinguishable Weather Patterns for Three Types of Sudden Stratospheric Warming During Northern Winter

Choi, Hyesun., **Kim, Joo-Hong.**, Kim, Baek-Min. and **Kim, Seong-Joong.**

Frontiers in Earth Science. 2021. 9.
doi: 10.3389/feart.2021.625868.

Sudden stratospheric warming (SSW) events often lead to a cold surface air temperature anomaly over the extratropical regions. In this study, we propose, through observational evidence, that the types of SSW determine the severity of the cold anomaly. Based on the three-type classification of SSW, it is found that the surface air temperature drops notably over central to eastern North America following an SSW-type transition, especially from displacement to split. Note, however, that the differences in mean surface air temperature anomalies between SSW types are not statistically significant, even though after SSW-type transition from displacement to split, surface air temperature anomalies are colder than the other two types. The development of an anomalous tropospheric ridge in the North Pacific Arctic sector, associated with the difference in the vertical and zonal propagation of planetary waves, characterizes the post-warming period of the displacement-split type. After the occurrence of the displacement-split type transition of SSW events, upward propagation of planetary waves of zonal wavenumber 1 is suppressed, whereas planetary waves of zonal wavenumber 2 increase in the troposphere. Accompanying the ridge in the North Pacific, a trough developed downstream over North America that carries cold polar air therein. The results in this study are relevant for the subseasonal time scale, within 20 days after an SSW occurrence.

keywords: sudden stratospheric warming; type-transition; North America; surface temperature; cold polar air

1-51 *Astronomy & Astrophysics*

Observations of the Aurora by Visible All-Sky Camera at Jang Bogo Station, Antarctica

Jee, Geonhwa., **Ham, Young-bae.**, **Choi, Yoonseung.**, **Kim, Eunsol.**, **Lee, Changsup.**, **Kwon, Hyuck-Jin.**, Trondsen,

Trond S., **Kim, Jieun.** and **Kim, Jeong-Han.**

Journal of Astronomy and Space Sciences. 2021. 38(4): 203-215.

doi: 10.5140/JASS.2021.38.4.203

The auroral observation has been started at Jang Bogo Station (JBS), Antarctica by using a visible All-sky camera (v-ASC) in 2018 to routinely monitor the aurora in association with the simultaneous observations of the ionosphere, thermosphere and magnetosphere at the station. In this article, the auroral observations are introduced with the analysis procedure to recognize the aurora from the v-ASC image data and to compute the auroral occurrences and the initial results on their spatial and temporal distributions are presented. The auroral occurrences are mostly confined to the northern horizon in the evening sector and extend to the zenith from the northwest to cover almost the entire sky disk over JBS at around 08 MLT (magnetic local time; 03 LT) and then retract to the northeast in the morning sector. At near the magnetic local noon, the occurrences are horizontally distributed in the northern sky disk, which shows the auroral occurrences in the cusp region. The results of the auroral occurrences indicate that JBS is located most of the time in the polar cap near the poleward boundary of the auroral oval in the nightside and approaches closer to the oval in the morning sector. At around 08 MLT (03 LT), JBS is located within the auroral oval and then moves away from it, finally being located in the cusp region at the magnetic local noon, which indicates that the location of JBS turns out to be ideal to investigate the variabilities of the poleward boundary of the auroral oval from long-term observations of the auroral occurrences. The future plan for the ground auroral observations near JBS is presented.

keywords: aurora; auroral occurrence; polar ionosphere; all-sky camera; Jang Bogo Station (JBS); antarctica

1-52 *Environmental Sciences & Ecology; Geology; Remote Sensing; Imaging Science & Photographic Technology*

Phytoplankton Bloom Changes under Extreme Geophysical Conditions in the Northern Bering Sea and the Southern Chukchi Sea

Park, Jinku., **Lee, Sungjae.**, Jo, Young-Heon. and **Kim, Hyun-Cheol.**

Remote Sensing. 2021. 13(20).

doi: 10.3390/rs13204035.

The northern Bering Sea and the southern Chukchi Sea are undergoing rapid regional biophysical changes in connection with the recent extreme climate change in the Arctic. The ice concentration in 2018 was the lowest since observations began in the 1970s, due to the unusually warm southerly wind in winter, which continued in 2019. We analyzed the characteristics of spring phytoplankton biomass distribution under the extreme environmental conditions in 2018 and 2019. Our results show that higher phytoplankton biomass during late spring compared to the 18-year average was observed in the Bering Sea in both years. Their spatial distribution is closely related to the open water extent following winter-onset sea ice retreat in association with dramatic atmospheric conditions. However, despite a similar level of shortwave heat flux, the 2019 springtime biomass in the Chukchi Sea was lower than that in 2018, and was delayed to summer. We confirmed that this difference in bloom timing in the Chukchi Sea was due to changes in seawater properties, determined by a combination of northward oceanic heat flux modulation by the disturbance from more extensive sea ice in winter and higher surface net shortwave heat flux than usual.

keywords: Bering and Chukchi Seas; phytoplankton bloom; satellite observation; anomalous biophysical condition

1-53 *Environmental Sciences & Ecology; Meteorology & Atmospheric Sciences*

Polar Middle Atmospheric Responses to Medium Energy Electron (MEE) Precipitation Using Numerical Model Simulations

Lee, Ji-Hee., **Jee, Geonhwa.**, Kwak, Young-Sil., **Hwang, Heejin.**, Seppala, Annika., **Song, In-Sun.** and 2 others.

Atmosphere. 2021. 12(2).

doi: 10.3390/atmos12020133.

Energetic particle precipitation (EPP) is known to be an important source of chemical changes in the polar middle atmosphere in winter. Recent modeling studies further suggest that chemical changes induced by EPP can also cause dynamic changes in the middle atmosphere. In this study, we investigated the atmospheric responses to the precipitation of medium-to-high energy electrons (MEEs) over the period 2005–2013 using the Specific Dynamics Whole Atmosphere Community Climate Model (SD-

WACCM). Our results show that the MEE precipitation significantly increases the amounts of NO_x and HO_x, resulting in mesospheric and stratospheric ozone losses by up to 60% and 25% respectively during polar winter. The MEE-induced ozone loss generally increases the temperature in the lower mesosphere but decreases the temperature in the upper mesosphere with large year-to-year variability, not only by radiative effects but also by adiabatic effects. The adiabatic effects by meridional circulation changes may be dominant for the mesospheric temperature changes. In particular, the meridional circulation changes occasionally act in opposite ways to vary the temperature in terms of height variations, especially at around the solar minimum period with low geomagnetic activity, which cancels out the temperature changes to make the average small in the polar mesosphere for the 9-year period.

keywords: medium energy electron (MEE); energetic electron precipitation (EEP); mesosphere; odd-nitrogen; odd-hydrogen; ozone loss

1-54 *Geology; Oceanography*

Provenance constraints on the Cretaceous-Paleocene erosional history of the Guiana Shield as determined from the geochemistry of clay-size fraction of sediments from the Arapaima-1 well (Guyana-Suriname basin)

Roddaz, Martin., Dera, Guillaume., Mourlot, Yannick., Calves, Gerome., **Kim, Jung-Hyun.** and 3 others.

Marine Geology. 2021. 434.
doi: 10.1016/j.margeo.2021.106433.

Recent studies have emphasized the role of the Equatorial Atlantic Ocean opening on the drainage reorganization and erosion of the West African and northeastern Brazilian cratons during the Cretaceous. However, such studies are lacking regarding the Guiana Shield. To fill this gap, we determined the provenance of sediments deposited in the Suriname-Guyana basin during the Cretaceous-Paleocene based on the total organic carbon (TOC) content, $\delta^{13}C_{TOC}$, major and trace element concentrations, and Sr-Nd isotopic data of nineteen clay-size fraction samples from one industrial well (Arapaima-1). Overall, the absence of correlation between the TOC content, $\delta^{13}C_{TOC}$ and provenance proxies as well as the lack of Ce anomaly indicate that marine authigenesis, reducing conditions, and weathering have not markedly affected the trace element ratios (Eu/Eu*, Cr/Th, Th/Sc) and Sr-Nd isotopic compositions used as provenance proxies. Three samples (Early Cretaceous, Cenomanian and Late Campanian) have radiogenic $\varepsilon_{Nd(0)}$ values > − 2.2. The Early Cretaceous sample may have been sourced by Precambrian or Mesozoic mafic rocks of the Guiana Shield or contemporaneous basic volcanic rocks. The Cenomanian sample is likely to have been sourced by basic volcanic rocks of the Caribbean Large Igneous Province or the Takutu rift whereas the Late Campanian sample may have recorded more acid volcanism in the Takutu Rift. The other samples have an overall Guiana cratonic provenance with variable contributions of the Paleoproterozoic and Mesoproterozoic terranes and Jurassic or Precambrian mafic dykes. Increases in $^{87}Sr/^{86}Sr$ ratios and trace element ratios characteristic of more differentiated sources suggest an increasing contribution from the inner part of the Guiana Shield after the Coniacian. Because of the possible presence of active volcanism during the deposition of analyzed samples, post rift mantle upwelling under the equatorial margin is the favored mechanism to explain the increasing erosion of the Guiana Shield inner parts.

keywords: Provenance; Cretaceous; Guiana Shield; Guyana-Suriname Basin

1-55 *Geochemistry & Geophysics*

A Pulse of Meteoric Subsurface Fluid Discharging Into the Chukchi Sea During the Early Holocene Thermal Maximum (EHTM)

Kim, Ji-Hoon., Hong, Wei-Li., Torres, Marta E., Ryu, Jong-Sik., Kang, Moo-Hee., Han, Dukki., **Nam, Seung-Il.**, Hur, Jin., Koh, Dong-Chan., Niessen, Frank., Lee, Dong-Hun., **Jang, Kwangchul.** and 2 others.

Geochemistry Geophysics Geosystems. 2021. 22(8).
doi: 10.1029/2021gc009750.

The response of Arctic Ocean biogeochemistry to subsurface flow driven by permafrost thaw is poorly understood. We present dissolved chloride and water isotopic data from the Chukchi Sea Shelf sediments that reveal the presence of a meteoric subsurface flow enriched in cations with a radiogenic Sr fingerprint. This subsurface fluid is also enriched

in dissolved inorganic carbon and methane that bear isotopic compositions indicative of a carbon reservoir modified by reactions in a closed system. Such fluid characteristics are in stark contrast with those from other sites in the Chukchi Sea where the pore water composition shows no sign of meteoric input, but reflect typical biogeochemical reactions associated with early diagenetic sequences in marine sediment. The most likely source of the observed subsurface flow at the Chukchi Sea Shelf is from the degradation of permafrost that had extended to the shelf region during the Last Glacial Maximum. Our data suggest that the permafrost-driven subsurface flow most likely took place during the 2–3°C warming in the Early Holocene Thermal Maximum. This time scale is supported by numerical simulation of pore water profiles, which indicate that a minimum of several thousand years must have passed since the cessation of the subsurface methane-bearing fluid flow.

keywords: subsurface meteoric fluid discharge; Arctic element; carbon cycle; permafrost; EHTM; Chukchi Sea

1-56 *Environmental Sciences & Ecology*

Record of North American boreal forest fires in northwest Greenland snow

Kang, Jung-Ho., **Hwang, Heejin.**, Lee, Sang-Jin., Choi, Sung-Deuk., Kim, Jin-Soo., **Hong, Sang-Bum.**, **Hur, Soon Do.** and Baek, Je-Hyun.

Chemosphere. 2021. 276.
doi: 10.1016/j.chemosphere.2021.130187.

We present boreal forest fire proxies in a northwest Greenland snowpit spanning a period of six years, from spring 2003 to summer 2009. Levoglucosan ($C_6H_{10}O_5$) is a specific organic molecular marker of biomass burning caused by boreal forest fires. In this study, levoglucosan was determined via liquid chromatography/negative ion electrospray ionization-tandem mass spectrometry, wherein isotope-dilution and multiple reaction monitoring methods are employed. Ammonium (NH_4^+) and oxalate ($C_2O_4^{2-}$), traditional biomass burning proxies, were determined using two-channel ion chromatography. In the northwest Greenland snowpit, peaks in levoglucosan, ammonium, and oxalate were observed in snow layers corresponding to the summer–fall seasons of 2004 and 2005. Considered together, these spikes are a marker for large boreal forest fires. The levoglucosan deposited in the Greenland snow was strongly dependent on long-range atmospheric transportation. A 10-day backward air mass trajectory analysis supports that the major contributors were air masses from North America. In addition, satellite-derived carbon monoxide (CO) and ammonia (NH_3) concentrations suggest that chemicals from North American boreal forest fires during the summer–fall of 2004 and 2005 were transported to Greenland. However, large boreal fires in Siberia in 2003 and 2008 were not recorded in the snowpit. The sub-annual resolution measurements of levoglucosan and ammonium can distinguish between the contributions of past boreal forest fires and soil emissions from anthropogenic activity to Greenland snow and ice.

keywords: Levoglucosan; Ammonium; Oxalate; Boreal forest fire; Greenland snow

1-57 *Chemistry; Geochemistry & Geophysics*

Reductive Adsorption of Atmospheric Oxidized Mercury on Ice: Insights from Density Functional Calculations

Yi, Yoo Soo., **Han, Yeongcheol.** and **Hur, Soon Do.**

Acs Earth and Space Chemistry. 2021. 5(11): 3170-3181.
doi: 10.1021/acsearthspacechem.1c00269.

The fate of atmospheric mercury (Hg) has been intensively investigated due to concerns about its global dispersion. The reduction of reactive oxidized Hg (Hg^{II}) to the stable form (Hg^0) is a significant process, in that it extends the mean atmospheric lifetime of Hg and allows for its long-range transport. While the reduction mechanisms of Hg^{II} in aqueous, particulate, and gas phases have drawn much attention, the reaction pathway and mechanism of Hg^{II} reduction in icy environments are still elusive, despite that ice particles have been expected to play an active role, from field and laboratory observations. With density functional theory calculations, we reveal the adsorptive and dissociative pathways of Hg^{II} on ice, including the catalytic role of the ice surface that facilitates the dissociative adsorption of Hg dihalides. Because ice is the most common phase of water in the upper atmosphere and cryosphere, its influence on Hg speciation can have profound implications on the global Hg cycle.

keywords: polar mercury cycle; Hg adsorption; ice surface; Hg reduction; dissociative adsorption

1-58 *Environmental Sciences & Ecology; Meteorology & Atmospheric Sciences*

Relationship between cloud condensation nuclei (CCN) concentration and aerosol optical depth in the Arctic region

Ahn, Seohee., **Yoon, Young Jun.**, **Choi, Taejin.**, Lee, J. Y., Kim, Y. P., **Lee, Bang Yong.** and 6 others.

Atmospheric Environment. 2021. 267.
doi: 10.1016/j.atmosenv.2021.118748.

To determine the direct and indirect effects of aerosols on climate, it is important to know the spatial and temporal variations in cloud condensation nuclei (CCN) concentrations. Although many types of CCN measurements are available, extensive CCN measurements are challenging because of the complexity and high operating cost, especially in remote areas. As aerosol optical depth (AOD) can be readily observed by remote sensing, many attempts have been made to estimate CCN concentrations from AOD. In this study, the CCN–AOD relationship is parameterized based on CCN ground measurements from the Zeppelin Observatory (78.91° N, 11.89° E, 474 m asl) in the Arctic region. The AOD measurements were obtained from the Ny-Ålesund site (78.923° N, 11.928° E) and Modern-Era Retrospective Analysis for Research and Applications, Version 2 reanalysis. Our results show a CCN-AOD correlation with a coefficient of determination R^2 of 0.59. Three additional estimation models for CCN were presented based on the following data: (i) in situ aerosol chemical composition, (ii) in situ aerosol optical properties, and (iii) chemical composition of AOD obtained from reanalysis data. The results from the model using in situ aerosol optical properties reproduced the observed CCN concentration most efficiently, suggesting that the contribution of BC to CCN concentration should be considered along with that of sulfate.

keywords: Arctic region; Cloud condensation nuclei; Aerosol optical depth; CCN-AOD relationship; Black carbon

1-59

The Relationship between the Arctic Oscillation and Heatwaves on the Korean Peninsula

Kim, Jeong-Hun. and 2 others.

THE KOREAN JOURNAL OF QUATERNARY RESEARCH. 2021. 33(1-2): 25-35.

In this study, we identified characteristics of heatwaves on the Korean Peninsula and related atmospheric circulation patterns using data on the daily maximum temperature (TMX) and reanalysis data for the past 42 years (1979–2020) and analyzed their connection to the Arctic oscillation (AO). The heatwave on the Korean Peninsula showed to be stronger and more frequent in the 2000s. The recent strong and frequent heatwaves on the Korean Peninsula are mainly affected by abnormal high-pressure over the Korean Peninsula on the middle/upper-level atmosphere and the strengthening of the North Pacific high pressure. Interestingly, composite difference of sea level pressure showed very similar results to the positive AO pattern. The correlation coefficients between the summertime AO and the TMX and HWD of the Korean Peninsula were 0.407 and 0.437, respectively, which showed a statistical significance in 1%, and showed a clear relationship with the abnormal high-pressure over the Korean Peninsula and the strengthening of the North Pacific high pressure. In addition, in the positive AO phase, the TMX and HWD of the Korean peninsula were approximately 30.1 °C and 14.6 days, which were about 1.2 °C and 8.8 days higher than in the negative AO phase, respectively. As a result of the 15-year moving average correlation analysis, the relationship between the heatwave and AO on the Korean Peninsula has increased significantly since 2003, and the linear relationship between them has become more apparent. Moreover, after the 2000s, when the relationship developed, AO had more strongly induced the atmospheric circulation pattern to be more favorable to the occurrence of heatwaves in the Korean Peninsula. This study implies that understanding the AO, which is the large-scale variability in the Northern Hemisphere, and the Arctic-mid latitude teleconnection, can improve the performance of global climate models and help predict the seasonality of the summer heatwave on the Korean Peninsula

keywords: Arctic oscillation; Heatwaves; Arctic-Mid latitude interaction; Teleconnection

1-60 *Physical Geography; Remote Sensing*

Retrieval of daily sea ice thickness from AMSR2 passive microwave data using ensemble convolutional neural networks

Chi, Junhwa. and **Kim, Hyun-Cheol.**

Giscience & Remote Sensing. 2021. 58(6): 812-830.
doi: 10.1080/15481603.2021.1943213.

Recently, measurement of sea ice thickness (SIT) has received increasing attention due to the importance of thinning ice in the context of global warming. Although altimeter sensors onboard satellite missions enable continuous SIT measurements over larger areas compared to in situ observations, these sensors are inadequate for mapping daily Arctic SIT because of their small footprints. We exploited passive microwave data from AMSR2 (Advanced Microwave Scanning Radiometer 2) by incorporating a state-of-the-art deep learning (DL) approach to address this limitation. Passive microwave data offer better temporal resolutions than those from a single altimeter sensors, but are rarely used for SIT estimations due to their limited physical relationship with SIT. In this study, we proposed an ensemble DL model with different modalities to produce daily pan-Arctic SIT retrievals. The proposed model determined the hidden and unknown relationships between the brightness temperatures of AMSR2 channels and SITs measured by CryoSat-2 (CS2) from the extended input features defined by our feature augmentation strategy. Although AMSR2-based SITs agreed well with CS2-derived gridded SIT values, they had similar uncertainties and errors in the CS2 SIT measurements, particularly for thin ice. However, based on quantitative validations using long-term unseen data and IceBridge data, the proposed retrieval model consistently generated SITs from AMSR2 at 25 km spatial resolution, regardless of time and space.

keywords: AMSR2; Arctic sea ice; convolutional neural network; deep learning; passive microwave; sea ice thickness

---

1-61 *Environmental Sciences & Ecology; Geology; Remote Sensing; Imaging Science & Photographic Technology*

Retrieval of Summer Sea Ice Concentration in the Pacific Arctic Ocean from AMSR2 Observations and Numerical Weather Data Using Random Forest Regression

Han, Hyangsun., **Lee, Sungjae.**, **Kim, Hyun-Cheol.** and Kim, Miae.

Remote Sensing. 2021. 13(12).

doi: 10.3390/rs13122283.

The Arctic sea ice concentration (SIC) in summer is a key indicator of global climate change and important information for the development of a more economically valuable Northern Sea Route. Passive microwave (PM) sensors have provided information on the SIC since the 1970s by observing the brightness temperature (T_B) of sea ice and open water. However, the SIC in the Arctic estimated by operational algorithms for PM observations is very inaccurate in summer because the T_B values of sea ice and open water become similar due to atmospheric effects. In this study, we developed a summer SIC retrieval model for the Pacific Arctic Ocean using Advanced Microwave Scanning Radiometer 2 (AMSR2) observations and European Reanalysis Agency-5 (ERA-5) reanalysis fields based on Random Forest (RF) regression. SIC values computed from the ice/water maps generated from the Korean Multi-purpose Satellite-5 synthetic aperture radar images from July to September in 2015–2017 were used as a reference dataset. A total of 24 features including the T_B values of AMSR2 channels, the ratios of T_B values (the polarization ratio and the spectral gradient ratio (*GR*)), total columnar water vapor (TCWV), wind speed, air temperature at 2 m and 925 hPa, and the 30-day average of the air temperatures from the ERA-5 were used as the input variables for the RF model. The RF model showed greatly superior performance in retrieving summer SIC values in the Pacific Arctic Ocean to the Bootstrap (BT) and Arctic Radiation and Turbulence Interaction STudy (ARTIST) Sea Ice (ASI) algorithms under various atmospheric conditions. The root mean square error (RMSE) of the RF SIC values was 7.89% compared to the reference SIC values. The BT and ASI SIC values had three times greater values of RMSE (20.19% and 21.39%, respectively) than the RF SIC values. The air temperatures at 2 m and 925 hPa and their 30-day averages, which indicate the ice surface melting conditions, as well as the *GR* using the vertically polarized channels at 23 GHz and 18 GHz (*GR*(23V18V)), TCWV, and *GR*(36V18V), which accounts for atmospheric water content, were identified as the variables that contributed greatly to the RF model. These important variables allowed the RF model to retrieve unbiased and accurate SIC values by taking into account the changes in T_B values of sea ice and open water caused by atmospheric effects.

keywords: summer sea ice concentration; Pacific Arctic Ocean; AMSR2; ERA-5; Random Forest regression

1-62

Review on the impact of Arctic Amplification on winter cold surges over east Asia

Kim, Seong-Joong., **Kim, Jeong-Hun.**, **Jun, Sang-Yoon.**, Kim, Maeng-Ki. and **Lee, Solji.**

THE KOREAN JOURNAL OF QUATERNARY RESEARCH. 33(1-2): 1-23.

In response to the increase in atmospheric carbon dioxide and greenhouse gases, the global mean temperature is rising rapidly. In particular, the warming of the Arctic is two to three times faster than the rest. Associated with the rapid Arctic warming, the sea ice shows decreasing trends in all seasons. The faster Arctic warming is due to ice-albedo feedback by the presence of snow and ice in polar regions, which have higher reflectivity than the ocean, the bare land, or vegetation, higher long-wave heat loss to space than lower latitudes by lower surface temperature in the Arctic than lower latitudes, different stability of atmosphere between the Arctic and lower latitudes, where low stability leads to larger heat losses to atmosphere from surface by larger latent heat fluxes than the Arctic, where high stability, especially in winter, prohibits losing heat to atmosphere, increase in clouds and water vapor in the Arctic atmosphere that subsequently act as green house gases, and finally due to the increase in sensible heat fluxes from low latitudes to the Arctic via lower troposphere. In contrast to the rapid Arctic warming, in midlatitudes, especially in eastern Asia and eastern North America, cold air outbreaks occur more frequently and last longer in recent decades. Two pathways have been suggested to link the Arctic warming to cold air outbreaks over midlatitudes. The first is through troposphere in synoptic-scales by enhancing the Siberian high via a development of Rossby wave trains initiated from the Arctic, especially the Barents-Kara Seas. The second is via stratosphere by activating planetary waves to stratosphere and beyond, that leads to warming in the Arctic stratosphere and increase in geopotential height that subsequently weakens the polar vortex and results in cold air outbreaks in midlatitudes for several months. There exists lags between the Arctic warming and cold events in midlatitudes. Thus, understanding chain reactions from the Arctic warming to midlatitude cooling could help improve a predictability of seasonal winter weather in midlatitudes. This study reviews the results on the Arctic warming and its connection to midlatitudes and examines the trends in surface temperature and the Arctic sea ice.

keywords: Arctic amplification; midlatitude cold air outbreaks; global warming; Arctic sea ice; surface temperature

1-63 *Meteorology & Atmospheric Sciences*

Role of Cloud Feedback in Continental Warming Response to CO_2 Physiological Forcing

Park, So-Won., Kug, Jong-Seong., **Jun, Sang-Yoon.** and 2 others.

Journal of Climate. 2021. 34(22): 8813-8828.

doi: 10.1175/jcli-d-21-0025.1.

Stomatal closure is a major physiological response to the increasing atmospheric carbon dioxide (CO_2), which can lead to surface warming by regulating surface energy fluxes—a phenomenon known as CO_2 physiological forcing. The magnitude of land surface warming caused by physiological forcing is substantial and varies across models. Here we assess the continental warming response to CO_2 physiological forcing and quantify the resultant climate feedback using carbon–climate simulations from phases 5 and 6 of the Coupled Model Intercomparison Project, with a focus on identifying the cause of intermodel spread. It is demonstrated that the continental (40°–70°N) warming response to the physiological forcing in summer (~0.55 K) is amplified primarily due to cloud feedback (~1.05 K), whereas the other climate feedbacks, ranging from –0.57 to 0.20 K, show relatively minor contributions. In addition, the strength of cloud feedback varies considerably across models, which plays a primary role in leading large diversity of the continental warming response to the physiological forcing.

keywords Atmosphere-land interaction; Feedback; Climate models; Model comparison; Model evaluation/performance

1-64 *Geology*

Role of Intense Arctic Storm in Accelerating Summer Sea Ice Melt: An In Situ Observational Study

Peng, Liran., Zhang, Xiangdong., **Kim, Joo-Hong.**, **Cho, Kyoung-Ho.** and 3 others.

Geophysical Research Letters. 2021. 48(8).
doi: 10.1029/2021gl092714.

Intense storms have been more frequently observed in the Arctic during recent years, in coincidence with extreme sea ice loss events. However, it is still not fully understood how storms drive such events due to deficient observations and modeling discrepancies. Here we address this problem by analyzing in situ observations acquired during an Arctic expedition, which uniquely captured an intense storm in summer 2016. The result shows a pronounced acceleration of sea ice loss during the storm process. Diagnostic analysis indicates a net energy loss at the ice surface, not supporting the accelerated melting. Although the open water surface gained net heat energy, it was insufficient to increase the mixed-layer temperature to the observed values. Dynamic analysis suggests that storm-driven increase in ocean mixing and upward Ekman pumping of the Pacific-origin warm water tremendously increased oceanic heat flux. The thermal advection by the Ekman pumping led to a warmed mixed layer by 0.05°C–0.12°C and, in consequence, an increased basal sea ice melt rate by 0.1–1.7 cm day^{-1}.

keywords: Arctic climate change; storm and cyclone; sea ice; air-ice-sea interaction; energy budgets; Ekman dynamics

1-65 *Environmental Sciences & Ecology; Geology*

Role of polar vortex weakening in cold events in central Asia during late winter

Kim, Seong-Joong. and **Choi, Hye-Sun.**

Polar Science. 2021. 30.
doi: 10.1016/j.polar.2021.100640.

The cause of cold events over central Asia was investigated. Since 1958, surface air temperature (SAT) has gradually increased over central Asia, but SAT has shown very strong multidecadal fluctuations, with cooling dominant in the 1960s–1970s and recent decades but warming dominant in the 1990s. SAT in February in central Asia has decreased by more than 7 °C compared to that in normal years. Analysis indicates that cold events over central Asia are related to the weakening of the polar vortex, which is indicated by the increase in polar cap height (PCH) and weaker zonal-mean zonal winds. The increase in PCH begins in January in the stratosphere and propagates down to the troposphere in February; it is well reflected in the weakening of zonal-mean zonal winds in the stratosphere in January, which extends to the troposphere in February. The January increase in PCH anomaly is associated with surface conditions in the Arctic region, especially the Barents–Kara seas, where sea level pressure increases substantially in January; high pressure then expands to the southeastern (downstream) branch of the Siberian high in February, bringing cold eastern Siberian air to central Asia.

keywords: Central Asia; Late winter; Cold events; Polar vortex; Siberian high

1-66 *Geology*

The Role of the Pacific-Japan Pattern in Extreme Heatwaves Over Korea and Japan

El Noh., Kim, Joowan., **Jun, Sang-Yoon.**, Cha, Dong-Hyun., Park, Myung-Sook., **Kim, Joo-Hong.** and Kim, Hyeong-Gyu.

Geophysical Research Letters. 2021. 48(18).
doi: 10.1029/2021gl093990.

In the Northwestern Pacific, the meridionally propagating Rossby waves, known as the Pacific-Japan (PJ) pattern, is the dominant teleconnection pattern and is considered as a source of heatwaves in East Asia. In this study, the circulation and thermodynamic characteristics of these patterns were investigated based on daily timescale to evaluate their relationship with the likelihood of heatwaves in Korea and Japan. The investigations reveal that stations in Korea and Japan record approximately 90% increase in extremely hot days (T_{max} > 35°C) during the positive PJ pattern events. According to thermodynamic budget, horizontal heat advection is a key factor for the observed near-surface warming during the positive PJ. The circulation pattern during the positive PJ largely explains the enhanced warm advection and physical heating due to the increased insolation and adiabatic heating are secondary factors for near-surface warming. This phenomenon is robustly observed regardless of the definition.

keywords: Pacific-Japan pattern; heatwaves; horizontal temperature advection

1-67 *Environmental Sciences & Ecology; Meteorology & Atmospheric Sciences*

Seasonality and Dynamics of Atmospheric Teleconnection from the Tropical Indian Ocean and the Western Pacific to West Antarctica

Lee, Hyun-Ju. and **Jin, Emilia-Kyung.**

Atmosphere. 2021. 12(7).
doi: 10.3390/atmos12070849.

The global impact of the tropical Indian Ocean and the Western Pacific (IOWP) is expected to increase in the future because this area has been continuously warming due to global warming; however, the impact of the IOWP forcing on West Antarctica has not been clearly revealed. Recently, ice loss in West Antarctica has been accelerated due to the basal melting of ice shelves. This study examines the characteristics and formation mechanisms of the teleconnection between the IOWP and West Antarctica for each season using the Rossby wave theory. To explicitly understand the role of the background flow in the teleconnection process, we conduct linear baroclinic model (LBM) simulations in which the background flow is initialized differently depending on the season. During JJA/SON, the barotropic Rossby wave generated by the IOWP forcing propagates into the Southern Hemisphere through the climatological northerly wind and arrives in West Antarctica; meanwhile, during DJF/MAM, the wave can hardly penetrate the tropical region. This indicates that during the Austral winter and spring, the IOWP forcing and IOWP-region variabilities such as the Indian Ocean Dipole (IOD) and Indian Ocean Basin (IOB) modes should paid more attention to in order to investigate the ice change in West Antarctica.

keywords: tropical-Antarctic teleconnection; barotropic Rossby wave theory; Indian Ocean and Western Pacific forcing; climate of West Antarctica

1-68 *Environmental Sciences & Ecology; Geology*

Seasonality of isotopic and chemical composition of snowpack in the vicinity of Jang Bogo Station, East Antarctica

Hur, Soon Do., **Chung, Jiwoong.**, **Nyamgerel, Yalalt.** and Lee, Jeonghoon.

Polish Polar Research. 2021. 42(4): 221-236.
doi: 10.24425/ppr.2021.137146.

Seasonal variations of the isotopic and chemical compositions of snowpits can provide useful tools for dating the age of the snowpit and examining the sources of aerosol. Based on the seasonal layers with δD and $\delta^{18}O$ maxima and minima, it was determined that the snowpit, conducted in the vicinity of the Jang Bogo Station in Antarctica, contained snow deposited over a three-year period (2008–2010). Distinct seasonal variations of stable water isotopes were observed, with a slope of 8.2 from the linear isotopic relationship between oxygen and hydrogen, which indicates that the snow accumulated during three years without a significant post-depositional process. The positive correlations ($r > 0.85$) between Na^+ and other ions in the winter period and the positive relationship with the concentrations of the methanesulphonic acid (MSA) and non-sea salt sulfate ($nssSO_4^{2-}$) in the warm period ($r = 0.6$, spring to summer) indicate the significant contributions of an oceanic source to the snowpit. Based on principal component analysis, the isotopic and chemical variables were classified into species representing input of sea-salt aerosol and suggesting potential seasonal markers. This study will support further investigations using ice cores in this region.

keywords: Antarctica; Terra Nova Bay; snowpit; water stable isotopes; snow chemistry

1-69 *Environmental Sciences & Ecology; Meteorology & Atmospheric Sciences*

Shallow soils are warmer under trees and tall shrubs across Arctic and Boreal ecosystems

Kropp, Heather., Loranty, Michael M., Natali, Susan M., Kholodov, Alexander L., Rocha, Adrian, V., Myers-Smith, Isla., Abbot, Benjamin W., Abermann, Jakob., Blanc-Betes, Elena., Blok, Daan., Blume-Werry, Gesche., Boike, Julia., Breen, Amy L., Cahoon, Sean M. P., Christiansen, Casper T., Douglas, Thomas A., Epstein, Howard E., Frost, Gerald, V., Goeckede, Mathias., Hoye, Toke T., Mamet, Steven D., O'Donnell, Jonathan A., Olefeldt, David., Phoenix, Gareth K., Salmon, Verity G., Sannel, A. Britta K., Smith, Sharon L., Sonnentag, Oliver., Vaughn, Lydia Smith., Williams, Mathew., Elberling, Bo., Gough, Laura., Hjort, Jan., Lafleur, Peter M., Euskirchen, Eugenie S., Heijmans, Monique M. P. D., Humphreys, Elyn R., Iwata, Hiroki., Jones, Benjamin M., Jorgenson, M. Torre., Gruenberg, Inge., Kim, Yongwon., Laundre, James., Mauritz, Marguerite., Michelsen, Anders., Schaepman-Strub, Gabriela., Tape, Ken D., Ueyama, Masahito., **Lee, Bang Yong.** and 2 others.

Environmental Research Letters. 2021. 16(1).
doi: 10.1088/1748-9326/abc994.

Soils are warming as air temperatures rise across the Arctic and Boreal region concurrent with the expansion of tall-statured shrubs and trees in the tundra. Changes in vegetation structure and function are expected to alter soil thermal regimes, thereby modifying climate feedbacks related to permafrost thaw and carbon cycling. However, current understanding of vegetation impacts on soil temperature is limited to local or regional scales and lacks the generality necessary to predict soil warming and permafrost stability on a pan-Arctic scale. Here we synthesize shallow soil and air temperature observations with broad spatial and temporal coverage collected across 106 sites representing nine different vegetation types in the permafrost region. We showed ecosystems with tall-statured shrubs and trees (>40 cm) have warmer shallow soils than those with short-statured tundra vegetation when normalized to a constant air temperature. In tree and tall shrub vegetation types, cooler temperatures in the warm season do not lead to cooler mean annual soil temperature indicating that ground thermal regimes in the cold-season rather than the warm-season are most critical for predicting soil warming in ecosystems underlain by permafrost. Our results suggest that the expansion of tall shrubs and trees into tundra regions can amplify shallow soil warming, and could increase the potential for increased seasonal thaw depth and increase soil carbon cycling rates and lead to increased carbon dioxide loss and further permafrost thaw.

keywords: Arctic; boreal forest; soil temperature; vegetation change; permafrost

1-70 *Geology*

Snow-Pit Record from a Coastal Antarctic Site and Its Preservation of Meteorological Features

Nyamgerel, Yalalt., **Hong, Sang-Bum.**, **Han, Yeongcheol.**, **Kim, Songyi.**, Lee, Jeonghoon. and **Hur, Soon Do.**

Earth Interactions. 2021. 25(1): 108-118.

doi: 10.1175/ei-d-20-0018.1.

Polar snow pits or ice cores preserve valuable information derived from the atmosphere on past climate and environment changes. A 1.57-m snow-pit record from the coastal site (Styx Glacier) in eastern Antarctica covering the period from January 2011 to January 2015 was discussed and compared with meteorological variables. The dominant contribution of the deposition of sea-salt aerosols due to the proximity of the site to the ocean and processes of sea ice formation was revealed in the ionic concentrations. Consistent seasonal peaks in $\delta^{18}O$, δD, MSA, $nssSO_4^{2-}$, and NO_3^- indicate the strong enhancement of their source during warm periods, whereas the sea-salt ions (Na^+, K^+, Mg^{2+}, Ca^{2+}, Cl^-, and $totSO_4^{2-}$) exhibit a distinct distribution. Monthly mean $\delta^{18}O$ positively correlates with the air temperature record from an automatic weather station (AWS) located in the main wind direction. Despite the shortness of the record, we suspect that the slight depletion of the isotopic composition and lowering of the snow accumulation could be related to the cooler air temperature with the decrease of open sea area. Consistency with previous studies and the positive correlation of sea-salt ions in the snow pit indicate the relatively good preservation of snow layers with noticeable climate and environmental signals [e.g., changes in sea ice extent (SIE) or sea surface temperature]. We report a new snow-pit record, which would be comparative and supportive to understand similar signals preserved in deeper ice cores in this location.

keywords: Antarctica; Sea ice; Snow

1-71 *Environmental Sciences & Ecology; Meteorology & Atmospheric Sciences*

Soil respiration strongly offsets carbon uptake in Alaska and Northwest Canada

Watts, Jennifer D., Natali, Susan M., Minions, Christina., Risk, Dave., Arndt, Kyle., Zona, Donatella., Euskirchen, Eugenie S., Rocha, Adrian, V., Sonnentag, Oliver., Helbig, Manuel., Kalhori, Aram., Oechel, Walt., Ikawa, Hiroki., Ueyama, Masahito., Suzuki, Rikie., Kobayashi, Hideki., Celis, Gerardo., Schuur, Edward A. G., Humphreys, Elyn., Kim, Yongwon., **Lee, Bang Yong.** and 13 others.

Environmental Research Letters. 2021. 16(8).

doi: 10.1088/1748-9326/ac1222.

Soil respiration (i.e. from soils and roots) provides one of the largest global fluxes of carbon dioxide (CO_2) to the atmosphere and is likely to increase with warming, yet the magnitude of soil respiration from rapidly thawing Arctic-boreal regions is not well understood. To address this knowledge gap, we first compiled a new CO_2 flux database for permafrost-affected tundra and boreal ecosystems in Alaska and

Northwest Canada. We then used the CO_2 database, multi-sensor satellite imagery, and random forest models to assess the regional magnitude of soil respiration. The flux database includes a new Soil Respiration Station network of chamber-based fluxes, and fluxes from eddy covariance towers. Our site-level data, spanning September 2016 to August 2017, revealed that the largest soil respiration emissions occurred during the summer (June–August) and that summer fluxes were higher in boreal sites (1.87 ± 0.67 g CO_2–C m^{-2} d^{-1}) relative to tundra (0.94 ± 0.4 g CO_2–C m^{-2} d^{-1}). We also observed considerable emissions (boreal: 0.24 ± 0.2 g CO_2–C m^{-2} d^{-1}; tundra: 0.18 ± 0.16 g CO_2–C m^{-2} d^{-1}) from soils during the winter (November–March) despite frozen surface conditions. Our model estimates indicated an annual region-wide loss from soil respiration of 591 ± 120 Tg CO_2–C during the 2016–2017 period. Summer months contributed to 58% of the regional soil respiration, winter months contributed to 15%, and the shoulder months contributed to 27%. In total, soil respiration offset 54% of annual gross primary productivity (GPP) across the study domain. We also found that in tundra environments, transitional tundra/boreal ecotones, and in landscapes recently affected by fire, soil respiration often exceeded GPP, resulting in a net annual source of CO_2 to the atmosphere. As this region continues to warm, soil respiration may increasingly offset GPP, further amplifying global climate change.

keywords: Arctic; boreal; soil respiration; carbon; CO_2; ecosystem vulnerability; climate change

1-72 *Environmental Sciences & Ecology; Geology; Remote Sensing; Imaging Science & Photographic Technology*

Spatial and Temporal Variability of Minimum Brightness Temperature at the 6.925 GHz Band of AMSR2 for the Arctic and Antarctic Oceans

Kwon, Young-Joo., Hong, Sungwook., **Park, Jeong-Won.**, **Kim, Seung Hee.**, **Kim, Jong-Min.** and **Kim, Hyun-Cheol.**

Remote Sensing. 2021. 13(11).
doi: 10.3390/rs13112122.

The minimum brightness temperature (mBT) of seawater in the polar region is an important parameter in algorithms for determining sea ice concentration or snow depth. To estimate the mBT of seawater at 6.925 GHz for the Arctic and Antarctic Oceans and to find their physical characteristics, we collected brightness temperature and sea ice concentration data from the Advanced Microwave Scanning Radiometer 2 (AMSR2) for eight years from 2012 to 2020. The estimated mBT shows constant annual values, but we found a significant difference in the seasonal variability between the Arctic and Antarctic Oceans. We calculated the mBT with the radiative transfer model parameterized by sea surface temperature (SST), sea surface wind speed (SSW), and integrated water vapor (IWV) and compared them with our observations. The estimated mBT represents the modeled mBT emitted from seawater under conditions of 2–5 m/s SSW and SST below 0 °C, except in the Arctic summer. The exceptional summer mBT in the Arctic Ocean was related to unusually high SST. We found evidence of Arctic amplification in the seasonal variability of Arctic mBT.

keywords: passive microwave; ocean; AMSR2; tie point; Arctic amplification

1-73 *Environmental Sciences & Ecology; Geology; Meteorology & Atmospheric Sciences*

Spatiotemporal Characterization of Mercury Isotope Baselines and Anthropogenic Influences in Lake Sediment Cores

Lee, Ju Hyeon., Kwon, Sae Yun., Yin, Runsheng., Motta, Laura C., Kurz, Aaron Y. and **Nam, Seung-Il.**

Global Biogeochemical Cycles. 2021. 35(10).
doi: 10.1029/2020gb006904.

Increasing mercury isotope ratios from pre-industrial (1510–1850) to present-day (1990–2014) in lake sediment cores have been suggested to be a global phenomenon. To assess factors leading to spatiotemporal changes, we compiled mercury concentration (THg) and mercury isotope ratios in 22 lake sediment cores located at various regions of the world. We find that the positive δ^{202}Hg shifts together with THg increases from pre-industrial to present-day are a widespread phenomenon. This is caused by increased contribution of mercury from local to regional anthropogenic mercury emission sources, which lead to higher sediment δ^{202}Hg (–1.07 ± 0.69 ‰, 1 SD) than pre-industrial sediments (–1.55 ± 0.96 ‰, 1 SD). The positive Δ^{199}Hg shifts were observed in 15 lake sediment cores, which have low pre-industrial

Δ^{199}Hg (–0.20 ± 0.32 ‰) compared to the sediment cores with near-zero to positive pre-industrial Δ^{199}Hg (0.08 ± 0.07 ‰). The magnitudes of δ^{202}Hg (r^2 = 0.09) and Δ^{199}Hg(r^2= 0.20, both $p > 0.05$) changes from pre-industrial to present-day did not correlate with the magnitude of THg changes. Instead, the magnitudes of δ^{202}Hg and Δ^{199}Hg changes decreased with increasing pre-industrial δ^{202}Hg and Δ^{199}Hg values, suggesting that the baseline mercury isotope ratios play a more important role in determining the magnitude of mercury isotope changes compared to the degree of THg input. We suggest that the spatiotemporal assessments of δ^{202}Hg in lake sediment cores can be used as an important proxy for monitoring changes in anthropogenic mercury sources for the Minamata Convention on Mercury.

keywords: Mercury isotope; sediment core; anthropogenic; baseline; Minamata Convention

1-74 *Environmental Sciences & Ecology; Geology; Remote Sensing; Imaging Science & Photographic Technology*

Spectral Characteristics of the Antarctic Vegetation: A Case Study of Barton Peninsula

Chi, Junhwa., **Lee, Hyoungseok.**, **Hong, Soon Gyu.** and **Kim, Hyun-Cheol.**

Remote Sensing. 2021. 13(13).
doi: 10.3390/rs13132470.

Spectral information is a proxy for understanding the characteristics of ground targets without a potentially disruptive contact. A spectral library is a collection of this information and serves as reference data in remote sensing analyses. Although widely used, data of this type for most ground objects in polar regions are notably absent. Remote sensing data are widely used in polar research because they can provide helpful information for difficult-to-access or extensive areas. However, a lack of ground truth hinders remote sensing efforts. Accordingly, a spectral library was developed for 16 common vegetation species and decayed moss in the ice-free areas of Antarctica using a field spectrometer. In particular, the relative importance of shortwave infrared wavelengths in identifying Antarctic vegetation using spectral similarity comparisons was demonstrated. Due to the lack of available remote sensing images of the study area, simulated images were generated using the developed spectral library. Then, these images were used to evaluate the potential performance of the classification and spectral unmixing according to spectral resolution. We believe that the developed library will enhance our understanding of Antarctic vegetation and will assist in the analysis of various remote sensing data.

keywords: Antarctic vegetation; Barton Peninsula; field spectroscopy; King George Island; lichen; moss; spectral characteristics; spectral library

1-75 *Biodiversity & Conservation; Environmental Sciences & Ecology*

Statistical upscaling of ecosystem CO_2 fluxes across the terrestrial tundra and boreal domain: Regional patterns and uncertainties

Virkkala, Anna-Maria., Aalto, Juha., Rogers, Brendan M., Tagesson, Torbern., Treat, Claire C., Natali, Susan M., Watts, Jennifer D., Potter, Stefano., Lehtonen, Aleksi., Mauritz, Marguerite., Schuur, Edward A. G., Kochendorfer, John., Zona, Donatella., Oechel, Walter., Kobayashi, Hideki., Humphreys, Elyn., Goeckede, Mathias., Iwata, Hiroki., Lafleur, Peter M., Euskirchen, Eugenie S., Bokhorst, Stef., Marushchak, Maija., Martikainen, Pertti J., Elberling, Bo., Voigt, Carolina., Biasi, Christina., Sonnentag, Oliver., Parmentier, Frans-Jan W., Ueyama, Masahito., Celis, Gerardo., St.Louis, Vincent L., Emmerton, Craig A., Peichl, Matthias., Chi, Jinshu., Jarveoja, Jarvi., Nilsson, Mats B., Oberbauer, Steven F., Torn, Margaret S., **Park, Sang-Jong.**, Dolman, Han., Mammarella, Ivan., **Chae, Namyi.** and 7 others.

Global Change Biology. 2021. 27(17): 4040-4059.
doi: 10.1111/gcb.15659.

The regional variability in tundra and boreal carbon dioxide (CO_2) fluxes can be high, complicating efforts to quantify sink-source patterns across the entire region. Statistical models are increasingly used to predict (i.e., upscale) CO_2 fluxes across large spatial domains, but the reliability of different modeling techniques, each with different specifications and assumptions, has not been assessed in detail. Here, we compile eddy covariance and chamber measurements of annual and growing season CO_2 fluxes of gross primary productivity (GPP), ecosystem respiration (ER), and net ecosystem exchange (NEE) during 1990–2015 from 148 terrestrial high-latitude (i.e., tundra and boreal) sites to analyze the spatial patterns and drivers of CO_2 fluxes and test the accuracy and uncertainty of

different statistical models. CO_2 fluxes were upscaled at relatively high spatial resolution (1 km²) across the high-latitude region using five commonly used statistical models and their ensemble, that is, the median of all five models, using climatic, vegetation, and soil predictors. We found the performance of machine learning and ensemble predictions to outperform traditional regression methods. We also found the predictive performance of NEE-focused models to be low, relative to models predicting GPP and ER. Our data compilation and ensemble predictions showed that CO_2 sink strength was larger in the boreal biome (observed and predicted average annual NEE −46 and −29 g C m^{-2} yr^{-1}, respectively) compared to tundra (average annual NEE +10 and −2 g C m^{-2} yr^{-1}). This pattern was associated with large spatial variability, reflecting local heterogeneity in soil organic carbon stocks, climate, and vegetation productivity. The terrestrial ecosystem CO_2 budget, estimated using the annual NEE ensemble prediction, suggests the high-latitude region was on average an annual CO_2 sink during 1990–2015, although uncertainty remains high.

keywords: Arctic; CO_2 balance; empirical; greenhouse gas; land; permafrost; remote sensing

1-76 *Environmental Sciences & Ecology; Marine & Freshwater Biology; Microbiology*

Survey of Bacterial Phylogenetic Diversity During the Glacier Melting Season in an Arctic Fjord

Han, Dukki., Richter-Heitmann, Tim., Kim, Il-Nam., **Choy, Eunjung.**, **Park, Ki-Tae.**, Unno, Tatsuya., Kim, Jungman. and **Nam, Seung-Il.**

Microbial Ecology. 2021. 81(3): 579-591.
doi: 10.1007/s00248-020-01616-4.

To understand bacterial biogeography in response to the hydrographic impact of climate change derived from the Arctic glacier melting, we surveyed bacterial diversity and community composition using bacterial 16S rRNA gene metabarcoding in the seawaters of Kongsfjorden, Svalbard, during summer 2016. In the present study, bacterial biogeography in the Kongsfjorden seawaters showed distinct habitat patterns according to water mass classification and habitat transition between Atlantic and fjord surface waters. Moreover, we estimated phylogenetic diversity of bacterial communities using the net relatedness, nearest taxon, and beta nearest taxon indices. We found the influence of freshwater input from glacier melting in shaping bacterial assemblage composition through the stochastic model. We further evaluated bacterial contributions to phytoplankton-derived dimethylsulfoniopropionate (DMSP) using a quantitative PCR (qPCR) measurement with demethylation (*dmdA*) and cleavage (*dddP*) genes of two fundamentally different processes. Our qPCR results imply that bacterial DMSP degradation follows the Atlantic inflow during summer in Kongsfjorden. These findings suggest that the Atlantic inflow and glacial melting influence bacterial community composition and assembly processes and thus affect the degradation of phytoplankton-derived organic matter in an Arctic fjord.

keywords: Arctic glacial fjord; Kongsfjorden; Bacterial biogeography; Stochastic-deterministic balance; SAR11; Phytoplankton-derived organic matter

1-77 *Geochemistry & Geophysics; Meteorology & Atmospheric Sciences*

Temperature tele-connections between the tropical and polar middle atmosphere in the Southern Hemisphere during the 2010 minor sudden stratospheric warming

Eswaraiah, Sunkara., **Lee, Changsup.** and 4 others.

Atmospheric Science Letters. 2021. 22(1).
doi: 10.1002/asl.1010.

Southern Hemispheric (SH) sudden stratospheric warmings (SSWs) are relatively rare compared to their Northern Hemisphere counterparts. No study has so far investigated the impacts of the SH minor SSWs on the tropical atmosphere and connection between the tropical and polar atmospheres. Here, we analyze the MERRA-2 and ERA-interim datasets, and *Microwave Limb Sounder* satellite temperature measurements to investigate the tropical and polar atmosphere tele-connections during the SH minor SSW that occurred in 2010. Our analysis shows the strong anti-correlation between the polar and tropical temperatures during the 2010 minor SSW in the stratosphere and mesosphere. This is the first observational study over the SH that reveals the tele-connection between the tropical and polar middle atmospheres through the

temperature during a minor SSW. We verified this tele-connection, using simulations of the Ground-to-topside model of Atmosphere and Ionosphere for Aeronomy (GAIA) model during the 2010 minor SSW. GAIA model simulations show the temperature anti-correlation between the tropical and polar middle atmosphere and zonal wind variations. The feature of meridional circulation changes was also observed during the SSW period. Hence, the present study strongly suggests that even minor SSW in the SH can affect the meridional circulation in the middle atmosphere via planetary wave activity.

keywords: GAIA simulations; MLS; polar middle atmosphere dynamics; stratosphere-mesosphere temperature; sudden stratospheric warming; tele-connection; tropical middle atmosphere

1-78 *Geochemistry & Geophysics*

Tephrochronology and Provenance of an Early Pleistocene (Calabrian) Tephra From IODP Expedition 374 Site U1524, Ross Sea (Antarctica)

Di Roberto, A., Scateni, B., Di Vincenzo, G., Petrelli, M., Fisauli, G., Barker, S. J., Del Carlo, P., Colleoni, F., Kulhanek, D. K., McKay, R., De Santis, L. and **Kim, Sunghan.**

Geochemistry Geophysics Geosystems. 2021. 22(8).
doi: 10.1029/2021gc009739.

We present a full characterization of a 20 cm-thick tephra layer found intercalated in the marine sediments recovered at Site U1524 during International Ocean Discovery Program (IODP) Expedition 374, in the Ross Sea, Antarctica. Tephra bedforms, mineral paragenesis, and major- and trace-element composition on individual glass shards were investigated and the tephra age was constrained by ^{40}Ar-^{39}Ar on sanidine crystals. The ^{40}Ar-^{39}Ar data indicate that sanidine grains are variably contaminated by excess Ar, with the best age estimate of 1.282 ± 0.012 Ma, based on both single-grain total fusion analyses and step-heating experiments on multi-grain aliquots. The tephra is characterized by a very homogeneous rhyolitic composition and a peculiar mineral assemblage, dominated by sanidine, quartz, and minor aenigmatite and arfvedsonite-riebeckite amphiboles. The tephra from Site U1524 compositionally matches with a ca. 1.3 Ma, rhyolitic pumice fall deposit on the rim of the Chang Peak volcano summit caldera, in the Marie Byrd Land, located ca. 1,300 km from Site U1524. This contribution offers important volcanological data on the eruptive history of Chang Peak volcano and adds a new tephrochronologic marker for the dating, correlation, and synchronization of marine and continental early Pleistocene records of West Antarctica.

keywords: Antarctica; Expedition 374IODP; marine tephra; Ross Sea; tephrochronology

1-79 *Environmental Sciences & Ecology; Physical Geography; Geology*

Topographical effect of the Antarctic Peninsula on a strong wind event

Kwon, Hataek., **Kim, Seong-Joong.** and 2 others.

Antarctic Science. 2021. 33(6): 674-684.
doi: 10.1017/s0954102021000444.

The topographical effect on a strong wind event that occurred on 7 January 2013 at King Sejong Station (KSJ), Antarctica, was investigated using the Polar Weather Research and Forecasting (WRF) model. Numerical experiments applying three different terrain heights of the Antarctic Peninsula (AP) were performed to quantitatively estimate the topographical effect on the selected strong wind event. The experiment employing original AP topography successfully represented the observed features in the strong wind event, both in terms of peak wind speed (by ~94%; ~19.7 m/s) and abrupt transitions of wind speed. In contrast, the experiment with a flattened terrain height significantly underestimated the peak wind speeds (by ~51%; ~10.4 m/s) of the observations. An absence of AP topography failed to simulate both a strong discontinuity of sea-level pressure fields around the east coast of the AP and a strong south-easterly wind over the AP. As a result, the observed downslope windstorm, driven by a flow overriding a barrier, was not formed at the western side of the AP, resulting in no further enhancement of the wind at KSJ. This result demonstrates that the topography of the AP played a critical role in driving the strong wind event at KSJ on 7 January 2013, accounting for ~50% of the total wind speed.

keywords: downslope windstorm; King Sejong Station; polar WRF; topography

1-80 *Environmental Sciences & Ecology; Toxicology*

Trace Level Determination of Saccharides in Pristine Marine Aerosols by Gas Chromatography—Tandem Mass Spectrometry

Choi, Na-Rae., **Yoon, Young Jun.**, **Park, Ki-Tae.** and 4 others.

Toxics. 2021. 9(4).
doi: 10.3390/toxics9040086.

The quantification and identification of saccharides in pristine marine aerosols can provide useful information for determining the contributions of anthropogenic and natural sources of the aerosol. However, individual saccharide compounds in pristine marine aerosols that exist in trace amounts are difficult to analyze due to their low concentrations. Thus, in this study, we applied gas chromatography–tandem mass spectrometry (GC-MS/MS) in multiple reaction monitoring (MRM) mode to analyze the particulate matter with an aerodynamic diameter equal or less than 2.5 μm ($PM_{2.5}$) samples, and the results were compared with those of conventional GC-MS. To investigate the chemical properties of pristine marine aerosols, 12 $PM_{2.5}$ samples were collected while aboard Araon, an ice-breaking research vessel (IBRV), as it sailed from Incheon, South Korea to Antarctica. The method detection limits of GC-MS/MS for 10 saccharides were 2–22-fold lower than those of GC-MS. Consequently, the advantages of GC-MS/MS include (1) more distinct peak separations, enabling the accurate identification of the target saccharides and (2) the quantification of all individual saccharide compounds with concentrations outside the quantifiable range of GC-MS. Accordingly, the time resolution for sampling saccharides in pristine marine aerosols can be improved with GC-MS/MS.

keywords: Antarctica; marine aerosol; gas chromatography; tandem mass spectrometry; saccharides; IBRV Araon

1-81 *Environmental Sciences & Ecology; Geology; Remote Sensing; Imaging Science & Photographic Technology*

Two-Stream Convolutional Long- and Short-Term Memory Model Using Perceptual Loss for Sequence-to-Sequence Arctic Sea Ice Prediction

Chi, Junhwa., **Bae, Jihyun.** and **Kwon, Young-Joo.**

Remote Sensing. 2021. 13(17).
doi: 10.3390/rs13173413.

Arctic sea ice plays a significant role in climate systems, and its prediction is important for coping with global warming. Artificial intelligence (AI) has gained recent attention in various disciplines with the increasing use of big data. In recent years, the use of AI-based sea ice prediction, along with conventional prediction models, has drawn attention. This study proposes a new deep learning (DL)-based Arctic sea ice prediction model with a new perceptual loss function to improve both statistical and visual accuracy. The proposed DL model learned spatiotemporal characteristics of Arctic sea ice for sequence-to-sequence predictions. The convolutional neural network-based perceptual loss function successfully captured unique sea ice patterns, and the widely used loss functions could not use various feature maps. Furthermore, the input variables that are essential to accurately predict Arctic sea ice using various combinations of input variables were identified. The proposed approaches produced statistical outcomes with better accuracy and qualitative agreements with the observed data.

keywords: Arctic sea ice; convolutional neural network; long- and short-term memory; visual geometry group (VGG); loss function; deep learning; future prediction

1-82 *Geology*

Ubiquity of human-induced changes in climate variability

Rodgers, Keith B., Lee, Sun-Seon., Rosenbloom, Nan., Timmermann, Axel., Danabasoglu, Gokhan., Deser, Clara., Edwards, Jim., Kim, Ji-Eun., Simpson, Isla R., Stein, Karl., Stuecker, Malte F., Yamaguchi, Ryohei., Bodai, Tamas., **Chung, Eui-Seok.** and 6 others.

Earth System Dynamics. 2021. 12(4): 1393-1411.
doi: 10.5194/esd-12-1393-2021.

While climate change mitigation targets necessarily concern maximum mean state changes, understanding impacts and developing adaptation strategies will be largely contingent on how climate variability responds to increasing anthropogenic perturbations. Thus far Earth system modeling efforts have primarily focused on projected mean state changes and the sensitivity of specific modes of climate variability, such as the El Niño–Southern Oscillation. However, our knowledge of forced changes in the overall spectrum of climate variability and higher-order statistics is relatively limited. Here we present a new 100-member large

ensemble of climate change projections conducted with the Community Earth System Model version 2 over 1850–2100 to examine the sensitivity of internal climate fluctuations to greenhouse warming. Our unprecedented simulations reveal that changes in variability, considered broadly in terms of probability distribution, amplitude, frequency, phasing, and patterns, are ubiquitous and span a wide range of physical and ecosystem variables across many spatial and temporal scales. Greenhouse warming in the model alters variance spectra of Earth system variables that are characterized by non-Gaussian probability distributions, such as rainfall, primary production, or fire occurrence. Our modeling results have important implications for climate adaptation efforts, resource management, seasonal predictions, and assessing potential stressors for terrestrial and marine ecosystems.

1-83 *Science & Technology*

Unexpected nascent atmospheric emissions of three ozone-depleting hydrochlorofluorocarbons

Vollmer, Martin K., Muhle, Jens., Henne, Stephan., Young, Dickon., Rigby, Matthew., Mitrevski, Blagoj., Park, Sunyoung., Lunder, Chris R., **Rhee, Tae Siek.** and 18 others.

Proceedings of the National Academy of Sciences of the United States of America. 2021. 118(5).

doi: 10.1073/pnas.2010914118.

Global and regional atmospheric measurements and modeling can play key roles in discovering and quantifying unexpected nascent emissions of environmentally important substances. We focus here on three hydrochlorofluorocarbons (HCFCs) that are restricted by the Montreal Protocol because of their roles in stratospheric ozone depletion. Based on measurements of archived air samples and on in situ measurements at stations of the Advanced Global Atmospheric Gases Experiment (AGAGE) network, we report global abundances, trends, and regional enhancements for HCFC-132b ($CH_2ClCClF_2$), which is newly discovered in the atmosphere, and updated results for HCFC-133a (CH_2ClCF_3) and HCFC-31 (CH_2ClF). No purposeful end-use is known for any of these compounds. We find that HCFC-132b appeared in the atmosphere 20 y ago and that its global emissions increased to 1.1 $Gg{\cdot}y^{-1}$ by 2019. Regional top-down emission estimates for East Asia, based on high-frequency measurements for 2016–2019, account for ~95% of the global HCFC-132b emissions and for ~80% of the global HCFC-133a emissions of 2.3 $Gg{\cdot}y^{-1}$ during this period. Global emissions of HCFC-31 for the same period are 0.71 $Gg{\cdot}y^{-1}$. Small European emissions of HCFC-132b and HCFC-133a, found in southeastern France, ceased in early 2017 when a fluorocarbon production facility in that area closed. Although unreported emissive end-uses cannot be ruled out, all three compounds are most likely emitted as intermediate by-products in chemical production pathways. Identification of harmful emissions to the atmosphere at an early stage can guide the effective development of global and regional environmental policy.

keywords: Montreal Protocol; atmospheric composition; ozone depletion

1-84 *Astronomy & Astrophysics*

Wind Variations in the Mesosphere and Lower Thermosphere Near 60°S Latitude During the 2019 Antarctic Sudden Stratospheric Warming

Liu, Guiping., Janches, Diego., Lieberman, Ruth S., Moffat-Griffin, Tracy., Mitchell, Nicholas J., **Kim, Jeong-Han.** and **Lee, Changsup.**

Journal of Geophysical Research-Space Physics. 2021. 126(5).

doi: 10.1029/2020ja028909.

Sudden stratospheric warmings (SSWs) could act as an important mediator in the vertical coupling of atmospheric regions and dramatic variations in the mesosphere and lower thermosphere (MLT) in response to SSWs have been documented. However, due to rare occurrences, SSWs in the Southern Hemisphere (SH) and their impacts on the MLT dynamics are not well understood. This study presents an analysis of MLT winds at ~80–98 km altitudes measured by meteor radars located at Tierra del Fuego (53.7°S, 67.7°W), King Edward Point (54.3°S, 36.5°W) and King Sejong Station (62.2°S, 58.8°W) near 60°S latitude during the Antarctic winter. Eastward zonal winds from these stations are observed to decrease significantly near the peak date of the 2019 Antarctic SSW, and both zonal and meridional winds in 2019 exhibit considerable differences to the mean winds

averaged over other non-SSW years. A quasi 6-day oscillation is observed at all three radar locations, being consistent with the presence of the westward propagating zonal wave-1 planetary wave. The vertical wavelength of this wave is estimated to be~55 km, and the enhancement of the wave amplitude during this SSW is noticeable. Evidence of the interaction between the 6-day wave and the semidiurnal diurnal tide is provided, which suggests a possible mechanism for SSWs to impact the upper atmosphere. This study reports the large-scale variations in winds in the MLT region at SH midlatitudes to high latitudes in a key dynamic but largely unexplored latitudinal band in response to the 2019 Antarctic SSW.

keywords: mesosphere and lower thermosphere; mesospheric wind; planetary wave; planetary wave-tide interaction; tides; upper atmosphere

PART2

Geosciences

2-1 *Geology; Oceanography*

A 100-km wide slump along the upper slope of the Canadian Arctic was likely preconditioned for failure by brackish pore water flushing

Paull, C. K., Dallimore, S. R., Caress, D. W., Gwiazda, R., Lundsten, E., Anderson, K., Melling, H., **Jin, Young Keun.**, Duchesne, M. J., **Kang, Seung-Goo.**, **Kim, Sookwan.** and 3 others.

Marine Geology. 2021. 435.
doi: 10.1016/j.margeo.2021.106453.

Exploration of the continental slope of the Canadian Beaufort Sea has revealed a remarkable coalescence of slide scars with headwalls between 130 and 1100 m water depth (mwd). With increased depth, the scars widen and merge into one gigantic regional slide scar that is more than 100 km wide below ~1100 mwd. To understand the development of these features, five sites were investigated with an Autonomous Underwater Vehicle, which provided 1-m bathymetric grids and Chirp profiles, and surveyed with a Remotely Operated Vehicle. The morphologies are consistent with retrograde failures that occurred on failure planes located between 30 and 75 m below the modern seafloor. At issue is whether the continental slope in this area is preconditioned for failure. While rapid sedimentation during glacial periods, and the presence of shallow gas cannot be ruled out, given the geological environment, it is unclear that they are primary preconditioning factors. Evidence of widespread flushing of the slope with brackish waters, and observed flows of brackish water within slide scars, suggest fluid venting and overpressure may play a role in the development of the extensive slope failures seen along this margin. The impact of pore water salinity changes at the depth of the failure plane on slope stability has not been considered in marine settings previously.

keywords: Submarine slope failures; Continental margin morphology; Cold venting process and products; Arctic Ocean; Autonomous Underwater Vehicles

2-2 *Geology*

Alkalic to tholeiitic magmatism near a mid-ocean ridge: petrogenesis of the KR1 Seamount Trail adjacent to the Australian-Antarctic Ridge

Yi, Sang-Bong., **Lee, Mi Jung.**, **Park, Sung-Hyun.**, Nagao, Keisuke., **Han, Seunghee.**, **Yang, Yun Seok.**, **Choi, Hakkyum.**, **Baek, Jongmin.** and Sumino, Hirochika.

International Geology Review. 2021. 63(10): 1215-1235.
doi: 10.1080/00206814.2020.1756002.

Coexisting alkalic and tholeiitic basalt lavas has been identified in a seamount chain located near the Australian–Antarctic spreading ridge. The KR1 Seamount Trail (KR1 ST) is a series of volcanic seamounts extending to the southeast in the spreading direction of the Australian–Antarctic Ridge (AAR). We herein report Sr, Nd and Pb isotopic compositions and (U–Th)/He and K–Ar geochronology for dredge samples from the KR1 ST in order to evaluate mantle processes and the role of enriched components for alkalic to tholeiitic magma generation in this region. The KR1 ST is a medium-sized seamount chain that extends for ~60 km, has a maximum height of ~1600 m above the seafloor, and consists of alkaline basalts and tholeiites with formation ages of ~0.4 Ma to ≤1.3 Ma. The isotopic characteristics of the alkaline basalts ($^{206}Pb/^{204}Pb$ = 19.52–19.91; $^{87}Sr/^{86}Sr$ = 0.7030–0.7033; $^{143}Nd/^{144}Nd$ = 0.5128–0.5130) from the KR1 ST reflect a dominant 'PREMA (or FOZO)' mantle component represented by radiogenic Pb and mildly enriched Sr and Nd isotopic compositions. On the other hand, the weak PREMA (FOZO)-affinity ($^{206}Pb/^{204}Pb$ = 18.89–18.93; $^{87}Sr/^{86}Sr$ = 0.7028–0.7029; $^{143}Nd/^{144}Nd$ = ~0.5130; $^{3}He/^{4}He$ = 7.64 ± 0.13 (R/R_A)) coupled with their enriched mid-ocean ridge basalt (E-MORB) characteristics of tholeiites from the KR1 ST largely overlap with the KR1 MORB composition. The potential source materials for the alkaline basalts are considered to be ancient, recycled oceanic crust (i.e. eclogite) as well as sub-KR1 depleted MORB mantle (DMM). Whereas the main source materials for the KR1 ST tholeiites are presumed to be the DMM-dominant lithology with minor recycled material. We interpret the KR1 ST as a submarine hotspot chain that was formed by asthenospheric upwelling and spreading processes that delivered fertile blobs of recycled oceanic crust to the sub-KR1 region. The fundamental reason for sub-KR1 upper mantle enrichment might be attributed to a mantle plume event that possibly occurred prior to the formation of the KR1 ST.

keywords: KR1 Seamount Trail; alkaline basalt; tholeiite; PREMA (FOZO); recycled oceanic crust

2-3 *Marine & Freshwater Biology; Oceanography*

Application of Column Chromatography for Accurate Determination of the Carbon Isotopic Compositions of n-alkanes in Diverse Environmental Samples

Lee, Dong-Hun., **Kim, Jung-Hyun.** and Shin, Kyung-Hoon.

Ocean Science Journal. 2021. 56(1): 46-54.
doi: 10.1007/s12601-021-00009-z.

The carbon isotopic compositions ($\delta^{13}C$) of *n*-alkanes in various environmental samples have been previously proposed as suitable fingerprints for assessing the origin of organic matter (OM) in diverse environmental systems. However, with respect to using gas chromatography–combustion–isotope ratio mass spectrometry for the carbon isotopic analysis of *n*-alkanes, analytical uncertainty may often be caused by the co-elution of interfering unsaturated compounds (e.g., aromatic and branched compounds). Hence, we propose a simple but reliable method for purification that uses column chromatography. The performance of two different solid stationary phases (i.e., aluminum oxide and Ag^+-impregnated silica) was compared in terms of their capacity to eliminate unsaturated compounds from total hydrocarbons and thus increase the precision of $\delta^{13}C$ measurements. Compared to the use of an activated aluminum oxide column, elution from an Ag^+-impregnated silica column allows more effective isolation of individual *n*-alkanes, which results in more precise $\delta^{13}C$ measurements for diverse environmental samples. Thus, Ag^+-impregnated silica column separation can be effective as a routine experimental technique for increasing the accuracy of the $\delta^{13}C$ values for *n*-alkanes in OM, which includes a large proportion of unsaturated compounds.

keywords: Ag^+-impregnated silica column; Carbon isotopic composition ($\delta^{13}C$); Gas chromatography–combustion–isotope ratio mass spectrometry (GC–C–IRMS); N-alkanes; Organic matter

2-4 *Geology; Oceanography*

A chronology of post-glacial mass-transport deposits on the Canadian Beaufort Slope

Riedel, M., **Han, Yeongcheol.** and 7 others.

Marine Geology. 2021. 433.
doi: 10.1016/j.margeo.2020.106407.

Extent and chronology of 24 buried and seabed-exposed mass transport deposits (MTDs) on the continental slope of the Canadian Beaufort Sea were compiled towards a regional geo-hazard assessment of the Beaufort region. A total of 2220 lines of 3.5 kHz sub-bottom profiler (SBP) data (~40,000-line kilometres) covering an area of 9740 km² were analyzed to allow a new understanding of slope instability in the region. Several sediment cores acquired across the region allow dating of the sediment cover. A regionally representative seismic-stratigraphy (type section, ca. 60 m thick) of the stratified sediments mantling the slope was defined. The MTDs all occur above a marked change in sedimentation style from a deeper-situated slope fan that varies substantially laterally to the above-lying stratified layers that host the MTDs. The type section comprises three sedimentary units bound by two prominent markers. Relative ages for the MTDs were defined by measuring the thickness of sediments overlying each MTD and linking that sediment package to the type section. Two 3-D seismic data volumes across the study region verified interpretations from 2D data by imaging internal deposit character and down-slope continuity of the MTDs. Seismic amplitude and similarity attributes enabled identification of further MTD events, incompletely imaged by the SBP data. A composite chronostratigraphy based on ^{14}C dating of foraminifera and shells was assembled despite the fact that the type section is far thicker than sediment coring limits. Sub-unit thickness varies up- and down-slope such that a selection of cores across the study region enabled its compilation. The marked change in sedimentation style at the base of the type section required substantial extrapolation to date. Simple (quadratic function) age models project that the base of the type section signals the end of the last glacial maximum (Wisconsinan, or marine isotope stage 2 glaciation) and initiation of pro-glacial plume sedimentation (the deglacial), and finally post-glacial (marine) ultimately from the Mackenzie River. The MTD abundance above this contact defines an average theoretical recurrence rate of one MTD per ~1000 yrs.; however, MTDs are clustered temporally with the highest number of events occurring just prior to the onset of the Younger Dryas at around 13 ka BP (cal.).

keywords: Seismic-stratigraphy; Sediment mass failure; MTD; Sub-bottom profiler; 3-D seismic similarity; Mass failure recurrence rate

2-5 *Environmental Sciences & Ecology*

Distribution of Rare Earth Elements and Their Applications as Tracers for Groundwater Geochemistry - A Review

Hwang, HeeJin. and 2 others.

The Journal of The Korean Earth Science Society. 2021. 42(4): 383-389.
doi: 10.5467/JKESS.2021.42.4.383.

Several studies investigating the behavior and environmental distribution of rare earth elements (REEs) have been reviewed to determine the geochemical processes that may affect their concentrations and fractionation patterns in groundwater and whether these elements can be used as tracers for groundwater-rock interactions and groundwater flow paths in small catchments. Inductively coupled plasma-mass spectrometry (ICP-MS), equipped with an ultrasonic nebulizer and active-film multiplier detector, is routinely used as an analytical technique to measure REEs in groundwater, facilitating the analysis of dissolved REE geochemistry. This review focuses on the distribution of REEs in groundwater and their application as tracers for groundwater geochemistry. Our review of existing literature suggests that REEs in ice cores can be used as effective tracers for atmospheric particles, aiding the identification of source regions.

keywords: rare earth element; groundwater-rock interaction; groundwater flow paths; ice core study

2-6 *Geochemistry & Geophysics*

An effect of variations in relative sensitivity factors on Al-Mg systematics of Ca-Al-rich inclusions in meteorites with secondary ion mass spectrometry

Kawasaki, Noriyuki., **Park, Changkun.**, Wakaki, Shigeyuki., **Kim, Hwayoung.**, **Park, Sunyoung.** and 5 others.

Geochemical Journal. 2021. 55(4): 283-287.
doi: 10.2343/geochemj.2.0634.

Instrumental mass fractionation of Mg-isotopes and the relative sensitivity factor (RSF) for $^{27}Al/^{24}Mg$ratios for *in situ* analysis by secondary ion mass spectrometry were investigated for minerals in Ca-Al-rich inclusions (CAIs) of meteorites, to verify systematic errors in Al-Mg chronological systematics of CAIs. We synthesized seventeen glasses with different chemical compositions that imitate those for CAI minerals and measured their Al-Mg isotopic compositions. In particular, the variation range of RSFs for six melilite glasses almost covering chemical compositions of CAI melilite is 2.0 ± 0.3%, indicating that systematic error for $^{27}Al/^{24}Mg$ for melilite is less than 2.0 ± 0.3% and likely corresponds to that of an ^{26}Al-^{26}Mg relative age of ~0.01 Myr for melilite-rich CAIs. Our data strongly support the robustness of variations in initial $^{26}Al/^{27}Al$ ratios among CAIs, corresponding to a formation age spread of ~0.4 Myr at the very beginning of the Solar System formation.

keywords: Ca-Al-rich inclusions; Al-Mg systematics; secondary ion mass spectrometry; instrumental mass fractionation; relative sensitivity factor

2-7 *Science & Technology*

Enduring evolutionary embellishment of cloudinids in the Cambrian

Park, Tae-Yoon S., **Jung, Jikhan.**, **Lee, Mirinae**. and 5 others.

Royal Society Open Science. 2021. 8(12).
doi: 10.1098/rsos.210829.

The Ediacaran–Cambrian transition and the following Cambrian Explosion are among the most fundamental events in the evolutionary history of animals. Understanding these events is enhanced when phylogenetic linkages can be established among animal fossils across this interval and their trait evolution monitored. Doing this is challenging because the fossil record of animal lineages that span this transition is sparse, preserved morphologies generally simple and lifestyles in the Ediacaran and Cambrian commonly quite different. Here, we identify derived characters linking some members of an enigmatic animal group, the cloudinids, which first appeared in the Late Ediacaran, to animals with cnidarian affinity from the Cambrian Series 2 and the Miaolingian. Accordingly, we present the first case of an animal lineage represented in the Ediacaran that endured and diversified successfully throughout the Cambrian Explosion by embellishing its overall robustness and structural complexity. Among other features, dichotomous branching, present in some early cloudinids, compares closely with a cnidarian asexual reproduction mode. Tracking this morphological change from Late Ediacaran to the Miaolingian provides a unique glimpse into how a primeval animal group responded during the Cambrian Explosion.

keywords: Cloudina; Cambrian Explosion; cnidarians

2-8 *Geochemistry & Geophysics*

Evolution of Microstructural Properties in Sheared Iron-Rich Olivine

Qi, Chao., Zhao, Yong-Hong., Zimmerman, Mark E., **Kim, Daeyeong.** and Kohlstedt, David L.

Journal of Geophysical Research-Solid Earth. 2021. 126(3).
doi: 10.1029/2020jb019629.

Iron-rich olivine is mechanically weaker than olivine of mantle composition, ca. Fo_{90}, and thus is more amenable to study under a wide range of laboratory conditions. To investigate the effects of iron content on deformation-produced crystallographic preferred orientation (CPO) and grain size, we analyzed the microstructures of olivine samples with compositions of Fo_{70}, Fo_{50}, and Fo_0 that were deformed in torsion under either anhydrous or hydrous conditions at 300 MPa. Electron backscatter diffraction (EBSD) observations reveal a transition in CPO from D-type fabric, induced by dislocation glide on both the (010)[100] and the (001)[100] slip systems, at low strains, to A-type fabric, caused by dislocation glide on the (010)[100] slip system, at high strains for all of our samples, independent of iron content and hydrous/anhydrous conditions. A similar evolution of fabric with increasing strain is also reported to occur for Fo_{90}. Radial seismic anisotropy increases with increasing strain, reaching a maximum value of ~1.15 at a shear strain of ~3.5 for each sample, demonstrating that the seismic anisotropy of naturally deformed olivine-rich rocks can be well approximated by that of iron-rich olivine. Based on EBSD observations, we derived a piezometer for which recrystallized grain size decreases inversely with stress to the similar to ~1.2 power. Also, recrystallized grain size increases with increasing iron content. Our experimental results contribute to understanding the microstructural evolution in the mantle of not only Earth but also Mars, where the iron content in olivine is higher.

keywords: crystallographic preferred orientation; grain size; olivine; piezometer

2-9

Exploration of the Gas Hydrates on the Southwestern Continental Slope of the Chukchi Plateau in the Arctic Ocean

Kang, Seung-Goo., Jang, Ugeun., **Kim, Sook-wan.**, **Choi, Yeonjin.**, Kim, Young Gyun., **Hong, Jong Kuk.** and **Jin, Young Keun.**

Journal of the Korean Society of Mineral and Energy Resources Engineers. 2021. 58(5): 418-432.
doi: 10.32390/ksmer.2021.58.5.418.

A single-channel sparker seismic survey was conducted to investigate the distribution of gas hydrates around a sea mound cluster on the southwestern slope of the Chukchi Plateau, where the gas hydrates were first recovered by gravity coring in 2016. Reflections with reversed polarity were discovered on the continental slope of the acquired seismic sections. The depths of the lower bound of the gas hydrate stability zone calculated from the heat flow data and the water temperature at the seafloor were used to confirm that these reflections were gas hydrate related bottom simulating reflections (BSRs). This implies that the regional distribution of gas hydrates in the southwestern continental slope of the Chukchi Plateau is being reported for the first time based on geophysical data. The proposed distribution map of the BSRs related to the gas hydrates is expected to be used as significant information for future gas hydrate surveys in the Chukchi Sea.

keywords: Arctic Ocean; bottom simulating reflection; gas hydrates; gas hydrate stability zone; single-channel sparker seismic survey

2-10 *Geology; Paleontology*

The first orthopteran fossils from the Lower Cretaceous (Albian) Jinju Formation of Korea: Ethological implications for elcanids

Kim, Do-Yoon., **Lee, Mirinae.**, Nam, Gi-Soo. and **Park, Tae-Yoon S.**

Cretaceous Research. 2021. 125.
doi: 10.1016/j.cretres.2021.104843.

The lower Albian Jinju Formation has produced various fossils of invertebrates. Of them, insect fossils have remained understudied, and especially, orthopteran fossils have never been described from the Jinju Formation. Here we report a new species of the Elcanidae (Orthoptera: Elcanoidea), *Panorpidium spica* sp. nov. based on three specimens from the Jinju Formation. Notably, we have applied Wavelength Dispersive Spectrometer (WDS) analysis for the first time on insect fossils, and discovered that the carbon elemental maps are helpful in recognizing crucial morphology. The presence of pterostigmata in forewing supports that elcanids evolved a unique flight mechanism distinct from other extant orthopterans. Based on a detailed morphological comparison with the paddles of the extant tridactylids, it is inferred that the leaf-shaped spurs on the metatibiae of elcanids were used for jumping on the water, although other possible functions cannot be ruled out. Diving into the water and jumping on the water surface must have been an effective way of escaping from predators, both for the flightless nymphs and the short-range flying adults.

keywords: Jinju Formation; Elcanidae; WDS analysis; Pterostigma; Spur; Tridactyloidea

2-11 *Geochemistry & Geophysics; Mineralogy; Mining & Mineral Processing*

Geochemistry and Geochronology of Early Paleozoic Intrusive Rocks in the Terra Nova Bay Area, Northern Victoria Land, Antarctica

Kim, Daeyeong., **Yi, Sang-Bong.**, Kim, Hyeoncheol., **Kim, Taehwan.**, Kim, Taehoon. and **Lee, Jong Ik.**

Minerals. 2021. 11(7).
doi: 10.3390/min11070787.

The Terra Nova Intrusive Complex (TNIC) in northern Victoria Land, Antarctica, results from widespread magmatism during the Early Paleozoic Ross Orogeny. According to field relationships, geochemistry, and geochronology data, the northern part of the TNIC comprises the Browning Intrusive Unit (BIU), which is associated with an arc crustal melting including migmatization of the Wilson Metamorphic Complex, and the later Campbell Intrusive Unit (CIU), which is attributed to the mantle and crustal melting processes. Zircon U-Pb ages suggest Late Neoproterozoic to Early Cambrian protolith with Late Cambrian metamorphism (502 ± 15 Ma) in the WMC, Late Cambrian formation (~500 Ma) of the BIU, and Early Ordovician formation

(~480–470 Ma) of the CIU. Sr-Nd isotopic characteristics of the BIU indicate predominant crustal component ($\varepsilon Nd_{(t)}$ = –8.7 to –8.9), whereas those of the CIU reflect both mantle ($\varepsilon Nd_{(t)}$ = 1.8 to 1.6) and crustal ($\varepsilon Nd_{(t)}$ = –4.0 to –7.5) compositions. These results suggest that the northern TNIC magmatism occurring at ~500–470 Ma originated from partial melting of the mantle–mafic crust components and mixing with felsic crust components. By integrating the results with previous studies, the TNIC is considered to be formed by a combination of the mantle and mafic crust melting, crustal assimilation, felsic crust melting, and magma mixing during the Ross Orogeny.

keywords: Ross Orogeny; Terra Nova Intrusive Complex (TNIC); northern Victoria Land (NVL); zircon U-Pb age; Sr-Nd isotopes

2-12 *Environmental Sciences & Ecology; Geology; Remote Sensing; Imaging Science & Photographic Technology*

Geomorphological and Spatial Characteristics of Underwater Volcanoes in the Easternmost Australian-Antarctic Ridge

Choi, Hakkyum., Kim, Seung-Sep., **Park, Sung-Hyun.** and **Kim, Hyoung Jun.**

Remote Sensing. 2021. 13(5).
doi: 10.3390/rs13050997.

Underwater volcanoes and their linear distribution on the flanks of mid-ocean ridges are common submarine topographic structures at intermediate- and fast-spreading systems, where sufficient melt supplies are often available. Such magma sources beneath the seafloor located within a few kilometers of the corresponding ridge-axis tend to concentrate toward the axis during the upwelling process and contribute to seafloor formation. As a result, seamounts on the flanks of the ridge axis are formed at a distance from the spreading axis and distributed asymmetrically about the axis. In this study, we examined three linearly aligned seamount chains on the flanks of the KR1 ridge, which is the easternmost and longest Australian-Antarctic Ridge (AAR) segment. The AAR is an intermediate-spreading rate system located between the Southeast Indian Ridge and Macquarie Triple Junction of the Australian-Antarctic-Pacific plates. By inspecting the high-resolution shipboard multi-beam bathymetric data newly acquired in the study area, we detected 20 individual seamounts. The volcanic lineament runs parallel to the spreading direction of the KR1 segment. The geomorphologic parameters of height, basal area, volume, and summit types of the identified seamounts were individually measured. We also investigated the spatial distribution of the seamounts along the KR1 segment, which exhibits large variations in axial morphology with depth along the ridge axis. Based on the geomorphology and spatial distribution, all the KR1 seamounts can be divided into two groups: the subset seamounts of volcanic chains distributed along the KR1 segment characterized by high elevation and large volume, and the small seamounts distributed mostly on the western KR1. The differences in the volumetric magnitude of volcanic eruptions on the seafloor and the distance from the given axis between these two groups indicate the presence of magma sources with different origins.

keywords: Australian-Antarctic Ridge; seamounts; underwater volcanism; multi-beam bathymetry; geomorphology

2-13 *Environmental Sciences & Ecology; Geology*

Gravity observations at Jang Bogo Station, Antarctica, and scale factor calibrations of different relative gravimeters

Fukuda, Yoichi., Okuno, Jun'ichi., Doi, Koichiro. and **Lee, Choon-Ki.**

Polar Science. 2021. 29.
doi: 10.1016/j.polar.2021.100702.

We conducted gravity observations in Antarctica at Jang Bogo Station (JBS) during the 2019 –2020 Austral summer season using an FG5-210 absolute gravimeter (AG) and a LaCoste & Romberg (LCR) Model D-58 relative gravimeter. Absolute gravity measurements were successfully made at reference gravity point JBSAG1 and newly established gravity point JBSAG2, yielding about 19,000 and 14,400 drops of data, respectively, with measurement precisions better than 0.4 μGal (1 μGal = 10^{-8} m s^{-2}). In addition, relative gravity measurements were conducted at 10 other newly established gravity points, with accuracies better than 10 μGal, to supplement the absolute gravity data. Superconducting gravimeter (SG) observation with an iGrav-021 instrument has been underway at JBS since 2016. Since an SG is a relative gravimeter, the

calibration of the scale factor is essential for long-term gravity monitoring. In addition, the D-58 instrument was required for scale factor calibration. To calibrate the scale factors of these gravimeters, we first estimated a value for the iGrav-021 using parallel observations with the FG5-210 instrument. The D-58 scale factor was then estimated indirectly from parallel observations with the iGrav-021. These calibrations should ensure accurate gravity monitoring in future work.

keywords: Gravity monitoring; Absolute gravimeter measurement; Superconducting gravimeter; Scale factor calibration; LaCoste D gravimeter

2-14 *Engineering*

Ground Penetrating Radar Imaging of a Circular Patterned Ground near King Sejong Station, Antarctica

Kim, Kwansoo., **Hyeontae, Ju.**, **Lee, Joohan.**, **Chung, Changhyun.**, **Kim, Hyoung-kwon.** and 2 others.

The journal of Engineering Geology. 2021. 31(3): 257-267.
doi: 10.9720/kseg.2021.3.257.

Constraints on the structure and composition of the active layer are important for understanding permafrost evolution. Soil convection owing to repeated moisture-induced freeze-thaw cycles within the active layer promotes the formation of self-organized patterned ground. Here we present the results of ground penetrating radar (GPR) surveys across a selected sorted circle near King Sejong Station, Antarctica, to better delineate the active layer and its relation to the observed patterned ground structure. We acquire GPR data in both bistatic mode (common mid-points) for precise velocity constraints and monostatic mode (common-offset) for subsurface imaging. Reflections are derived from the active layer-permafrost boundary, organic layer-weathered soil boundary within the active layer, and frozen rock-fracture-filled ice boundary within the permafrost. The base of the imaged sorted circle possesses a convex-down shape in the central silty zone, which is typical for the pattern associated with convection-like soil motion within the active layer. The boundary between the central fine-silty domain and coarse-grained stone border is effectively identified in a radar amplitude contour at the assumed active layer depth, and is further examined in the frequency spectra of the near- and far-offset traces. The far-offset traces and the traces from the lower frequency components dominant on the far-offset traces would be associated with rapid absorption of higher frequency radiowave due to the voids in gravel-rich zone. The presented correlation strategies for analyzing very shallow, thin-layered GPR reflection data can potentially be applied to the various types of patterned ground, particularly for acquiring time-lapse imaging, when electric resistivity tomography is incorporated into the analysis.

keywords: patterned ground; active layer; ground penetrating radar (GPR); common mid-point (CMP); frequency spectrum; King Sejong Station

2-15 *Geology*

Imaging the P-Wave Velocity Structure of Arctic Subsea Permafrost Using Laplace-Domain Full-Waveform Inversion

Kang, Seung-Goo., **Jin, Young Keun.**, Jang, Ugeun., Duchesne, Mathieu J., Shin, Changsoo., **Kim, Sookwan.**, Riedel, Michael., Dallimore, Scott R., Paull, Charles K., **Choi, Yeonjin.** and **Hong, Jong Kuk.**

Journal of Geophysical Research-Earth Surface. 2021. 126(3).
doi: 10.1029/2020jf005941.

Climate change in the Arctic has recently become a major scientific issue, and detailed information on the degradation of subsea permafrost on continental shelves in the Arctic is critical for understanding the major cause and effects of global warming, especially the release of greenhouse gases. The subsea permafrost at shallow depths beneath the Arctic continental shelves has significantly higher P-wave velocities than the surrounding sediments. The distribution of subsea permafrost on Arctic continental shelves has been studied since the 1970s using seismic refraction methods. With seismic refraction data, the seismic velocity and the depth of the upper boundary of subsea permafrost can be determined. However, it is difficult to identify the lower boundary and the internal shape of permafrost. Here, we present two-dimensional P-wave velocity models of the continental shelf in the Beaufort Sea by applying the Laplace-domain full-waveform inversion method to acquired multichannel seismic reflection data. With the inverted P-wave velocity model, we identify anomalous high seismic velocities that originated from the subsea

permafrost. Information on the two-dimensional distribution of subsea permafrost on the Arctic continental shelf area, including the upper and lower bounds of subsea permafrost, are presented. Also, the two-dimensional P-wave velocity model allows us to estimate the thawing pattern and the shape of subsea permafrost structures. Our proposed P-wave velocity models were verified by comparison with the previous distribution map of subsea permafrost from seismic refraction analyses, geothermal modeling, and well-log data.

keywords: continental shelf of the Canadian Beaufort Sea; laplace domain full-waveform inversion; lower boundaries of permafrost; spatial distribution; subsea permafrost

2-16 *Environmental Sciences & Ecology*

The impact of the abnormal salinity enrichment in pore water on the thermodynamic stability of marine natural gas hydrates in the Arctic region

Choi, Wonjung., Lee, Joonseop., Kim, Young-Gyun., Kim, Hanwoong., **Rhee, Tae Siek.**, **Jin, Young Keun.** and 2 others.

Science of the Total Environment. 2021. 799.
doi: 10.1016/j.scitotenv.2021.149357.

In this study, the thermodynamic and structural characteristics of natural gas hydrates (NGHs) retrieved from gas hydrate mounds (ARAON Mound 03 (AM03) and ARAON Mound 06 (AM06)) in the Chukchi Sea in the Arctic region were investigated. The gas compositions, crystalline structure, and cage occupancy of the NGHs at AM03 and AM06 were experimentally measured using gas chromatography (GC), ^{13}C nuclear magnetic resonance (NMR), Raman spectroscopy, and powder X-ray diffraction (PXRD). In the NGHs from AM03 and AM06, a significantly large fraction of CH_4 (> 99%) and a very small amount of H_2S were enclathrated in small (5^{12}) and large ($5^{12}6^2$) cages of sI hydrate. The NGHs from AM03 and AM06 were almost identical in composition, guest distributions, and existing environment to each other. The salinity of the residual pore water in the hydrate-bearing sediment (AM06) was measured to be 50.32‰, which was much higher than that of seawater (34.88‰). This abnormal salinity enrichment in the pore water of the low-permeability sediment might induce the dissociation of NGHs at a lower temperature than expected. The saturation changes in the NGHs that corresponded with an increase in the seawater temperature were also predicted on the basis of the salinity changes in the pore water. The experimental and predicted results of this study would be helpful for understanding the thermodynamic stability of NGHs and potential CH_4-releasing phenomena in the Arctic region.

keywords: Natural gas hydrates; Arctic; Salinity; Structure I; Thermodynamic stability; Saturation

2-17 *Geology*

Magmatic-Hydrothermal Processes of Vein-Type Haman-Gunbuk-Daejang Copper Deposits in the Gyeongnam Metallogenic Belt in South Korea

Lee, Tong Ha., Seo, Jung Hun., Yoo, Bong Chul., Lee, Bum Han., **Han, Seunghee.**, **Yang, Yun Seok.** and Lee, Jun Hee.

Frontiers in Earth Science. 2021. 9.
doi: 10.3389/feart.2021.752908.

Haman, Gunbuk, and Daejang deposits are neighboring vein-type hydrothermal Cu deposits located in the SE part of the Korean Peninsula. These three deposits are formed by magmatic-hydrothermal activity associated with a series of Cretaceous granodioritic intrusions of the Jindong Granitoids, which have created a series of veins and alterations in a hornfelsed shale formation. The copper deposits have common veining and alteration features: 1) a pervasive chlorite-epidote alteration, cut by 2) Cu-Pb-Zn-bearing quartz veins with a tourmaline-biotite alteration, and 3) the latest barren calcite veins. Chalcopyrite, pyrite, and pyrrhotite are common ore minerals in the three deposits. Whereas magnetite is a dominant mineral in the Haman and Gunbuk deposits, no magnetite is present, but sphalerite and galena are abundant in the Daejang deposit. Ore-bearing quartz veins have three types of fluid inclusions: 1) liquid-rich, 2) vapor-rich, and 3) brine inclusions. Hydrothermal temperatures obtained from the brine inclusion assemblages are about 340–600, 250–500, and 320–460°C in the Haman, Gunbuk, and Daejang deposits, respectively. The maximum temperatures (from 460 to 600°C) recorded in the fluid inclusions of the three deposits are higher than those of the Cu ore precipitating temperature of typical porphyry-like deposits (from 300 to 400°C). Raman spectroscopy

of vapor inclusions showed the presence of CO_2 and CH_4 in the three deposits, which indicates relatively reduced hydrothermal conditions as compared with typical porphyry deposits. The Rb/Sr ratios and Cs concentrations of brine inclusions suggest that the Daejang deposit was formed by a later and more fractionated magma than the Haman and Gunbuk deposits, and the Daejang deposit has lower Fe/Mn ratios in brine inclusions than the Haman and Gunbuk deposits, which indicates contrasting redox conditions in hydrothermal fluids possibly caused by an interaction with a hosting shale formation. In brines, concentrations of base metals do not change significantly with temperature, which suggests that significant ore mineralization precipitation is unlikely below current exposure levels, especially at the Haman deposit. Ore and alteration mineral petrography and fluid inclusions suggest that the Haman deposit was formed near the top of the deep intrusion center, whereas the Gunbuk deposit was formed at a shallower intrusion periphery. The Daejang deposit was formed later at a shallow depth by relatively fractionated magma.

keywords: haman; gunbuk; daejang; gyeongnam metallogenic belt; hydrothermal alteration; fluid inclusions; LA-ICP-MS

2-18 *Geochemistry & Geophysics*

Magnetic Constraints on Off-Axis Seamount Volcanism in the Easternmost Segment of the Australian-Antarctic Ridge

Choi, Hakkyum., Kim, Seung-Sep. and **Park, Sung-Hyun.**

Geochemistry Geophysics Geosystems. 2021. 22(9).
doi: 10.1029/2020gc009576.

The Australian-Antarctic Ridge (AAR) is an intermediate-spreading rate system located between the Southeast Indian Ridge and Macquarie Triple Junction of the Australian-Antarctic-Pacific plates. KR1 is the easternmost and longest AAR segment and exhibits unique axial morphology and various volcanic structures. We identified three asymmetric seamount chains positioned parallel to the seafloor spreading direction, which were indicative of prevalent off-axis volcanism in the vicinity of segment KR1. Two-dimensional magnetic modeling was used to predict the magnetization polarity of the seamounts, as well as to constrain their formation time and duration. The magnetic modeling revealed that the majority of the examined seamounts were formed over a period of less than ~600 kyrs. The seamount formation primarily occurred during two distinct volcanic pulses from 0.16–1.14 to 1.58–2.69 Ma. A temporal gap of 200–650 kyrs between the formation time of the seamounts and seafloor was estimated for certain seamounts that were formed much later than their underlying seafloor and at a distance of 10–20 km from the KR1 axis. Typically, such off-axis seamount activity is related to axial mantle convection caused by excessive magma supply near the ridge crest. Considering the scale of off-axis volcanism and thickening lithosphere ~20 km away from the axis with intermediate-spreading rates, small-scale upwelling made feasible by the fertile mantle heterogeneity is proposed as the mechanism for the seamount formations at off-axis distances, and the geochemically enriched compositions of the seamounts support this alternative explanation.

keywords: Australian-Antarctic Ridge; seamount; marine magnetism; off-axis volcanism

2-19 *Physical Geography; Geology*

Mega-scale glacial lineations formed by ice shelf grounding in the Canadian Beaufort Sea during multiple glaciations

Riedel, Michael., Dallimore, Scott., Wamsteeker, Michael., Taylor, Gary., King, Edward L., Rohr, Kristin M. M., **Hong, Jong Kuk.** and **Jin, Young Keun.**

Earth Surface Processes and Landforms. 2021. 46(8): 1568-1585.
doi: 10.1002/esp.5125.

Mega-scale glacial lineations formed by the raking of ice shelves across the seafloor have been reported from multiple polar regions. Here, we present the first evidence of continental slope situated buried lineations in the southern Canadian Beaufort Sea in present-day water depths of 220 to 800 m. Three separate surfaces with lineations are defined at sub-seafloor depths of 40 m to 390 m. All lineations are mostly parallel to the general trend of slope contours. The uppermost surface is recognized over a distance of 56 km. In water depths > 500 m the lineations are parallel to each other at a consistent direction (43°–44°). The second lineated surface is a regionally occurring erosional unconformity. This event has two sub-sets of lineations: mid-slope situated lineations oriented at 42°–48°, and lineations closer to the

continental shelf break at 55°–59°. The third lineated surface is an unconformable horizon buried up to 390 m below seafloor with lineaments oriented between 30° and 55°. All three sets of lineations are interpreted to have been produced by ice-ploughing on the paleo-seafloor through the grounding of an ice shelf. Our observations are similar to those documented along the slope off northern Alaska, Chukchi Rise, and Lomonosov Ridge. Collectively, these observations support the concept of an extensive ice shelf across the Arctic Ocean that grounded locally along its margins during multiple glaciations, including during the penultimate (or an earlier) glaciation. The youngest set of lineations indicates ice movement to the southwest with a suggested source in Amundsen Gulf and/or M'Clure Strait. Tentative age considerations for these youngest lineations indicate the first evidence for an analogous extensive ice shelf configuration for the Last Glacial Maximum.

keywords: 3D seismic data; Canadian Beaufort Sea; ice shelf grounding; Last Glacial Maximum; mega-scale glacial lineations

2-20

Microstructure and Crystallographic Preferred Orientations of an Azimuthally Oriented Ice Core from a Lateral Shear Margin: Priestley Glacier, Antarctica

Thomas, Rilee E., Negrini, Marianne., Prior, David J., Mulvaney, Robert., Still, Holly., Bowman, M. Hamish., Craw, Lisa., Fan, Sheng., Hubbard, Bryn., Hulbe, Christina., **Kim, Daeyeong.** and Lutz, Franz.

Frontiers in Earth Science. 2021. 9: 1-22.
doi: 10.3389/feart.2021.702213

A 58m long azimuthally oriented ice core has been collected from the floating lateral sinistral shear margin of the lower Priestley Glacier, Terra Nova Bay, Antarctica. The crystallographic preferred orientations (CPO) and microstructures are described in order to correlate the geometry of anisotropy with constrained large-scale kinematics. Cryogenic Electron Backscatter Diffraction analysis shows a very strong fabric (*c*-axis primary eigenvalue ~0.9) with *c*-axes aligned horizontally sub-perpendicular to flow, rotating nearly 40° clockwise (looking down) to the pole to shear throughout the core. The *c*-axis maximum is sub-perpendicular to vertical layers, with the pole to layering always clockwise of the *c*-axes. Priestley ice microstructures are defined by largely sub-polygonal grains and constant mean grain sizes with depth. Grain long axis shape preferred orientations (SPO) are almost always 1–20°clockwise of the *c*-axis maximum. A minor proportion of "oddly" oriented grains that are distinct from the main *c*-axis maximum, are present in some samples. These have horizontal *c*-axes rotated clockwise from the primary *c*-axis maximum and may define aweaker secondary maximum up to 30° clockwise of the primary maximum. Intragranular misorientations are measured along the core, and although the statistics are weak, this could suggest recrystallization by subgrain rotation to occur. These microstructures suggest subgrain rotation (SGR) and recrystallization by grain boundary migration recrystallization (GBM) are active in the Priestley Glacier shear margin. Vorticity analysis based on intragranular distortion indicates a vertical axis of rotation in the shear margin. The variability in *c*-axis maximum orientation with depth indicates the structural heterogeneity of the Priestley Glacier shear margin occurs at the meter to tens of meters scale. We suggest that CPO rotations could relate to rigid rotation of blocks of ice within the glacial shear margin. Rotation either post-dates CPO and SPO development or is occurring faster than CPO evolution can respond to a change in kinematics.

keywords: lateral glacial shear margin; crystallographic preferred orientations; ice microstructure; ice deformation and flow; electron backscatter diffraction; Priestley Glacier

2-21 *Geology*

Middle Cambrian slope deposits in northern Victoria Land, Antarctica: Fingerprinting small carbonate platforms dominated by grainy carbonates and microbial reefs

Hong, Jongsun., Woo, Jusun., **Park, Tae-Yoon S.**, **Kihm, Ji-Hoon.** and 2 others.

Episodes. 2021. 44(3): 299-315.
doi: 10.18814/epiiugs/2020/020090.

Carbonate-bearing slope strata are reported from the upper Miaolingian-lower Furongian Spurs Formation in northern Victoria Land, Antarctica, deposited in a backarc basin during the Ross Orogeny. The Spurs Formation consists mainly of shale interbedded with conglomerate and sandstone. It overlies the middle Miaolingian Glasgow Volcanics and volcaniclastic Molar Formation and is overlain by the lower

Furongian sandstone-dominated Eureka Formation. The Spurs conglomerate is composed of randomly-oriented, granule- to boulder-sized, polymictic clasts of shale, sandstone and various limestone. These limestone clasts are variable in texture, such as microbial boundstone composed of calcimicrobe Epiphyton and subordinate microbial crust, oolitic-peloidal packstone to grainstone, and minor lime mudstone to wackestone. These are collectively interpreted as slope deposits, in which limestone clasts may have been derived from missing platform margin carbonate, analogous to Cambrian to Lower Ordovician slope successions elsewhere. On the other hand, the rarity of thinly bedded micritic limestones in the Spurs slope successions is markedly distinctive, and possibly reflects subdued production of lime muds behind the platform edge. It suggests that the vanished carbonate platform may have formed within a narrow shelf margin, dominated by coarse-grained carbonate and microbial reefs. Such style of carbonate platforms would contribute to understand how syn-orogenic carbonates initiated and developed in back-arc basins along the pacific margin of Gondwana (i.e., southern Australia and New Zealand).

2-22 *Geology*

Oxygen isotope record of magmatic evolution of alkaline volcanic rocks at The Pleiades, northern Victoria Land, Antarctica

Kim, Nak Kyu., **Lee, Mi Jung.**, **Lee, Jong Ik.** and Kim, Ji-hyuk.

Geosciences Journal. 2021. 25(6): 787-797.
doi: 10.1007/s12303-021-0002-x.

Oxygen isotopes are used to examine the well-documented magmatic evolution of alkaline volcanic rocks at The Pleiades in northern Victoria Land (NVL), Antarctica. Oxygen isotopes were measured in olivine, clinopyroxene, and plagioclase phenocrysts to better understand the origin and evolution of the sodic and potassic differentiation lineages. The volcanic rocks at The Pleiades evolved from a parental basanite by fractional crystallization in crustal magma chambers. Olivine which crystallizes first in the mafic magmas provides the initial oxygen isotope composition of the magmatic lineages. The $\delta^{18}O_{OL}$ values for the mafic lavas in the sodic lineage are lower than the potassic lineage. The primary melt derived from the metasomatized lithospheric mantle may have consumed a low-$\delta^{18}O$ amphibole metasome. Subsequently, the melt would have evolved to the normal-$\delta^{18}O$ potassic lineage magma by a large contribution from surrounding peridotite. In contrast, the sodic lineage magma might preserve low-$\delta^{18}O$ characteristics because of insufficient reaction with the surrounding mantle peridotite. Intermediate rocks of the potassic lineage exhibit a wide variation in their oxygen isotope compositions and it deviates from the theoretical normal-$\delta^{18}O$ trend. Hence, variable $\delta^{18}O_{OL}$ values of the intermediate rocks suggest that high-$\delta^{18}O$ recorded in olivine could be reconciled with an assimilation of crustal rocks in NVL, and hydrothermally altered material may have contributed to low-$\delta^{18}O$ signature of the olivines.

keywords: The Pleiades volcanic complex; McMurdo Volcanic Group; Antarctica; oxygen isotope; AFC process

2-23 *Geochemistry & Geophysics; Mineralogy*

Petrogenesis of coeval shoshonitic and high-K calc-alkaline igneous suites in the Eopyeong granitoids, Taebaeksan Basin, South Korea: Lithospheric thinning-related Early Cretaceous magmatism in the Korean Peninsula

Im, Sunghwan., Park, Jung-Woo., Kim, Jihyuk., Choi, Seon-Gyu. and **Lee, Mi Jung.**

Lithos. 2021. 392.
doi: 10.1016/j.lithos.2021.106127.

The Early Cretaceous was the initial period of prolonged Cretaceous-Tertiary magmatic episode in the Korean Peninsula, during which a tectonic transition from compression to extension occurred. The Early Cretaceous Eopyeong granitoids in the Taebaeksan Basin consist of two distinct series of magmas: shoshonitic and high-K calc-alkaline series. We investigated the petrology, whole-rock major and trace element geochemistry, and Sr-Nd-Pb isotope compositions of the Eopyeong granitoids to understand their magma evolution processes and source characteristics. Sensitive high-resolution ion microprobe zircon U-Pb analysis was performed on the Eopyeong granitoids to constrain their intrusion ages. Zircon U-Pb ages of the shoshonitic and high-K calc-alkaline series are 110.63±0.52 and

110.65±0.66 Ma, respectively, indicating that the two series formed during the same magmatic event. The mafic mineral assemblages of the shoshonitic series change from two-pyroxene+biotite to clinopyroxene+amphibole+biotite through magma evolution, whereas those of the high-K calc-alkaline series consist of more hydrous assemblages of amphibole+biotite. The shoshonitic series is also distinguished from the high-K calc-alkaline series by its higher La/Yb ratio and negative anomalies of Rb, Ba, and Eu. Mineral geothermobarometry and hygrometry data and geochemical mass balance modeling results show that the two series evolved mainly by fractional crystallization from two distinct parental magmas containing different water contents. Primitive rocks from each series have high compatible element contents such as MgO, Cr, and Ni with high Mg# compared to crustal melts in a similar range of SiO_2, suggesting their mantle origin. They also have abundant incompatible elements and 'crust-like' isotopic compositions [$(^{87}Sr/^{86}Sr)_i$ = 0.7093–0.7098; εNd(t) = −7.1 to −8.8; $(^{206}Pb/^{204}Pb)_i$ = 18.133–18.327; $(^{207}Pb/^{204}Pb)_i$ = 15.621–15.665; $(^{208}Pb/^{204}Pb)_i$ = 38.691–38.862] with negative Nb-Ta anomalies in the primitive mantle-normalized patterns. The enrichment in both compatible and incompatible elements can be best explained by partial melting of phlogopite-bearing lithospheric mantle metasomatized by isotopically enriched upper crustal sediment-derived melt or fluid. The two magma series may have been generated by different degrees of partial melting of the mantle sources with varying water contents. Changes in subduction angle and direction of the paleo-Pacific plate during the Early Cretaceous may have led to lithospheric thinning and upwelling of asthenospheric mantle, which triggered the partial melting of fusible domains of metasomatized lithospheric mantle. The small igneous bodies of the Early Cretaceous shoshonitic to alkaline mafic rocks occur sporadically throughout the southern part of the Korean Peninsula in close spatial association with the Cretaceous basins. They also show crust-like geochemistry and isotopic compositions, similar to the Eopyeong granitoids, implying that the lithospheric thinning-related melting of the metasomatized lithospheric mantle may have been widespread in the southern part of the Korean Peninsula.

keywords: High-K calc-alkaline magma; Shoshonitic magma; Lithospheric thinning; Partial melting of enriched lithospheric mantle; Early cretaceous; Korean Peninsula

2-24 *Geology*

Recent anomalous seismic activity in the Bransfield Strait, near King Sejong Station, Antarctic Peninsula (August 2020-February 2021)

Lee, Won Sang., **Park, Yongcheol.** and **Lee, Choon-Ki.**

Journal of the Geological Society of Korea. 2021. 57(5): 717-726.
doi: 10.14770/jgsk.2021.57.5.717.

There have been 170 earthquakes with seismic magnitudes ranging from 4.0-6.9 in the Bransfield Strait, Antarctic Peninsula, reported by the USGS since the first event (*Mw* 4.9) occurred on 29 August 2020, which is anomalously high seismicity in this region. The largest event in the earthquake swarm sequence occurred ~200 km northeast of the Orca submarine volcano on 23 January 2021, which has a magnitude *Mw* 6.9. We investigated the seismic data recorded at JUBA where is located in the King George Island and found that total 34,101 events were detected by applying the STA/LTA method and the daily occurrence exceeds 100 events until early November 2020 then gets smaller. Furthermore, the Focal Mechanisms Classification analysis for 27 earthquakes that moment tensor solutions are provided by the USGS indicates that most events are characterized by strike-slip faultings and a few normal faulting events. Some events with a compensated linear vector dipole component of more than 10% may implicate volumetric changes associated with submarine volcanic environments, even though it should be carefully examined by collecting more data through international collaborations.

keywords: anomalously high seismicity; earthquake swarm; Bransfield Strait; Antarctic Peninsula

2-25 *Biochemistry & Molecular Biology; Chemistry*

Review on Applications of ^{17}O in Hydrological Cycle

Nyamgerel, Yalalt., **Han, Yeongcheol**. and 3 others.

Molecules. 2021. 26(15).
doi: 10.3390/molecules26154468.

The triple oxygen isotopes (^{16}O, ^{17}O, and ^{18}O) are very useful in hydrological and climatological studies because of their sensitivity to environmental

conditions. This review presents an overview of the published literature on the potential applications of ^{17}O in hydrological studies. Dual-inlet isotope ratio mass spectrometry and laser absorption spectroscopy have been used to measure ^{17}O, which provides information on atmospheric conditions at the moisture source and isotopic fractionations during transport and deposition processes. The variations of $\delta^{17}O$ from the developed global meteoric water line, with a slope of 0.528, indicate the importance of regional or local effects on the ^{17}O distribution. In polar regions, factors such as the supersaturation effect, intrusion of stratospheric vapor, post-depositional processes (local moisture recycling through sublimation), regional circulation patterns, sea ice concentration and local meteorological conditions determine the distribution of ^{17}O-excess. Numerous studies have used these isotopes to detect the changes in the moisture source, mixing of different water vapor, evaporative loss in dry regions, re-evaporation of rain drops during warm precipitation and convective storms in low and mid-latitude waters. Owing to the large variation of the spatial scale of hydrological processes with their extent (i.e., whether the processes are local or regional), more studies based on isotopic composition of surface and subsurface water, convective precipitation, and water vapor, are required. In particular, in situ measurements are important for accurate simulations of atmospheric hydrological cycles by isotope-enabled general circulation models.

keywords: ^{17}O-excess; kinetic fractionation; stable water isotopes

2-26 *Physical Geography; Geology*

Role of dense shelf water in the development of Antarctic submarine canyon morphology

Gales, J., Rebesco, M., De Santis, L., Bergamasco, A., Colleoni, F., **Kim, Sookwan.** and 8 others.

Geomorphology. 2021. 372.
doi: 10.1016/j.geomorph.2020.107453.

Increased ocean heat supply to the Antarctic continental shelves is projected to cause accelerated ice sheet loss and contribute significantly to global sea-level rise over coming decades. Changes in temperature or salinity of dense shelf waters around Antarctica, resulting from increased glacial meltwater input, have the potential to significantly impact the location and structure of the global Meridional Overturning Circulation, with seabed irregularities such as submarine canyons, driving these flows toward the abyss. Submarine canyons also influence the location of intruding warm water currents by acting as preferential routes for rising Circumpolar Deep Water. These global changes have implications for large-scale effects to atmospheric and oceanic circulation. The ability for numerical modellers to predict these future behaviours is dependent upon our ability to understand both modern and past oceanic, sedimentological and glaciological processes. This knowledge allows ocean models to better predict the flux and pathways of Circumpolar Deep Water delivery to the shelf, and consequently to ice shelf cavities where melt is concentrated. Here we seek to understand how dense shelf water and other continental slope processes influence submarine canyon morphology by analysing newly collected geophysical and oceanographic data from a region of significant and prolonged dense shelf water export, the Hillary Canyon in the Ross Sea. We find that cascading flows of dense shelf water do not contribute to significant gully incision at the shelf edge during interglacial periods, however, are strong enough to prevent gully infilling and contribute to canyon-levee aggradation down-slope. We find buried paleo-gullies beneath gullies incising the modern seafloor. Paleo-gullies occur as single gullies and in complexes indicating that gully activity was continuous over multiple glacial cycles and formed an important role in the development of the shelf edge and upper slope. Glacial cycles likely drive large-scale shifts in canyon head processes with periods of intense seafloor erosion and significant gully incision likely occurring when ice grounded near to the shelf edge, during glacial and deglacial periods, when sediment-laden subglacial meltwater was released at the shelf edge. We put slope morphology observed at the Hillary Canyon head into global perspective to show that cascading flows of dense shelf water do not exert consistent patterns of erosion on high-latitude continental margins.

keywords: Slope process; Continental slope; Submarine gully; Meltwater

2-27 *Geology*

Seismostratigraphic and Geomorphic Evidence for the Glacial History of the Northwestern Chukchi Margin, Arctic Ocean

Kim, Sookwan., Polyak, Leonid., **Joe, Young Jin.**, Niessen, Frank., **Kim, Hyoung Jun.**, **Choi, Yeonjin.**, **Kang, Seung-Goo.**, **Hong, Jong Kuk.**, **Nam, Seung-Il.** and **Jin, Young Keun.**

Journal of Geophysical Research-Earth Surface. 2021. 126(4).

doi: 10.1029/2020jf006030.

High-resolution seafloor mapping provides insights into the dynamics of past ice sheets/ice shelves on high-latitude continental margins. Geological/geophysical studies in the Arctic Ocean suggest widespread Pleistocene ice grounding on the Chukchi–East Siberian continental margin. However, flow directions, timing, and behavior of these ice masses are not yet clear due to insufficient data. We present a combined seismostratigraphic and morphobathymetric analysis of the Chukchi Rise off the northwestern Chukchi margin using the densely acquired subbottom profiler (SBP) and multibeam echosounder (MBES) data. Comparison with deeper airgun seismic records shows that the SBP data cover most of the glaciogenic stratigraphy possibly spanning ca. 0.5–1 Ma. Based on the stratigraphic distribution and geometry of acoustically transparent glaciogenic diamictons, the lateral and vertical extent of southern-sourced grounded ice became smaller over time. The older deposits are abundant as debris lobes on the slope contributing to a large trough mouth fan, whereas younger grounding-zone wedges are found at shallower depths. MBES data show two sets of mega-scale lineations indicating at least two fast ice-streaming events of different ages. Contour-parallel recessional morainic ridges mark a stepwise retreat of the grounded ice margin, likely controlled by rising sea levels during deglaciation(s). The different inferred advance and retreat directions of the southern-sourced ice reflect complex geomorphic settings. The overall picture shows that the Chukchi Rise was an area where different ice streams had complex interactions. In addition to glaciogenic deposits, we identify a number of related or preceding seabed features including mounds, gullies/channels, and sediment waves.

keywords: Arctic Ocean; Chukchi Rise; glaciogenic sedimentary processes; ice-sheet dynamics; morphobathymetry; seismostratigraphy

2-28 *Environmental Sciences & Ecology*

Subsea permafrost as a potential major source of dissolved organic matter to the East Siberian Arctic Shelf

Chen, Meilian., Kim, Ji-Hoon., Lee, Yun Kyung., Lee, Dong-Hun., **Jin, Young Keun.** and Hur, Jin.

Science of the Total Environment. 2021. 777.

doi: 10.1016/j.scitotenv.2021.146100.

Arctic subsea permafrost contains more organic carbon than the terrestrial counterpart (~1400 Pg C vs. ~1000 Pg C) and is undergoing fast degradation (at rates of ~10 to 30 cm yr^{-1} over the past 3 decades) in response to climate warming. Yet the flux of organic carbon sequestered in the sediments of subsea permafrost to overlying water column, which can trigger enormous positive carbon-climate feedbacks, remain unclear. In this study, we examined the dissolved organic matter (DOM) diffusion to bottom seawaters from East Siberian Sea (ESS) sediments, which was estimated at about 943–2240 g C m^{-2} yr^{-1} and 10–55 g C m^{-2} yr^{-1} at the continuous-discontinuous transition zone of subsea permafrost and the remainder shelf and slope sites, respectively. The released DOM is characterized by prevailing dominance (≥ 98%) of low molecular weight (M_n < 350 Da) fractions. A red-shifted (emission wavelength >500 nm) fluorescence fingerprint, a typical feature of sediment/soil DOM, accounts for 4–6% and 7–8% in the fluorescence distributions of seawaters and pore waters, respectively, on ESS shelf. Statistical analysis revealed that seawaters and pore waters possessed similar DOM composition. The estimated total benthic efflux of dissolved organic carbon (DOC) was ~0.7–1.0 Pg C yr^{-1} when the estimate was scaled up to the entire Arctic shelf underlain with subsea permafrost assuming the width of continuous-discontinuous transition zone is 1 to 10 m. This estimation is consistent with the established ~10–30 cm yr^{-1} degradation rates of subsea permafrost by estimating its thaw-out time. Compiled observation data suggested that subsea permafrost might be a major DOM source to the Arctic Ocean, which could release tremendous carbon upon remineralization via its degradation to CO_2 and CH_4 in the water column.

keywords: Carbon release; Subsea permafrost; Low molecular weight fraction; Fluorescence; Benthic efflux; Arctic sediment

2-29 *Geology*

Tectonic constraints on formation and evolution of microplates in the Indian and Pacific Oceans: reviews and statistical inferences

Choi, Hakkyum., Kim, Seung-Sep. and **Park, Sung-Hyun.**

Geosciences Journal. 2021. 25(6): 799-811.
doi: 10.1007/s12303-021-0005-7.

Oceanic plates are growing through narrow boundaries, such as mid-ocean ridges and transform faults. However, the discovery of diffuse plate boundary suggests another type of plate boundary that accommodates difference in plate motion via internal deformation. Along the Central and Southeast Indian ridges, for example, the Capricorn and Macquarie microplates exhibit widespread diffuse boundaries and hence divide the Indo-Australian Plate further into the Indian, Australian, Capricorn, and Macquarie plates. As for microplates distributed along the East Pacific Rise and Pacific-Antarctic Ridge in the Pacific Ocean, however, the typical plate boundaries surrounding the given microplate are distinctly established. Global plate reorganization involving the changes in plate motion or in spreading direction can be accommodated by forming a microplate through ridge extinction, ridge propagation, and pseudofault formation. However, relations between these tectonic processes have not been quantitatively assessed. In particular, we aim to examine tectonic constrains on the formation processes of microplates with diffuse plate boundary. In this study, we compare plate size, plate age, full-spreading rates, thermal structures, total rotation, and rotation rate for the 9 microplates including extinct plates (i.e., Capricorn, Macquarie, and Mammerickx* microplates in the Indian and Southern Oceans; Galapagos, Easter, Juan Fernandez, Bauer*, Friday*, and Selkirk* microplates in the Pacific Ocean; extinct plates are denoted with asterisks). From this comparison, we find that the microplate formation would require certain tectonic conditions (e.g., full-spreading rates faster than 70-80 mm/yr and rotation rates faster than 5-6°/m.y.) to evolve into an independent and rigid plate with respect to the neighboring plates. If the conditions are not met, the same tectonic reorganization would result in a microplate with diffuse plate boundaries.

keywords: microplate; ridge propagation; diffuse plate boundary; plate reorganization

2-30 *Geology*

Time-lapse electrical resistivity tomography and ground penetrating radar mapping of the active layer of permafrost across a snow fence in Cambridge Bay, Nunavut Territory, Canada: correlation interpretation using vegetation and meteorological data

Kim, Kwansoo., **Lee, Joohan.**, **Ju, Hyeontae.**, **Jung, Ji Young.**, Chae, Namyi., **Chi, Junhwa.**, Kwon, Min Jung., **Lee, Bang Yong.** and 2 others.

Geosciences Journal. 2021. 25(6): 877-890.
doi: 10.1007/s12303-021-0021-7.

The active layer thickness (ALT) is a key parameter for permafrost studies. Changes in the ALT are affected mainly by air and ground temperatures, physical and thermal properties of the surface and subsurface materials, soil moisture, vegetation, and the duration and thickness of snow cover. Ground penetrating radar (GPR) and electrical resistivity tomography (ERT) were employed across a snow fence during the thawing season to delineate and monitor the active layer of permafrost in Cambridge Bay, Nunavut, Canada. The variation of the ALT is well captured by the high-resolution time-lapse radargram. At the position of the fence, the active layer thickens over the thawing period from 0.5 m depth at the beginning to 1.0 m depth at the end. The active layer is thicker in the pre-fence area (C zone) than in the post-fence area (H zone). As the air temperature increases with time, the difference in thickness between the two zones decreases, eventually becoming almost equal. Changes in the ALT are represented in the ERT by low resistivities (< 200 Ωm), which decrease gradually with time. This occurs most significantly in the H zone due to the rapidly increasing temperature in the absence of snow cover. The electrical resistivity structure of the active layer is well correlated with the vegetation activity, as measured by the normalized difference vegetation index, air/ground temperatures, soil moisture, snow cover, and snow accumulation controlled by the

fence. Geophysical data interpretation and correlation schemes with vegetation and meteorological data explored in this paper can be applied to monitor the active layer, which is expected to thin during the freezing season.

keywords: snow fence; geophysical survey; active layer; normalized difference vegetation index (NDVI); permafrost

2-31 *Geology*

Uncharted Permian to Jurassic continental deposits in the far north of Victoria Land, East Antarctica

Bomfleur, Benjamin., Mors, Thomas., Unverfaerth, Jan., Liu, Feng., Laeufer, Andreas., Castillo, Paula., Oh, Changhwan., **Park, Tae-Yoon S.** and 2 others.

Journal of the Geological Society. 2021. 178(1).
doi: 10.1144/jgs2020-062.

The remote lower reaches of the Rennick Glacier in the far north of Victoria Land hold some of the least-explored outcrop areas of the Transantarctic basin system. Following recent international field-work efforts in the Helliwell Hills, we here provide a comprehensive emendation to the regional stratigraphy. Results of geological and palaeontological reconnaissance and of petrographic, geochemical and palynostratigraphic analyses reveal a stack of three previously unknown sedimentary units in the study area: the Lower Triassic Van der Hoeven Formation (new unit, 115+ m thick) consists mainly of quartzose sandstone and non-carbonaceous mudstone rich in continental trace fossils. The Middle to Upper Triassic Helliwell Formation (new unit, 235 m thick) consists of coal-bearing overbank deposits and volcaniclastic sandstone and yielded typical plant fossils of the Gondwanan *Dicroidium* flora together with plant-bearing silicified peat. The succession is capped by *c*. 14 m of the sandstone-dominated Section Peak Formation (uppermost Triassic-Lower Jurassic). Our results enable more detailed correlation of the Palaeozoic–Mesozoic successions throughout East Antarctica and into Tasmania. Of particular interest is one section that spans the end-Permian mass extinction interval, which promises to allow detailed reconstructions of high-latitude vegetation dynamics across this critical interval in Earth history.

2-32 *Geology*

Upper mantle seismic anisotropy beneath the Northern Transantarctic Mountains inferred from peridotite xenoliths near Mt. Melbourne, northern Victoria Land, Antarctica

Kim, Daeyeong., Park, Munjae., **Park, Yongcheol.**, Qi, Chao., **Kim, Hwayoung.**, **Lee, Mi Jung.** and Michibayashi, Katsuyoshi.

Journal of Structural Geology. 2021. 143.
doi: 10.1016/j.jsg.2020.104237.

Microstructural investigations of mantle xenoliths from the Mt. Melbourne area were undertaken to reveal the origin of S-wave splitting beneath northern Victoria Land, Antarctica. The six analyzed peridotites contain various deformation features. The rotated olivine maxima of [100] and [010] into horizontal and vertical orientations, respectively, are classified into five samples with a D-type crystallographic preferred orientation (CPO) and one sample as an A-type CPO. The D-type olivine fabric can be explained by multiple slip systems of {0kl} [100] at low-temperature and high-stress conditions; therefore, both compressional and extensional regimes during subduction and rifting, respectively, could be applied in this study. With an assumption that olivine α-axes are aligned along the direction of mantle flow to form maximum S-wave splitting, the observed delay time of 0.9–1.3 s beneath northern Victoria Land can be partially explained by the anisotropy in the mantle peridotites. The remaining seismic anisotropy can be explained by the presence of melt pockets trapped along tectonic faults that developed perpendicular to the fast S-wave splitting direction. This study therefore demonstrates that the NE–SW-trending S-wave splitting beneath northern Victoria Land, Antarctica, results from the existence of both mantle peridotites as well as melt pockets trapped along the tectonic faults.

keywords: Mantle xenolith; Mt. Melbourne; Seismic anisotropy; Olivine; Crystallographic preferred orientation; Electron backscatter diffraction

2-33 *Physical Geography; Geology; Paleontology*

Variable redox conditions as an evolutionary driver? A multi-basin comparison of redox in the middle and later Cambrian oceans (Drumian-Paibian)

LeRoy, Matthew A., Gill, Benjamin C., Sperling, Erik A., McKenzie, N. Ryan. and **Park, Tae-Yoon S.**

Palaeogeography Palaeoclimatology Palaeoecology. 2021. 566.
doi: 10.1016/j.palaeo.2020.110209.

The middle to later Cambrian (Drumian-Jiangshanian Ages, 505–490 Ma) was a time of unique evolutionary dynamics that remain enigmatic. This interval records unusually high rates of faunal turnover that produced a "plateau" within the broader trajectory of rapidly increasing biodiversity seen across the Cambrian Explosion and Great Ordovician Biodiversification Event (GOBE). The oceans during this time are generally thought to have been less oxygenated than later in the Phanerozoic, yet knowledge of oceanic redox structure and the influence this exerted upon the biosphere remains limited. Importantly, this interval also encompasses two large carbon cycle perturbations—the DICE and SPICE events—that are thought to involve the expansion of anoxic and, more specifically euxinic regions in the ocean. Despite this supposition, direct characterization of redox conditions across this time remains limited. Here we explore these conditions using new and previously published Fespeciation data from seven basins distributed across five paleocontinents representing a range of depositional conditions. Our analysis reveals anoxia was a common and persistent feature of deeper-water environments and that it was generally absent from shallower-waters across this timespan. An exception to this broad pattern is seen during the SPICE when these deeper-water anoxic conditions expanded into shallower-water environments. These anoxic conditions were dominantly ferruginous and rare instances of euxinia were spatiotemporally limited to environments of high productivity, low clastic sedimentation and high sulfate availability within a generally low-sulfate ocean. Intriguingly, during these events faunal turnover was concentrated in inner-shelf areas suggesting a mechanistic link to the variable redox conditions characteristic of these environments. More broadly this instability in nearshore environments appears a likely cause of the high rates of faunal turnover seen across the later Cambrian and into the Early Ordovician, but further detailed paleontological and redox investigation of these environments are needed to adequately evaluate this view.

keywords: Cambrian; Marine redox; Sedimentary redox; Iron speciation; DICE; SPICE

2-34 *Geochemistry & Geophysics*

Water-susceptible primordial noble gas components in less-altered CR chondrites: A possible link to cometary materials

Obase, Tomoya., Nakashima, Daisuke., **Choi, Jisu.** and 3 others.

Geochimica Et Cosmochimica Acta. 2021. 312: 75-105.
doi: 10.1016/j.gca.2021.08.012.

We report detailed characterizations of the petrology, mineralogy, and noble gas signatures of Renazzo-type (CR) chondrites EET 92048, MIL 090657, NWA 801, and hydrothermally treated MIL 090657 samples to investigate primordial noble gases hosted by water-susceptible materials in aqueously less-altered CR chondrites. The noble gases were extracted by a stepwise heating method. The hydrothermal treatment on MIL 090657 resulted in the alteration of amorphous silicates in the matrix and the removal of large amounts of He and Ne that were released at low temperature from the untreated sample. The $^{36}Ar/^{132}Xe$ ratios in EET 92048 and MIL 090657 are ~5 times higher than that of the Q noble gas component, although both meteorites do not show any evidence for solar wind noble gases. The analyses revealed that aqueously less-altered CR chondrites contain two distinct primordial noble gas components hosted by water-susceptible materials: an isotopically Q-like Ne-rich component and an Ar-rich component. The characteristics of the Q-like Ne-rich component are consistent with those of Q-like Ne in cometary materials. We propose that the CR chondrites formed at a greater heliocentric distance and share similar materials hosting the Q-like Ne-rich component with comets. The presence of the Ar-rich component in the CR chondrites, as well as in ordinary chondrites and other anhydrous carbonaceous chondrites, provides evidence of the global distribution of the Ar-rich carriers in the ordinary and carbonaceous chondrite forming regions.

keywords: CR chondrites; Primitive meteorites; Noble gases; Aqueous alteration

PART3

Marine Sciences

3-1 *Environmental Sciences & Ecology; Marine & Freshwater Biology*

Advanced Remote Data Acquisition Using a Pop-Up Data Shuttle (PDS) to Report Data From Current- and Pressure-Recording Inverted Echo Sounders (CPIES)

Jeon, Chanhyung., Park, Jae-Hun., Kennelly, Maureen., Sousa, Erran., Watts, D. Randolph., Lee, Eun-Joo., **Park, Taewook.** and Peacock, Thomas.

Frontiers in Marine Science. 2021. 8.
doi: 10.3389/fmars.2021.679534.

A current- and pressure-recording inverted echo sounder (CPIES) placed on the sea floor monitors aspects of the physical ocean environment for periods of months to years. Until recently, acoustic telemetry of daily-processed data was the existing method for data acquisition from CPIES without full instrument recovery. However, this approach, which requires positioning a ship at the mooring site and operator time, is expensive and time-consuming. Here, we introduce a new method of obtaining data remotely from CPIES using a popup-data-shuttle (PDS), which enables straightforward data acquisition without a ship. The PDS data subsampled from CPIES has 30–60 min temporal resolution. The PDS has a scheduled pop-up-type release system, so each data pod floats to the sea surface at a user-specified date and relays the recorded data via the Iridium satellite system. We demonstrated the capability of an array of PDS-CPIES via two successful field experiments in the Arctic Ocean. The data acquired through the PDS were in agreement with the fully recovered datasets. An example of the data retrieved from the PDS shows that time-varying signals of tides and high-frequency internal waves were well captured. GPS-tracked trajectories of the PDS floating free at the sea surface can provide insights into ice drift or ocean surface currents. This PDS technology provides an alternative method for remote deep-ocean mooring data acquisition.

keywords: pop-up data shuttle; remote data acquisition; advanced technology; temporal high-resolution data; deep-ocean mooring

3-2 *Chemistry; Oceanography*

Assessment of the nutrient diol index (NDI) as a sea surface nutrient proxy using sinking particles in the East Sea

Gal, Jong-Ku., **Kim, Jung-Hyun.** and 3 others.

Marine Chemistry. 2021. 231.
doi: 10.1016/j.marchem.2021.103937.

The Nutrient Diol Index (NDI) has been proposed as a paleo sea surface nutrient proxy. However, the NDI's broad applicability needs to be further assessed by examining its temporal variability in association with modern sea surface nutrient concentrations. This study is the first report to evaluate the NDI with respect to sinking particles in the East Sea. The NDI values showed seasonal variations resembling those of the surface phosphate concentrations in the study area. However, the calibration based on the sinking particles at 1000 m water depth ($NDI = 1.134 \times [PO^{4-}] + 0.115$, $R^2 = 0.59$, $n = 26$) deviated from the newly compiled global surface sediment dataset ($NDI = 0.392 \times [PO^{4-}] + 0.023$; $R^2 = 0.58$, $n = 566$). This local calibration predicted the phosphate concentrations in surface sediments in the East Sea better than the global calibration. Our study suggests that the difference of the calibration slope between the East Sea trap dataset and the global surface sediment dataset might be associated with different 1,14-diol producers and their sensitivity to nutrient concentrations in the East Sea. Accordingly, the NDI should be further assessed in various oceanic settings before it is routinely used to reconstruct sea surface nutrient conditions.

keywords: Nutrient diol index; Long chain diol; Paleo nutrient proxy; Sinking particle; East Sea

3-3 *Geology*

Atlantic-Origin Cold Saline Water Intrusion and Shoaling of the Nutricline in the Pacific Arctic

Jung, Jinyoung., **Cho, Kyoung-Ho.**, **Park, Taewook.**, Yoshizawa, Eri., **Lee, Youngju.**, **Yang, Eun Jin.**, **Gal, Jong-Ku.**, **Ha, Sun-Yong.**, Kim, Soobin., **Kang, Sung-Ho.** and Grebmeier, Jacqueline M.

Geophysical Research Letters. 2021. 48(6).
doi: 10.1029/2020gl090907.

Atlantic-origin cold saline water has previously not been considered an important contributor to the nutrient supply in the Pacific Arctic due to the effective insulation by the overlying Pacific-origin waters that separate the surface mixed layer from the deeper Atlantic Water. Based on hydrographic observations in the northwestern Chukchi Sea from 2015 to 2017, we demonstrate that the intrusion of Atlantic-origin cold saline water into the halocline boundary between Pacific and Atlantic-origin waters in 2017 lifted Pacific-origin nutrients up to the surface layer. We find that the cyclonic atmospheric circulation in 2017 was considerably strengthened, leading to lateral intrusions of two bodies of cold halocline water from the Eurasian marginal seas into the northwestern Chukchi Sea. Our results reveal that the intrusions of cold halocline waters caused unprecedented shoaling of the nutricline and anomalously high surface phytoplankton blooms in typically highly oligotrophic surface waters in the region during summer.

3-4 *Geology*

Effects of Geophony and Anthrophony on the Underwater Acoustic Environment in the East Siberian Sea, Arctic Ocean

Han, Dong-Gyun., Joo, Jongmin., **Son, Wuju.**, **Cho, Kyoung-Ho.**, Choi, Jee Woong., **Yang, Eun Jin.**, **Kim, Jeong-Hoon.**, **Kang, Sung-Ho.** and **La, Hyoung Sul.**

Geophysical Research Letters. 2021. 48(12).
doi: 10.1029/2021gl093097.

As Arctic warming accelerates, the underwater acoustic environment in the Arctic Ocean is rapidly changing. We present the first results of passive acoustic monitoring in the marginal ice zone of the East Siberian Sea (ESS). A high sea ice concentration (SIC) and seasonal variations in ice cover make the ESS an ideal region to verify how ambient sound levels respond to natural physical processes and anthropogenic activities during summer. Our observations show that the sound level in the ESS exhibits a strong negative correlation with SIC, and the sound level in September, which was higher than that in other months, was 16 dB higher than the annual average. This increase resulted from geophony and anthrophony with the reduction in the SIC, and sound level increased by 13 dB without anthrophony. Our results indicate that ambient sound level in the Arctic Ocean may increase as climate change accelerates sea ice melting.

keywords: Arctic Ocean; East Siberian Sea; ambient sound; anthrophony; seismic airguns; sea ice

3-5 *Oceanography*

Exploring the Roles of Iron and Irradiance in Dynamics of Diatoms and *Phaeocystis* in the Amundsen Sea Continental Shelf Water

Kwon, Young Shin., **La, Hyoung Sul.**, **Jung, Jin-young.**, Lee, Sang Heon., **Kim, Tae-Wan.**, Kang, Hyoun-Woo. and **Lee, SangHoon.**

Journal of Geophysical Research-Oceans. 2021. 126(3).
doi: 10.1029/2020jc016673.

The Amundsen Sea continental shelf (ACS) water ecosystem is expected to undergo changes since increasing melt rate of glacier and decreasing sea ice extent by global warming would lead to the mitigation of iron and light limitation. We investigated how diatoms and *Phaeocystis*, two dominant taxa, and primary production in the ACS water would respond to variations in iron and light availabilities by using a 1-D pelagic ecosystem model. In the model, we added sea ice effects that reduce light penetration and optimized model parameters for diatoms and *Phaeocystis*. The results from our model showed good agreement with 20-year observations of Chl-*a* as well as the biomass proportion of diatoms and *Phaeocystis* and nutrient distributions during the growing season. Our model experimental results suggest that the current moderate iron and high light conditions favor the growth of *Phaeocystis* over diatoms. Moreover, as iron increases, the organic carbon exudation by phytoplankton increases more rapidly than net primary production (NPP), leading to a decline in phytoplankton biomass. On the other hand, irradiance plays a role in controlling NPP in terms of photoinhibition which is reduced by increasing iron. Increases in both iron and irradiance lead to an advance in the timing of the bloom peak (surface Chl-*a* maximum) due to increases in phytoplankton carbon loss and photoinhibition. Our results imply that the dominance of *Phaeocystis* can continue and that

the carbon uptake capacity of the ACS in the summer seasons might increase given that iron availability will increase with future climate change.

3-6 *Environmental Sciences & Ecology; Meteorology & Atmospheric Sciences*

First High-Frequency Underway Observation of DMS Distribution in the Southern Ocean during Austral Autumn

Kim, Intae., Zhang, Miming., **Kim, Kitae.** and **Park, Keyhong.**

Atmosphere. 2021. 12(1).

doi: 10.3390/atmos12010122.

We investigate the distribution of dimethyl sulfide (DMS) in the Southern Ocean's (50° W to 170° W) surface water, including the Antarctic Peninsula and the marginal sea ice zone (MIZ) in the Ross and Amundsen Seas. This is the first high-frequency observation conducted in the austral autumn (in April) in the Southern Ocean. The mean DMS concentration was 2.7 ± 2.5 nM (1 σ) for the entire study area. Noticeably enhanced DMS (5 to 28 nM) concentrations were observed in the MIZ around the Ross and Amundsen Seas and the coastal regions in the Antarctic Peninsula; this could be attributed to biological production of local ice algae, which appears to be supplied with nutrients from glacial or sea ice melt water. These observed DMS inventories were significantly higher (an order of magnitude) than current climatological DMS inventories. The local DMS sources being transported outward from the polynyas, where strong bloom occurs during summer, could result in larger discrepancies between observed DMS and climatological DMS in the MIZ area (in the Amundsen Sea). Overall, this study is the first to highlight the significance of the underestimation of current DMS fluxes in the austral autumn, which consequently results in significant errors in the climate models.

keywords: dimethyl sulfide; Southern Ocean; austral autumn; climate; high-frequency underway observation

3-7 *Environmental Sciences & Ecology; Marine & Freshwater Biology*

Geochemical and Microbial Signatures of Siboglinid Tubeworm Habitats at an Active Mud Volcano in the Canadian Beaufort Sea

Lee, Dong-Hun., **Kim, Jung-Hyun.**, **Lee, Yung Mi.**, Kim, Ji-Hoon., **Jin, Young Keun.** and 3 others.

Frontiers in Marine Science. 2021. 8.

doi: 10.3389/fmars.2021.656171.

During the ARA08C expedition in 2017, sediment push cores were collected at an active mud volcano (420 m water depth) in the Canadian Beaufort Sea from two visually discriminative siboglinid tubeworm (ST) habitats that were colonized densely and less densely (ST1 and ST2, respectively). In this study, we investigated the biogeochemical and microbial community characteristics at ST1 by analyzing the geochemical properties, microbial lipids, and nucleic acid signatures, and comparing them with the data previously reported from ST2. The two ST sites showed distinct differences in vertical geochemical gradients [methane, sulfate, dissolved inorganic carbon (DIC), total organic carbon, and total sulfur], with a higher methane flux recorded at ST1 (0.05 mmol cm^{-2} y^{-1}) than at ST2 (0.01 mmol cm^{-2} y^{-1}). Notably, the $\delta^{13}C$ values of DIC were more depleted at ST1 than at ST2, resulting in a higher proportion of DIC derived from the anaerobic oxidation of methane (AOM) at ST1 than at ST2. Moreover, both the ST1 and ST2 sites revealed the dominance of AOM-related lipid biomarkers (especially *sn*-2-hydroxyarchaeol), showing highly ^{13}C-depleted values. The 16S rRNA analyses showed the presence of AOM-related archaea, predominantly anaerobic methanotrophic archaea (ANME)-3 at ST1 and ST2. Our results suggest that AOM-related byproducts (sulfide and DIC) potentially derived from ANME-3 were more abundant at ST1 than at ST2. This variation was attributed to the intensity and persistence of ascending methane. Therefore, our study suggests that AOM-derived byproducts are possibly an essential energy source for tubeworms during chemosynthetic metabolism, shaping different colony types on the seafloor.

keywords: mud volcano; methane oxidation; *Oligobrachia haakonmosbiensis*; lipid biomarkers; 16S rRNA

3-8 *Environmental Sciences & Ecology; Marine & Freshwater Biology*

Impact of Freshwater Discharge on the Carbon Uptake Rate of Phytoplankton During Summer (January–February 2019) in Marian Cove, King George Island, Antarctica

Kim, Bo Kyung., **Jeon, Misa.**, **Joo, Hyoung Min.**, **Kim, Tae-Wan.**, **Park, Sang-Jong.**, **Park, Jisoo.** and **Ha, Sun-Yong.**

Frontiers in Marine Science. 2021. 8.
doi: 10.3389/fmars.2021.725173.

Rapidly changing conditions in high-latitude coastal systems can significantly impact biogeochemical cycles because these systems are strongly influenced by freshwater discharged from melting glaciers and streams on land. Generally, Antarctic coastal areas are considered high-productivity areas in which phytoplankton growth prevails under various environmental conditions (e.g., oceanographic and meteorological conditions). This study provides carbon uptake rates of phytoplankton in Marian Cove during summer (January-February 2019). Daily depth-integrated carbon uptake varied greatly and averaged 0.8 g C m^{-2} day^{-1}, with a maximum of 4.52 mg g C m^{-2} day^{-1} recorded on 14 January. Similarly, the observed biomass standing stocks were very high (up to 19.5 mg m^{-3} chlorophyll *a*) and were dominated by microphytoplankton (20–200 µm), representing 84% of total chlorophyll *a* (chl-*a*). The depth-integrated chl-*a* and carbon uptake decreased from outer to inner areas (close to the glacial front) in the cove. As the austral summer progressed, the freshening of the surface waters coincided with high water stability and suspended material and with low productivity when nanophytoplankton were present (2–20 µm; >60%). These findings suggest that both photosynthetically active radiation penetrating the water column and enhanced turbidity control light availability for phytoplankton, as well as their community compositions.

keywords: phytoplankton; carbon uptake rate; stable isotope; Marian Cove; Antarctica

3-9 *Engineering; Environmental Sciences & Ecology*

Importance of seasonal sea ice in the western Arctic ocean to the Arctic and global microplastic budgets

Kim, Seung-Kyu., Lee, Hee-Jee., Kim, Ji-Su., **Kang, Sung-Ho.**, **Yang, Eun Jin.**, **Cho, Kyoung-Ho.** and 2 others.

Journal of Hazardous Materials. 2021. 418.
doi: 10.1016/j.jhazmat.2021.125971.

Arctic sea ice entraps microplastics (MP) from seawater and atmosphere and is recognized as sink and transport vector of MPs. However, ice-trapped fraction in the global MP budget, contribution of atmospheric input, and linkage among Arctic basins remain unclear. To assess them, we investigated the number- and mass-based data separated by size and shape geometry for MPs in sea ice, snow, and melt pond water from the western Arctic Ocean (WAO). A significant dependency of MP data on measured cutoff size and geometry was found. For the same size range and geometry, sea ice MPs in WAO ($(11.4 \pm 9.12) \times 10^3$ N m^{-3} for ≥ 100 µm) were within comparable levels with those in other Arctic basins, but showed closer similarity in polymer and shape compositions between WAO and Arctic Central Basin, indicating the strong linkage of the two basins by the Transpolar Drift. Our budgeting shows that a significant amount of plastic particles ($(3.4 \pm 2.6) \times 10^{16}$ N; 280 ± 701 kilotons), which are missed from the global inventory, is trapped in WAO seasonal sea ice, with < 1% snowfall contribution. Our findings highlight that WAO ice zone may play a role as a sink of global MPs as well as a source of Arctic MPs.

keywords: Microplastics; Western Arctic ocean; Ice-trapping; Seasonal sea ice; Snow; Melt pond water; Mass budget

3-10 *Oceanography*

Interannual Variation of Modified Circumpolar Deep Water in the Dotson-Getz Trough, West Antarctica

Kim, Tae-Wan., **Yang, Hee Won.**, Dutrieux, Pierre., Wahlin, Anna K., Jenkins, Adrian., **Kim, Yeong Gi.**, Ha, Ho Kyung., Kim, Chang-Sin., **Cho, Kyoung-Ho.**, **Park, Taewook.**, **Park, Jisoo.**, **Lee, SangHoon.** and Cho, Yang-Ki.

Journal of Geophysical Research-Oceans. 2021. 126(12).
doi: 10.1029/2021jc017491.

Widespread ice shelf thinning has been recorded in the Amundsen Sea in recent decades, driven by basal melting and intrusions of relatively warm Circumpolar Deep Water (CDW) onto the continental shelf. The Dotson Ice Shelf (DIS) is located to the south of the Amundsen Sea polynya, and has a high basal melting rate because modified CDW (mCDW) fills the Dotson-Getz Trough (DGT) and reaches the base of the ice shelf. Here, hydrographic data in the DGT obtained during seven oceanographic surveys from 2007 to 2018 were used to study the interannual variation in mCDW volume and properties and their causes. Although mCDW volume showed relatively weak interannual variations at the continental shelf break, these variations intensified southward and reached a maximum in front of the DIS. There, the mCDW volume was ~8,000 km³ in 2007, rapidly decreased to 4,700 km³ in 2014 before rebounding to 7,300 km³ in 2018. We find that such interannual variability is coherent with local Ekman pumping integrated along the DGT modulated by the presence of sea ice, and complementing earlier theories involving shelf break winds only. The interannual variability in strength of the dominant south-southeast coastal wind modulates the amplitude of Ekman upwelling along the eastern boundary of the Amundsen Sea polynya during the austral summers of the surveyed years, apparently leading to change in the volume of mCDW along the DGT. We note a strong correlation between the wind variability and the longitudinal location of the Amundsen Sea Low.

keywords: Ekman upwelling; Amundsen Sea; Dotson Ice Shelf; Dotson-Getz Trough; hydrographic data

3-11 *Engineering; Environmental Sciences & Ecology*

Large Plastic Debris Dumps: New Biodiversity Hot Spots Emerging on the Deep-Sea Floor

Song, Xikun., Lyu, Mingxin., Zhang, Xiaodi., Ruthenstein-er, Bernhard., **Ahn, In-Young.** and 9 others.

Environmental Science & Technology Letters. 2021. 8(2): 148-154.

doi: 10.1021/acs.estlett.0c00967.

Macroplastic debris recorded in the Mariana Trench and accumulated on some deep-sea canyons worldwide has aroused great public concerns. Large plastic debris dumps found in canyons of the Xisha Trough, South China Sea have become hot spots for deep-sea pollution, with 1 order of magnitude higher abundance than in other investigated canyons. Here we adopted an integrative specimen-based approach to examine macroplastic items from large debris dumps in the Xisha Trough and comparative items from continental shelves with rare macroplastics. On the investigated items, we found an epibenthic ecosystem with relatively high species diversity, comprised of 49 mm-sized fungi and invertebrate species dominated by scyphozoan polyps and brachiopod juveniles according to inhabiting density. These large dumps are functioning as new biodiversity hot spots hosting endemic species like soft corals or aplacophoran molluscs, providing a spawning habitat for gastropods and even specialized parasitic flatworms, and can be inferred as potential scattered regional sources releasing deep-sea coronate jellyfish. We hypothesize that macroplastics can boost population extension of sessile and some free-living (Mollusca) invertebrates and affect the deep-sea benthic-pelagic coupling process. The baseline of associated organisms needs to be set up and monitored in more canyons, where debris is transported to and accumulated at the highest density.

3-12 *Environmental Sciences & Ecology; Marine & Freshwater Biology*

Long-term environmental changes in the Geum Estuary (South Korea): Implications of river impoundments

Kang, Sujin., **Kim, Jung-Hyun.**, **Joe, Young Jin.**, **Jang, Kwangchul.**, **Nam, Seung-Il.** and Shin, Kyung-Hoon.

Marine Pollution Bulletin. 2021. 168.

doi: 10.1016/j.marpolbul.2021.112383.

We investigated a sediment core collected from the Geum Estuary through sedimentological and geochemical analyses. Three lithological units were classified based on sedimentological characteristics. Unit 1 and Unit 3 were geochemically distinct, while Unit 2 was the transitional phase between them. The geochemical results suggest that the contribution of terrestrial organic carbon (OC) to the sedimentary OC pool in the coarse-grained Unit 1 was lesser than that of fine-grained Unit 3. The excess activity ($^{210}Pb_{ex}$) and the sedimentation rate indicate that Unit 1 corresponded to 1977 Common Era (CE). Since the first dam construction

on the Geum River began in 1975 CE, the deposition of Unit 1 in the Geum Estuary is likely associated with river impoundments, which reduce the delivery of fine-grained sediment and terrestrial OC to the estuary. This study highlights the role of river impoundments in altering the sedimentary OC and thus the sedimentary environment in the estuary.

keywords: Geum Estuary; Sedimentary organic carbon; Stable carbon isotope; *n*-Alkanes; River impoundment

3-13 *Microbiology*

Monthly Variation in the Macromolecular Composition of Phytoplankton Communities at Jang Bogo Station, Terra Nova Bay, Ross Sea

Kim, Kwanwoo., **Park, Jisoo.** and 5 others.

Frontiers in Microbiology. 2021. 12.
doi: 10.3389/fmicb.2021.618999.

Organic carbon fixed by photosynthesis of phytoplankton during the polar growing period could be important for their survival and consumers during the long polar night. Differences in biochemical traits of phytoplankton between ice-free and polar night periods were investigated in biweekly water samples obtained at the Korean "Jang Bogo Station" located in Terra Nova Bay, Antarctica. The average concentration of total Chl-*a* from phytoplankton dominated by micro-sized species from the entire sampling period was 0.32 μg L^{-1} (SD = ± 0.88 μg L^{-1}), with the highest concentration of 4.29 μg L^{-1} in February and the lowest concentration of 0.01 μg L^{-1} during the ice-covered polar night (April–October) in 2015. The highest protein concentration coincided with the peak Chl-*a* concentration in February and decreased rapidly relative to the carbohydrate and lipid concentrations in the early part of polar night. Among the different biochemical components, carbohydrates were the predominant constituent, accounting for 69% (SD = ± 14%) of the total particulate organic matter (POM) during the entire study period. The carbohydrate contributions to the total POM markedly increased from 39 ± 8% during the ice-free period to 73 ± 9% during the polar night period. In comparison, while we found a significant negative correlation (r^2 = 0.92, p < 0.01) between protein contributions and carbohydrate contributions, lipid contributions did not show any particular trend with relatively small temporal variations during the entire observation period. The substantial decrease in the average weight ratio of proteins to carbohydrates from the ice-free period (mean ± SD = 1.0 ± 0.3) to the ice-covered period (mean ± SD = 0.1 ± 0.1) indicates a preferential loss of nitrogen-based proteins compared to carbohydrates during the polar night period. Overall, the average food material (FM) concentration and calorific contents of FM in this study were within the range reported previously from the Southern Ocean. The results from this study may serve as important background data for long-term monitoring of the regional and interannual variations in the physiological state and biochemical compositions of phytoplankton resulting from future climate change in Antarctica.

keywords: Ross Sea (Antarctica); phytoplankton biomass; macromolecular composition; food material; polar night

3-14 *Chemistry; Oceanography*

A multiproxy approach to characterize the sedimentation of organic carbon in the Amazon continental shelf

Sobrinho, Rodrigo de L., Bernardes, Marcelo C., de Rezende, Carlos Eduardo., **Kim, Jung-Hyun.** and 2 others.

Marine Chemistry. 2021. 232.
doi: 10.1016/j.marchem.2021.103961.

Surface sediments were collected in a transect from the Amazon river delta to open marine sites in the north Atlantic Ocean in order to characterize spatial contrasts in the deposited organic carbon (OC), allowing to uncover the role of the river plume on the sedimentation of OC. Analysis of isoprenoidal and branched glycerol dialkyl glycerol tetraethers (GDGTs), lignin phenols, fatty acids, *n*-alkanes and bulk parameters were performed to characterize the sedimentary OC. An end-member approach based on biomarkers (lignin phenols and GDGTs), and the stable carbon isotopic composition of bulk organic carbon ($\delta^{13}C_{OC}$), was used to estimate the fraction of marine (OC_{mar}) and continental sources (OC_{cont}) of sedimentary organic carbon. Similar estimates based on lignin phenols were obtained and indicates that the OC_{cont} was on average 30 ± 37%; based on the GDGTs it was 29 ± 35% while based on the $\delta^{13}C_{OC}$ it was 30 ± 32%. The OC content of the surface sediments remained relatively constant from the delta to the marine sites

northward (ca. 0.6%) but the fractions of continental and marine OC were variable. In the deltaic region, OC_{cont} was ca. 84%, while in the open marine sites, OC_{mar} was ca. 86%. In the stations southward the delta, the OC content was about 0.03% with high OC_{mar} and low OC_{cont}, which indicates a low influence of the river plume on this location. The accumulation rates of OC_{cont} and OC_{mar} were estimated and showed that both were higher in the deltaic region in comparison to the marine sites. The results suggested that only 10–15% of the OC_{cont} is deposited offshore and that river plume conditions stimulated primary production and, thus, ultimately the sedimentation of OC_{mar} in the continental shelf and offshore sediments. Finally, our estimates showed that the Amazon River Delta has an accumulation rate above the global average and the material transported horizontally by the river plume fuels the primary production in adjacent areas, which improves the relevance of the Amazon continental shelf to the global carbon budget.

keywords: Organic carbon; Continental organic matter; Marine organic matter; Biomarkers

3-15 *Science & Technology*

N_2O dynamics in the western Arctic Ocean during the summer of 2017

Heo, Jang-Mu., Kim, Seong-Su., **Kang, Sung-Ho.**, **Yang, Eun Jin.**, **Park, Ki-Tae.**, **Jung, Jinyoung.**, **Cho, Kyoung-Ho.** and 7 others.

Scientific Reports. 2021. 11(1).
doi: 10.1038/s41598-021-92009-1.

The western Arctic Ocean (WAO) has experienced increased heat transport into the region, sea-ice reduction, and changes to the WAO nitrous oxide (N_2O) cycles from greenhouse gases. We investigated WAO N_2O dynamics through an intensive and precise N_2O survey during the open-water season of summer 2017. The effects of physical processes (i.e., solubility and advection) were dominant in both the surface (0–50 m) and deep layers (200–2200 m) of the northern Chukchi Sea with an under-saturation of N_2O. By contrast, both the surface layer (0–50 m) of the southern Chukchi Sea and the intermediate (50–200 m) layer of the northern Chukchi Sea were significantly influenced by biogeochemically derived N_2O production (i.e., through nitrification), with N_2O over-saturation. During summer 2017, the southern region acted as a source of atmospheric N_2O (mean: + 2.3 ± 2.7 μmol N_2O m^{-2} day^{-1}), whereas the northern region acted as a sink (mean – 1.3 ± 1.5 μmol N_2O m^{-2} day^{-1}). If Arctic environmental changes continue to accelerate and consequently drive the productivity of the Arctic Ocean, the WAO may become a N_2O "hot spot", and therefore, a key region requiring continued observations to both understand N_2O dynamics and possibly predict their future changes.

3-16 *Environmental Sciences & Ecology*

On the impact of wastewater effluent on phytoplankton in the Arctic coastal zone: A case study in the Kitikmeot Sea of the Canadian Arctic

Back, Dong-Young., **Ha, Sun-Yong.** and 9 others.

Science of the Total Environment. 2021. 764.
doi: 10.1016/j.scitotenv.2020.143861.

We present a case study on the impact of effluent from a wastewater lagoon-wetland system on phytoplankton and local primary production near a coastal Arctic community (Cambridge Bay) over spring to fall 2018. Results are also placed within an interannual and regional context for the surrounding Kitikmeot Sea. We find the shallow, relatively fresh Kitikmeot Sea is one of the most nutrient-deplete regions of the Arctic Ocean with NO_3^- + NO_2^- concentrations below the surface mixed layer rarely exceeding 2 μmol L^{-1} and a N:Si:P ratio of 1:6:1. The fjordal-type bathymetry of the main study site and a persistent pycnocline below the bay's exit sill led to slightly elevated N:Si:P of 3:11:1 through trapping of wastewater-sourced N at depth via sinking and remineralization of primary production. Total production in Cambridge Bay over the 3-month open water period was 12.1 g C m^{-2} with 70% of this production occurring during the 1-month discharge of wastewater into the system. Local primary production responded rapidly to high NO_3^- + NO_2^-, NO_4^+ and PON concentrations provided by wastewater effluent, comprising up to 20% of the production during the discharge period. Remaining production was mostly explained by the deep nutrient pool in the bay, which was only accessed towards the end of the discharge period as the diatom-dominated deep chlorophyll maximum settled below the pycnocline. Although not yet eutrophic, caution is raised at the rapid response of the marine system to wastewater release with a strong

recommendation to develop a research and monitoring plan for the bay.

keywords: Wastewater; Phytoplankton; Primary production; Arctic Ocean; Stratification; Nitrogen budget

3-17 *Science & Technology*

One Year of GOCI-II Launch Present and Future

Choi, Jong-kuk., Park, Myung-sook., Han, Kyung-soo., **Kim, Hyun-Cheol.** and Im, Jungho.

Korean Journal of Remote Sensing. 2021. 37(5): 1229-1234.
doi: 10.7780/kjrs.2021.37.5.2.1.

GOCI-II, which succeeded the mission of GOCI, was successfully launched in February 2020 and is in operation. GOCI-II is expected to be highly useful in a wide range of fields, including detailed changes in the coastal seawater environment using improved spatial and spectral resolution, increased number of observation and full disk observation mode. This special issue introduces the assessment of the current GOCI-II data quality and the studies on the accuracy improvement and applications at this time of one year after launch and data disclosure. We expect that this issue can be an opportunity for GOCI-II data to be actively utilized not only in the ocean but also in various fields of land and atmosphere.

keywords: GOCI-II; Data quality assessment; Accuracy improvement; Applications

3-18 *Science & Technology*

An open access dataset for developing automated detectors of Antarctic baleen whale sounds and performance evaluation of two commonly used detectors

Miller, Brian S., The IWC-SORP/SOOS Acoustic Trends Working Group., Balcazar, Naysa., Nieukirk, Sharon., Leroy, Emmanuelle C., Aulich, Meghan., Shabangu, Fannie W., Dziak, Robert P., **Lee, Won Sang.** and **Hong, Jong Kuk.**

Scientific Reports. 2021. 11(1).
doi: 10.1038/s41598-020-78995-8.

Since 2001, hundreds of thousands of hours of underwater acoustic recordings have been made throughout the Southern Ocean south of 60°S. Detailed analysis of the occurrence of marine mammal sounds in these circumpolar recordings could provide novel insights into their ecology, but manual inspection of the entirety of all recordings would be prohibitively time consuming and expensive. Automated signal processing methods have now developed to the point that they can be applied to these data in a cost-effective manner. However training and evaluating the efficacy of these automated signal processing methods still requires a representative annotated library of sounds to identify the true presence and absence of different sound types. This work presents such a library of annotated recordings for the purpose of training and evaluating automated detectors of Antarctic blue and fin whale calls. Creation of the library has focused on the annotation of a representative sample of recordings to ensure that automated algorithms can be developed and tested across a broad range of instruments, locations, environmental conditions, and years. To demonstrate the utility of the library, we characterise the performance of two automated detection algorithms that have been commonly used to detect stereotyped calls of blue and fin whales. The availability of this library will facilitate development of improved detectors for the acoustic presence of Southern Ocean blue and fin whales. It can also be expanded upon to facilitate standardization of subsequent analysis of spatiotemporal trends in call-density of these circumpolar species.

3-19 *Biodiversity & Conservation; Environmental Sciences & Ecology*

Patterns, drivers and implications of ascidian distributions in a rapidly deglaciating fjord, King George Island, West Antarctic Peninsula

Kim, Dong-U., Khim, Jong Seong. and **Ahn, In-Young.**

Ecological Indicators. 2021. 125.
doi: 10.1016/j.ecolind.2021.107467.

We report strong evidence for the utility of ascidian communities as sentinel organisms for monitoring nearshore Antarctic marine ecosystem response to climate-induced warming and glacial melting. Ascidians are one of the most common Antarctic

epibenthic megafauna, but information on their distribution and the determinants is still scarce. In this study we investigated spatial patterns of ascidians in Marian Cove (MC), a rapidly deglaciating fjord in the West Antarctic Peninsula, one of the most rapidly warming regions on earth. We also analyzed key drivers structuring the communities and assessed their relevance to glacial retreat and following processes. The first applied ROV survey in MC discovered that ascidians were the most diverse (14 out of 64 taxa) taxa with the greatest abundance (~264 inds·m^{-2}). Ascidian abundance and diversity greatly varied in space, by distance from glacier and/or depths, explaining ~64% of total megafaunal variations. Notably, in deep seabed (50–90 m) they shifted distinctly from early colonization communities near glacier (0.2 km to glacier) with predominance of two opportunistic species, *Molgula pedunculata* and *Cnemidocarpa verrucosa*, to mature communities at the most remote site (3.5 km). A set of analyses revealed that such shifts were related mostly to changes in sediment properties that develop in association with glacial retreat and consequent processes. Sediment composition, grain size and sorting collectively explained outward increasing physical stability apparently with decreased influence of glacial retreat, supporting ascidian community maturing at the deep and distant site. BIOENV analysis indicated that "distance" to glacier is one key factor influencing ascidian community structure in the deep seabed. Overall, the results of the analyses strongly indicated that physical disturbances (mainly sedimentation and ice scouring) accompanying glacial retreat are an important force shaping ascidian assemblages in the cove, and that these forces are altered by the distance from the glacier and water depth. Notably, in this fjord, the period of seabed deglaciation was roughly proportional to the distance to glacier over the last six decades. This suggested that the ascidian shift identified in this study reflects a long-term successional process associated with glacial retreat in the past in MC, which in turn warrants to project future changes in this glacial fjord and possibly other similar environments.

keywords: Marian Cove; Antarctic fjord; Glacial retreat; Ascidian distribution and succession; Distance to glacier; Ice scouring; Sedimentation

3-20 *Biodiversity & Conservation; Environmental Sciences & Ecology*

Phytoplankton succession during a massive coastal diatom bloom at Marian Cove, King George Island, Antarctica

Jeon, Misa., Iriarte, Jose Luis., **Yang, Eun Jin.**, **Kang, Sung-Ho.**, **Lee, Youngju.**, **Joo, Hyoung Min.**, **Ahn, In-Young.**, **Park, Jisoo.**, Min, Gi-Sik. and **Park, Sang-Jong.**

Polar Biology. 2021. 44(10): 1993-2010.
doi: 10.1007/s00300-021-02933-1.

To understand the community structure and the functional dynamics of phytoplankton over the long term, it is essential to identify rapid changes in the properties of Antarctic phytoplankton communities in relation to ongoing changes in environmental factors due to climate change. This study investigated short-term variability in the phytoplankton biomass and its composition over the summer of 2010 when the sea surface temperature was lowest and chlorophyll-a (chl-a) concentrations were the highest, relative to a 15-year monitoring period (1996–2011). We assessed the intraseasonal variability of the phytoplankton assemblage structure and its synchrony with changes in the main environmental variables in Marian Cove of King George Island, Antarctica. Chlorophyll-a concentrations in summer 2010 (January–February) were significantly higher (up to 24 μg L^{-1}) when the high phytoplankton carbon biomass (603 μg C L^{-1}) was dominated by the sympagic diatom *Navicula glaciei*, the benthic diatoms *Licmophora belgicae* and *Fragilaria striatula*, the planktonic diatoms *Thalassiosira antarctica* and *Thalassiosira* spp. (cell size <10 μm), and the Haptophyceae nanoplanktonic cells of *Phaeocystis antarctica*. Intraseasonal processes such as easterly winds direction on Maxwell Bay appeared to be the main factors affecting the advection of cold, nutrient-rich waters, and water stability that enhanced phytoplankton growth in Marian Cove.

keywords: Phytoplankton blooms; Marian Cove; Sympagic diatom; Benthic diatom; 2010 summer bloom

3-21 *Chemistry*

Proton Transport and Related Chemical Processes of Ice

Lee, Du Hyeong. and Kang, Heon.

Journal of Physical Chemistry B. 2021. 125(30): 8270-8281.
doi: 10.1021/acs.jpcb.1c04414.

Excess protons play a key role in the chemical reactions of ice because of their exceptional mobility, even when the diffusion of atoms and molecules is suppressed in ice at low temperatures. This article reviews the current state of knowledge on the properties of excess protons in ice, with a focus on the involvement of protons in chemical reactions. The mechanism of efficient proton transport in ice, which involves a proton-hopping relay along the hydrogen-bond ice network and the reorientation of water, is discussed and compared with the inefficient transport of hydroxide in ice. Distinctly different properties of protons residing in the ice interior and on the ice surface are emphasized. Recent observations of the spontaneous occurrence of reactions in ice at low temperatures, which include the dissociation of protic acids and the hydrolysis of acidic oxides, are discussed with regard to the kinetic and thermodynamic effects of mobile protons on the promotion of unique chemical processes of ice.

3-22 *Oceanography*

Quality Control Methods for CTD Data Collected by Using Instrumented Marine Mammals: A Review and Case Study

Yoon, Seung-Tae. and **Lee, Won Young.**

Ocean and Polar Research. 2021. 43(4): 321-334.
doi: 10.4217/opr.2021.43.4.321.

'Marine mammals-based observations' refers to data acquisition activities from marine mammals by instrumenting CTD (Conductivity-Temperature-Depth) sensors on them for recording vertical profiles of ocean variables such as temperature and salinity during animal diving. It is a novel data collecting platform that significantly improves our abilities in observing extreme environments such as the Southern Ocean with low cost compared to the other conventional methods. Furthermore, the system continues to create valuable information until sensors are detached, expanding data coverage in both space and time. Owing to these practical advantages, the marine mammals-based observations become popular to investigate ocean circulation changes in the Southern Ocean. Although these merits may bring us more opportunities to understand ocean changes, the data should be carefully qualified before we interpret it incorporating shipboard/autonomous vehicles/moored CTD data. In particular, we need to pay more attention to salinity correction due to the usage of an unpumped-CTD sensor tagged on marine mammals. In this article, we introduce quality control methods for the marine mammals-based CTD profiles that have been developed in recent studies. In addition, we discuss strategies of quality control specifically for the seal-tagging CTD profiles, successfully having been obtained near Terra Nova Bay, Ross Sea, Antarctica since February 2021. It is the Korea Polar Research Institute's research initiative of animal-borne instruments monitoring in the region. We anticipate that this initiative would facilitate collaborative efforts among Polar physical oceanographers and even marine mammal behavior researchers to understand better rapid changes in marine environments in the warming world.

keywords: instrumented marine mammals; CTD data quality control; temperature; salinity; southern ocean

3-23 *Environmental Sciences & Ecology; Marine & Freshwater Biology*

Quantifying Soundscapes in the Ross Sea, Antarctica Using Long-Term Autonomous Hydroacoustic Monitoring Systems

Yun, Sukyoung., **Lee, Won Sang.**, Dziak, Robert P., Roche, Lauren., Matsumoto, Haruyoshi., Lau, Tai-Kwan., Sremba, Angela., Mellinger, David K., Haxel, Joseph H., **Kang, Seung-Goo.**, **Hong, Jong Kuk.** and **Park, Yongcheol.**

Frontiers in Marine Science. 2021. 08.
doi: 10.3389/fmars.2021.703411.

Deployment of long-term, continuously recording passive-acoustic sensors in the ocean can provide insights into sound sources related to ocean dynamics, air–sea interactions, and biologic and human activities, all which contribute to shaping ocean soundscapes. In the polar regions, the changing ocean climate likely contributes to seasonal and long-term variation in cryogenic sounds, adding to the complexity of these soundscapes. The Korea Polar Research Institute and the U.S. National Oceanic and Atmospheric Administration have jointly operated two arrays of autonomous underwater hydrophones in the Southern Ocean, one in the Terra Nova Bay Polynya (TNBP) during December 2015–January 2019 and the other in the Balleny Islands (BI) region during January 2015–March 2016, to monitor changes in ocean soundscapes. In the BI region, we found

distinct seasonal variations in the cryogenic signals that were attributed to collisions and thermal/mechanical fracturing of the surface sea ice. This is consistent with sea-ice patterns due to annual freeze–thaw cycles, which are not clearly observed in TNBP, where frequent blowing out of sea ice by katabatic winds and icequakes from nearby ice shelves generate strong noise even in austral winters. Another advantage of passive acoustic recordings is that they provide opportunities to measure biodiversity from classifying spectral characteristics of marine mammals: we identified 1. Leopard seals (*Hydrurga leptonyx*; 200–400 Hz), most abundant in the BI region and TNBP in December; 2. Antarctic blue whales (*Balaenoptera musculus*; distinctive vocalization at 18 and 27 Hz), strong signals in austral winter and fall in the BI region and TNBP; 3. Fin whales (*B. physalus*; fundamental frequency in the 15–28 Hz and overtones at 80 and 90 Hz), maximum presence in the BI region during the austral summer and spring months; 4. Antarctic minke whales (*B. bonaerensis*; 100–200 Hz), strongest signals from June to August in the BI region; 5. Humpback whales in TNBP; 6. Unidentified whales (long-duration downsweeping from 75 to 62 Hz), detected in TNBP. Long-term soundscape monitoring can help understand the spatiotemporal changes in the Southern Ocean and cryosphere and provide a means of assessing the status and trends of biodiversity in the Ross Sea Region Marine Protected Area.

keywords: passive acoustic monitoring; Southern Ocean; cryogenic signals; air–sea interaction; biodiversity; Marine Protected Area

3-24 *Environmental Sciences & Ecology; Toxicology*

Reductive transformation of hexavalent chromium by ferrous ions in a frozen environment: Mechanism, kinetics, and environmental implications

Nguyen, Quoc Anh., **Kim, Bomi.**, **Chung, Hyun Young.**, Nguyen, Anh Quoc Khuong., Kim, Jungwon. and **Kim, Kitae.**

Ecotoxicology and Environmental Safety. 2021. 208.
doi: 10.1016/j.ecoenv.2020.111735.

The transformation between hexavalent chromium (Cr^{6+}) and trivalent chromium (Cr^{3+}) has a significant impact on ecosystems, as Cr^{6+} has higher levels of toxicity than Cr^{3+}. In this regard, a variety of Cr^{6+} reduction processes occurring in natural environments have been studied extensively. In this work, we investigate the reductive transformation of Cr^{6+} by ferrous ions (Fe^{2+}) in ice at –20 °C, and compare the same process in water at 25 °C. The Fe^{2+}-mediated reduction of Cr^{6+} occurred much faster in ice than it did in water. The accelerated reduction of Cr^{6+} in ice is primarily ascribed to the accumulation of Cr^{6+}, Fe^{2+}, and protons in the grain boundaries formed during freezing, which constitutes favorable conditions for redox reactions between Cr^{6+} and Fe^{2+}. This freeze concentration phenomenon was verified using UV–visible spectroscopy with *o*-cresolsulfonephthalein (as a pH indicator) and confocal Raman spectroscopy. The reductive transformation of Cr^{6+} (20 μM) by Fe^{2+} in ice proceeded rapidly under various Fe^{2+} concentrations (20–140 μM), pH values (2.0–5.0), and freezing temperatures (–10 to –30 °C) with a constant molar ratio of oxidized Fe^{2+} to reduced Cr^{6+} (3:1). This result implies that the proposed mechanism (i.e., the redox reaction between Cr^{6+} and Fe^{2+} in ice) can significantly contribute to the natural conversion of Cr^{6+} in cold regions. The Fe^{2+}-mediated Cr^{6+} reduction kinetics in frozen Cr^{6+}-contaminated wastewater was similar to that in frozen Cr^{6+} solution. This indicates that the variety of substrates typically present in electroplating wastewater have a negligible effect on the redox reaction between Cr^{6+} and Fe^{2+} in ice; it also proposes that the Fe^{2+}/freezing process can be used for the treatment of Cr^{6+}-contaminated wastewater.

keywords: Ice chemistry; Hexavalent chromium; Ferrous ion; Natural detoxification; Cr^{6+}-contaminated wastewater

3-25 *Environmental Sciences & Ecology; Marine & Freshwater Biology*

Ross Sea Dissolved Organic Matter Optical Properties During an Austral Summer: Biophysical Influences

D'Sa, Eurico J., **Kim, Hyun-Cheol.**, **Ha, Sun-Yong.** and Joshi, Ishan.

Frontiers in Marine Science. 2021. 08.
doi: 10.3389/fmars.2021.749096.

The Ross Sea, one of the most productive regions in the Southern Ocean, plays a significant role in deep water formation and carbon cycling. Dissolved organic carbon (DOC) concentrations and chromophoric dissolved organic matter (CDOM) absorption and

fluorescence (FDOM) properties were studied in conjunction with biophysical properties during austral summer. Elevated values of both DOC (mean 47.82 ± 5.70 µM) and CDOM (absorption coefficient at 325 nm, $a_{cdom}325$: mean 0.31 ± 0.18 m^{-1}) observed in the upper shelf waters in the southwest (SW), north of the Ross Ice Shelf (RIS), the northwest and along a transect inward of the shelf break, suggested *in situ* production and accumulation linked to the productive spring/summer season. However, regional differences were observed in CDOM with $a_{cdom}325$ higher (0.63 ± 0.19 m^{-1}) and its spectral slope $S_{275-295}$ lower (24.06 ± 2.93 μm^{-1}) in the SW compared to other regions (0.25 ± 0.08 m^{-1} and 28.92 ± 2.67 μm^{-1}, respectively). Similarly, the specific UV absorption coefficient or $SUVA_{254}$ determined at 254 nm was greater (1.85 ± 0.55 m^2 mg^{-1} C) compared to other regions (1.07 ± 0.24 m^2 mg^{-1} C), indicating CDOM of greater molecular weight and aromaticity in the SW. Phytoplankton absorption spectra indicated the shallow mixed layer of SW Ross Sea to be dominated by diatoms (e.g., *Fragilariopsis spp.*), a preferential food source for grazers such as the Antarctic krill, which in large numbers have been shown to enhance CDOM absorption, a likely source in the SW. Excitation-emission matrix (EEM) fluorescence combined with parallel factor analysis (PARAFAC) retrieved one protein-like and two humic-like FDOM fractions commonly observed in the global ocean. In contrast to $a_{cdom}325$ which was uncorrelated to DOC, we observed weak but significant positive correlations between the humic-like FDOM with salinity and DOC, high value of the biological index parameter BIX and an instance of increasing FDOM with depth at a location with sinking organic matter, suggesting autochthonous production of FDOM. The absorption budget showed a relatively higher contribution by CDOM (70.7 ± 18.3%) compared to phytoplankton (22.5 ± 15.2%) absorption coefficients at 443 nm with implications to ocean color remote sensing. This first study of DOM optical properties provides additional insights on carbon cycling in the Ross Sea.

keywords: Ross Sea; Southern Ocean; DOM; CDOM; FDOM; DOC

3-26 *Engineering; Oceanography*

Seasonal Dietary Shifts of the Gammarid Amphipod *Gondogeneia antarctica* in a Rapidly Warming Fjord of the West Antarctic Peninsula

Ahn, In-Young., **Elias-Piera, Francyne.**, **Ha, Sun-Yong.**, Rossi, Sergio. and **Kim, Dong-U.**

Journal of Marine Science and Engineering. 2021. 9(12). doi: 10.3390/jmse9121447.

The amphipod *Gondogeneia antarctica* is among the most abundant benthic organisms, and a key food web species along the rapidly warming West Antarctic Peninsula (WAP). However, little is known about its trophic strategy for dealing with the extreme seasonality of Antarctic marine primary production. This study, using trophic markers, for the first time investigated seasonal dietary shifts of *G. antarctica* in a WAP fjord. We analyzed $\delta^{13}C$ and $\delta^{15}N$ in *G. antarctica* and its potential food sources. The isotopic signatures revealed a substantial contribution of red algae to the amphipod diet and also indicated a significant contribution of benthic diatoms. The isotope results were further supported by fatty acid (FA) analysis, which showed high similarities in FA composition (64% spring-summer, 58% fall-winter) between *G. antarctica* and the red algal species. *G. antarctica* $\delta^{13}C$ showed a small shift seasonally (–18.9 to –21.4‰), suggesting that the main diets do not change much year-round. However, the relatively high $\delta^{15}N$ values as for primary consumers indicated additional dietary sources such as animal parts. Interestingly, *G. antarctica* and its potential food sources were significantly enriched with $\delta^{15}N$ during the fall-winter season, presumably through a degradation process, suggesting that *G. antarctica* consumes a substantial portion of its diets in the form of detritus. Overall, the results revealed that *G. antarctica* relies primarily on food sources derived from benthic primary producers throughout much of the year. Thus, *G. antarctica* is unlikely very affected by seasonal Antarctic primary production, and this strategy seems to have allowed them to adapt to shallow Antarctic nearshore waters.

keywords: *Gondogeneia antarctica*; seasonal dietary shift; macroalgae; benthic diatoms; C and N stable isotopes; West Antarctic Peninsula; King George Island; Marian Cove (62°13′ S; 58°47′ W)

3-27 *Environmental Sciences & Ecology; Water Resources*

Seasonal Variations in the Biochemical Compositions of Phytoplankton and Transparent Exopolymer Particles (TEPs) at Jang Bogo Station (Terra Nova Bay, Ross Sea), 2017–2018

Park, Sanghoon., **Park, Jisoo.**, **Yoo, Kyu-Cheul.**, **Yoo, Jaeill.** and 7 others.

Water. 2021. 13(16).

doi: 10.3390/w13162173.

The biochemical composition of particulate organic matter (POM) mainly originates from phytoplankton. Transparent exopolymer particles (TEPs) depend on environmental conditions and play a role in the food web and biogeochemical cycle in marine ecosystems. However, little information on their characteristics in the Southern Ocean is available, particularly in winter. To investigate the seasonal characteristics of POM and TEPSs, seawater samples were collected once every two weeks from November 2017 to October 2018 at Jang Bogo Station (JBS) located on the coast of Terra Nova Bay in the Ross Sea. The total chlorophyll-*a* (Chl-*a*) concentrations increased from spring (0.08 ± 0.06 μg L^{-1}) to summer (0.97 ± 0.95 μg L^{-1}) with a highest Chl-*a* value of 2.15 μg L^{-1}. After sea ice formation, Chl-*a* rapidly decreased in autumn (0.12 ± 0.10 μg L^{-1}) and winter (0.01 ± 0.01 μg L^{-1}). The low phytoplankton Chl-*a* measured in this study was related to a short ice-free period in summer. Strong seasonal variations were detected in the concentrations of proteins and lipids (one-way ANOVA test, $p < 0.05$), whereas no significant difference in carbohydrate concentrations was observed among different seasons (one-way ANOVA test, $p > 0.05$). The phytoplankton community was mostly composed of diatoms (88.8% ± 11.6%) with a large accumulation of lipids. During the summer, the POM primarily consisted of proteins. The composition being high in lipids and proteins and the high caloric content in summer indicated that the phytoplankton would make a good food source. In winter, the concentrations of proteins decreased sharply. In contrast, relatively stable concentrations of carbohydrates and lipids have been utilized for respiration and long-term energy storage in the survival of phytoplankton. The TEPS values were significantly correlated with variations in the biomass and species of the phytoplankton. Our study site was characterized by dominant diatoms and low Chl-*a* concentrations, which could have resulted in relatively low TEP concentrations compared to other areas. The average contributions of TEP-C to the total POC were relatively high in autumn (26.9% ± 6.1%), followed by those in summer (21.9% ± 7.1%), winter (13.0% ± 4.2%), and spring (9.8% ± 3.1%).

keywords: phytoplankton; macromolecular composition; transparent exopolymer particles; Ross Sea; polar night

3-28 *Oceanography*

Spatial and Temporal Variations of Aragonite Saturation States in the Surface Waters of the Western Arctic Ocean

Kim, Dongseon., **Yang, Eun Jin.**, Cho, S., Kim, H. -J., **Cho, Kyoung-Ho.**, **Jung, Jinyoung.** and **Kang, Sung-Ho.**

Journal of Geophysical Research-Oceans. 2021. 126(11).

doi: 10.1029/2021jc017738.

The aragonite saturation state (Ω_{arag}) was determined for the surface waters of the western Arctic Ocean over 3 years, from 2016 to 2018, in an investigation of the present state of acidification of its waters and the main factors controlling the spatial and temporal variations in the surface Ω_{arag}. The study area was divided into the Chukchi marginal area (CMA) and the East Siberian marginal area (ESMA) along a longitude of 180°E. In the CMA, the surface Ω_{arag} during the study period ranged from 0.86 to 1.77, with an average of 1.16, indicating near saturation with respect to aragonite. In the ESMA, the surface Ω_{arag} during the study period ranged from 1.01 to 2.21, with a higher average (1.59) than the CMA. Aragonite undersaturation in the ESMA was not observed during any of the measurement periods, so ocean acidification was less serious there than in the CMA. The surface Ω_{arag} of the CMA was mainly determined by the mixing of seawater and freshwater introduced from rivers and/or sea ice, whereas in the ESMA it was influenced by the mixing of seawater and freshwater but also biological production and lateral mixing.

keywords: aragonite saturation state; carbonate chemistry; ocean acidification; Chukchi marginal area; East Siberian marginal area

3-29 *Environmental Sciences & Ecology; Water Resources*

Spatial Patterns of Macromolecular Composition of Phytoplankton in the Arctic Ocean

Choe, Keyseok., Yun, Misun., Park, Sanghoon., **Yang, Eun Jin.**, **Jung, Jinyoung.** and 5 others.

Water. 2021. 13(18).
doi: 10.3390/w13182495.

The macromolecular concentrations and compositions of phytoplankton are crucial for the growth or nutritional structure of higher trophic levels through the food web in the ecosystem. To understand variations in macromolecular contents of phytoplankton, we investigated the macromolecular components of phytoplankton and analyzed their spatial pattern on the Chukchi Shelf and the Canada Basin. The carbohydrate (CHO) concentrations on the Chukchi Shelf and the Canada Basin were 50.4–480.8 μg L^{-1} and 35.2–90.1 μg L^{-1}, whereas the lipids (LIP) concentrations were 23.7–330.5 μg L^{-1} and 11.7–65.6 μg L^{-1}, respectively. The protein (PRT) concentrations were 25.3–258.5 μg L^{-1} on the Chukchi Shelf and 2.4–35.1 μg L^{-1} in the Canada Basin. CHO were the predominant macromolecules, accounting for 42.6% on the Chukchi Shelf and 60.5% in the Canada Basin. LIP and PRT contributed to 29.7% and 27.7% of total macromolecular composition on the Chukchi Shelf and 30.8% and 8.7% in the Canada Basin, respectively. Low PRT concentration and composition in the Canada Basin might be a result from the severe nutrient-deficient conditions during phytoplankton growth. The calculated food material concentrations were 307.8 and 98.9 μg L^{-1} , and the average calorie contents of phytoplankton were 1.9 and 0.6 kcal m^{-3} for the Chukchi Shelf and the Canada Basin, respectively, which indicates the phytoplankton on the Chukchi Shelf could provide the large quantity of food material and high calories to the higher trophic levels. Overall, our results highlight that the biochemical compositions of phytoplankton are considerably different in the regions of the Arctic Ocean. More studies on the changes in the biochemical compositions of phytoplankton are still required under future environmental changes.

keywords: macromolecules; phytoplankton; Chukchi Shelf; Canada Basin; food material

3-30 *Environmental Sciences & Ecology; Water Resources*

Spectral Characterization of Dissolved Organic Matter in Seawater and Sediment Pore Water from the Arctic Fjords (West Svalbard) in Summer

Chen, Meilian., Kim, Ji-Hoon., Hong, Sungwook., Lee, Yun Kyung., Kang, Moo Hee., **Jin, Young Keun.** and Hur, Jin.

Water. 2021. 13(2).
doi: 10.3390/w13020202.

Fjords in the high Arctic, as aquatic critical zones at the interface of land-ocean continuum, are undergoing rapid changes due to glacier retreat and climate warming. Yet, little is known about the biogeochemical processes in the Arctic fjords. We measured the nutrients and the optical properties of dissolved organic matter (DOM) in both seawater and sediment pore water, along with the remote sensing data of the ocean surface, from three West Svalbard fjords. A cross-fjord comparison of fluorescence fingerprints together with downcore trends of salinity, Cl^-, and PO_4^{3-} revealed higher impact of terrestrial inputs (fluorescence index: ~1.2–1.5 in seawaters) and glaciofluvial runoffs (salinity: ~31.4 ± 2.4 psu in pore waters) to the southern fjord of Hornsund as compared to the northern fjords of Isfjorden and Van Mijenfjorden, tallying with heavier annual runoff to the southern fjord of Hornsund. Extremely high levels of protein-like fluorescence (up to ~4.5 RU) were observed at the partially sea ice-covered fjords in summer, in line with near-ubiquity ice-edge blooms observed in the Arctic. The results reflect an ongoing or post-phytoplankton bloom, which is also supported by the higher levels of chlorophyll *a* fluorescence at the ocean surface, the very high apparent oxygen utilization through the water column, and the nutrient drawdown at the ocean surface. Meanwhile, a characteristic elongated fluorescence fingerprint was observed in the fjords, presumably produced by ice-edge blooms in the Arctic ecosystems. Furthermore, alkalinity and the humic-like peaks showed a general downcore accumulation trend, which implies the production of humic-like DOM via a biological pathway also in the glaciomarine sediments from the Arctic fjords.

keywords: dissolved organic matter; excitation emission matrix; glaciofluvial runoff; ice algal bloom; Arctic glaciomarine sediment

3-31 *Environmental Sciences & Ecology; Marine & Freshwater Biology*

Temporal and Spatial Variations in Particle Fluxes on the Chukchi Sea and East Siberian Sea Slopes From 2017 to 2018

Kim, Ho-Jung., Kim, Hyung Jeek., **Yang, Eun Jin.**, **Cho, Kyoung-Ho.**, **Jung, Jinyoung.**, **Kang, Sung-Ho.** and 3 others.

Frontiers in Marine Science. 2021. 7.

doi: 10.3389/fmars.2020.609748.

Time-series sediment traps were deployed on the Chukchi Sea and East Siberian Sea slopes from August 2017 to August 2018 with the aim of elucidating the temporal and spatial variations in particle fluxes and identifying the main processes affecting those variations. Particle fluxes showed a typical seasonal pattern, with high values in summer and low values in other seasons, and a large inter-annual variation was observed only on the East Siberian Sea slope, where particle fluxes were one order of magnitude higher in early August 2018 than in late August 2017. This large inter-annual variation in particle flux resulted from the episodic intrusion of nutrient-enriched shelf water in the East Siberian Sea, which enhanced biological production at the surface and particle fluxes. The Chukchi Sea slope was influenced by the inflow of Anadyr Water, with high salinity and high nutrient concentrations, which had little annual variability. Therefore, particle flux showed little inter-annual variation on the Chukchi Sea slope. Under-ice phytoplankton blooms were observed in both the Chukchi Sea and East Siberian Sea slopes, and increases in particulate organic carbon (POC) flux and the C:N ratio under the sea ice were related to transparent exopolymer (TEP) production by ice algae. On the East Siberian Sea slope, particle fluxes increased slightly from 115 to 335 m, indicating lateral transport of suspended particulate matter; POC and lithogenic particles may be laterally transported to the slope as nutrient-rich shelf waters flowed from the East Siberian Sea to the Makarov Basin. Annual POC fluxes were 2.3 and 2.0 g C m^{-2} $year^{-1}$ at 115 and 335 m, respectively, on the East Siberian Sea slope and was 2.1 g C m^{-2} $year^{-1}$ at 325 m on the Chukchi Sea slope. Annual POC fluxes were higher on the Chukchi Sea and East Siberian Sea slopes than in Arctic basins, lower than on Arctic shelves, and generally similar to those on western Arctic slopes.

keywords: particle flux; biological pump; time-series sediment trap; seasonal variation; western Arctic Ocean

3-32 *Polymer Science*

Ten-Minute Synthesis of Highly Conductive Polymer Nanosheets on Ice Surfaces: Role of Ice Crystallinity

Kim, Kyoungwook., **Kim, Bomi.**, **Kim, Kitae.** and Park, Moon Jeong.

Macromolecular Rapid Communications. 2021. 42(24).

doi: 10.1002/marc.202100565.

Conducting polymers have been studied widely over the past decades for use as organic electrode materials owing to their high electrical conductivity and low-cost synthesis. Among the various synthesis methods reported, the recently established ice-assisted approach for developing conducting polymer nanosheets is regarded as an advanced technology that allows for easy fabrication in an eco-friendly manner. However, the role of the crystallinity of the underlying ice surface in determining the physicochemical properties of the conducting polymers remains unclear. Here, the electronic properties and packing structures of polyaniline (PANI) nanosheets formed on ice surfaces are studied by controlling the ice crystallinity. Intriguingly, the crystallinity of the PANI nanosheets resembles that of the ice surfaces, in that the anisotropic growth of the PANI crystals with a face-on orientation occurs preferentially on high-crystalline ice surfaces. In addition, it is found that the development of highly crystalline PANI nanosheets results in efficient charge transport, owing to polaron delocalization in PANI with extended chain conformations and the improvement in the degree of backbone ordering because of the preorganized aniline moieties on the ice surface.

keywords: conducting polymers; electronic properties; ice crystallinity; ice-template; polyaniline

3-33 *Chemistry; Oceanography*

Tracing Circumpolar Deep Water and glacial meltwater using humic-like fluorescent dissolved organic matter in the Amundsen Sea, Antarctica

Jeon, Mi Hae., **Jung, Jinyoung.**, Park, Mi Ok., Aoki, Shige-

ru., **Kim, Tae-Wan.** and Kim, Seung-Kyu.
Marine Chemistry. 2021. 235.
doi: 10.1016/j.marchem.2021.104008.

The Amundsen Sea is the most rapidly melting part of the West Antarctic Ice Sheet, due to increased heat transport by Circumpolar Deep Water (CDW). Tracing CDW and resulting glacial meltwater is important since glacial meltwater may change the water mass properties, leading to the change of the biogeochemical cycles. In this study, in order to investigate the potential for using the humic-like component of fluorescent dissolved organic matter (FDOM) as a tracer for CDW and glacial meltwater in the Amundsen Sea, a hydrographic survey was conducted during the austral summer of 2018 aboard the Korean icebreaker IBR/V *Araon*. The meteoric water and CDW fractions calculated using the humic-like component (f_{mw_humic} and f_{cdw_humic}) were compared to those using oxygen isotope ($\delta^{18}O$) (f_{mw}) and optimum multiparameter analysis (OMP) (f_{cdw_OMP}), respectively. The fluorescence intensity of the humic-like component varied from 0.007 to 0.021, with higher values in the deeper layer and lower intensities in the surface waters. The range of f_{cdw_humic} (0.5–1.0) was narrower than that of f_{cdw_OMP} (0.1–1.0), indicating that the f_{cdw_humic} values were overestimated due to the remained humic-like C1. To minimize the effect of the remained humic-like C1 on the calculation of CDW fraction, we used newly derived empirical equations (i.e., $f_{cdw\_OMP} = 105.17 \times$ C1–1.14 for transect 1 and $f_{cdw\_OMP} = 126.04 \times$ C1–1.41 for transect 2). The CDW fraction calculated using the empirical equations ($f_{cdw\_humic\_empirical}$) was in good agreement with the f_{cdw_OMP}. We also found a significant positive relationship between f_{mw} and f_{mw_humic}, indicating that a reasonable method can be applied with a high percentage of explained variance and that f_{mw} can be largely explained by f_{mw_humic}. Our results show that the humic-like component can be a useful tracer for identifying CDW and glacial meltwater in the Amundsen Sea.

keywords: Amundsen Sea; Fluorescent dissolved organic matter; Humic-like component; CDW; Glacial meltwater

3-34 *Environmental Sciences & Ecology*

Tracing riverine dissolved organic carbon and its transport to the halocline layer in the Chukchi Sea (western Arctic Ocean) using humic-like fluorescence fingerprinting

Jung, Jinyoung., Son, Jin Eui., Lee, Yun Kyung., **Cho, Kyo-ung-Ho.**, **Lee, Youngju.**, **Yang, Eun Jin.**, **Kang, Sung-Ho.** and Hur, Jin.

Science of the Total Environment. 2021. 772.
doi: 10.1016/j.scitotenv.2021.145542.

Dissolved organic carbon (DOC) and the fluorescence properties of dissolved organic matter (FDOM) were investigated using parallel factor analysis (PARAFAC) for seawater samples collected in the Chukchi Sea (65°N–78°N, 170°E–160°W) during summer 2017. River water (f_{river}) and sea-ice meltwater ($f_{sea\ ice\ melt}$) fractions were also derived using oxygen isotopes ratios ($\delta^{18}O$) to examine the influence of sea ice on riverine DOM. The spatial distributions of f_{river}, riverine DOC, and the humic-like fluorescent component (C1) showed an overall south-north gradient, with higher values in the northern Chukchi Sea in summer. Pronounced accumulation of river water and riverine DOM was also observed in the anticyclonic Beaufort Gyre at the eastern stations of the northern Chukchi Sea in association with a long water residence time. Estimated riverine DOC in the surface layer accounted for 27 ± 9% (range: 17–47%) of the total DOC in the southern Chukchi Sea, and 39 ± 6% (range: 32–49%) and 31 ± 4% (range: 25–37%) for the eastern and western stations of the northern Chukchi Sea, respectively. Humic-like Cl showed negative and positive relationships with sea-ice meltwater-corrected salinity ($S_{sim\_corrected}$) and f_{river}, respectively. However, Arctic river waters with distinct humic-like C1 characteristics were likely mixed in the northern Chukchi Sea. The vertical distributions of riverine DOC, humic-like C1 fluorescence, and f_{river} generally decreased with water depth, reflecting the strong influence of riverine DOM in the surface layer. Although riverine DOM and f_{river} were dominant in the upper 50 m of the water column, they were also pronounced in the upper halocline (50–200 m), in which $f_{sea\ ice\ melt}$ dropped below zero. Our results indicated the existence of brine rejected from growing sea ice, and that sea-ice formation was a key factor for the transport of riverine DOM to the upper halocline layer in the northern Chukchi Sea.

keywords: Riverine DOC; Humic-like fluorescence; River water; Chukchi Sea; Western Arctic

3-35 *Oceanography*

Trophic Dynamics of Calanus *hyperboreus* in the Pacific Arctic Ocean

Choi, Hyuntae., Won, Haemin., **Kim, Jee-Hoon.**, **Yang, Eun Jin.**, **Cho, Kyoung-Ho.**, **Lee, Youngju.**, **Kang, Sung-Ho.** and Shin, Kyung-Hoon.

Journal of Geophysical Research-Oceans. 2021. 126(3).

doi: 10.1029/2020jc017063.

The zooplankton community composition in the Pacific Arctic Ocean depends heavily on the sea ice and hydrodynamic conditions. The calanoid copepod *Calanus hyperboreus* is a dominant Arctic zooplankton, but its diet sources in the Pacific Arctic are unclear. *C. hyperboreus* individuals were collected in the northern Chukchi Sea (NCS) and the northern-East Siberian Sea (NESS), which display contrasting chlorophyll abundance and sea ice concentration in summer 2018. Nitrogen isotopes of individual amino acid and fatty acid compositions were measured to determine its trophic level (TL) and dominant diet. *C. hyperboreus* collected in the NCS had higher TL values (3.0 ± 0.2) and a relatively low proportion of C20:5(n-3). In the NESS, *C. hyperboreus* had lower TL values (2.7 ± 0.2) and a larger percentage of C20:5(n-3), suggesting a greater proportion of diatoms in its diet. Spatial TL variations of *C. hyperboreus* between the NCS and NESS may be caused by variations in phytoplankton composition (micro-phytoplankton vs. nano- and picophytoplankton) as a result of surface seawater stratification triggered by the inflow of sea ice meltwater as well as summer Bering Sea water through the Bering Strait. These results suggest that the filter-feeding copepod *C. hyperboreus* could be a useful indicator to understand trophic dynamics in zooplankton food web.

keywords: amino acid; Pacific Arctic; stable isotope; trophic level; zooplankton

3-36 *Marine & Freshwater Biology; Oceanography*

Trophic niche of seabirds on the Barton Peninsula, King George Island, Antarctica

Gal, Jong-Ku., Choi, Bohyung., **Kim, Bo Kyung.**, Jung, Jin-Woo., **Min, Jun-Oh.**, **Lee, Won Young.**, Shin, Kyung-Hoon., **Kim, Jeong-Hoon.** and **Ha, Sun-Yong.**

Estuarine Coastal and Shelf Science. 2021. 258.

doi: 10.1016/j.ecss.2021.107443.

Drastic sea ice retreats in the Antarctic Peninsula, and the consequent environmental changes have brought about the consequences of biological adaptation and food competition. The isotopic niche is reflected by the ecological position and functional role of a species, which can be altered depending on these environmental changes. We assessed the isotopic niche and trophic positions (TP) of 3 seabirds on the Barton Peninsula, King George Island, Antarctica, to understand ecological interaction among the species. The average TP of Antarctic krill (*Euphausia superba*) (hereafter "krill") (2.6 ± 0.1) was estimated by using the compiled published data of the compound-specific nitrogen isotope ratio of glutamic acid and phenylalanine in the Southern Ocean, and TP values of the seabirds based on that of krill to be reliable according to ecological knowledge. Our results on the overlap of the isotopic niches of seabirds suggests potential diet competition among the consumers, such as the brown skua (*Stercorarius antarcticus*) and south polar skua (*Stercorarius maccormicki*), whereas the distinct and broad isotopic niche width of kelp gulls (*Larus dominicanus*) suggesting that their adaptation through generalization was related to their extended habitat and various food sources. Our research indicates that isotopic niche of seabirds reflects their survival strategy for food competition. Consequently, these seabirds can be easily influenced by alternative food sources, including terrestrial and human-derived sources, by rapid environmental changes, indicating that they are valuable as key environmental species and require long-term monitoring in the Antarctic Peninsula.

keywords: Antarctic seabirds; Isotopic niche; Trophic position; Stable isotope analysis; Antarctic Peninsula

3-37 *Environmental Sciences & Ecology*

Type II photosensitized oxidation in senescent microalgal cells at different latitudes: Does low under-ice irradiance in polar regions enhance efficiency?

Rontani, Jean-Francois., Amiraux, Remi., Smik, Lukas., Wakeham, Stuart G., Paulmier, Aurelien., Vaultier, Frederic., **Ha, Sun-Yong.**, **Min, Jun-Oh.** and Belt, Simon T.

Science of the Total Environment. 2021. 779.

doi: 10.1016/j.scitotenv.2021.146363.

Comparison of Type II photosensitized oxidation of lipids (the photodynamic effect) and

photodegradation of chlorophyll (sensitizer photobleaching) in samples of particulate matter collected previously from locations representing a diverse range of latitudes reveals an enhancement of the photooxidation of lipids at the expense of chlorophyll photodegradation in the polar regions. The efficiency of the photodynamic effect appears to be particularly high in sinking particles collected under sea ice and is attributed to the rapid settling of highly aggregated sympagic algae to depths of low light transmission favouring the photodynamic effect at the expense of photobleaching of the sensitizer. Paradoxically, the low efficiency of Type II photosensitized oxidation of lipids observed in temperate and equatorial regions is associated with high solar irradiances in these regions. Type II photosensitized oxidation of lipids in senescent phytoplankton seems thus to be strongly dependent of the intensity of solar irradiance.

keywords: Photodynamic effect; Senescent phytoplankton; Latitude; Polar regions; Solar irradiance

3-38 *Environmental Sciences & Ecology; Geology; Meteorology & Atmospheric Sciences*

Unravelling Surface Seawater DMS Concentration and Sea-To-Air Flux Changes After Sea Ice Retreat in the Western Arctic Ocean

Zhang, Miming., Marandino, Christa A., Yan, Jinpei., Wu, Yanfang., **Park, Keyhong.** and 3 others.

Global Biogeochemical Cycles. 2021. 35(6).
doi: 10.1029/2020gb006796.

The receding of the seasonal ice cover in the Arctic due to climate change has been predicted by models to increase climate-active biogenic trace gas emissions, specifically those of dimethylsulfide (DMS). However, insufficient DMS measurements are currently available to either support or refute this hypothesis and to fully understand the various responses of oceanic DMS in a rapidly changing Arctic Ocean environment. Here, we present high-resolution surface water DMS data collected in the summer of 2014 in combination with a suite of ancillary variables including sea ice cover, salinity, and nutrients. We show that surface seawater DMS concentrations, generally below 0.5 nmol L^{-1}, remained unchanged in the Canada Basin after sea ice retreat probably due to insufficient nutrients supply to the upper mixed layer and resulting low primary production. Moreover, in the Chukchi shelf region, DMS concentrations decreased following a phytoplankton bloom due to the rapid depletion and slow resupply of nutrients. Although the DMS sea-to-air fluxes were not high from a global perspective, they increased by a factor of 4-fold after sea ice retreat in the Arctic Ocean high latitudes. This increase in DMS flux was mainly driven by increased wind speed. This work provides unique observations and insights on how surface seawater DMS and flux to the atmosphere may change in the future Arctic Ocean.

keywords: dimethylsulfide; Arctic Ocean; sea ice retreat; changes; surface seawater

3-39 *Science & Technology*

Widespread increase in dynamic imbalance in the Getz region of Antarctica from 1994 to 2018

Selley, Heather L., Hogg, Anna E., Cornford, Stephen., Dutrieux, Pierre., Shepherd, Andrew., Wuite, Jan., Floricioiu, Dana., Kusk, Anders., Nagler, Thomas., Gilbert, Lin., Slater, Thomas. and **Kim, Tae-Wan.**

Nature Communications. 2021. 12(1).
doi: 10.1038/s41467-021-21321-1.

The Getz region of West Antarctica is losing ice at an increasing rate; however, the forcing mechanisms remain unclear. Here we use satellite observations and an ice sheet model to measure the change in ice speed and mass balance of the drainage basin over the last 25-years. Our results show a mean increase in speed of 23.8 % between 1994 and 2018, with three glaciers accelerating by over 44 %. Speedup across the Getz basin is linear, with speedup and thinning directly correlated confirming the presence of dynamic imbalance. Since 1994, 315 Gt of ice has been lost contributing 0.9 ± 0.6 mm global mean sea level, with increased loss since 2010 caused by a snowfall reduction. Overall, dynamic imbalance accounts for two thirds of the mass loss from this region of West Antarctica over the past 25-years, with a longer-term response to ocean forcing the likely driving mechanism.

PART4

Life Sciences

4-1 *Physiology*

Abiotic Stress-Induced *Actin-Depolymerizing Factor* 3 From *Deschampsia antarctica* Enhanced Cold Tolerance When Constitutively Expressed in Rice

Byun, Mi Young., Cui, Li Hua., Lee, Andosung., Oh, Hyung Geun., **Yoo, Yo-Han.**, **Lee, Jungeun.**, Kim, Woo Taek. and **Lee, Hyoungseok.**

Frontiers in Physiology. 2021. 12.
doi: 10.3389/fpls.2021.734500.

The Antarctic flowering plant *Deschampsia antarctica* is highly sensitive to climate change and has shown rapid population increases during regional warming of the Antarctic Peninsula. Several studies have examined the physiological and biochemical changes related to environmental stress tolerance that allow *D. antarctica* to colonize harsh Antarctic environments; however, the molecular mechanisms of its responses to environmental changes remain poorly understood. To elucidate the survival strategies of *D. antarctica* in Antarctic environments, we investigated the functions of actin depolymerizing factor (ADF) in this species. We identified eight *ADF* genes in the transcriptome that were clustered into five subgroups by phylogenetic analysis. DaADF3, which belongs to a monocot-specific clade together with cold-responsive ADF in wheat, showed significant transcriptional induction in response to dehydration and cold, as well as under Antarctic field conditions. Multiple drought and low-temperature responsive elements were identified as possible binding sites of C-repeat-binding factors in the promoter region of *DaADF3*, indicating a close relationship between DaADF3 transcription control and abiotic stress responses. To investigate the functions of DaADF3 related to abiotic stresses *in vivo*, we generated transgenic rice plants overexpressing *DaADF3*. These transgenic plants showed greater tolerance to low-temperature stress than the wild-type in terms of survival rate, leaf chlorophyll content, and electrolyte leakage, accompanied by changes in actin filament organization in the root tips. Together, our results imply that DaADF3 played an important role in the enhancement of cold tolerance in transgenic rice plants and in the adaptation of *D. antarctica* to its extreme environment.

keywords: abiotic stress; actin cytoskeleton; Antarctic; *Deschampsia antarctica* actin-depolymerizing factor 3; low temperature; polar adaptation

4-2 *Environmental Sciences & Ecology; Public, Environmental & Occupational Health*

Accelerated chromate reduction by tea waste: Comparison of chromate reduction properties between water and ice systems

Han, Tae Uk., Kim, Jungwon. and **Kim, Kitae.**

Environmental Research. 2021. 197.
doi: 10.1016/j.envres.2021.111059.

The concentration of chromium (Cr) in natural water and soil environments has gradually increased in recent decades, owing to intensive use of Cr in industry and its subsequent disposal. In this study, we performed a comparison study on chromate (Cr^{6+}) reduction by tea waste (green tea, black tea, red tea, and chamomile) in water (25 °C) and ice (−20 °C) to develop a new strategy for environmental-friendly stabilization of hazardous Cr^{6+} by freezing. This study shows that the freezing process can enhance the reduction of Cr^{6+} by tea waste. The residual Cr^{6+} concentration ratios (C/C_0, where C is the concentration of Cr^{6+} after the reaction (5 h) and C_0 is the initial concentration of Cr^{6+} (20 μM) in the system) by tea wastes in water were in the range of 0.71 (green tea) to 0.92 (chamomile); however, the ratios dramatically decreased under the freezing process (i.e., 0.06 by green tea, 0.13 by black tea, 0.18 by red tea, and 0.08 by chamomile). According to the results obtained from the fluorescent, chromatographic, and spectroscopic analyses, under the freezing process, the enhanced reduction of Cr^{6+} could be explained by the freeze concentration of Cr^{6+}, phenolic components in tea extracts, and protons in small liquid pockets in liquid-like layers (LLLs). In addition, the proposed system can efficiently purify the real Cr^{6+}-containing wastewater (i.e., electroplating wastewater), indicating that the system will be economically feasible in cold regions (i.e., polar regions).

keywords: Waste utilization; Chromate; Ice; Liquid-like layer; Freezing

4-3 *Environmental Sciences & Ecology*

Activation of peroxymonosulfate by bicarbonate and acceleration of the reaction by freezing

Ahn, Yong-Yoon., Kim, Jungwon. and **Kim, Kitae.**

Science of the Total Environment. 2021. 785.
doi: 10.1016/j.scitotenv.2021.147369.

This study demonstrates the positive effects of dissolved bicarbonate and carbonate anions on peroxymonosulfate (PMS) induced oxidation and the remarkable acceleration of the reaction by freezing. More than 90% of the initial 4-chlorophenol (4-CP) decomposed in the frozen case, whereas only less than 20% of the 4-CP was removed in the aqueous case in the same time period. This accelerated reaction is attributed to the freeze-concentration of the dissolved substrates (i.e., PMS, bicarbonate, and pollutants) in the quasi-liquid layer at the ice grain boundaries between ice crystals. The reaction between bicarbonate and PMSwas found to be unique because none of the effects were observed in the phosphate and hydroxide cooperated system with freezing, although the base activation of PMS could participate under basic conditions (pH > 9). Based on electron paramagnetic resonance spectroscopy measurements and comparison with the photo-excited Rose Bengal system as a reference system for singlet oxygen ($^1O_2$) generation, $^1O_2$ was found to have a minor effect on the oxidation of 4-CP in the frozen bicarbonate-PMS system. While, direct electron transfer from the target organic substrate to the PMS was suggested as a major mechanism of 4-CP oxidation, because the selected target organic substrates were decomposed with different tendencies, and the consumption of PMS was accelerated by the presence of an electron donating compound. The results show the potential applicability of the freezing phenomenon, which occurs naturally in the mid-latitude and polar area, to help a decomposition of water dissolved organic pollutants by the imitation of the natural purification process.

keywords: Peroxymonosulfate; Bicarbonate; Oxidation; Freeze-concentration effect; Water treatment; Organic pollutant

4-4 *Life Sciences & Biomedicine*

Antarctic ecosystems in transition - life between stresses and opportunities

Gutt, Julian., Isla, Enrique., Xavier, Jose C., Adams, Byron J., **Ahn, In-Young.** and 20 others.

Biological Reviews. 2021. 96(3): 798-821.
doi: 10.1111/brv.12679.

Important findings from the second decade of the 21st century on the impact of environmental change on biological processes in the Antarctic were synthesised by 26 international experts. Ten key messages emerged that have stakeholder-relevance and/or a high impact for the scientific community. They address (*i*) altered biogeochemical cycles, (*ii*) ocean acidification, (*iii*) climate change hotspots, (*iv*) unexpected dynamism in seabed-dwelling populations, (*v*) spatial range shifts, (*vi*) adaptation and thermal resilience, (*vii*) sea ice related biological fluctuations, (*viii*) pollution, (*ix*) endangered terrestrial endemism and (*x*) the discovery of unknown habitats. Most Antarctic biotas are exposed to multiple stresses and considered vulnerable to environmental change due to narrow tolerance ranges, rapid change, projected circumpolar impacts, low potential for timely genetic adaptation, and migration barriers. Important ecosystem functions, such as primary production and energy transfer between trophic levels, have already changed, and biodiversity patterns have shifted. A confidence assessment of the degree of 'scientific understanding' revealed an intermediate level for most of the more detailed sub-messages, indicating that process-oriented research has been successful in the past decade. Additional efforts are necessary, however, to achieve the level of robustness in scientific knowledge that is required to inform protection measures of the unique Antarctic terrestrial and marine ecosystems, and their contributions to global biodiversity and ecosystem services.

keywords: adaptation; benthic dynamism; biogeochemical cycles; climate change; invasion; new habitats; ocean acidification; primary production; range shifts; sea ice

4-5 *Zoology*

Antarctic population of Anteholosticha sigmoidea (Foissner, 1982) Berger, 2003 (Ciliophora: Urostylidae) with notes on its phylogenetic position

Kim, Kang-San., Ji, Su-Jung., **Kim, Sanghee.** and Min, Gi-Sik.

Zootaxa. 2021. 4942(2): 290-300.
doi: 10.11646/zootaxa.4942.2.9.

Anteholosticha sigmoidea (Foissner, 1982) Berger, 2003 was isolated from a wet soil sample collected on King George Island, Antarctica. Morphological observations and molecular phylogenetic analyses based on the gene sequences of small subunit ribosomal RNA (18S rRNA) were used to identify the species. *Anteholosticha sigmoidea* can be divided into two groups: group I (three populations described by Foissner 1982) and group II (described by Foissner 1984) based on the morphological differences. Group I differs from group II by the length of the midventral complex (65.1% vs. 52.5% of the cell length), the number of adoral membranelles (25–28 vs. 16–24), and the number of dorsal bristles in kinety 1 (16 bristles vs. nine bristles). Group I differs from the Antarctica population by the absence/presence of the collecting canals of the contractile vacuole and the number of macronuclear nodules (6–12 vs. 13–19). Group II differs from the Antarctica population by the number of macronuclear nodules (five to nine vs. 13–19); the arrangement of cortical granules (forming longitudinal rows vs. irregularly distributed); the length of the midventral complex (64.7% vs. 53.8% of cell length). In the phylogenetic analyses, *A. sigmoidea* was not nested with any species, and the gene tree indicated polyphyly of the genus *Anteholosticha*.

keywords: Antarctic ciliate; *Anteholosticha*; phylogeny; terrestrial; 18S rRNA gene

4-6 *Food Science & Technology*

Anti-cancer effects of lucidadiol against malignant melanoma cells

Shin, Seong-Ah., Lee, Jun Seob., Joo, Byeong Jun., Ryu, Gyoungah., Han, Minjoo., Kim, Huiji., An, Jangeun., **Koo, Man Hyung.**, **Youn, Ui Joung.**, **Lee, Jun Hyuck.** and 2 others.

Applied Biological Chemistry. 2021. 64(1).
doi: 10.1186/s13765-021-00647-w.

Melanoma is one of the most aggressive and lethal skin cancers. Lucidadiol is a triterpenoid isolated from *Ganoderma lucidum* and is known to have various biological functions, including antibacterial effects. However, the anti-cancer effects and mechanism of action of lucidadiol in malignant melanoma are unknown. In this study, lucidadiol significantly reduced B16 melanoma cell viability in a dose- and time-dependent manner. In addition, lucidadiol induced apoptosis and suppressed cell mobility in B16 melanoma cells. Moreover, our findings revealed that lucidadiol remarkably downregulated phospho-Akt/ERK/JNK, but not p38. Taken together, our results suggest that lucidadiol could exerts its anti-cancer effects by inducing apoptosis via modulation of the Akt/MAPK pathway. Therefore, lucidadiol may be a potential cancer therapeutic agent for malignant melanoma.

keywords: Melanoma; Lucidadiol; Anti-cancer; Akt; MAPK

4-7 *Pharmacology & Pharmacy; Chemistry*

Anti-fibrotic effects of brevilin A in hepatic fibrosis via inhibiting the STAT3 signaling pathway

Park, Yong Joo., Jeon, Mi Seon., **Lee, Seulah.** and 4 others.

Bioorganic & Medicinal Chemistry Letters. 2021. 41.
doi: 10.1016/j.bmcl.2021.127989.

Hepatic fibrosis is a chronic liver disease characterized by the accumulation of extracellular matrix (ECM). Activation of hepatic stellate cells (HSCs) after repetitive liver damage is a key event in hepatic fibrogenesis. As part of ongoing research projects to identify pharmacologically effective natural products, the phytochemical investigation of a MeOH extract of *Centipeda minima* led to the isolation of a sesquiterpene lactone, brevilin A, which was explored to elucidate potential anti-fibrotic effects by reversing HSC activation. First, we observed that transforming growth factor (TGF)-β1 treatment significantly increased the expression levels of HSC activation marker, α-smooth muscle actin (α-SMA), and ECM protein such as collagen and fibronectin. Then, we demonstrated that brevilin A reversed the TGF-β1-induced increase in protein and mRNA expression levels of α-SMA and collagen. To investigate the underlying molecular mechanism of brevilin A, we

evaluated the effects of brevilin A on the STAT3 signaling pathway. STAT3 phosphorylation, increased by TGF- β1 treatment, was strongly inhibited by brevilin A; the expression levels of fibronectin and connective tissue growth factor were also significantly decreased by brevilin A. The present study indicated that brevilin A has a preventive and therapeutic potential against hepatic fibrosis.

keywords: *Centipeda minima*; brevilin A; Hepatic fibrosis; Hepatic stellate cells; STAT3

4-8 *Biotechnology & Applied Microbiology; Research & Experimental Medicine*

Anti-Inflammatory Effects of Antarctic Lichen *Umbilicaria antarctica* Methanol Extract in Lipopolysaccharide-Stimulated RAW 264.7 Macrophage Cells and Zebrafish Model

Hong, Ju-Mi., **Kim, Jung Eun.**, **Min, Seul Ki.**, **Kim, Kyung Hee.**, **Han, Se Jong.**, **Yim, Joung Han.**, Park, Hyun., **Kim, Jin-Hyoung.** and **Kim, Il-Chan.**

Biomed Research International. 2021. 2021.
doi: 10.1155/2021/8812090.

Umbilicaria antarctica (UA) is a member of the family Umbilicariaceae. To the best of our knowledge, no studies on its anti-inflammatory effects have been reported yet. In the present study, we examined its ability to suppress inflammatory responses and the molecular mechanisms underlying these abilities using lipopolysaccharide- (LPS-) stimulated RAW 264.7 cells and a zebrafish model of inflammation. We investigated the effects of UA on the production of nitric oxide (NO) and prostaglandin E_2 (PGE_2) in LPS-stimulated RAW 264.7 cells. To explore the anti-inflammatory mechanisms of UA, we measured the mRNA and protein expression of proinflammatory mediators in LPS-stimulated RAW 264.7 cells using quantitative RT-PCR and western blot analyses, respectively. UA significantly inhibited the production of NO, PGE_2, interleukin- (IL-) 6, and tumor necrosis factor- (TNF-) α in the LPS-stimulated RAW 264.7 cells. It also suppressed the mRNA and protein expression of inducible nitric oxide synthase (iNOS), cyclooxygenase-2 (COX-2), and nuclear factor- (NF-) ***κ***B activation in LPS-stimulated RAW 264.7 cells and tail pin-cutting-induced zebrafish model. Collectively, these findings indicate that UA significantly inhibits LPS-stimulated inflammatory responses. These effects were considered to be strongly associated with the suppression of NF-***κ***B activation. Overall, our results demonstrate that UA extract exerts strong anti-inflammatory activities in *in vitro* and *in vivo* models and suggest that UA may be an effective novel therapeutic agent for the treatment of inflammatory diseases.

4-9 *Biochemistry & Molecular Biology; Chemistry*

Anti-Inflammatory Effects of Metabolites from Antarctic Fungal Strain *Pleosporales* sp. SF-7343 in HaCaT Human Keratinocytes

Dong, Linsha., Kim, Hye Jin., Thao Quyen Cao., Liu, Zhiming., Lee, Hwan., Ko, Wonmin., Kim, Youn-Chul., Sohn, Jae Hak., **Kim, Tai Kyoung.**, **Yim, Joung Han.** and 2 others.

International Journal of Molecular Sciences. 2021. 22(18).
doi: 10.3390/ijms22189674.

Chemical investigation of the Antarctic fungi *Pleosporales* sp. SF-7343 revealed four known secondary fungal metabolites: alternate C (**1**), altenusin (**2**), alternariol (**3**), and altenuene (**4**). The compound structures were identified primarily by NMR and MS analyses. Atopic dermatitis, an inflammatory disease, is driven by the abnormal activation of T helper (Th) 2 cells and barrier dysfunction. We attempted to identify the anti-inflammatory components of SF-7343. Initial screening showed that compounds **1** and **3** inhibited the secretion of interleukin-8 and -6 in tumor necrosis factor-α/interferon-γ-treated HaCaT cells, and these compounds also showed inhibitory effects on CCL5 and CCL22. Compounds **1** and **3** also downregulated the protein expression levels of intercellular adhesion molecule-1 and upregulated the expression of filaggrin and involcurin. The mechanism study results showed that compounds **1** and **3** inhibited nuclear translocation of nuclear factor-kappa B p65 and the phosphorylation of STAT1 and STAT3. Compound **1**, but not compound **3**, significantly promoted the expression of heme oxygenase (HO)-1. The effects of compound **1** were partly reversed by co-treatment with a HO-1 inhibitor, tin protoporphyrin IX. Taken together, this study demonstrates the potential value of Antarctic fungal strain SF-7343 isolates as a bioresource for bioactive compounds to prevent skin inflammation.

keywords: Antarctic fungi; inflammation; ICAM-1; NF-κB; HO-1; HaCaT

4-10 *Biochemistry & Molecular Biology; Chemistry*

Anti-inflammatory spiroditerpenoids from *Penicillium bialowiezense*

Kwon, Jaeyoung., Kim, Min Jee., Kim, Dong-Cheol., Kwon, Haeun., Ryu, Seung Mok., Shim, Sang Hee., Guo, Yuanqiang., Hong, Seung-Beom., **Yim, Joung Han.** and 3 others.

Bioorganic Chemistry. 2021. 113.
doi: 10.1016/j.bioorg.2021.105012.

Inflammation is a vital process that maintains tissue homeostasis. However, it is widely known that uncontrolled inflammation can contribute to the development of various diseases. This study aimed to discover antiinflammatory metabolites from *Penicillium bialowiezense*. Seven spiroditerpenoids, including two new compounds, breviones P and Q (**1** and **2**), were isolated and characterized by various spectroscopic and spectrometric methods. All isolated compounds were initially tested for their inhibitory effects against lipopolysaccharideinduced nitric oxide (NO) production in RAW 264.7 macrophages. Of these, brevione A (**3**) exhibited this activity with a half-maximal inhibitory concentration value of 9.5 μM. Further mechanistic studies demonstrated that **3** could suppress the expression of pro-inflammatory cytokines and mediators, such as NO, prostaglandin E_2, interleukin (IL)-1β, tumor necrosis factor-α, IL-6, and IL-12 by inhibiting the activation of nuclear factor-kappa B and c-Jun *N*-terminal kinase.

keywords: *Penicillium bialowiezense*; Spiroditerpenoid; Brevione; Anti-inflammatory effect

4-11 *Biochemistry & Molecular Biology; Chemistry*

Anticancer Activity of 2-*O*-caffeoyl Alphitolic Acid Extracted from the Lichen, *Usnea barbata* 2017-KL-10

Chae, Hae-Jung., Kim, Geum-Jin., Deshar, Barsha., Kim, Hyun-Jin., Shin, Min-Ji., Kwon, Hyukbean., **Youn, Ui Joung.** and 4 others.

Molecules. 2021. 26(13).
doi: 10.3390/molecules26133937.

Colorectal cancer is one of the life-threatening ailments causing high mortality and morbidity worldwide. Despite the innovation in medical genetics, the prognosis for metastatic colorectal cancer in patients remains unsatisfactory. Recently, lichens have attracted the attention of researchers in the search for targets to fight against cancer. Lichens are considered mines of thousands of metabolites. Researchers have reported that lichen-derived metabolites demonstrated biological effects, such as anticancer, antiviral, anti-inflammatory, antibacterial, analgesic, antipyretic, antiproliferative, and cytotoxic, on various cell lines. However, the exploration of the biological activities of lichens' metabolites is limited. Thus, the main objective of our study was to evaluate the anticancer effect of secondary metabolites isolated from lichen (*Usnea barbata* 2017-KL-10) on the human colorectal cancer cell line HCT116. In this study, 2OCAA exhibited concentration-dependent anticancer activities by suppressing antiapoptotic genes, such as *MCL-1*, and inducing apoptotic genes, such as *BAX*, *TP53*, and *CDKN1A*(p21). Moreover, 2OCAA inhibited the migration and invasion of colorectal cancer cells in a concentration-dependent manner. Taken together, these data suggest that 2OCAA is a better therapeutic candidate for colorectal cancer.

keywords: colorectal cancer; 2-*O*-caffeoyl alphitolic acid; lichen; *Usnea barbata*; apoptosis; HCT116

4-12 *Chemistry; Pharmacology & Pharmacy*

Antiinflammatory lanostane triterpenoids from *Ganoderma lucidum*

Koo, Man Hyung., Chae, Hae-Jung., **Lee, Jun Hyuck.**, Suh, Sung-Suk. and **Youn, Ui Joung.**

Natural Product Research. 2021. 35(22): 4295-4302.
doi: 10.1080/14786419.2019.1705815.

Phytochemical and biological studies of the methanolic extracts from *Ganoderma lucidum* (Polyporaceae) have led to the identification and isolation of a new lanostane triterpenoid, ganosidone A (**1**), and its eight known derivatives (**2–9**). The structure of new compound was determined by HREIMS, 1 D and 2 D NMR experiments and by comparing the acquired physicochemical data with the published values. All the compounds were evaluated for cancer chemopreventive potential based on their ability to inhibit nitric oxide (NO) production induced by lipopolysaccharides (LPS) in mouse

macrophage RAW 264.7 cells in vitro. Notably, at a concentration of 50 μM, compounds **4** and **7** inhibited NO production by 86.5% and 88.2%, respectively.

keywords: *Ganoderma lucidum*; polyporaceae; lanostane triterpenoid; inhibit nitric oxide production

4-13 *Paleontology*

Articulated trilobite ontogeny: suggestions for a methodological standard

Hughes, Nigel C., Adrain, Jonathan M., Holmes, James D., Hong, Paul S., Hopkins, Melanie J., Hou, Jin-Bo., Minelli, Alessandro., **Park, Tae-Yoon S.** and 6 others.

Journal of Paleontology. 2021. 95(2): 298-304.
doi: 10.1017/jpa.2020.96.

In order to maximize the utility of future studies of trilobite ontogeny, we propose a set of standard practices that relate to the collection, nomenclature, description, depiction, and interpretation of ontogenetic series inferred from articulated specimens belonging to individual species. In some cases, these suggestions may also apply to ontogenetic studies of other fossilized taxa.

4-14 *Chemistry; Crystallography; Materials Science*

Characterization of high-H_2O_2-tolerant bacterial cytochrome P450 CYP105D18: insights into papaverine N-oxidation

Pardhe, Bashu Dev., **Do, Hackwon.**, **Jeong, Chang-Sook.**, Kim, Ki-Hwa., **Lee, Jun Hyuck.** and Oh, Tae-Jin.

lucrj. 2021. 8: 684-694.
doi: 10.1107/s2052252521005522.

The bacterial CYP105 family is involved in secondary metabolite biosynthetic pathways and plays essential roles in the biotransformation of xenobiotics. This study investigates the newly identified H_2O_2-mediated CYP105D18 from *Streptomyces laurentii* as the first bacterial CYP for N-oxidation. The catalytic efficiency of CYP105D18 for papaverine N-oxidation was 1.43 s^{-1} μM^{-1}. The heme oxidation rate (*k*) was low (<0.3 min^{-1}) in the presence of 200 m*M* H_2O_2. This high H_2O_2 tolerance capacity of CYP105D18 led to higher turnover prior to heme oxidation. Additionally, the high-resolution papaverine complexed structure and substrate-free structure of CYP105D18 were determined. Structural analysis and activity assay results revealed that CYP105D18 had a strong substrate preference for papaverine because of its bendable structure. These findings establish a basis for biotechnological applications of CYP105D18 in the pharmaceutical and medicinal industries.

keywords: CYP105D18; papaverine *N*-oxide; H_2O_2 tolerance; *Streptomyces laurentii*; enzyme mechanisms; crystal morphology; co-crystals.

4-15 *Genetics & Heredity*

Characterization of the complete mitochondrial genome of the Macaroni penguin *Eudyptes chrysolophus* from the Barton Peninsula, King George Island, Antarctica

Kim, Jong-U. and **Kim, Jeong-Hoon.**

Mitochondrial DNA Part B-Resources. 2021. 6(3): 972-973.
doi: 10.1080/23802359.2021.1888329.

The Macaroni penguin *Eudyptes chrysolophus* is a small crested penguin. In this study, the complete mitochondrial genome of *E. chrysolophus* is revealed for the first time. The mitogenome sequence is circular and 17,059 bp in length. It contains 13 protein-coding genes (PCGs), 22 transfer RNA (tRNA) genes, and two ribosomal RNA (rRNA) genes similar to other Spheniscidae species. The total nucleotide composition is 30.53% (A), 32.86% (C), 13.96% (G), and 22.66% (T), and 46.81% for overall GC contents. The phylogenetic analysis shows a close relationship between *E. chrysolophus* and *E. schlegeli*. Our findings would be useful for further studies on phylogenetics and evolutionary history of the genus *Eudyptes*.

keywords: Crested penguin; *Eudyptes chrysolophus*; Macaroni penguin mitogenome

4-16 *Genetics & Heredity*

Characterization of the complete mitochondrial genome of the scale worm, *Eunoe nodosa* (Phyllodocida; Polynoidae) from the Beaufort Sea

Kim, Bo-Mi., Nam, Sang-Eun., Lee, Somyeong., **Kihm, Ji-Hoon.**, **Park, Tae-Yoon S.** and Rhee, Jae-Sung.

Mitochondrial DNA Part B-Resources. 2021. 6(10): 2835-2837.
doi: 10.1080/23802359.2021.1955768.

To increase the mitogenome data available for robust phylogeny, we sequenced the complete mitochondrial DNA of the scale worm *Eunoe nodosa* (Sars, 1861) in the family Polynoidae of the order Phyllodocida. The complete mitogenome has 15,366 bp and has 28.9% A, 13.2% C, 19.0% G, and 38.8% T. Using MITOS and tRNAscan-SE, we identified the 13 typical protein-coding genes (PCGs), 2 ribosomal RNA (rRNA) genes, 22 transfer RNA (tRNA) genes, and a non-coding region. Phylogenomic analysis based on 27 in-group taxa belonging to five families of the subclass Errantia show congruence with the published phylogenetic relationship within the Polynoidae, in which *E. nodosa* lies in the clade of shallow water species.

keywords: Complete mitogenome; Phyllodocida; Polynoidae; *Eunoe nodosa*; scale worm

4-17 *Biochemistry & Molecular Biology; Chemistry*

Chemical constituents from basidiomycete *Basidioradulum radula* culture medium and their cytotoxic effect on human prostate cancer DU-145 cells

Ryu, Seung Mok., Nguyen, Quynh Nhu., Lee, Sullim., Kwon, Haeun., Kwon, Jaeyoung., Lee, Hyaemin., Kwon, Sun Lul., Lee, Jun., Hwang, Bang Yeon., **Yim, Joung Han.** and 4 others.

Bioorganic Chemistry. 2021. 114.
doi: 10.1016/j.bioorg.2021.105064.

Eight new naphtho [1,2-*c*]furan derivatives (**1–8**) along with six known analogues (**9–14**) were isolated from culture medium of the basidiomycete *Basidioradulum radula*. The structures of these compounds were identified using spectroscopic analysis, and their absolute configurations were resolved using X-ray diffraction, ECD, and VCD. Compounds **7** and **14** inhibited the cell viability of human prostate cancer DU-145 cells with IC_{50} values of 7.54 ± 0.03 μM and 5.04 ± 0.03 μM, respectively. At 8 μM, compounds **7** and **14** increased the percentage of apoptotic cells and upregulated the protein expression related to the apoptosis caspase pathways in DU-145 cells. Furthermore, the hallmarks of cells undergoing apoptosis, such as chromatin condensation, were also observed at this concentration. However, compound **7** and **14** showed no effect on the proliferation of splenocytes isolated from cyclophosphamide-induce immunosuppressed mice.

keywords: Basidiomycete; *Basidioradulum radula*; Hyphodermin; DU-145 prostate cancer cell; Cytotoxicity

4-18 *Zoology*

Chromosomal assembly of the Antarctic toothfish (*Dissostichus mawsoni*) genome using third-generation DNA sequencing and Hi-C technology

Lee, Seung Jae., **Kim, Jeong-Hoon.**, **Jo, Euna.** and 6 others.

Zoological Research. 2021. 42(1): 124-129.
doi: 10.24272/j.issn.2095-8137.2020.264.

4-19 *Biodiversity & Conservation; Environmental Sciences & Ecology*

Chromosomal-Level Assembly of Antarctic Scaly Rockcod, *Trematomus loennbergii* Genome Using Long-Read Sequencing and Chromosome Conformation Capture (Hi-C) Technologies

Jo, Euna., Lee, Seung Jae., **Kim, Jeong-Hoon.** and 6 others.

Diversity-Basel. 2021. 13(12).
doi: 10.3390/d13120668.

Trematomus species (suborder Notothenioidei; family Nototheniidae) are widely distributed in the southern oceans near Antarctica. There are 11 recognized species in the genus Trematomus, and notothenioids are known to have high chromosomal diversity (2n = 24–58) because of relatively recent and rapid adaptive radiation. Herein, we report the chromosomal-level genome assembly of T. loennbergii, the first characterized genome representative of the genus Trematomus. The final genome assembly of T. loennbergii was obtained using a Pacific Biosciences long-read sequencing platform and high-throughput chromosome conformation capture technology. Twenty-three chromosomal-level scaffolds were assembled to 940 Mb in total size, with a longest contig size of 48.5 Mb and contig N50 length of 24.7 Mb. The genome contained 42.03% repeat sequences, and a total of 24,525 protein-coding genes were annotated. We produced a high-quality genome assembly of T. loennbergii. Our results provide a first

reference genome for the genus Trematomus and will serve as a basis for studying the molecular taxonomy and evolution of Antarctic fish.

keywords: Antarctic fish; notothenioids; long-read sequencing; Hi-C; chromosomal-level assembly

4-20 *Environmental Sciences & Ecology*

Climate predicts both visible and near-infrared reflectance in butterflies

Kang, Changku., **Im, Sehyeok.**, **Lee, Won Young.** and 3 others.

Ecology Letters. 2021. 24(9): 1869-1879.
doi: 10.1111/ele.13821.

Climatic gradients frequently predict large-scale ecogeographical patterns in animal coloration, but the underlying causes are often difficult to disentangle. We examined ecogeographical patterns of reflectance among 343 European butterfly species and isolated the role of selection for thermal benefits by comparing animal-visible and near-infrared (NIR) wavebands. NIR light accounts for~50% of solar energy but cannot be seen by animals so functions primarily in thermal control. We found that reflectance of both dorsal and ventral surfaces shows thermally adaptive correlations with climatic factors including temperature and precipitation. This adaptive variation was more prominent in NIR than animal-visible wavebands and for body regions (thorax-abdomen and basal wings) that are most important for thermoregulation. Thermal environments also predicted the reflectance difference between dorsal and ventral surfaces, which may be due to modulation between requirements for heating and cooling. These results highlight the importance of climatic gradients in shaping the reflectance properties of butterflies at a continent-wide scale.

keywords: Bogert's rule; ecogeographical patterns; Gloger's rule; thermal melanism; thermoregulation

4-21 *Genetics & Heredity; Marine & Freshwater Biology*

Complete genome of *Polaromonas vacuolata* KCTC 22033^T isolated from beneath Antarctic Sea ice

Hwang, Kyuin., Choe, Hanna., Nasir, Arshan. and **Kim, Kyung Mo.**

Marine Genomics. 2021. 55.
doi: 10.1016/j.margen.2020.100790.

Polaromonas vacuolata KCTC 22033^T is an obligate aerobic, Gram-negative, psychrophilic and rod-shaped bacterium isolated from beneath the sea ice off the coast of the Palmer Peninsula, Anvers Islands, Antarctica. *P. vacuolata* is the type species of *Polaromonas* genus and the first example of gas vacuolate *Betaproteobacteria* isolated from marine habitats. Here, we report a complete genome of *P. vacuolata* KCTC 22033^T, which consists of 3,837,686 bp (G + C content of 52.07%) with a single chromosome, 3461 protein-coding genes, 56 tRNAs and 6 rRNA operons. Genomic analysis revealed the presence of genes involved in bacterial adaptation under saline conditions, cold adaptation via the production of gas vesicles and cell adhesion proteins, and a photoheterotrophic lifestyle when challenged by starvation. Intriguingly, several of these genes were likely acquired from species outside the *Polaromonas* genus. The genomic information therefore describes the unique evolution and adaptation of *P. vacuolata* to its extraordinary habitat, i.e., beneath the Antarctic sea ice.

keywords: Betaine; Genome reduction; Horizontal gene transfer; Psychrophile; Rhodopsin

4-22 *Genetics & Heredity; Marine & Freshwater Biology*

Complete genome sequence of *Paenibacillus xylanexedens* PAMC 22703, a xylan-degrading bacterium

Hwang, Junsang., **Shin, Seung Chul.** and 5 others.

Marine Genomics. 2021. 55.
doi: 10.1016/j.margen.2020.100788.

Paenibacillus is widely distributed in various environments and has the potential for use as a biotechnological agent in industrial processes. Here, we report the complete genome sequence of the marine bacterium, *Paenibacillus xylanexedens* PAMC 22703, which utilizes xylan. The *P. xylanexedens* PAMC 22703 strain was isolated from marine sediments. *P. xylanexedens* PAMC 22703 utilizes xylan as a carbon source to grow. The genome sequence clarified that this strain possesses genes for utilizing xylan. The complete genome sequence contained one chromosome (7,053,622 bp with 46.0% GC content)

and one plasmid (44,617 bp with 44.1% C + G content). The genome harbored genes that fully deploy the xylan assimilation pathway. The complete genome sequence of *P. xylanexedens* PAMC 22703 would prove useful in acquiring information for its application with xylan in various industries.

keywords: Metabolic pathway; *Paenibacillus xylanexedens*; Xylan; Xylose utilization

4-23 *Microbiology*

Complete genome sequencing and comparative CAZyme analysis of *Rhodococcus* sp. PAMC28705 and PAMC28707 provide insight into their biotechnological and phytopathogenic potential

Ghimire, Nisha., Han, So-Ra., Kim, Byeollee., Jung, Sang-Hee., Park, Hyun., **Lee, Jun Hyuck.** and Oh, Tae-Jin.

Archives of Microbiology. 2021. 203(4): 1731-1742.
doi: 10.1007/s00203-020-02177-3.

Study of carbohydrate-active enzymes (CAZymes) can reveal information about the lifestyle and behavior of an organism. *Rhodococcus* species is well known for xenobiotic metabolism; however, their carbohydrate utilization ability has been less discussed till date. This study aimed to present the CAZyme analysis of two *Rhodococcus* strains, PAMC28705 and PAMC28707, isolated from lichens in Antarctica, and compare them with other *Rhodococcus*, *Mycobacterium*, and *Corynebacterium* strains. Genome-wide computational analysis was performed using various tools. Results showed similarities in CAZymes across all the studied genera. All three genera showed potential for significant polysaccharide utilization, including starch, cellulose, and pectin referring their biotechnological potential. Keeping in mind the pathogenic strains listed across all three genera, CAZymes associated to pathogenicity were analyzed too. Cutinase enzyme, which has been associated with phytopathogenicity, was abundant in all the studied organisms. CAZyme gene cluster of *Rhodococcus* sp. PAMC28705 and *Rhodococcus* sp. PAMC28707 showed the insertion of cutinase in the cluster, further supporting their possible phytopathogenic properties.

keywords: CAZyme; *Rhodococcus*; Polysaccharide; Biotechnological potential; Cutinase; Phytopathogenic property

4-24 *Genetics & Heredity*

Complete mitochondrial genome of the marine polychaete, *Nereis zonata* (Phyllodocida, Nereididae) isolated from the Beaufort Sea

Nam, Sang-Eun., Lee, Somyeong., **Park, Tae-Yoon S.** and Rhee, Jae-Sung.

Mitochondrial DNA Part B-Resources. 2021. 6(1): 231-233.
doi: 10.1080/23802359.2020.1861994.

Here, we present the first whole mitogenome sequence of the marine polychaete, *Nereis zonata*, isolated from the Beaufort Sea. The mitochondrial genome of *N. zonata* is 15,757 bp in length and consists of 13 protein-coding genes (PCGs), 22 transfer RNA (tRNA) genes, 2 ribosomal RNA (rRNA) genes, and a non-coding region that is typical of polychaetes. GC content of the *N. zonata* mitogenome is 37.2%. A maximum-likelihood gene tree based on the *N. zonata* mitogenome combined with previously published annelid mitogenome data revealed that *N. zonata* is clustered with *Cheilonereis cyclurus*, which form a sister group to *Nereis* sp.

keywords: Beaufort Sea; mitogenome; Nereididae; Nereis zonata; polychaete

4-25 *Genetics & Heredity*

The complete mitochondrial genome of the terebellid polychaete *Thelepus plagiostoma* (Terebellida; Terebellidae)

Nam, Sang-Eun., Park, Hyoung Sook., Kim, Sung Ah., **Kim, Bo-Mi**. and Rhee, Jae-Sung.

Mitochondrial DNA Part B-Resources. 2021. 6(11): 3114-3116.
doi: 10.1080/23802359.2021.1975510.

Here, we report the complete mitogenome information of the terebellid polychaete, *Thelepus plagiostoma* (Schmarda, 1861). Genome sequencing by Illumina HiSeq platform permitted assembly of a circular mitochondrial genome of 15,628 bp from *T. plagiostoma* consisting of 67% AT nucleotides, 13 protein-coding genes (PCGs), 2 ribosomal RNA (rRNA) genes, 22 transfer RNA (tRNA) genes, and a non-coding region in the typical annelid gene composition. Gene order of the *T. plagiostoma* mitochondrion is identical to those of the Terebelliformia mitogenomes.

Phylogenetic reconstruction places *T. plagiostoma* within the monophyletic subclass Sedentaria, a sister to *Pista cristata* in the suborder Terebelliformia.

keywords: Complete mitogenome; Terebellida; Terebellidae; *Thelepus plagiostoma*; polychaete

4-26 *Genetics & Heredity*

The complete mitochondrial genome of *Trematomus loennbergii* (Perciformes, Nototheniidae)

Choi, Eunkyung., Im, Tae-Eul., Lee, Seung Jae., Jo, Euna., Kim, Jinmu., Kim, Sun Hee., Chi, Young Min., **Kim, Jeong-Hoon.** and Park, Hyun.

Mitochondrial DNA Part B-Resources. 2021. 6(3): 1032-1033.
doi: 10.1080/23802359.2021.1899070.

The complete mitochondrial genome of *Trematomus loennbergii* was studied using NGS technology with PacBio platform. The mitochondrial genome size was 19,374bp and it had 13 protein-coding genes, 22 tRNAs and 2 rRNAs. There were 4 types of stop codons which were TAA, TAG, AGG and T(AA) but start codon type was only one (ATG). The contents of GC were 44.09% and AT contents were 55.91%. To conduct phylogenetic analysis, 12 species in 3 families were used. The result suggested that *T. loennbergii* was close to *Pagothenia borchgrevinki* in Nototheniidae. This study would provide a fundamental data for molecular evolution of *T. loennbergii*.

keywords: Mitochondrial genome; *Trematomus loennbergii*; Scaly rockcod; PacBio

4-27 *Biochemistry & Molecular Biology; Plant Sciences; Chemistry*

Compositional variation of atranorin-related components of lichen *Myelochroa leucotyliza* dependent on extraction solvent and their quantitative analysis by qHNMR

Ojha, Manju., Kil, Yun-Seo., **Youn, Ui Joung.** and 3 others.

Phytochemical Analysis. 2021. 32(6): 1067-1073.
doi: 10.1002/pca.3048.

Introduction: Quantitative nuclear magnetic resonance (qNMR) is one of the effective and reliable quantification tools for natural product research. *Myelochroa leucotyliza* belongs to the genus *Myelochroa*, a common foliose lichen genus found in the Korean Peninsula, and has not been quantitatively analysed using NMR. Previous chemical studies on *M. leucotyliza* have been limited to the main components by traditional thin-layer chromatography (TLC) experiments.
Objective: We explored the stability of atranorin, a major component of *M. leucotyliza*, in methanol and acetone using NMR and characterised the changes in the chemical profiles of the lichen extracts in methanol and acetone using qNMR.
Methodology: Atranorin transformation in the presence of methanol was analysed using time-dependent proton (^{1}H)-NMR analysis (600 MHz NMR spectrometer). A ^{1}H qNMR (qHNMR) method was established using dimethyl sulfone as the internal standard for quantifying the selected components isolated from *M. leucotyliza*. Homogenous mixtures of the samples were dissolved in deuterated chloroform.
Results: Time-dependent ^{1}H -NMR experiments revealed that atranorin (**5**) from lichen *M. leucotyliza* decomposed into atraric acid (**1**) and methyl haemmatommate (**2**) in methanol. Four components were identified from *M. leucotyliza*: **1**, **2**, usnic acid (**4**), and **5**, and their respective contents were determined using qHNMR. The percentages (*w/w*) of **1**, **2**, and **4** in the methanol extract were calculated as 5.66%, 0.69%, and 0.90%, while those of **1**, **4**, and **5** in the acetone extract were 1.70%, 1.68%, and 19.11%, respectively.
Conclusion: We used qHNMR to effectively analyse quantitative compositional variations in two different *M. leucotyliza* extracts and reliably determined the chemical conversion of the unstable compound atranorin.

keywords: atranorin; *Myelochroa leucotyliza*; qNMR

4-28 *Biotechnology & Applied Microbiology; Genetics & Heredity*

A computational approach to identify CRISPR-Cas loci in the complete genomes of the lichen-associated *Burkholderia* sp. PAMC28687 and PAMC26561

Shrestha, Prasansah., Han, So-Ra., **Lee, Jun Hyuck.** and 2 others.

Genomics. 2021. 113(3): 881-888.
doi: 10.1016/j.ygeno.2021.01.019.

The genus *Burkholderia* and its strains PAMC28687 and PAMC26561 are lichen-associated bacteria isolated from the Antarctic region. Our study is the first to provide the genome sequence of the *Burkholderia* sp. PAMC26561 strain. The genus *Burkholderia* includes bacteria that are pathogenic to plants, animals, and humans. Computational analysis of complete genomes of strains from the uncategorized *Burkholderia* group was performed using the NCBI databank and PATRIC (for genome sequence information) and CRISPRCasFinder (online and offline versions) software in order to predict the CRISPR loci and Cas genes. The RNAfold Webserver online software was used to predict RNA secondary structures. Our study showed that strain MSMB0852 (plasmid) possesses CRISPR-Cas system Class 2, and two lichen-associated strains, PAMC28687 (chromosome I) and PAMC26561 (chromosome I), possess CRISPR-Cas system Class 1. Additionally, only the two lichen-associated strains possess a variety of Cas genes.

keywords: CRISPR-Cas classification; *Burkholderia* PAMC26561; *Burkholderia* PAMC28687; Lichen

4-29 *Biochemistry & Molecular Biology; Environmental Sciences & Ecology; Evolutionary Biology*

Contrasting early successional dynamics of bacterial and fungal communities in recently deglaciated soils of the maritime Antarctic

Gyeong, Hyeryeon., Hyun, Chang-Uk., Kim, Seok Cheol., **Tripathi, Binu Mani.**, Yun, Jeongeun., Kim, Jinhyun., Kang, Hojeong., **Kim, Ji Hee.**, **Kim, Sanghee.** and **Kim, Mincheol.**

Molecular Ecology. 2021. 30(17): 4231-4244.
doi: 10.1111/mec.16054.

Although microorganisms are the very first colonizers of recently deglaciated soils even prior to plant colonization, the drivers and patterns of microbial community succession at early-successional stages remain poorly understood. The successional dynamics and assembly processes of bacterial and fungal communities were compared on a glacier foreland in the maritime Antarctic across the ~10-year soil-age gradient from bare soil to sparsely vegetated area. Bacterial communities shifted more rapidly than fungal communities in response to glacial retreat; species turnover (primarily the transition from glacier-to soil-favouring taxa) contributed greatly to bacterial beta diversity, but this pattern was less clear in fungi. Bacterial communities underwent more predictable (more deterministic) changes along the soil-age gradient, with compositional changes paralleling the direction of changes in soil physicochemical properties following deglaciation. In contrast, the compositional shift in fungal communities was less associated with changes in deglaciation-induced changes in soil geochemistry and most fungal taxa displayed mosaic abundance distribution across the landscape, suggesting that the successional dynamics of fungal communities are largely governed by stochastic processes. A co-occurrence network analysis revealed that biotic interactions between bacteria and fungi are very weak in early succession. Taken together, these results collectively suggest that bacterial and fungal communities in recently deglaciated soils are largely decoupled from each other during succession and exert very divergent trajectories of succession and assembly under different selective forces.

keywords: bacterial community; fungal community; glacier foreland; microbial ecology; microbial succession

4-30 *Chemistry; Crystallography; Materials Science*

Crystal structure of a MarR family protein from the psychrophilic bacterium *Paenisporosarcina* sp. TG-14 in complex with a lipid-like molecule

Hwang, Jisub., **Park, Sun-Ha.**, **Lee, Chang Woo.**, **Do, Hackwon.**, **Shin, Seung Chul.**, **Kim, Han-Woo.**, **Lee, Sung Gu.**, Park, Hyun Ho., Kwon, Sung-hark. and **Lee, Jun Hyuck.**

Iucrj. 2021. 8: 842-852.
doi: 10.1107/s2052252521005704.

MarR family proteins regulate the transcription of multiple antibiotic-resistance genes and are widely found in bacteria and archaea. Recently, a new MarR family gene was identified by genome analysis of the psychrophilic bacterium *Paenisporosarcina* sp. TG-14, which was isolated from sediment-laden basal ice in Antarctica. In this study, the crystal structure of the MarR protein from *Paenisporosarcina* sp. TG-14 (*Pa*MarR) was determined at 1.6 Å resolution. In the crystal structure, a novel lipid-type compound (palmitic acid) was found in a deep cavity, which was assumed to be an effector-binding site. Comparative

structural analysis of homologous MarR family proteins from a mesophile and a hyperthermophile showed that the DNA-binding domain of *Pa*MarR exhibited relatively high mobility, with a disordered region between the β1 and β2 strands. In addition, structural comparison with other homologous complex structures suggests that this structure constitutes a conformer transformed by palmitic acid. Biochemical analysis also demonstrated that *Pa*MarR binds to cognate DNA, where *Pa*MarR is known to recognize two putative binding sites depending on its molar concentration, indicating that *Pa*MarR binds to its cognate DNA in a stoichiometric manner. The present study provides structural information on the cold-adaptive MarR protein with an aliphatic compound as its putative effector, extending the scope of MarR family protein research.

keywords: MarR family proteins; transcription factors; psychrophilic bacteria; *Paenisporosarcina* sp. TG-14; palmitic acid; conformational change; protein structure; molecular recognition.

4-31 *Biochemistry & Molecular Biology; Biophysics*

Crystal structure of a novel putative sugar isomerase from the psychrophilic bacterium *Paenibacillus* sp. R4

Kwon, Sunghark., Ha, Hyun Ji., Kang, Yong Jun., Sung, Ji Hye., **Hwang, Jisub.**, **Lee, Min Ju.**, **Lee, Jun Hyuck.** and Park, Hyun Ho.

Biochemical and Biophysical Research Communications. 2021. 585: 48-54.

doi: 10.1016/j.bbrc.2021.11.026.

Sugar isomerases (SIs) catalyze the reversible conversion of aldoses to ketoses. A novel putative SI gene has been identified from the genome sequence information on the psychrophilic bacterium *Paenibacillus* sp. R4. Here, we report the crystal structure of the putative SI from *Paenibacillus* sp. R4 (*Pb*SI) at 2.98 Å resolution. It was found that the overall structure of *Pb*SI adopts the triose-phosphate isomerase (TIM) barrel fold. *Pb*SI was also identified to have two heterogeneous metal ions as its cofactors at the active site in the TIM barrel, one of which was confirmed as a Zn ion through X-ray anomalous scattering and inductively coupled plasma mass spectrometry analysis. Structural comparison with homologous SI proteins from mesophiles, hyperthermophiles, and a psychrophile revealed that key residues in the active site are well conserved and that dimeric *Pb*SI is devoid of the extended C-terminal region, which tetrameric SIs commonly have. Our results provide novel structural information on the cold-adaptable SI, including information on the metal composition in the active site.

keywords: Sugar isomerase; Xylose isomerase; Glucose isomerase; *Paenibacillus*; Psychrophilic bacteria; Cold adaptation

4-32 *Biochemistry & Molecular Biology; Endocrinology & Metabolism*

Crystal structure of an apo 7α-hydroxysteroid dehydrogenase reveals key structural changes induced by substrate and co-factor binding

Kim, Ki-Hwa., **Lee, Chang Woo.**, Pardhe, Bashu Dev., **Hwang, Jisub.**, **Do, Hackwon.**, **Lee, Yung Mi.**, **Lee, Jun Hyuck.** and Oh, Tae-Jin.

Journal of Steroid Biochemistry and Molecular Biology. 2021. 212.

doi: 10.1016/j.jsbmb.2021.105945.

7α -Hydroxysteroid dehydrogenase (7α-HSDH) catalyzes the dehydrogenation of a hydroxyl group at the 7α position in steroid substrates using NAD^+ or $NADP^+$ as a co-factor. Although studies have determined the binary and ternary complex structures, detailed structural changes induced by ligand and co-factor binding remain unclear, because ligand-free structures are not yet available. Here, we present the crystal structure of apo 7α-HSDH from *Escherichia coli* (*Eco*-7α-HSDH) at 2.7 Å resolution. We found that the apo form undergoes substantial conformational changes in the β4-α4 loop, α7-α8 helices, and C-terminus loop among the four subunits comprising the tetramer. Furthermore, a comparison of the apo structure with the binary (NAD^+)-complex and ternary (NADH and 7-oxoglycochenodeoxycholic acid)-complex *Eco*-7α -HSDH structures revealed that only the ternary-complex structure has a fully closed conformation, whereas the binary-complex and apo structures have a semi-closed or open conformation. This open-to-closed transition forces several catalytically important residues (S146, Y159, and K163) into correct positions for catalysis. To confirm the catalytic activity, we used alcohol dehydrogenase

for NAD^+ regeneration to allow efficient conversion of chenodeoxycholic acid to 7-ketolithocholic acid by *Eco*-7α-HSDH. These findings demonstrate that apo *Eco*-7α-HSDH exhibits intrinsically flexible characteristics with an open conformation. This structural information provides novel insight into the 7α-HSDH reaction mechanism.

keywords: Crystal structure; Conformational change; 7α-hydroxysteroid dehydrogenase; X-ray crystallography

4-33 *Microbiology*

Different Biochemical Compositions of Particulate Organic Matter Driven by Major Phytoplankton Communities in the Northwestern Ross Sea

Jo, Naeun., **La, Hyoung Sul.**, **Kim, Jeong-Hoon.**, Kim, Kwanwoo., **Kim, Bo Kyung.**, Kim, Myung Joon., **Son, Wuju.** and Lee, Sang Heon.

Frontiers in Microbiology. 2021. 12.
doi: 10.3389/fmicb.2021.623600.

Marine particulate organic matter (POM) largely derived from phytoplankton is a primary food source for upper trophic consumers. Their biochemical compositions are important for heterotrophs. Especially, essential amino acids (EAAs) in phytoplankton are well known to have impacts on the survival and egg productions of herbivorous zooplankton. To estimate the nutritional quality of POM, the biochemical compositions [biomolecular and amino acid (AA) compositions] of POM were investigated in the northwestern Ross Sea during the late austral summer in 2018. Carbohydrates (CHO) accounted for the highest portion among different biomolecules [CHO, proteins (PRT), and lipids (LIP)] of POM. However, the higher contribution of PRT and lower contribution of CHO were observed in the southern section of our study area compared to those in the northern section. The spatial distribution of total hydrolyzable AAs in POM was considerably influenced by phytoplankton biomass, which indicates that the main source of particulate AA was generated by phytoplankton. Our results showed that the relative contribution of EAA to the total AAs was strongly associated with EAA index (EAAI) for determining protein quality. This result indicates that higher EAA contribution in POM suggests a better protein quality in consistency with high EAAI values. In this study, variations in the biochemical compositions in POM were principally determined by two different bloom-forming taxa (diatoms and *Phaeocystis antarctica*). The southern region dominated majorly by diatoms was positively correlated with PRT, EAA, and EAAI indicating a good protein quality, while *P. antarctica*-abundant northern region with higher CHO contribution was negatively correlated with good protein quality factors. Climate-driven environmental changes could alter not only the phytoplankton community but also the physiological conditions of phytoplankton. Our findings could provide a better understanding for future climate-induced changes in the biochemical compositions of phytoplankton and consequently their potential impacts on higher trophic levels.

keywords: phytoplankton; biomolecular composition; amino acid composition; food quality; Ross Sea

4-34 *Biodiversity & Conservation; Environmental Sciences & Ecology*

Disproportionate microbial responses to decadal drainage on a Siberian floodplain

Kwon, Min Jung., **Tripathi**, **Binu Mani.**, Goeckede, Mathias., **Shin, Seung Chul.**, **Myeong, Nu Ri.**, **Lee, Yoo Kyung.** and **Kim, Mincheol.**

Global Change Biology. 2021. 27(20): 5124-5140.
doi: 10.1111/gcb.15785.

Permafrost thaw induces soil hydrological changes which in turn affects carbon cycle processes in the Arctic terrestrial ecosystems. However, hydrological impacts of thawing permafrost on microbial processes and greenhouse gas (GHG) dynamics are poorly understood. This study examined changes in microbial communities using gene and genome-centric metagenomics on an Arctic floodplain subject to decadal drainage, and linked them to CO_2 and CH_4 flux and soil chemistry. Decadal drainage led to significant changes in the abundance, taxonomy, and functional potential of microbial communities, and these modifications well explained the changes in CO_2 and CH_4 fluxes between ecosystem and atmosphere—increased fungal abundances potentially increased net CO_2 emission rates and highly reduced CH_4 emissions in drained sites corroborated the marked decrease in the abundance of methanogens and methanotrophs. Interestingly, various microbial taxa disproportionately responded to drainage: *Methanoregula*, one of the key players in methanogenesis under saturated conditions,

almost disappeared, and also *Methylococcales* methanotrophs were markedly reduced in response to drainage. Seven novel methanogen population genomes were recovered, and the metabolic reconstruction of highly correlated population genomes revealed novel syntrophic relationships between methanogenic archaea and syntrophic partners. These results provide a mechanistic view of microbial processes regulating GHG dynamics in the terrestrial carbon cycle, and disproportionate microbial responses to long-term drainage provide key information for understanding the effects of warming-induced soil drying on microbial processes in Arctic wetland ecosystems.

keywords: CO_2 and CH_4 flux; long-term drainage; metagenome-assembled genomes; methanogens; permafrost thaw; soil microbiome

4-35 *Microbiology*

Distinct Microbial Communities in Adjacent Rock and Soil Substrates on a High Arctic Polar Desert

Choe, Yong-Hoe., **Kim, Mincheol.** and **Lee, Yoo Kyung.**

Frontiers in Microbiology. 2021. 11.
doi: 10.3389/fmicb.2020.607396.

Understanding microbial niche variability in polar regions can provide insights into the adaptive diversification of microbial lineages in extreme environments. Compositions of microbial communities in Arctic soils are well documented but a comprehensive multidomain diversity assessment of rocks remains insufficiently studied. In this study, we obtained two types of rocks (sandstone and limestone) and soils around the rocks in a high Arctic polar desert (Svalbard), and examined the compositions of archaeal, bacterial, fungal, and protistan communities in the rocks and soils. The microbial community structure differed significantly between rocks and soils across all microbial groups at higher taxonomic levels, indicating that Acidobacteria, Gemmatimonadetes, Latescibacteria, Rokubacteria, Leotiomycetes, Pezizomycetes, Mortierellomycetes, Sarcomonadea, and Spirotrichea were more abundant in soils, whereas Cyanobacteria, Deinococcus-Thermus, FBP, Lecanoromycetes, Eurotiomycetes, Trebouxiophyceae, and Ulvophyceae were more abundant in rocks. Interestingly, fungal communities differed markedly between two different rock types, which is likely to be ascribed to the predominance of distinct lichen-forming fungal taxa (Verrucariales in limestone, and Lecanorales in sandstone). This suggests that the physical or chemical properties of rocks could be a major determinant in the successful establishment of lichens in lithic environments. Furthermore, the biotic interactions among microorganisms based on co-occurrence network analysis revealed that *Polyblastia* and *Verrucaria* in limestone, and *Atla*, *Porpidia*, and *Candelariella* in sandstone play an important role as keystone taxa in the lithic communities. Our study shows that even in niches with the same climate regime and proximity to each other, heterogeneity of edaphic and lithic niches can affect microbial community assembly, which could be helpful in comprehensively understanding the effects of niche on microbial assembly in Arctic terrestrial ecosystems.

keywords: polar desert; lithic niche; edaphic niche; rock microbes; Arctic

4-36 *Microbiology*

Diversity and Physiological Characteristics of Antarctic Lichens-Associated Bacteria

Noh, Hyun-Ju., **Park, Yerin.**, **Hong, Soon Gyu.** and **Lee, Yung Mi.**

Microorganisms. 2021. 9(3).
doi: 10.3390/microorganisms9030607.

The diversity of lichen-associated bacteria from lichen taxa *Cetraria*, *Cladonia*, *Megaspora*, *Pseudephebe*, *Psoroma*, and *Sphaerophorus* was investigated by sequencing of 16S *rRNA* gene amplicons. Physiological characteristics of the cultured bacterial isolates were investigated to understand possible roles in the lichen ecosystem. Proteobacteria (with a relative abundance of 69.7–96.7%) were mostly represented by the order Rhodospirillales. The 117 retrieved isolates were grouped into 35 phylotypes of the phyla Actinobacteria (27), Bacteroidetes (6), Deinococcus-Thermus (1), and Proteobacteria (Alphaproteobacteria (53), Betaproteobacteria (18), and Gammaproteobacteria (12)). Hydrolysis of macromolecules such as skim milk, polymer, and (hypo)xanthine, solubilization of inorganic phosphate, production of phytohormone indole-3-acetic acid, and fixation of atmospheric nitrogen were observed in different taxa. The potential phototrophy of the

strains of the genus *Polymorphobacter* which were cultivated from a lichen for the first time was revealed by the presence of genes involved in photosynthesis. Altogether, the physiological characteristics of diverse bacterial taxa from Antarctic lichens are considered to imply significant roles of lichen-associated bacteria to allow lichens to be tolerant or competitive in the harsh Antarctic environment.

keywords: Antarctic lichens; lichen-associated bacteria; macromolecule hydrolysis; indole-3-acetic acid; phosphate solubilization; nitrogen fixation.

4-37

Draft Genome Sequence of the Chitin Degrading Psychrotolerant Bacterium *Pedobacter jejuensis* TN23 Isolated from Antarctic Soil

Cho, Ahnna., Cho, Yong-Joon. and **Kim, Ok-Sun.**

Microbiology Resource Announcements. 2021.10(26).
doi: 10.1128/MRA.00523-21.

Pedobacter jejuensis TN23 was isolated from soil from Terra Nova Bay, Victoria Land, Antarctica. The assembled draft genome size is 4,795,808 bp, and it contains a total of 4,095 genes with 3,970 coding sequences, including genes putatively involved in the degradation of chitin.

4-38 *Life Sciences & Biomedicine*

Draft genome sequence of *Aurantimonas coralicida* DM33-3 isolated from Amundsen Sea Polynya

Kim, So-Jeong., Kim, Jong-Geol., Jung, Gi-Yong., **Park, Jisoo.** and **Yang, Eun Jin.**

Korean Journal of Microbiology. 2021. 57(2): 116-118.
doi: 10.7845/kjm.2021.1024.

Here, we report the draft genome sequence of *Aurantimonas coralicida* DM33-3 isolated from Amundsen Sea Polynya. The genome size is 4,620,302 bp, 4,415 coding sequences, one rRNA operon (additionally two 5S ribosomal RNA genes), and 45 tRNA genes. Genes related to manganese oxidation and thiosulfate oxidation are also included in the genome. The genome harbors genes coding for enzymes having varying affinities to oxygen and nitrate reduction. This showed that strain DM33-3 might play the potential role in biogeochemical cycling (manganese, sulfur and nitrogen cycle) in the Amundsen Sea Polynya.

keywords: *Aurantimonas coralicida*; Antarctica; Polynya

4-39 *Science & Technology*

Dynamic bacterial community response to *Akashiwo sanguinea* (Dinophyceae) bloom in indoor marine microcosms

Jung, Seung Won., Kang, Junsu., Park, Joon Sang., **Joo, Hyoung Min.** and 4 others.

Scientific Reports. 2021. 11(1).
doi: 10.1038/s41598-021-86590-8.

We investigated the dynamics of the bacterial composition and metabolic function within *Akashiwo sanguinea* bloom using a 100-L indoor microcosm and metagenomic next-generation sequencing. We found that the bacterial community was classified into three groups at 54% similarity. Group I was associated with "during the A. sanguinea bloom stage" and mainly consisted of Alphaproteobacteria, Flavobacteriia and Gammaproteobacteria. Meanwhile, groups II and III were associated with the "late bloom/decline stage to post-bloom stage" with decreased Flavobacteriia and Gammaproteobacteria in these stages. Upon the termination of the A. *sanguinea* bloom, the concentrations of inorganic nutrients (particularly PO_4^{3-}, NH_4^+ and dissolved organic carbon) increased rapidly and then decreased. From the network analysis, we found that the A. *sanguinea* node is associated with certain bacteria. After the bloom, the specific increases in NH_4^+ and PO_4^{3-} nodes are associated with other bacterial taxa. The changes in the functional groups of the bacterial community from chemoheterotrophy to nitrogen association metabolisms were consistent with the environmental impacts during and after A. *sanguinea* bloom. Consequently, certain bacterial communities and the environments dynamically changed during and after harmful algal blooms and a rapid turnover within the bacterial community and their function can respond to ecological interactions.

4-40 *Fisheries*

Enzymes and Their Reaction Mechanisms in Dimethylsulfoniopropionate Cleavage and Biosynthesis of Dimethylsulfide by Marine Bacteria

Do, Hackwon., **Hwang, Jisub.**, **Lee, Sung Gu.** and **Lee, Jun Hyuck.**

Journal of Marine Life Science. 2021. 6(1): 1-8.
doi: 10.23005/ksmls.2021.6.1.1.

In marine ecosystems, the biosynthesis and catabolism of dimethylsulfoniopropionate (DMSP) by marine bacteria is critical to microbial survival and the ocean food chain. Furthermore, these processes also influence sulfur recycling and climate change. Recent studies using emerging genome sequencing data and extensive bioinformatics analysis have enabled us to identify new DMSP-related genes. Currently, seven bacterial DMSP lyases (DddD, DddP, DddY, DddK, DddL, DddQ and DddW), two acrylate degrading enzymes (DddA and DddC), and four demethylases (DmdA, DmdB, DmdC, and DmdD) have been identified and characterized in diverse marine bacteria. In this review, we focus on the biochemical properties of DMSP cleavage enzymes with special attention to DddD, DddA, and DddC pathways. These three enzymes function in the production of acetyl coenzyme A (CoA) and CO_2 from DMSP. DddD is a DMSP lyase that converts DMSP to 3-hydroxypropionate with the release of dimethylsulfide. 3-Hydroxypropionate is then converted to malonate semialdehyde by DddA, an alcohol dehydrogenase. Then, DddC transforms malonate semialdehyde to acetyl-CoA and CO_2 gas. DddC is a putative methylmalonate semialdehyde dehydrogenase that requires nicotinamide adenine dinucleotide and CoA cofactors. Here we review recent insights into the structural characteristics of these enzymes and the molecular events of DMSP degradation.

keywords: Dimethylsulfide; Dimethylsulfoniopropionate; Molecular modeling; Methylmalonate semialdehyde dehydrogenase; Sulfur recycle

4-41 *Chemistry*

Ergopyrone, a Styrylpyrone-Fused Steroid with a Hexacyclic 6/5/6/6/6/5 Skeleton from a Mushroom *Gymnopilus orientispectabilis*

Lee, Seulah., Kim, Chung Sub., Yu, Jae Sik., Kang, Hee-sun., Yoo, Min Jeong., **Youn, Ui Joung.** and 3 others.

Organic Letters. 2021. 23(9): 3315-3319.
doi: 10.1021/acs.orglett.1c00790.

A styrylpyrone-fused ergosterol derivative, ergopyrone (**1**), was isolated and structurally characterized from a mushroom, *Gymnopilus orientispectabilis*, along with five biosynthetically related metabolites (**2**–**6**). Compound **1** features an unprecedented hexacyclic 6/5/6/6/6/5 skeleton that would be formed from ergosterol and styrylpyrone precursors via [3 + 2] cycloaddition. The chemical structure of **1** was elucidated by conventional spectroscopic and spectrometric data analysis coupled with computational methods including DP4+ probability and ECD simulation and an NOE/ROE-based interproton distance measurement technique via peak amplitude normalization for the improved cross-relaxation (PANIC) method. Plausible biosynthetic pathways of **1**–**6** are proposed, and compound **6** significantly regulated lipid metabolism in adipocytes through the upregulation of the mRNA expression of *Adipsin*, *Fabp4*, *SREBP1*, and *ATGL*.

4-42 *Zoology*

Feather mites (Acariformes, Astigmata) from marine birds of the Barton Peninsula (King George Island, Antarctica), with descriptions of two new species

Han, Yeong-Deok., Mironov, Sergey V., **Kim, Jeong-Hoon.** and Min, Gi-Sik.

ZOOKEYS. 2021.1061: 109-130.
doi: 10.3897/zookeys.1061.71212.

We report on the first investigation of feather mites associated with birds living on the Barton Peninsula (King George Island, Antarctica). We found seven feather mite species of the superfamily Analgoidea from four host species. Two new species are described from two charadriiform hosts: *Alloptes (Sternalloptes) antarcticus* **sp. nov.** (Alloptidae) from *Stercorarius*

maccormicki Saunders (Stercorariidae), and *Ingrassia chionis* **sp. nov.** (Xolalgidae) from *Chionis albus* (Gmelin) (Chionidae). Additionally, we provide partial sequences of the mitochondrial cytochrome c oxidase subunit I (COI), which was utilized as a DNA barcode, for all seven feather mite species.

keywords: *Alloptes*; Analgoidea; Antarctica; feather mites; *Ingrassia*; systematics

4-43 *Genetics & Heredity*

The first complete mitochondrial genome from the family Solasteridae, *Crossaster papposus* (Echinodermata, Asteroidea)

Nam, Sang-Eun., Kim, Sung Ah., **Park, Tae-Yoon S.** and Rhee, Jae-Sung.

Mitochondrial DNA Part B-Resources. 2021. 6(1): 45-47.
doi: 10.1080/23802359.2020.1846001.

The common sunstar, *Crossaster papposus*, belongs to the family Solasteridae whose ordinal classification has been unstable. Here, for the first time, we assembled and annotated the complete mitochondrial genome of the common sunstar, *C. papposus* Linnaeus, 1767. The circular genome of *C. papposus* is 16,335 bp in length and contains 13 protein-coding genes (PCGs), 22 transfer RNA (tRNA) genes, a control region, and large and small ribosomal subunits. The overall genomic structure and gene arrangement were identical to the reported mitochondrial genomes of sea star species, and a phylogenetic analysis of 13 PCGs recovers a closest relationship with the derived cluster of the paraphyletic order Valvatida.

keywords: Mitochondrion; sunstar; Valvatida; Solasteridae; phylogeny

4-44 *Agriculture; Veterinary Sciences; Zoology*

A First Genome Survey and Genomic SSR Marker Analysis of *Trematomus loennbergii* Regan, 1913

Choi, Eunkyung., Kim, Sun Hee., Lee, Seung Jae., **Jo, Euna.**, Kim, Jinmu., **Kim, Jeong-Hoon.** and 3 others.

Animals. 2021. 11(11).
doi: 10.3390/ani11113186.

Trematomus loennbergii Regan, 1913, is an evolutionarily important marine fish species distributed in the Antarctic Ocean. However, its genome has not been studied to date. In the present study, whole genome sequencing was performed using next-generation sequencing (NGS) technology to characterize its genome and develop genomic microsatellite markers. The 25-mer frequency distribution was estimated to be the best, and the genome size was predicted to be 815,042,992 bp. The heterozygosity, average rate of read duplication, and sequencing error rates were 0.536%, 0.724%, and 0.292%, respectively. These data were used to analyze microsatellite markers, and a total of 2,264,647 repeat motifs were identified. The most frequent repeat motif was di-nucleotide with 87.00% frequency, followed by tri-nucleotide (10.45%), tetra-nucleotide (1.94%), penta-nucleotide (0.34%), and hexa-nucleotide (0.27%). The AC repeat motif was the most abundant motif among di-nucleotides and among all repeat motifs. Among microsatellite markers, 181 markers were selected and PCR technology was used to validate several markers. A total of 15 markers produced only one band. In summary, these results provide a good basis for further studies, including evolutionary biology studies and population genetics of Antarctic fish species.

keywords: *Trematomus loennbergii*; scaly rockcod; repeat motif; SSR; microsatellite; Illumina

4-45 *Biochemistry & Molecular Biology; Research & Experimental Medicine; Pharmacology & Pharmacy*

Generation of Stilbene Glycoside with Promising Cell Rejuvenation Activity through Biotransformation by the Entomopathogenic Fungus *Beauveria bassiana*

Ha, Sang Keun., Kang, Min Cheol., **Lee, Seulah.** and 5 others.

Biomedicines. 2021. 9(5).
doi: 10.3390/biomedicines9050555.

A stilbene glycoside (resvebassianol A) (**1**) with a unique sugar unit, 4-*O*-methyl-D-glucopyranose, was identified through biotransformation of resveratrol (RSV) by the entomopathogenic fungus *Beauveria bassiana* to obtain a superior RSV metabolite with enhanced safety. Its structure, including its absolute configurations, was determined using spectroscopic data, HRESIMS, and chemical reactions. Microarray analysis showed that the expression levels of

filaggrin, HAS2-AS1, and CERS3 were higher, while those of IL23A, IL1A, and CXCL8 were lower in the resvebassianol A-treated group than in the RSV-treated group, as confirmed by qRT-PCR. Compound **1** exhibited the same regenerative and anti-inflammatory effects as RSV with no cytotoxicity in skin keratinocytes and TNF-α/IFN-γ-stimulated HIEC-6 cells, suggesting that compound **1** is a safe and stable methylglycosylated RSV. Our findings suggest that our biotransformation method can be an efficient biosynthetic platform for producing a broad range of natural glycosides with enhanced safety.

keywords: Beauveria bassiana; resveratrol; biotransformation; microarray analysis; cell rejuvenation

4-46 *Agriculture; Veterinary Sciences; Zoology*

Genome of the Southern Giant Petrel Assembled Using Third-Generation DNA Sequencing and Linked Reads Reveals Evolutionary Traits of Southern Avian

Kim, Sun-Hee., Lee, Seung-Jae., **Jo, Euna.**, Kim, Jangyeon., **Kim, Jong-U.**, **Kim, Jeong-Hoon.** and 2 others.

Animals. 2021. 11(7).
doi: 10.3390/ani11072046.

The southern giant petrel *Macronectes giganteus*, a large seabird of the southern oceans, is one of only two members of the genus *Macronectes* and is the largest species in the order Procellariiformes. Although these two families account for the vast majority of the avian fauna inhabiting the Antarctic and sub-Antarctic regions, studies on the status of some populations and the associated genetic data are currently extremely limited. In this study, we assembled the genome of *M. giganteus* by integrating Pacific Biosciences single-molecule real-time sequencing and the Chromium system developed by 10x Genomics. The final *M. giganteus* genome assembly was 1.248 Gb in size with a scaffold N50 length of 27.4 Mb and a longest scaffold length of 120.4 Mb. The *M. giganteus* genome contains 14,993 predicted protein-coding genes and has 11.06% repeat sequences. Estimated historical effective population size analysis indicated that the southern giant petrel underwent a severe reduction in effective population size during a period coinciding with the early Pleistocene. The availability of this newly sequenced genome will facilitate more effective genetic monitoring of threatened species. Furthermore, the genome will provide a valuable resource for gene functional studies and further comparative genomic studies on the life history and ecological traits of specific avian species.

keywords: southern giant petrel; *Macronectes giganteus*; genome assembly; annotation; PacBio sequencing; 10x Genomics Chromium technology

4-47 *Biochemistry & Molecular Biology; Cell Biology*

Genome survey and microsatellite motif identification of *Pogonophryne albipinna*

Jo, Euna., Cho, Yll Hwan., Lee, Seung Jae., Choi, Eunkyung., Kim, Jinmu., **Kim, Jeong-Hoon.** and 2 others.

Bioscience Reports. 2021. 41(7).
doi: 10.1042/bsr20210824.

The genus *Pogonophryne* is a speciose group that includes 28 species inhabiting the coastal or deep waters of the Antarctic Southern Ocean. The genus has been divided into five species groups, among which the *P. albipinna* group is the most deep-living group and is characterized by a lack of spots on the top of the head. Here, we carried out genome survey sequencing of *P. albipinna* using the Illumina HiSeq platform to estimate the genomic characteristics and identify genome-wide microsatellite motifs. The genome size was predicted to be ~883.8 Mb by K-mer analysis (K = 25), and the heterozygosity and repeat ratio were 0.289 and 39.03%, respectively. The genome sequences were assembled into 571624 contigs, covering a total length of ~819.3 Mb with an N50 of 2867 bp. A total of 2217422 simple sequence repeat (SSR) motifs were identified from the assembly data, and the number of repeats decreased as the length and number of repeats increased. These data will provide a useful foundation for the development of new molecular markers for the *P. albipinna* group as well as for further whole-genome sequencing of *P. albipinna*.

4-48 *Biochemistry & Molecular Biology*

Identification and Characterization of a Novel, Cold-Adapted D-Xylobiose- and D-Xylose-Releasing Endo-β-1,4-Xylanase from an Antarctic Soil Bacterium, *Duganella* sp. PAMC 27433

Kim, Do Young., Kim, Jonghoon., **Lee, Yung Mi.** and 5 others.

Biomolecules. 2021. 11(5).
doi: 10.3390/biom11050680.

Endo-β-1,4-xylanase is a key enzyme in the degradation of β-1,4-D-xylan polysaccharides through hydrolysis. A glycoside hydrolase family 10 (GH10) endo-β-1,4-xylanase (XylR) from *Duganella* sp. PAMC 27433, an Antarctic soil bacterium, was identified and functionally characterized. The XylR gene (1122-bp) encoded an acidic protein containing a single catalytic GH10 domain that was 86% identical to that of an uncultured bacterium BLR13 endo-β-1,4-xylanase (ACN58881). The recombinant enzyme (rXylR: 42.0 kDa) showed the highest beechwood xylan-degrading activity at pH 5.5 and 40 °C, and displayed 12% of its maximum activity even at 4 °C. rXylR was not only almost completely inhibited by 5 mM *N*-bromosuccinimide or metal ions (each 1 mM) including Hg^{2+}, Ca^{2+}, or Cu^{2+} but also significantly suppressed by 1 mM Ni^{2+}, Zn^{2+}, or Fe^{2+}. However, its enzyme activity was upregulated (>1.4-fold) in the presence of 0.5% Triton X-100 or Tween 80. The specific activities of rXylR toward beechwood xylan, birchwood xylan, oat spelts xylan, and *p*-nitrophenyl-β-D-cellobioside were 274.7, 103.2, 35.6, and 365.1 U/mg, respectively. Enzymatic hydrolysis of birchwood xylan and d-xylooligosaccharides yielded d-xylose and d-xylobiose as the end products. The results of the present study suggest that rXylR is a novel cold-adapted d-xylobiose- and d-xylose-releasing endo-β-1,4-xylanase.

keywords: Antarctic bacterium; *Duganella* sp.; GH10; cold-adapted; endo-β-1,4-xylanase

4-49 *Plant Sciences*

Improvement of moss photosynthesis by humic acids from Antarctic tundra soil

Byun, Mi Young., **Kim, Dockyu.**, **Youn, Ui Joung.**, **Lee, Seulah.** and **Lee, Hyoungseok.**

Plant Physiology and Biochemistry. 2021. 159: 37-42.
doi: 10.1016/j.plaphy.2020.12.007.

There have been several published reports regarding the growth promoting effect of humic acids (HA) on vascular plants; however, the effect of HA on bryophytes is still unknown. Due to the ecological importance of mosses, which dominate the Antarctic flora, we assessed the effectiveness of HA as a biostimulant using three moss species: Antarctic *Ceratodon purpureus* KMA5038, Arctic *Bryum* sp. KMR5045, and *Physcomitrella patens* which inhabits temperate regions. Natural HA (KS1-3_HA) were extracted through acidic precipitation of alkaline extracts from Antarctic tundra soil. Spectroscopic structural properties of KS1-3_HA were characterized and determined to possess several functional groups such as hydroxyl (R–OH) and carboxyl (R–COOH), implying they could have a growth-related biological function. For two polar mosses, increasing HA concentrations correlated with increased growth and photosynthesis. The efficiency for temperate moss increased at lower concentrations tested, but rather began to reduce at the highest HA concentration, indicating that effective concentrations of HA vary depending on the moss species and habitat. Based on these results, Antarctic HA may have ecological role in enhancing the growth and photosynthesis of Antarctic mosses. We believe this is the first study to establish a positive physiological effect of HA on mosses and hope it may serve as a basis for studying the role of HA in preserving the terrestrial ecosystem of Antarctica.

keywords: Antarctic; Humic acids; Humic substances; Photosynthetic activity; Plant growth promoting

4-50 *Agriculture; Veterinary Sciences; Zoology*

Inter-Specific and Intra-Specific Competition of Two Sympatrically Breeding Seabirds, Chinstrap and Gentoo Penguins, at Two Neighboring Colonies

Lee, Won Young., **Park, Seongseop.**, Kim, Kil Won., **Kim, Jeong-Hoon.**, **Gal, Jong-Ku.** and **Chung, Hosung.**

Animals. 2021. 11(2).
doi: 10.3390/ani11020482.

Simple Summary Under limited resources, different species may coexist by segregating their food items and foraging time, but neighboring colonies within the same species may have highly overlapping foraging habits. Thus, it is hypothesized that intra-specific competition is more intense than the inter-specific competition. To test this hypothesis, we chose sympatrically breeding Chinstrap and Gentoo penguins at two neighboring colonies and tracked their foraging space and dive depths during chick-

rearing. Here we report that there was a larger overlap in the foraging space between the two species than within each species, whereas there was lower inter-specific isotopic niche overlap than intra-specific isotopic niche overlap. Despite the low intra-specific spatial overlap, diets of conspecifics remained similar, resulting in the higher isotopic niche overlaps. Our results suggest that intra-specific competition is higher than inter-specific competition due to a lack of niche partitioning. Theory predicts that sympatric predators compete for food under conditions of limited resources. Competition would occur even within the same species, between neighboring populations, because of overlapping foraging habits. Thus, neighboring populations of the same species are hypothesized to face strong competition. To test the hypothesis that intra-specific competition is more intense than inter-specific competition owing to a lack of niche partitioning, we estimated the foraging area and diving depths of two colonial seabird species at two neighboring colonies. Using GPS and time-depth recorders, we tracked foraging space use of sympatric breeding Chinstrap and Gentoo penguins at Ardley Island (AI) and Narębski Point (NP) at King George Island, Antarctica. GPS tracks showed that there was a larger overlap in the foraging areas between the two species than within each species. In dive parameters, Gentoo penguins performed deeper and longer dives than Chinstrap penguins at the same colonies. At the colony level, Gentoo penguins from NP undertook deeper and longer dives than those at AI, whereas Chinstrap penguins did not show such intra-specific differences in dives. Stable isotope analysis of $\delta^{13}C$ and $\delta^{15}N$ isotopes in blood demonstrated both inter- and intra-specific differences. Both species of penguin at AI exhibited higher $\delta^{13}C$ and $\delta^{15}N$ values than those at NP, and in both locations, Gentoo penguins had higher $\delta^{13}C$ and lower $\delta^{15}N$ values than Chinstrap penguins. Isotopic niches showed that there were lower inter-specific overlaps than intra-specific overlaps. This suggests that, despite the low intra-specific spatial overlap, diets of conspecifics from different colonies remained more similar, resulting in the higher isotopic niche overlaps. Collectively, our results support the hypothesis that intra-specific competition is higher than inter-specific competition, leading to spatial segregation of the neighboring populations of the same species.

keywords: inter-specific competition; intra-specific competition; niche partitioning; Chinstrap penguin; Gentoo penguin

4-51 *Biotechnology & Applied Microbiology; Microbiology*

Involvement of laccase-like enzymes in humic substance degradation by diverse polar soil bacteria

Park, Ha Ju., **Lee, Yung Mi.**, **Do, Hackwon.**, **Lee, Jun Hyuck.**, Kim, Eungbin., **Lee, Hyoungseok.** and **Kim, Dockyu.**

Folia Microbiologica. 2021. 66(3): 331-340.
doi: 10.1007/s12223-020-00847-9.

Humic substances (HS) in soil are widely distributed in cold environments and account for a significant fraction of soil's organic carbon. Bacterial strains (n = 281) were isolated at 15 °C using medium containing humic acids (HA), a principal component of HS, from a variety of polar soil samples: 217 from the Antarctic and 64 from the Arctic. We identified 73 potential HA-degrading bacteria based on 16S rRNA sequence similarity, and these sequences were affiliated with phyla *Proteobacteria* (73.9%), *Actinobacteria* (20.5%), and *Bacteroidetes* (5.5%). HA-degrading strains were further classified into the genera *Pseudomonas* (51 strains), *Rhodococcus* (10 strains), or others (12 strains). Most strains degraded HA between 10 and 25 °C, but not above 30 °C, indicating cold-adapted degradation. Thirty unique laccase-like multicopper oxidase (LMCO) gene fragments were PCR-amplified from 71% of the 73 HA-degrading bacterial strains, all of which included conserved copper-binding regions (CBR) I and II, both essential for laccase activity. Bacterial LMCO sequences differed from known fungal laccases; for example, a cysteine residue between CBR I and CBR II in fungal laccases was not detected in bacterial LMCOs. This suggests a bacterial biomarker role for LMCO to predict changes in HS-degradation rates in tundra regions as global climate changes. Computer-aided molecular modeling showed these LMCOs contain a highly-conserved copper-dependent active site formed by three histidine residues between CBR I and CBR II. Phylogenetic- and modeling-based methods confirmed the wide occurrence of LMCO genes in HA-degrading polar soil bacteria and linked their putative gene functions with initial HS-degradation processes.

4-52 *Pharmacology & Pharmacy*

Isolation of Sesquiterpenoids and Steroids from the Soft Coral *Sinularia brassica* and Determination of Their Absolute Configuration

Pham, Giang Nam., Kang, Da Yeun., **Kim, Min Ju.**, **Han, Se Jong.**, **Lee, Jun Hyuck.** and Na, MinKyun.

Marine Drugs. 2021. 19(9).

doi: 10.3390/md19090523.

Two undescribed rearranged cadinane-type sesquiterpenoids (**1–2**), named sinulaketol A-B, together with one new chlorinated steroid (**3**), one new gorgosterol (**4**), one known sesquiterpene (**5**), one known dibromoditerpene (**6**) and two known polyhydroxylated steroids (**7–8**) were isolated from the soft coral *Sinularia brassica*. The structures of these compounds were established by extensive spectroscopic analysis, including HRESIMS, 1D, and 2D NMR spectroscopy. Their absolute configurations were also determined by the ECD calculations and DP4+ probability analysis. Antileishmanial activity of compounds **1–8** was evaluated in vitro against the amastigote forms of *Leishmania donovani*, in which compounds **3**, **6**, and **7** inhibited the growth of *L. donovani* by 58.7, 74.3, 54.7%, respectively, at a concentration of 50 μM. Antimicrobial effect of the isolated compounds were also evaluated against *Candida albicans*, *Staphylococcus aureus*, and *Escherichia coli*. Compound **6**, a brominated diterpene, exhibited antimicrobial effect against *S. aureus*.

keywords: *Sinularia brassica*; sesquiterpenoids; steroids; antileishmanial activity; antimicrobial activity

4-53 *Chemistry; Geochemistry & Geophysics*

Isotope Fractionation from *In Vivo* Methylmercury Detoxification in Waterbirds

Poulin, Brett A., Janssen, Sarah E., Rosera, Tylor J., Krabbenhoft, David P., Eagles-Smith, Collin A., Ackerman, Joshua T., Stewart, A. Robin., Kim, Eunhee., Baumann, Zofia., **Kim, Jeong-Hoon.** and Manceau, Alain.

Acs Earth and Space Chemistry. 2021. 5(5): 990-997.

doi: 10.1021/acsearthspacechem.1c00051.

The robust application of stable mercury (Hg) isotopes for mercury source apportionment and risk assessment necessitates the understanding of mass-dependent fractionation (MDF) as a result of internal transformations within organisms. Here, we used high energy-resolution X-ray absorption near edge structure spectroscopy and isotope ratios of total mercury (δ^{202}THg) and methylmercury (δ^{202}MeHg) to elucidate the chemical speciation of Hg and the resultant MDF as a result of internal MeHg demethylation in waterbirds. In three waterbirds (Clark's grebe, Forster's tern, and south polar skua), between 17 and 86% of MeHg was demethylated to inorganic mercury (iHg) species primarily in the liver and kidneys as Hg–tetraselenolate [$Hg(Sec)_4$] and minor Hg–dithiolate [$Hg(SR)_2$] complexes. Tissular differences between δ^{202}THg and δ^{202}MeHg correlated linearly with %iHg [$Hg(Sec)_4$ + $Hg(SR)_2$] and were interpreted to reflect a kinetic isotope effect during *in vivo* MeHg demethylation. The product–reactant isotopic enrichment factor ($\varepsilon_{p/r}$) for the demethylation of MeHg → $Hg(Sec)_4$ was −2.2 ± 0.1‰. δ^{202}MeHg values were unvarying within each bird, regardless of $Hg(Sec)_4$ abundance, indicating fast internal cycling or replenishment of MeHg relative to demethylation. Our findings document a universal selenium-dependent demethylation reaction in birds, provide new insights on the internal transformations and cycling of MeHg and $Hg(Sec)_4$, and allow for mathematical correction of δ^{202}THg values as a result of the MeHg → $Hg(Sec)_4$ reaction.

keywords: mercury; demethylation; isotopes; MDF; birds

4-54 *Biochemistry & Molecular Biology; Endocrinology & Metabolism; Toxicology; Zoology*

iTRAQ-based proteomic profiling, pathway analyses, and apoptotic mechanism in the Antarctic copepod *Tigriopus kingsejongensis* in response to ultraviolet B radiation

Lee, Young Hwan., Lee, Min-Chul., Han, Jeonghoon., Park, Jun Chul., Kim, Min-Sub., Kim, Duck-Hyun., Byeon, Eunjin., **Kim, Sanghee.**, **Yim, Joung Han.** and Lee, Jae-Seong.

Comparative Biochemistry and Physiology C-Toxicology & Pharmacology. 2021. 248.

doi: 10.1016/j.cbpc.2021.109120.

iTRAQ proteomic profiling was conducted to examine the proteomic responses of the Antarctic copepod *Tigriopus kingsejongensis* under ultraviolet B (UVB)

exposure. Of the 5507 proteins identified, 3479 proteins were annotated and classified into 25 groups using clusters of orthologous genes analysis. After exposing the *T. kingsejongensis* to 12 kJ/m² UVB radiation, 77 biological processes were modulated over different time periods (0, 6, 12, 24, and 48 h) compared with the control. A Kyoto Encyclopedia of Genes and Genomes pathway enrichment analysis showed that UVB exposure in *T. kingsejongensis* downregulated ribosome and glyoxylate and dicarboxylate metabolism at all time points. Furthermore, antioxidant and chaperone proteins were highly downregulated in response to UVB exposure, causing protein damage and activating apoptotic processes in the 48 h UVB exposure group. These proteomic changes show the mechanisms that underlie the detrimental effects of UVB on the cellular defense systems of the Antarctic copepod *T. kingsejongensis*.

keywords: iTRAQ; Antarctic copepod; *Tigriopus kingsejongensis;* Proteome; UVB radiation

4-55 *Environmental Sciences & Ecology; Public, Environmental & Occupational Health*

Mare incognita: Adélie penguins foraging in newly exposed habitat after calving of the Nansen Ice Shelf

Park, Seongseop., Thiebot, Jean-Baptiste., **Kim, Jeong-Hoon.**, Kim, Kil Won., **Chung, Hosung.** and **Lee, Won Young.**

Environmental Research. 2021. 201.
doi: 10.1016/j.envres.2021.111561.

Rapid environmental changes can dramatically and durably affect the animal's foraging behavior. In the Ross Sea (Antarctica), calving of the Nansen Ice Shelf in 2016 opened a newly accessible marine area of 214 km². In this study, we examined the foraging behavior of Adélie penguins from the nearby Inexpressible Island in December 2018, by tracking 27 penguins during their at-sea trips using GPS, depth and video loggers. The penguins mainly foraged within 88.2 ± 42.9 km of their colony, for 23.4 ± 6.8 h. Five penguins headed south to the newly exposed habitat along the Nansen Ice Shelf, whereas 22 penguins exploited previously available foraging areas. There was no significant difference in any of the foraging trip or diving parameters between the two penguin groups; however, in the calved region the penguins were diving into shallow areas more often than did the other penguins. These results show that Adélie penguins on Inexpressible Island had explored the newly exposed area after calving. We conclude that the penguins respond to newly available habitat following stochastic environmental events, either through information sharing at the colony, and/or by balancing prey availability per capita across the foraging sites. Considering that this penguin breeding area is under investigation for the establishment of an Antarctic Specially Protected Area (ASPA), the results of this study may provide insights for evaluating the ecological importance of this area and formulating an ASPA management plan for conservation.

keywords: Foraging area; GPS; Time-depth recorder; Nansen ice shelf; Antarctic specially protected area

4-56 *Microbiology*

Massilia aromaticivorans sp. nov., a BTEX Degrading Bacterium Isolated from Arctic Soil

Son, Jigwan., Lee, Hyosun., **Kim, Mincheol.** and 2 others.

Current Microbiology. 2021. 78(5): 2143-2150.
doi: 10.1007/s00284-021-02379-y.

A novel BTEX degrading bacterial strain, designated ML15P13^T, was isolated from Arctic soil at the Svalbard Islands, Norway, using an enrichment culture technique. This isolate is Gram-negative, aerobic, motile with multiple flagella at one polar end, and rod-shaped. Growth was observed at 4–35 °C, pH 6.0–8.0, and 0–0.5% (w/v) NaCl. According to 16S rRNA gene analysis, strain ML15P13^T was grouped with members of the genus *Massilia* and closely related to *Massilia atriviolacea* SOD^T (98.4%), *Massilia violaceinigra* B2^T (98.3%), *Massilia eurypsychrophila* B528-3^T (97.7%), *Massilia glaciei* B448-2^T (97.7%), and *Massilia psychrophila* B115-1^T (96.6%). Average nucleotide identity, digital DNA-DNA hybridization, and average amino acid identity between genome sequences of strain ML15P13^T and the closely related species ranged from 75.8 to 84.3%, from 19.6 ± 1.0 to 21.6 ± 0.3%, and from 68.8 to 71.0%, respectively. The major fatty acids were $C_{16:0}$, summed feature 3 ($C_{16:1}$ ω6c and/or $C_{16:1}$ ω7c), and summed feature 8 ($C_{18:1}$ ω7c and/or $C_{18:1}$ ω6c). Q-8 was the major ubiquinone. The polar lipid profile showed the presence of phosphatidylethanolamine, phosphatidylglycerol, diphosphatidylglycerol, one

unidentified phospholipid, and five unidentified polar lipids. The G + C content of the genomic DNA was 64.2 mol%. Based on the results for genotypic and phenotypic study, we conclude that strain ML15P13^T represents a novel species of the genus *Massilia*, for which the name *Massilia aromaticivorans* sp. nov. is proposed. The type strain is ML15P13^T (= KACC 21773^T= JCM 34089^T).

4-57 *Genetics & Heredity*

Mitochondrial genome of the Antarctic microalga *Micractinium simplicissimum* KSF0127 (Chlorellaceae, Trebouxiophyceae)

Kim, Eun Jae., **Chae, Hyunsik.**, **Yu, Jihyeon.**, **Kim, Hyun-joong.**, **Cho, Sung Mi.**, **Shin, Seung Chul.**, **Choi, Han-Gu.**, **Kim, Sanghee.** and **Han, Se Jong.**

Mitochondrial DNA Part B-Resources. 2021. 6(3): 878-879.

doi: 10.1080/23802359.2021.1886010.

We report the first mitochondrial genome of the Antarctic microalga *Micractinium simplicissimum* KSF0127. The circular mitochondrial genome was 67,923 bp in length and contained 45 protein-coding genes, one ribosomal RNA gene, and 60 transfer RNA genes. The phylogenetic tree was constructed with eight previously reported mitogenome sequences and showed the phylogenetic position of *M. simplicissimum* KSF0127 within the Chlorellaceae family.

keywords: Micractinium simplicissimum; Chlorellaceae; Trebouxiophyceae; Antarctic microalga; mitochondrial genome

4-58 *Chemistry; Crystallography; Materials Science*

Molecular basis of dimerization of lytic transglycosylase revealed by the crystal structure of MltA from *Acinetobacter baumannii*

Jang, Hyunseok., **Do, Hackwon.**, Kim, Chang Min., Kim, Gi Eob., **Lee, Jun Hyuck.** and Park, Hyun Ho.

Iucrj. 2021. 8: 921-930.

doi: 10.1107/s2052252521008666.

Peptidoglycan digestion by murein-degrading enzymes is a critical process in bacterial cell growth and/or cell division. The membrane-bound lytic murein transglycosylase A (MltA) is a murein-degrading enzyme; it catalyzes the cleavage of the β-1,4-glycosidic linkage between *N*-acetylmuramic acid and *N*-acetylglucosamine in peptidoglycans. Although substrate recognition and cleavage by MltA have been examined by previous structural and mutagenesis studies, the overall mechanism of MltA in conjunction with other functionally related molecules on the outer membrane of bacterial cells for peptidoglycan degradation has remained elusive. In this study, the crystal structure of MltA from the virulent human pathogen *Acinetobacter baumannii* is characterized and presented. The study indicated that MltA from *A. baumannii* forms homodimers via an extra domain which is specific to this species. Furthermore, the working mechanism of MltA with various functionally related proteins on the bacterial outer membrane was modeled based on the structural and biochemical analysis.

keywords: *Acinetobacter baumannii*; crystal structure; MltA; lytic transglycosylases; peptidoglycan remodeling; superbugs

4-59 *Biodiversity & Conservation; Environmental Sciences & Ecology*

Molecular characteristics of Bombus (*Alpinobombus*) polaris from North Greenland with comments on its general biology and phylogeography

Namin, Saeed Mohamadzade., **Park, Tae-Yoon S.** and 2 others.

Polar Biology. 2021. 44(12): 2209-2216.

doi: 10.1007/s00300-021-02952-y.

The bumble bee *Bombus polaris* (Curtis 1835) is known from the northernmost region of Greenland. But how it can survive there, where in terms of geographic origin it came from, and which species in addition to *B. pyrrhopygus* (Friese 1902) genetically it is most closely related to are insufficiently answered questions that have motivated us to carry out this study. On the basis of a molecular analysis of the cytochrome oxidase I gene of a *B. (Alpinobombus) polaris* from North Greenland (82° 48′ N; 42° 14′ W), we conclude that the female specimen we analysed was most closely related to the Canadian populations of *B. polaris*. Geographic proximity, occurrence of *B. polaris*

on Ellesmere Island and wind direction are likely factors that have aided *B. polaris* to establish itself in northern and eastern Greenland. The presence of five haplotypes in the studied sequences from Greenland indicates a moderately high level of genetic diversity of *B. polaris* in Greenland, reflecting the successful adaptation of *B. polaris* populations. In the broader context of entomological life in the high Arctic, our results on *B. polaris* allow us to conclude that the survival of pollinating species in the high Arctic under the changing climate scenario depends not only on the weather but also on an individual's opportunity to continue to locate suitable food sources, i.e. pollen and nectar in the case of *B. polaris*. This aspect, briefly touched upon in this study, is of relevance not just to *B. polaris*, but the Arctic entomofauna generally.

keywords: Arctic pollinator; Polar insects; DNA extraction and sequencing; Haplotypes; Population relationships

4-60 *Plant Sciences; Marine & Freshwater Biology*

Morphology and phylogenetic relationships of two new Antarctic species in phylogroup *Chloromonadinia* (Volvocales, Chlorophyceae)

Chae, Hyunsik., **Kim, Eun Jae.**, Lim, Sooyeon., Kim, Han Soon., **Choi, Han-Gu.**, **Kim, Sanghee.** and **Kim, Ji Hee.**

Phycologia. 2021. 60(3): 225-236.
doi: 10.1080/00318884.2021.1893005.

The phylogroup *Chloromonadinia* (Volvocales, Chlorophyceae) comprises green microalgae that inhabit a variety of environments, including freshwater, soil, and snow. Two strains were isolated from two sites in the South Shetland Islands in maritime Antarctica, and their morphological and molecular characteristics were studied. Light microscopy of the strain KSF0090 revealed ellipsoidal or broad ellipsoidal, sometimes almost spherical cells with a chloroplast without a pyrenoid, a prominent eyespot, and a hemispherical papilla. The vegetative cells of KSF0208 were ellipsoidal to ovoid cells with a chloroplast with a central pyrenoid, a linear eyespot, and a papilla. The two strains differed from other closely related species based on size and the aforementioned morphological characteristics. Nuclear small subunit rDNA sequence data indicated that each strain formed a distinct well-supported lineage within the phylogroup *Chloromonadinia*. In addition, comparative analyses of the secondary structures of internal transcribed spacer 2 and compensatory base changes were used to identify and characterize the two strains. Based on their morphological and molecular characteristics, we propose KSF0090 and KSF0208 as two new species, *Chloromonas deceptionensis sp. nov.* and *Ostravamonas greenwichensis sp. nov.*, respectively.

keywords: *Chloromonas deceptionensis*; Internal transcribed spacer 2; Molecular phylogeny; *Ostravamonas greenwichensis*

4-61 *Food Science & Technology*

A Multi-Elements Isotope Approach to Assess the Geographic Provenance of Manila Clams (*Ruditapes philippinarum*) via Recombining Appropriate Elements

Won, Eun-Ji., Kim, Seung Hee., Go, Young-Shin., Kumar, K. Suresh., Kim, Min-Seob., Yoon, Suk-Hee., Bayon, Germain., **Kim, Jung-Hyun.** and Shin, Kyung-Hoon.

Foods. 2021. 10(3).
doi: 10.3390/foods10030646.

The increasing global consumption of seafood has led to increased trade among nations, accompanied by mislabeling and fraudulent practices that have rendered authentication crucial. The multi-isotope ratio analysis is considered as applicable tool for evaluating geographical authentications but requires information and experience to select target elements such as isotopes, through a distinction method based on differences in habitat and physiology due to origin. The present study examined recombination conditions of multi-elements that facilitated geographically distinct classifications of the clams to sort out appropriate elements. Briefly, linear discriminant analysis (LDA) analysis was performed according to several combinations of five stable isotopes (carbon $\delta^{13}C$), nitrogen ($\delta^{15}N$), oxygen ($\delta^{18}O$), hydrogen (δD), and sulfur ($\delta^{34}S$)) and two radiogenic elements (strontium ($^{87}Sr/^{86}Sr$) and neodymium ($^{143}Nd/^{144}Nd$)), and the geographical classification results of the Manila clam *Ruditapes philippinarum* from Democratic People's Republic of Korea (DPR Korea), Korea and China were compared. In conclusion, linear discriminant analysis (LDA) with at least four elements (C, N, O, and S) including S revealed a remarkable cluster distribution of the clams. These findings

expanded the application of systematic multi-elements analyses, including stable and radiogenic isotopes, to trace the origins of *R. philippinarum* collected from the Korea, China, and DPR Korea.

keywords: authentication; Manila clam; stable isotope; traceability; linear discriminant analysis

4-62 *Biotechnology & Applied Microbiology; Immunology; Microbiology; Pharmacology & Pharmacy*

A new α-pyrone from *Arthrinium pseudosinense* culture medium and its estrogenic activity in MCF-7 cells

Kwon, Haeun., Nguyen, Quynh Nhu., Na, Myung Woo., Kim, Ki Hyun., Guo, Yuanqiang., **Yim, Joung Han.** and 4 others.

Journal of Antibiotics. 2021. 74(12): 893-897.
doi: 10.1038/s41429-021-00473-8.

A new *α*-pyrone analog, arthrifuranone A (**1**) was isolated from an EtOAc-extract of *Arthrinium pseudosinense* culture medium. The isolation workflow was guided by a Molecular Networking-based dereplication strategy. The chemical structure of the new compound was elucidated using MS and NMR spectroscopic techniques, and the absolute configuration was established by the Mosher's method and gauge-including atomic orbital NMR chemical shift calculations, followed by DP4 + analysis. The isolated compound was evaluated for its estrogenic activity using the MCF-7 estrogen responsive human breast cancer cells. Compound **1** showed estrogenic activity by increasing the proliferation of MCF-7 cells at the concentration of 3.125 μM via phosphorylation of estrogen receptor-*α*.

4-63 *Engineering; Environmental Sciences & Ecology*

Occurrence, distribution, and bioaccumulation of new and legacy persistent organic pollutants in an ecosystem on King George Island, maritime Antarctica

Kim, Jun-Tae., Choi, Yun-Jeong., Barghi, Mandana., **Kim, Jeong-Hoon.**, **Jung, Jin-Woo.**, **Kim, Kitae.**, **Kang, Jung-Ho.** and 2 others.

Journal of Hazardous Materials. 2021. 405.
doi: 10.1016/j.jhazmat.2020.124141.

The occurrence and bioaccumulation of new and legacy persistent organic pollutants (POPs), organochlorine pesticides (OCPs), polychlorinated biphenyls (PCBs), polychlorinated naphthalenes (PCNs), hexabromocyclododecanes (HBCDs), and Dechlorane Plus (DPs) and their related compounds (Dechloranes) in an ecosystem on King George Island, Antarctica are investigated. The new and legacy POPs were widely detected in the animal samples collected from Antarctica, which included Limpet, Antarctic cod, Amphipods, Antarctic icefish, Gentoo and Chinstrap penguins, Kelp gull, and South polar skua. The trophic magnification factors indicated that the levels of PCNs and HBCDs, as well as the legacy POPs, were magnified through the food web, whereas DPs might be diluted through the trophic levels contradicting the classification of Dechloranes as POPs. This is one of the first extensive surveys on PCNs, HBCDs, and Dechloranes, which provides unique information on the distribution and trophic biomagnification potential of the new and legacy POPs in the Antarctic region.

keywords: Persistent organic pollutants; Polychlorinated naphthalenes; Hexabromocyclododecane; Dechloranes; Trophic magnification factor

4-64 *Biodiversity & Conservation; Environmental Sciences & Ecology*

Penguins Strike Back: A Report on the Unusual Case of Adélie Penguin (*Pygoscelis adeliae*) Attacks on South Polar Skua Nests Distant from the Breeding Colony

Kim, Youmin., **Kim, Jong-U.**, **Chung, Hosung.**, **Oh, Yeon-Soo.**, **Oh, Young-Geun.** and **Kim, Jeong-Hoon.**

Diversity-Basel. 2021. 13(5).
doi: 10.3390/d13050181.

keywords: inter-specific behavior; *Pygoscelis adeliae*; Ross Sea region; *Stercorarius maccormicki*

4-65 *Biochemistry & Molecular Biology; Chemistry*

Potential of Ramalin and Its Derivatives for the Treatment of Alzheimer's Disease

Kim, Tai Kyoung., **Hong, Ju-Mi.**, **Kim, Kyung Hee.**, **Han, Se Jong.**, **Kim, Il-Chan.**, Oh, Hyuncheol. and **Yim, Joung Han.**

Molecules. 2021. 26(21).
doi: 10.3390/molecules26216445.

The pathogenesis of Alzheimer's disease (AD) is still unclear, and presently there is no cure for the disease that can be used for its treatment or to stop its progression. Here, we investigated the therapeutic potential of ramalin (isolated from the Antarctic lichen, *Ramalina terebrata*), which exhibits various physiological activities, in AD. Specifically, derivatives were synthesized based on the structure of ramalin, which has a strong antioxidant effect, BACE-1 inhibition activity, and anti-inflammatory effects. Therefore, ramalin and its derivatives exhibit activity against multiple targets associated with AD and can serve as potential therapeutic agents for the disease.

keywords: Alzheimer's disease; ramalin; derivatives; therapeutic potential; antioxidant; β-secratase; anti-inflammatory

4-66 *Biochemistry & Molecular Biology; Chemistry*

PTP1B Inhibitory Secondary Metabolites from an Antarctic Fungal Strain *Acremonium* sp. SF-7394

Kim, Hye Jin., Li, Xiao-Jun., Kim, Dong-Cheol., **Kim, Tai Kyoung.**, Sohn, Jae Hak., Kwon, Haeun., Lee, Dongho., Kim, Youn-Chul., **Yim, Joung Han.** and Oh, Hyuncheol.

Molecules. 2021. 26(18).
doi: 10.3390/molecules26185505.

Chemical investigation of the Antarctic lichen-derived fungal strain *Acremonium* sp. SF-7394 yielded a new amphilectane-type diterpene, acrepseudoterin (**1**), and a new acorane-type sesquiterpene glycoside, isocordycepoloside A (**2**). In addition, three known fungal metabolites, (−)-ternatin (**3**), [D-Leu]-ternatin (**4**), and pseurotin A (**5**), were isolated from the EtOAc extract of the fungal strain. Their structures were mainly elucidated by analyzing their NMR and MS data. The absolute configuration of **1** was proposed by electronic circular dichroism calculations, and the absolute configuration of the sugar unit in **2** was determined by a chemical method. The inhibitory effects of the isolated compounds on protein tyrosine phosphatase 1B (PTP1B) were evaluated by enzymatic assays; results indicated that acrepseudoterin (**1**) and [D-Leu]-ternatin (**4**) dose-dependently inhibited the enzyme activity with IC_{50} values of 22.8 ± 1.1 μM and 14.8 ± 0.3 μM, respectively. Moreover, compound **1** was identified as a competitive inhibitor of PTP1B.

keywords: *Acremonium* sp.; terpenoids; Antarctic fungal metabolites; PTP1B

4-67 *Crystallography; Materials Science*

Purification and Crystallographic Analysis of a Novel Cold-Active Esterase (*Ha*Est1) from *Halocynthiibacter arcticus*

Jeon, Sangeun., **Hwang, Jisub.**, Yoo, Wanki., Chang, Joo Won., **Do, Hackwon.**, **Kim, Han-Woo.**, Kim, Kyeong Kyu., **Lee, Jun Hyuck.** and Kim, T. Doohun.

Crystals. 2021. 11(2).
doi: 10.3390/cryst11020170.

This report deals with the purification, characterization, and a preliminary crystallographic study of a novel cold-active esterase (*Ha*Est1) from *Halocynthiibacter arcticus*. Primary sequence analysis reveals that *Ha*Est1 has a catalytic serine in G-x-S-x-G motif. The recombinant *Ha*Est1 was cloned, expressed, and purified. SDS-PAGE and zymographic analysis were carried out to characterize the properties of *Ha*Est1. A single crystal of *Ha*Est1 was obtained in a solution containing 10% (*w/v*) PEG 8000/8% ethylene glycol, 0.1 M Hepes-NaOH, pH 7.5. Diffraction data were collected to 2.10 Å resolution with $P2_1$ space group. The final R_{merge} and $R_{p.i.m}$ values were 7.6% and 3.5% for 50–2.10 Å resolution. The unit cell parameters were a = 35.69 Å, b = 91.21 Å, c = 79.15 Å, and β = 96.9°.

keywords: esterase; enzyme assay; crystallization; diffraction

4-68 *Life Sciences & Biomedicine*

Purification, crystallization, and preliminary X-ray diffraction analysis of an *S*-formylglutathione hydrolase (*Va*SFGH) homolog from *Variovorax* sp. PAMC 28711

Hwang, Jisub., **Lee, Min Ju.**, **Lee, Sung Gu.**, **Do, Hackwon.** and **Lee, Jun Hyuck.**

Biodesign. 2021. 9(4): 67-71.
doi: 10.34184/kssb.2021.9.4.67.

S-formylglutathione hydrolase (SFGH) is an esterase

that hydrolyzes *S*-formylglutathione into formic acid and glutathione. As SFGHs are also able to hydrolyze thioesters as well as non-thioester substrates, they have attracted considerable attention as potential biocatalysts. Although the substrate specificity of various SFGHs has been determined, the detailed structural differences relating to substrate preference remain unclear. Here, we present overexpression, purification, and preliminary X-ray crystallographic data for an SFGH from *Variovorax* sp. PAMC 28711 (*Va*SFGH). The *Va*SFGH protein was over-expressed in *Escherichia coli* and successfully crystallized in 0.2 M sodium chloride, 0.1 M Bis-Tris:HCl (pH 6.5), and 20% (w/v) PEG 3350. A complete native X-ray diffraction dataset was collected up to 2.38 Å resolution and processed in the C2 space group with unit-cell parameters a = 53.2 Å, b = 76.4 Å, c = 199.9 Å, α = 90°, β = 90.2°, and γ = 90°. Moreover, *Va*SFGH exhibited higher esterase activity toward shorter-chain esters. Based on its structural determination, future studies will elucidate the substrate-binding mechanism and specificity of *Va*SFGH at the molecular level.

4-69 *Chemistry; Crystallography; Materials Science*

Putative hexameric glycosyltransferase functional unit revealed by the crystal structure of *Acinetobacter baumannii* MurG

Jung, Kyoung Ho., Kwon, Sunghark., Kim, Chang Min., **Lee, Jun Hyuck.** and Park, Hyun Ho.

Iucrj. 2021. 8: 574-583.

doi: 10.1107/s2052252521003729.

Lipid II, the main component of the bacterial cell wall, is synthesized by the addition of UDP-*N*-acetylglucosamine to the UDP-*N*-acetylmuramic acid pentapeptide catalyzed by the glycosyltransferase MurG. Owing to its critical role in cell-wall biosynthesis, MurG is considered to be an attractive target for antibacterial agents. Although the Mur family ligases have been extensively studied, the molecular mechanism of the oligomeric scaffolding assembly of MurG remains unclear. In this study, MurG from *Acinetobacter baumannii* (abMurG), a human pathogen, was characterized and its hexameric crystal structure was unveiled; this is the first homo-oligomeric structure to be described in the MurG family and the Mur family. Homogeneous protein samples were produced for structural studies using size-exclusion chromatography, the absolute molecular mass was calculated via multi-angle light scattering, and protein-protein interactions were analyzed using the *PDBePISA* server. abMurG was found to form homo-oligomeric complexes in solution, which might serve as functional units for the scaffolding activity of MurG. Furthermore, analysis of this structure revealed the molecular assembly mechanism of MurG. This structural and biochemical study elucidated the homo-oligomerization mechanism of MurG and suggests a new potential antibiotic target on MurG.

keywords: *Acinetobacter baumannii*; cell-wall peptidoglycan biosynthesis; crystal structure; glycosyltransferases; MurG; superbugs

4-70 *Agriculture; Veterinary Sciences; Zoology*

Regional Differences in the Diets of Adélie and Emperor Penguins in the Ross Sea, Antarctica

Hong, Seo-Yeon., **Gal, Jong-Ku.**, **Lee, Bo-Yeon.**, **Son, Wuju.**, **Jung, Jin-Woo.**, **La, Hyoung Sul.**, Shin, Kyung-Hoon., **Kim, Jeong-Hoon.** and **Ha, Sun-Yong.**

Animals. 2021. 11(9).

doi: 10.3390/ani11092681.

To identify the dietary composition and characteristics of both Adélie (*Pygoscelis adeliae*) and Emperor (*Aptenodytes forsteri*) penguins at four breeding sites, we performed stable carbon ($\delta^{13}C$) and nitrogen ($\delta^{15}N$) isotope analysis of down samples taken from penguin chicks. Adélie Penguin chicks at Cape Hallett mostly fed on Antarctic krill (*Euphausia superba*; 65.5 ± 3.5%), a reflection of the prevalence of that species near Cape Hallett, and no significant differences were noted between 2017 and 2018. However, Adélie Penguin chicks at Inexpressible Island, located near Terra Nova Bay, fed on both Antarctic silverfish (*Pleuragramma antarctica*; 42.5%) and ice krill (*Euphausia crystallorophias*; 47%), reflecting the high biomass observed in Terra Nova Bay. Meanwhile, no significant difference was noted between the two breeding sites of the Emperor Penguin. Emperor Penguin chicks predominantly fed on Antarctic silverfish (74.5 ± 2.1%) at both breeding sites (Cape Washington and Coulman Island), suggesting that diet preference represents the main factor influencing Emperor Penguin foraging.

In contrast, the diet of the Adélie Penguin reflects presumed regional differences in prey prevalence, as inferred from available survey data.

keywords: stable isotope analysis; Adélie Penguin; Emperor Penguin; Ross Sea; SIAR

4-71 *Environmental Sciences & Ecology*

The relationships of present vegetation, bacteria, and soil properties with soil organic matter characteristics in moist acidic tundra in Alaska

Nam, Sungjin., Alday, Josu G., **Kim, Mincheol.**, Kim, Hyemin., Kim, Yongkang., Park, Taesung., Lim, Hyoun Soo., **Lee, Bang Yong.**, **Lee, Yoo Kyung.** and **Jung, Ji Young.**

Science of the Total Environment. 2021. 772.
doi: 10.1016/j.scitotenv.2021.145386.

Soil organic matter (SOM) is related to vegetation, soil bacteria, and soil properties; however, not many studies link all these parameters simultaneously, particularly in tundra ecosystems vulnerable to climate change. Our aim was to describe the relationships between vegetation, bacteria, soil properties, and SOM composition in moist acidic tundra by integrating physical, chemical, and molecular methods. A total of 70 soil samples were collected at two different depths from 36 spots systematically arranged over an area of about 300 m x 50 m. Pyrolysis-gas chromatography/mass spectrometry and pyrosequencing of the 16S rRNA gene were used to identify the molecular compositions of the SOM and bacterial community, respectively. Vegetation and soil physicochemical properties were also measured. The sampling sites were grouped into three, based on their SOM compositions: *Sphagnum* moss-derived SOM, lipid-rich materials, and aromatic-rich materials. Our results show that SOM composition is spatially structured and linked to microtopography; however, the vegetation, soil properties, and bacterial community composition did not show overall spatial structuring. Simultaneously, soil properties and bacterial community composition were the main factors explaining SOM compositional variation, while vegetation had a residual effect. Verrucomicrobia and Acidobacteria were related to polysaccharides, and Chloroflexi was linked to aromatic compounds. These relationships were consistent across different hierarchical levels. Our results suggest that SOM composition at a local scale is closely linked with soil factors and the bacterial community. Comprehensive observation of ecosystem components is recommended to understand the in-situ function of bacteria and the fate of SOM in the moist acidic tundra.

keywords: Soil organic matter (SOM); *Sphagnum* moss; Soil properties; Microbiome; Moist acidic tundra; Pyrolysis GC/MS

4-72 *Chemistry; Science & Technology; Instruments & Instrumentation; Physics*

Remote Recognition of Moving Behaviors for Captive Harbor Seals Using a Smart-Patch System via Bluetooth Communication

Kim, Seungyeob., Jeong, Jinheon., Seo, Seung Gi., **Im, Sehyeok.**, **Lee, Won Young.** and Jin, Sung Hun.

Micromachines. 2021. 12(3).
doi: 10.3390/mi12030267.

Animal telemetry has been recognized as a core platform for exploring animal species due to future opportunities in terms of its contribution toward marine fisheries and living resources. Herein, biologging systems with pressure sensors are successfully implemented via open-source hardware platforms, followed by immediate application to captive harbor seals (HS). Remotely captured output voltage signals in real-time mode via Bluetooth communication were reproducibly and reliably recorded on the basis of hours using a smartphone built with data capturing software with graphic user interface (GUI). Output voltages, corresponding to typical behaviors on the captive HS, such as stopping (A), rolling (B), flapping (C), and sliding (D), are clearly obtained, and their analytical interpretation on captured electrical signals are fully validated via a comparison study with consecutively captured images for each motion of the HS. Thus, the biologging system with low cost and light weight, which is fully compatible with a conventional smartphone, is expected to potentially contribute toward future anthology of seal animals.

keywords: biologging system; harbor seals; remote data capturing; Bluetooth communication

4-73 *Marine & Freshwater Biology; Oceanography*

A Review: Marine Bio-logging of Animal Behaviour and Ocean Environments

Chung, Hyunjae., **Lee, Jongchan.** and **Lee, Won Young.**

Ocean Science Journal. 2021. 56(2): 117-131.

doi: 10.1007/s12601-021-00015-1.

Recent technologies have allowed researchers to observe animal behaviour and monitor their surrounding environments by deploying electronic sensors onto the animals. So-called 'bio-logging' (also known as animal telemetry, biotelemetry, or animal-borne sensors) has been widely used to study marine animals that are difficult for humans to observe. In this study, we (1) review the types of sensors used, the animal taxa studied, and the study areas in marine bio-logging publications from 1974 to 2019; (2) introduce the main topics in behavioural and environmental marine bio-logging studies; and (3) discuss suggestions for future marine bio-logging studies. We expect that technological advances in new sensors will enhance the ability of both behavioural ecologists and oceanographers to explore animal movements, physiology and marine environments. In addition, we discuss future perspectives of bio-loggers to improve data acquisition and accuracy with longer battery life for applying bio-logging techniques to broader species.

keywords: Animal telemetry; Bio-logging; Marine animal; Marine ecosystem; Tagging

4-74 *Physical Geography; Geology*

Scientific access into Mercer Subglacial Lake: scientific objectives, drilling operations and initial observations

Priscu, John C., Kalin, Jonas., Winans, John., Campbell, Timothy., Siegfried, Matthew R., Skidmore, Mark., Dore, John E., Leventer, Amy., Harwood, David M., Duling, Dennis., Zook, Robert., Burnett, Justin., Gibson, Dar., Krula, Edward., Mironov, Anatoly., McManis, Jim., Roberts, Graham., Rosenheim, Brad E., Christner, Brent C., Kasic, Kathy., Fricker, Helen A., Lyons, W. Berry., Barker, Joel., Bowling, Mark., Collins, Billy., Davis, Christina., Gagnon, Al., Gardner, Christopher., Gustafson, Chloe., **Kim, Ok-Sun.** and 8 others.

Annals of Glaciology. 2021. 62(85-86): 340-352.

doi: 10.1017/aog.2021.10.

The Subglacial Antarctic Lakes Scientific Access (SALSA) Project accessed Mercer Subglacial Lake using environmentally clean hot-water drilling to examine interactions among ice, water, sediment, rock, microbes and carbon reservoirs within the lake water column and underlying sediments. A ~0.4 m diameter borehole was melted through 1087 m of ice and maintained over ~10 days, allowing observation of ice properties and collection of water and sediment with various tools. Over this period, SALSA collected: 60 L of lake water and 10 L of deep borehole water; microbes >0.2 μm in diameter from in situ filtration of ~100 L of lake water; 10 multicores 0.32–0.49 m long; 1.0 and 1.76 m long gravity cores; three conductivity–temperature–depth profiles of borehole and lake water; five discrete depth current meter measurements in the lake and images of ice, the lake water–ice interface and lake sediments. Temperature and conductivity data showed the hydrodynamic character of water mixing between the borehole and lake after entry. Models simulating melting of the ~6 m thick basal accreted ice layer imply that debris fall-out through the ~15 m water column to the lake sediments from borehole melting had little effect on the stratigraphy of surficial sediment cores.

keywords: Antarctic glaciology; basal ice; biogeochemistry; glacial sedimentology; subglacial lakes

4-75 *Genetics & Heredity*

Screening and Genetic Network Analysis of Genes Involved in Freezing and Thawing Resistance in *DaMDHAR*—Expressing *Saccharomyces cerevisiae* Using Gene Expression Profiling

Kim, Il-Sup., **Choi, Woong.**, **Son, Jonghyeon.**, **Lee, Jun Hyuck.**, **Lee, Hyoungseok.**, **Lee, Jungeun.**, **Shin, Seung Chul.** and **Kim, Han-Woo.**

Genes. 2021. 12(2).

doi: 10.3390/genes12020219.

The cryoprotection of cell activity is a key determinant in frozen-dough technology. Although several factors that contribute to freezing tolerance have been reported, the mechanism underlying the manner in which yeast cells respond to freezing and thawing (FT) stress is not well established. Therefore, the present study demonstrated the relationship between *DaMDHAR* encoding monodehydroascorbate

reductase from Antarctic hairgrass *Deschampsia antarctica* and stress tolerance to repeated FT cycles (FT2) in transgenic yeast *Saccharomyces cerevisiae*. *DaMDHAR*-expressing yeast (DM) cells identified by immunoblotting analysis showed high tolerance to FT stress conditions, thereby causing lower damage for yeast cells than wild-type (WT) cells with empty vector alone. To detect FT2 tolerance-associated genes, 3′-quant RNA sequencing was employed using mRNA isolated from DM and WT cells exposed to FT (FT2) conditions. Approximately 332 genes showed ≥2-fold changes in DM cells and were classified into various groups according to their gene expression. The expressions of the changed genes were further confirmed using western blot analysis and biochemical assay. The upregulated expression of 197 genes was associated with pentose phosphate pathway, NADP metabolic process, metal ion homeostasis, sulfate assimilation, β-alanine metabolism, glycerol synthesis, and integral component of mitochondrial and plasma membrane (PM) in DM cells under FT2 stress, whereas the expression of the remaining 135 genes was partially related to protein processing, selenocompound metabolism, cell cycle arrest, oxidative phosphorylation, and α-glucoside transport under the same condition. With regard to transcription factors in DM cells, *MSN4* and *CIN5* were activated, but *MSN2* and *MGA1* were not. Regarding antioxidant systems and protein kinases in DM cells under FT stress, *CTT1*, *GTO*, *GEX1*, and *YOL024W* were upregulated, whereas *AIF1*, *COX2*, and *TRX3* were not. Gene activation represented by transcription factors and enzymatic antioxidants appears to be associated with FT2-stress tolerance in transgenic yeast cells. *RCK1*, *MET14*, and *SIP18*, but not *YPK2*, have been known to be involved in the protein kinase-mediated signalling pathway and glycogen synthesis. Moreover, *SPI18* and *HSP12* encoding hydrophilin in the PM were detected. Therefore, it was concluded that the genetic network via the change of gene expression levels of multiple genes contributing to the stabilization and functionality of the mitochondria and PM, not of a single gene, might be the crucial determinant for FT tolerance in *DaMDAHR*-expressing transgenic yeast. These findings provide a foundation for elucidating the *DaMDHAR*-dependent molecular mechanism of the complex functional resistance in the cellular response to FT stress.

keywords: Antarctic plant; *Deschampsia antarctica*; monodehydroascorbate reductase; freezing and thawing; gene expression profiling; transgenic yeast

4-76 *Agriculture; Veterinary Sciences; Zoology*

Sex-Biased Gene Expression and Isoform Profile of Brine Shrimp *Artemia franciscana* by Transcriptome Analysis

Jo, Euna., Lee, Seung-Jae., Choi, Eunkyung., Kim, Jin-mu., **Lee, Jun-Hyuck.** and Park, Hyun.

Animals. 2021. 11(9).
doi: 10.3390/ani11092630.

The brine shrimp *Artemia* has a ZW sex determination system with ZW chromosomes in females and ZZ chromosomes in males. *Artemia* has been considered a promising model organism for ZW sex-determining systems, but the genes involved in sex determination and differentiation of *Artemia* have not yet been identified. Here, we conducted transcriptome sequencing of female and male *A. franciscana* using PacBio Iso-Seq and Illumina RNA-Seq techniques to identify candidate sex determination genes. Among the 42,566 transcripts obtained from Iso-Seq, 23,514 were analyzed. Of these, 2065 (8.8%) were female specific, 2513 (10.7%) were male specific, and 18,936 (80.5%) were co-expressed in females and males. Based on GO enrichment analysis and expression values, we found 10 female-biased and 29 male-biased expressed genes, including *DMRT1* and *Sad* genes showing male-biased expression. Our results showed that *DMRT1* has three isoforms with five exons, while *Sad* has seven isoforms with 2-11 exons. The *Sad* gene is involved in ecdysteroid signaling related to molting and metamorphosis in arthropods. Further studies on ecdysteroid biosynthetic genes are needed to improve our understanding of *Artemia* sex determination. This study will provide a valuable resource for sex determination and differentiation studies on *Artemia* and other crustaceans with ZW systems.

keywords: *Artemia franciscana*; transcriptome; isoforms; sex-biased gene expression; sex determination

4-77 *Biotechnology & Applied Microbiology; Marine & Freshwater Biology*

Sexually Dimorphic Growth Stimulation in a Strain of Growth Hormone Transgenic Coho Salmon (*Oncorhynchus kisutch*)

Chan, Michelle T. T., Muttray, Annette., Sakhrani, Di-onne., Woodward, Krista., **Kim, Jin-Hyoung.** and 3 others.

Marine Biotechnology. 2021. 23(1): 140-148.

doi: 10.1007/s10126-020-10012-5.

Growth hormone (GH) transgenic fish often exhibit remarkable transformations in growth rate and other phenotypes relative to wild-type. The 5750A transgenic coho salmon strain exhibits strong sexually dimorphic growth, with females possessing growth stimulation at a level typical of that seen for both sexes in other strains harbouring the same gene construct (e.g. M77), while males display a modest level of growth stimulation. GH mRNA levels were significantly higher in females than in males of the 5750A strain but equivalent in the M77 strain, indicating sex and transgene insertion locus altered transgene expression. We found that acute estradiol treatments did not influence GH expression in either strain (5750A and M77) or the transgene promoter (metallothionein-B), suggesting that estradiol level was not a significant factor influencing transgene activity. The feminization of XX and XY fish of the 5750A and M77 strains generated all-female groups and resulted in equalized growth of the two genetic sexes, suggesting that the presence of the Y chromosome was not directly capable of influencing the GH transgene-mediated growth in a physiological female conditions. These data suggest that the difference in growth rate seen between the sexes in the 5750A strain arises from non-estradiol-mediated sex influences on gene regulation at the transgene locus. This study shows how genetic factors and transgene insertion sites can influence transgene expression with significant consequent effects on phenotype.

keywords: Sexually dimorphic growth; Transgenic coho; Growth hormone; Metallothionein-B; Estradiol

4-78 *Science & Technology*

Shift in polar benthic community structure in a fast retreating glacial area of Marian Cove, West Antarctica

Bae, Hanna., **Ahn, In-Young.** and 5 others.

Scientific Reports. 2021. 11(1).
doi: 10.1038/s41598-020-80636-z.

Glacier retreat is a major long-standing global issue; however, the ecological impacts of such retreats on marine organisms remain unanswered. Here, we examined changes to the polar benthic community structure of "diatoms" under current global warming in a recently retreated glacial area of Marian Cove, Antarctica. The environments and spatiotemporal assemblages of benthic diatoms surveyed in 2018–2019 significantly varied between the intertidal (tidal height of 2.5 m) and subtidal zone (10 and 30 m). A distinct floral distribution along the cove (~ 4.5 km) was characterized by the adaptive strategy of species present, with chain-forming species predominating near the glacier. The predominant chain-forming diatoms, such as *Fragilaria striatula and Paralia* sp., are widely distributed in the innermost cove over years, indicating sensitive responses of benthic species to the fast-evolving polar environment. The site-specific and substrate-dependent distributions of certain indicator species (e.g., *F.striatula*, *Navicula glaciei*, *Cocconeis* cf. *pinnata*) generally reflected such shifts in the benthic community. Our review revealed that the inner glacier region reflected trophic association, featured with higher diversity, abundance, and biomass of benthic diatoms and macrofauna. Overall, the polar benthic community shift observed along the cove generally represented changing environmental conditions, (in) directly linked to ice-melting due to the recent glacier retreat.

4-79

Soil Metagenome Sequences from a Geothermal Site at Mount Melbourne in Antarctica

Park, Mira., **Choe, Yong-Hoe.** and **Kim, Mincheol.**

Microbiology Resource Announcements. 2021. 10(10).
doi: 10.1128/MRA.01490-20.

Here, we examined two soil metagenome data sets obtained from a geothermal site at the summit of Mount Melbourne in Antarctica. The geothermal soil microbiome exhibits very unique features of prokaryotic diversity and functions, which will provide deeper insight into the adaptation and evolution of soil microbes in Antarctic geothermal habitats.

4-80 *Biochemistry & Molecular Biology; Chemistry; Polymer Science*

Structural basis of the cooperative activation of type II citrate synthase (*Hy*CS) from *Hymenobacter* sp. PAMC 26554

Park, Sun-Ha., **Lee, Chang Woo.**, Bae, Da-Woon., **Do, Hackwon.**, **Jeong, Chang-Sook.**, **Hwang, Ji-sub.**, Cha, Sun-Shin. and **Lee, Jun Hyuck.**

International Journal of Biological Macromolecules. 2021. 183: 213-221.

doi: 10.1016/j.ijbiomac.2021.04.141.

Citrate synthase (CS) catalyzes the formation of citrate and coenzyme A from acetyl-CoA and oxaloacetate. CS exists in two forms: type I and type II. We determined the citrate-bound crystal structure of type II CS from the *Hymenobacter* sp. PAMC 26554 bacterium (*Hy*CS; isolated from Antarctic lichen). Citrate molecules bound to a cleft between the large and small domains of *Hy*CS. Structural comparison of *Hy*CS with other type II CSs revealed that type II CSs have a highly conserved flexible hinge region (residues G264–P265 in *Hy*CS), enabling correct positioning of active site residues. Notably, the catalytic His266 residue of *Hy*CS interacted with Trp262 in the inactive (unliganded open) state of other type II CSs, whereas the His266 residue moved to the active site via a small-domain swing motion, interacting with the bound citrate in the closed conformation of *Hy*CS. However, type I CSs lack this tryptophan residue and face-to-edge interactions. Thus, type II CSs might have a unique domain-motion control mechanism enabling a tight allosteric regulation. An activity assay using a W262A mutant showed a Hill coefficient of 2.4; thus, the interaction between Trp262 and His266 was closely related to the positive cooperative ligand binding of type II CS.

keywords: Crystal structure; Citrate synthase; *Hymenobacter* sp. PAMC 26554; Domain movement; X-ray crystallography

4-81

The Study on the Application of Citizen Science to the Penguin Monitoring project

Kim, Hyung-Joon., **Kim, Jeong-Hoon.** and Kim, Ji-Yeon.

과학기술학연구. 2021. 21(2): 168-202.

We reviewed previous research cases to examine the feasibility of applying citizen science to the monitoring and research of penguins in the Antarctic. Because access to the Antarctic region is limited, some people interested in polar research have participated in citizen science programs integrated with tourism, or census projects of weddell seals and penguins using crowdsourcing platforms.

Since 2017, the Korean government (Ministry of Oceans and Fisheries) has been supporting a research and development project (R&D) on the ecosystem structure and function of the Ross Sea region MPA to contribute to CCAMLR(The Commission for the Conservation of Antarctic Marine Living Resources)'s efforts to conserve the area.

We suggest that citizens could participate in producing CEMP(CCAMLR Ecosystem Monitoring Program) data from large-scale photographs with scientists. Through the participation of penguin citizen science, ordinary citizens experience the process of knowledge co-production with scientists. It could not only provide a national-level scientific contribution to CCAMLR's monitoring program, but also affect the direction and justification of polar research.

keywords: Antarctic Research; Citizen Science; CCAMLR; Penguin Count; Penguin Citizen Science Model

4-82 *Pharmacology & Pharmacy*

Svalbamides A and B, Pyrrolidinone-Bearing Lipodipeptides from Arctic *Paenibacillus* sp.

Du, Young Eun., Bae, Eun Seo., Lim, Yeonjung., Cho, Jang-Cheon., Nam, Sang-Jip., Shin, Jongheon., Lee, Sang Kook., **Nam, Seung-Il.** and Oh, Dong-Chan.

Marine Drugs. 2021. 19(4).

doi: 10.3390/md19040229.

Two new secondary metabolites, svalbamides A (**1**) and B (**2**), were isolated from a culture extract of *Paenibacillus* sp. SVB7 that was isolated from surface sediment from a core (HH17-1085) taken in the Svalbard archipelago in the Arctic Ocean. The combinational analysis of HR-MS and NMR spectroscopic data revealed the structures of **1** and **2** as being lipopeptides bearing 3-amino-2-pyrrolidinone, D-valine, and 3-hydroxy-8-methyldecanoic acid. The absolute configurations of the amino acid residues in svalbamides A and B were determined using the advanced Marfey's method, in

which the hydrolysates of **1** and **2** were derivatized with L- and D- forms of 1-fluoro-2,4-dinitrophenyl-5-alanine amide (FDAA). The absolute configurations of **1** and **2** were completely assigned by deducing the stereochemistry of 3-hydroxy-8-methyldecanoic acid based on DP4 calculations. Svalbamides A and B induced quinone reductase activity in Hepa1c1c7 murine hepatoma cells, indicating that they represent chemotypes with a potential for functioning as chemopreventive agents.

keywords: *Paenibacillus*; Arctic; Svalbard; Marfey's method; DP4 calculation; quinone reductase; lipopeptide; 3-amino-2-pyrrolidinone

4-83

Through a glass darkly, but with more understanding of arthropod origin

Park, Tae-Yoon S.

Peer Community In Paleontology. 2021.
doi: 10.24072/pci.paleo.100009

4-84 *Chemistry; Engineering; Materials Science; Physics*

Toxic Effects of Heavy Metals and Organic Polycyclic Aromatic Hydrocarbons in Sediment Porewater on the Amphipod *Hyalella azteca* and Zebrafish *Brachydanio rerio* Embryos from Different Rivers in Taiwan

Hu, Shao-Yang., Hsieh, Chi-Ying., Dahms, Hans-Uwe., Tseng, Yu-Hsien., Chen, Jesse., Wu, Meng-Chun., **Kim, Jin-Hyoung.** and Liu, Cheng-Han.

Applied Sciences-Basel. 2021. 11(17).
doi: 10.3390/app11178021.

The amphipod (*Hyalella azteca*) and zebrafish (*Brachydanio rerio*) embryos were used for toxicological sediment porewater testing. Porewaters from 35 sampling stations of eight streams in southern Taiwan were screened for toxic effects and their relationship with 6 metal and 16 polycyclic aromatic hydrocarbons (PAHs). Concentration analysis results showed that the following PAHs, naphththalene, benzo(b)fluoranthene, dibenz(a,h)anthracene, acenaphthalene, and the heavy metal cadmium were not detected in 35 sampling stations. The highest detection rate of 94.1% was caused by the PAHs fluoranthene and pyrene. The highest detection rate of the metal zinc was 88.6% of 35 analyzed samples. The majority of samples (88%) were classified as level tier 1 according to USEPA national sediment inventory. This indicates the probability of adverse effects on aquatic life or human health. The results of a zebrafish embryo test showed that heart rate and survival were significantly reduced with all porewater samples. Therefore, fish exposed to contaminated river conditions may be affected in their cardiovascular functions. Looking at correlations between toxic effects of metals and PAHs, we found that phenanthrene, anthracene, pyrene, benzo(a) anthracene, chrysene, benzo(b)fluoranthene, and benzo(a)pyrene were low, while fluorene was highly correlated with toxic effects of metals.

keywords: river sediment pollution; trace metal; PAHs; toxic chemical; biomarker; circulatory function

4-85 *Plant Sciences*

Transfection of Arctic *Bryum* sp. KMR5045 as a Model for Genetic Engineering of Cold-Tolerant Mosses

Byun, Mi Young., Seo, Suyeon., Lee, Jungeun., Yoo, Yo-Han. and **Lee, Hyoungseok.**

Frontiers in Plant Science. 2021. 11.
doi: 10.3389/fpls.2020.609847.

Mosses number about 13,000 species and are an important resource for the study of the plant evolution that occurred during terrestrial colonization by plants. Recently, the physiological and metabolic characteristics that distinguish mosses from terrestrial plants have received attention. In the Arctic, in particular, mosses developed their own distinct physiological features to adapt to the harsh environment. However, little is known about the molecular mechanisms by which Arctic mosses survive in extreme environments due to the lack of basic knowledge and tools such as genome sequences and genetic transfection methods. In this study, we report the axenic cultivation and transfection of Arctic *Bryum* sp. KMR5045, as a model for bioengineering of Arctic mosses. We also found that the inherent low-temperature tolerance of KMR5045 permitted it to maintain slow growth even at 2°C, while the model moss species *Physcomitrium patens* failed to grow at all, implying that KMR5045 is suitable for studies of cold-tolerance mechanisms. To achieve genetic transfection of KMR5045, some steps of the

existing protocol for *P. patens* were modified. First, protoplasts were isolated using 1% driselase solution. Second, the appropriate antibiotic was identified and its concentration was optimized for the selection of transfectants. Third, the cell regeneration period before transfer to selection medium was extended to 9 days. As a result, KMR5045 transfectants were successfully obtained and confirmed transfection by detection of intracellular Citrine fluorescence derived from expression of a *pAct5:Citrine* transgene construct. This is the first report regarding the establishment of a genetic transfection method for an Arctic moss species belonging to the Bryaceae. The results of this study will contribute to understanding the function of genes involved in environmental adaptation and to application for production of useful metabolites derived from stress-tolerant mosses.

keywords: Arctic moss; axenic culture; *Bryum* sp.; protoplast; transfection

4-86 *Biochemistry & Molecular Biology; Biophysics; Cell*

The ultrastructure of resurrection: Post-diapause development in an Antarctic freshwater copepod

Reed, Katherine A., **Lee, Sung Gu.**, **Lee, Jun Hyuck.** and 2 others.

Journal of Structural Biology. 2021. 213(1).
doi: 10.1016/j.jsb.2021.107705.

The copepod, *Boeckella poppei*, is broadly distributed in Antarctic and subantarctic maritime lakes threatened by climate change and anthropogenic chemicals. Unfortunately, comparatively little is known about freshwater zooplankton in lakes influenced by the Southern Ocean. In order to predict the impact of climate change and chemicals on freshwater species like *B. poppei*, it is necessary to understand the nature of their most resilient life stages. Embryos of *B. poppei* survive up to two centuries in a resilient dormant state, but no published studies evaluate the encapsulating wall that protects theses embryos or their development after dormancy. This study fills that knowledge gap by using microscopy to examine development and the encapsulating wall in *B. poppei* embryos from Antarctica. The encapsulating wall of *B. poppei* is comprised of three layers that appear to be conserved among crustacean zooplankton, but emergence and hatching are uniquely delayed until the nauplius is fully formed in this species. Diapause embryos in Antarctic sediments appear to be in a partially syncytial midgastrula stage. The number of nuclei quadruples between the end of diapause and hatching. Approximately 75% of yolk platelets are completely consumed during the same time period. However, some yolk platelets are left completely intact at the time of hatching. Preservation of complete yolk platelets suggests an all-or-none biochemical process for activating yolk consumption that is inactivated during dormancy to preserve yolk for post-dormancy development. The implications of these and additional ultrastructural features are discussed in the context of anthropogenic influence and the natural environment.

keywords: Crustacean; Zooplankton; Diapause; Developmental biology; Partial syncytium; Electron microscopy

4-87 *Chemistry; Engineering*

Use of spent coffee ground as a reducing agent for enhanced reduction of chromate by freezing process

Han, Tae Uk., Kim, Jungwon. and **Kim, Kitae.**

Journal of Industrial and Engineering Chemistry. 2021. 100: 310-316.
doi: 10.1016/j.jiec.2021.05.008.

In this study, the freezing-mediated reduction of chromate (Cr(VI)) was investigated using spent coffee ground (SCG) as a reducing agent. The results obtained showed that the rate of Cr(VI) reduction using SCG was dramatically enhanced in the frozen phase (–20 °C) compared with the aqueous phase (25 °C), and after 3 h of reaction, the residual Cr(VI) concentration in the aqueous phase was 15.25 ± 0.58 μM, while that in the frozen phase was only 1.89 ± 0.16 μM (initial experimental conditions: $[Cr(VI)]_i$ = 20 μM, $[SCG]_i$ = 0.1 g/L, and pH_i = 3.0). Additionally, based on the results obtained under different experimental conditions, the accelerated reduction of Cr(VI) using SCG in the frozen solution could be attributed to the freeze concentration phenomenon, which is associated with the accumulation of Cr(VI) and protons, as well as the phenolic compounds in SCG extracts.

keywords: Waste biomass; Spent coffee ground; Freeze concentration effect; Chromate; Phenolic compound

4-88 *Biochemistry & Molecular Biology; Cell Biology*

Whole genome survey and microsatellite motif identification of *Artemia franciscana*

Jo, Euna., Lee, Seung Jae., Choi, Eunkyung., Kim, Jin-mu., **Lee, Sung Gu.**, **Lee, Jun Hyuck.**, **Kim, Jeong-Hoon.** and Park, Hyun.

Bioscience Reports. 2021. 41(3).
doi: 10.1042/bsr20203868.

Artemia is an industrially important genus used in aquaculture as a nutritious diet for fish and as an aquatic model organism for toxicity tests. However, despite the significance of *Artemia*, genomic research remains incomplete and knowledge on its genomic characteristics is insufficient. In particular, *Artemia franciscana* of North America has been widely used in fisheries of other continents, resulting in invasion of native species. Therefore, studies on population genetics and molecular marker development as well as morphological analyses are required to investigate its population structure and to discriminate closely related species. Here, we used the Illumina Hi-Seq platform to estimate the genomic characteristics of *A. franciscana* through genome survey sequencing (GSS). Further, simple sequence repeat (SSR) loci were identified for microsatellite marker development. The predicted genome size was ~867 Mb using K-mer (a sequence of k characters in a string) analysis (K = 17), and heterozygosity and duplication rates were 0.655 and 0.809%, respectively. A total of 421467 SSRs were identified from the genome survey assembly, most of which were dinucleotide motifs with a frequency of 77.22%. The present study will be a useful basis in genomic and genetic research for *A. franciscana*.

4-89 *Biochemistry & Molecular Biology; Biophysics; Cell Biology*

Wide-open conformation of UDP-MurNc-tripeptide ligase revealed by the substrate-free structure of MurE from *Acinetobacter baumannii*

Jung, Kyoung Ho., Kim, Yeon-Gil., Kim, Chang Min., Ha, Hyun Ji., Lee, Chang Sup., **Lee, Jun Hyuck.** and Park, Hyun Ho.

Febs Letters. 2021. 595(2): 275-283.
doi: 10.1002/1873-3468.14007.

MurE ligase catalyzes the attachment of *meso*-diaminopimelic acid to the UDP-MurNAc-$_{L}$-Ala-$_{D}$-Glu using ATP and producing UDP-MurNAc-$_{L}$-Ala-$_{D}$-Glu-*meso*-A_2pm during bacterial cell wall biosynthesis. Owing to the critical role of this enzyme, MurE is considered an attractive target for antibacterial drugs. Despite extensive studies on MurE ligase, the structural dynamics of its conformational changes are still elusive. In this study, we present the substrate-free structure of MurE from *Acinetobacter baumannii*, which is an antibiotic-resistant superbacterium that has threatened global public health. The structure revealed that MurE has a wide-open conformation and undergoes wide-open, intermediately closed, and fully closed dynamic conformational transition. Unveiling structural dynamics of MurE will help to understand the working mechanism of this ligase and to design next-generation antibiotics targeting MurE.

keywords: *Acinetobacter baumannii*; ATP-dependent ligase; cell wall peptidoglycan biosynthesis; crystal structure; MurE

4-90 *Biochemistry & Molecular Biology; Environmental Sciences & Ecology; Evolutionary Biology*

Zooming on dynamics of marine microbial communities in the phycosphere of *Akashiwo sanguinea* (Dinophyta) blooms

Kang, Junsu., Park, Joon Sang., Jung, Seung Won., Kim, Hyun-Jung., **Joo, Hyoung Min.** and 8 others.

Molecular Ecology. 2021. 30(1): 207-221.
doi: 10.1111/mec.15714.

Characterizing ecological relationships between viruses, bacteria and phytoplankton in the ocean is critical to understanding the ecosystem; however, these relationships are infrequently investigated together. To understand the dynamics of microbial communities and environmental factors in harmful algal blooms (HABs), we examined the environmental factors and microbial communities during *Akashiwo sanguinea* HABs in the Jangmok coastal waters of South Korea by metagenomics. Specific bacterial species showed complex synergistic and antagonistic relationships with the *A. sanguinea* bloom. The endoparasitic dinoflagellate *Amoebophrya* sp. 1 controlled the bloom dynamics and correlated with HAB decline. Among nucleocytoplasmic large DNA viruses (NCLDVs), two Pandoraviruses and six Phycodnaviruses were strongly and positively

correlated with the HABs. Operational taxonomic units of microbial communities and environmental factors associated with *A. sanguinea* were visualized by network analysis: *A. sanguinea–Amoebophrya* sp. 1 (r = .59, time lag: 2 days) and *A. sanguinea–Ectocarpus siliculosus* virus 1 in Phycodnaviridae (0.50, 4 days) relationships showed close associations. The relationship between *A. sanguinea* and dissolved inorganic phosphorus relationship also showed a very close correlation (0.74, 0 day). Microbial communities and the environment changed dynamically during the *A. sanguinea* bloom, and the rapid turnover of microorganisms responded to ecological interactions. *A. sanguinea* bloom dramatically changes the environments by exuding dissolved carbohydrates via autotrophic processes, followed by changes in microbial communities involving host-specific viruses, bacteria and parasitoids. Thus, the microbial communities in HAB are composed of various organisms that interact in a complex manner.

keywords: *Akashiwo sanguinea*; endoparasitic *Amoebophrya* sp.; environmental change; harmful algal bloom; microbial community nucleocytoplasmic large DNA viruses

PART5

Policy & Technology

5-1 *Automation & Control Systems*

Development of Unmanned Ground Vehicle (UGV) for Detecting Crevasses in Glaciers

Chung, Changhyun., **Kim, Hyoung-Kwon.**, **Yoon, Dong-Jin.** and **Lee, Joohan.**

Journal of Institute of Control, Robotics and Systems. 2021. 27(1): 61-68.

doi: 10.5302/j.Icros.2021.20.0136.

Research activities in Antarctica face a number of risk factors, such as cold, strong winds, and isolated or dangerous environments. Among them, crevasses, which are deep cracks in glaciers, can cause fatal accidents since they are difficult to locate as they are covered with snow. In this paper, we present the development, design, and deployment of an UGV (Unmanned Ground Vehicle) that can explore ice-sheets and be used in various polar research fields. The developed UGV was customized to remotely detect crevasses and prevent related accidents. In order to adapt to the harsh terrain of Antarctica, the vehicle features ground clearance over 260mm, four-wheel-drive ability with a 400W high-power motor, as well as passive joints and differential links to allow for four-point contact on rough terrain. The UGV is also designed to run for more than two hours on the Antarctic ice sheet at a speed of 2.5m/sec. The control unit uses open-source hardware and software for rapid function implementation and ease of future customization. In November 2019, the UGV detected crevasses successfully by towing an IPR (Ice Penetrating Radar) along the 2.6 km section of the Browning Pass around Jang Bogo Station, Antarctica. Further improvement is required for heading angle errors due to magnetic compass malfunctions in Antarctica, and for the vibration and misalignment of the traction device for the towing research equipment.

keywords: unmanned ground vehicle; polar rover; polar science

5-2 *Engineering; Physical Geography; Remote Sensing; Imaging Science & Photographic Technology*

A Novel SAR Fractal Roughness Modeling of Complex Random Polar Media and Textural Synthesis Based on a Numerical Scattering Distribution Function Processing

Shahrezaei, Iman Heidarpour. and **Kim, Hyun-Cheol.**

Ieee Journal of Selected Topics in Applied Earth Observations and Remote Sensing. 2021. 14: 7386-7409.

doi: 10.1109/jstars.2021.3084822.

In this article, complex random polar media (CRPM) are synthesized by a forward numerical modeling based on the fractal statistical properties of the marginal ice zone (MIZ) in terms of its energy balance under sea state conditions. The proposed modeling was carried out by the parallel processing of a modified JONSWAP directional spectrum function in a two-dimensional hybrid domain. As a novel approach, the scattering formulation has been modified in the form of a two-scale implementation, which is optimized by the product of cosine-power and Gamma probability distribution function (PDF). As a result, a composite model of CRPM under different sea state conditions, including wind speed and direction, has been made possible. Due to the high dynamics of CRPM under sea state conditions, the presence of high entropy samples in the form of random roughness fluctuations is inevitable. These highly textured areas not only reduce the ability to resolve fine details but also make the interpretation difficult from a remote sensing point of view. According to the importance of synthetic aperture radar in the observation of MIZ and analysis of scattering properties, the spectral distribution modeling of these roughness anomalies and their electromagnetic interactions, along with surface tension synthesis, are presented here. Meanwhile, several objective quality metrics under different sea state conditions have been derived. The results show that the sea state not only changes the spectral components, but also affects their contribution to the roughness fluctuations and texture compositions. In short, this is for the first time that the composite modeling of CRPM based on directional spectrum function under sea state conditions along with electromagnetic interactions investigation and its pertinent texture analysis has been done.

keywords: Analytical models; Sea surface; Fluctuations; Computational modeling; Wind speed; Sea state; Parallel processing; Composite directional spectrum function; numerical modeling; roughness; synthetic aperture radar (SAR)

5-3 *Environmental Sciences & Ecology; Geology; Remote Sensing; Imaging Science & Photographic Technology*

An Optimal Image–Selection Algorithm for Large-Scale Stereoscopic Mapping of UAV Images

Lim, Pyung-chae., Rhee, Sooahm., Seo, Junghoon., **Kim, Jae-In.**, **Chi, Junhwa.** and 2 others.

Remote Sensing. 2021. 13(11).

doi: 10.3390/rs13112118.

Recently, the mapping industry has been focusing on the possibility of large-scale mapping from unmanned aerial vehicles (UAVs) owing to advantages such as easy operation and cost reduction. In order to produce large-scale maps from UAV images, it is important to obtain precise orientation parameters as well as analyzing the sharpness of they themselves measured through image analysis. For this, various techniques have been developed and are included in most of the commercial UAV image processing software. For mapping, it is equally important to select images that can cover a region of interest (ROI) with the fewest possible images. Otherwise, to map the ROI, one may have to handle too many images, and commercial software does not provide information needed to select images, nor does it explicitly explain how to select images for mapping. For these reasons, stereo mapping of UAV images in particular is time consuming and costly. In order to solve these problems, this study proposes a method to select images intelligently. We can select a minimum number of image pairs to cover the ROI with the fewest possible images. We can also select optimal image pairs to cover the ROI with the most accurate stereo pairs. We group images by strips and generate the initial image pairs. We then apply an intelligent scheme to iteratively select optimal image pairs from the start to the end of an image strip. According to the results of the experiment, the number of images selected is greatly reduced by applying the proposed optimal image-composition algorithm. The selected image pairs produce a dense 3D point cloud over the ROI without any holes. For stereoscopic plotting, the selected image pairs were map the ROI successfully

on a digital photogrammetric workstation (DPW) and a digital map covering the ROI is generated. The proposed method should contribute to time and cost reductions in UAV mapping.

keywords: UAV images; monoscopic mapping; stereoscopic plotting; image overlap; optimal image selection

5-4 *Engineering; Environmental Sciences & Ecology*

Oxygen vacancy engineering of cerium oxide for the selective photocatalytic oxidation of aromatic pollutants

Bui, Hoang Tran., Weon, Seunghyun., Bae, Ji Won., Kim, Eun-Ju., Kim, Bupmo., **Ahn, Yong-Yoon.**, **Kim, Kitae.** and 2 others.

Journal of Hazardous Materials. 2021. 404.
doi: 10.1016/j.jhazmat.2020.123976.

The engineering of oxygen vacancies in CeO_2 nanoparticles (NPs) allows the specific fine-tuning of their oxidation power, and this can be used to rationally control their activity and selectivity in the photocatalytic oxidation (PCO) of aromatic pollutants. In the current study, a facile strategy for generating exceptionally stable oxygen vacancies in CeO_2 NPs through simple acid (CeO_2-A) or base (CeO_2-B) treatment was developed. The selective (or mild) PCO activities of CeO_2-A and CeO_2-B in the degradation of a variety of aromatic substrates in water were successfully demonstrated. CeO_2-B has more oxygen vacancies and exhibits superior photocatalytic performance compared to CeO_2-A. Control of oxygen vacancies in CeO_2 facilitates the adsorption and reduction of dissolved O_2 due to their high oxygen-storage ability. The oxygen vacancies in CeO_2-B as active sites for oxygen-mediated reactions act as (i) adsorption and reduction reaction sites for dissolved O_2, and (ii) photo-generated electron scavenging sites that promote the formation of H_2O_2 by multi-electron transfer. The oxygen vacancies in CeO_2-B are particularly stable and can be used repeatedly over 30 h without losing activity. The selective PCOs of organic substrates were studied systematically, revealing that the operating mechanisms for UV-illuminated CeO_2-B are very different from those for conventional TiO_2 photocatalysts. Thus, the present study provides new insights into the design of defect-engineered metal oxides for the development of novel photocatalysts.

keywords: CeO_2; Oxygen vacancy; Photocatalytic mild oxidation

5-5 *Area Studies*

A Research on the Historical Perspectives of Russia's Arctic Policy

Seo, Hyun Kyo.

Korean journal of Siberian studies. 2021. 25(3): 1-39.
doi: 10.22892/ksc.2021.25.3.01.

Russia, the country with the largest territories in the Arctic among Arctic countries, has laid the foundation for its Arctic policy by starting its advance into Siberia from the feudal era before the imperial Russia. From then on, during the Imperial Russia era, the era of the Soviet regime (the former Soviet Union), and the current Russian federal government that became independent after the collapse of the former Soviet Union in 1991, policy views on Siberia were very different. In other words, after step by step colonization, territorialization, and industrialization, the current federal government defined its own Arctic region and promoted a systematic and comprehensive Arctic policy. Moreover, Russia is carrying out the various programmes to fortify its leadership in the Arctic, becoming the chair of the Arctic Council this year (2021-2023). In this paper, from the perspective of strengthening cooperation with Russia, the history of Russia's Arctic policy is divided by period and important policy areas are reviewed. In particular, Russia's national interest in the Arctic presented in the '2020 Basic Principle for Arctic Policy' in 2008, and '2035 Basic Principles for the Russian Arctic Policy' in 2020 which is the current federal government's representative Arctic policy was analyzed.
So, from the historical point of view, the top priority and the latest themes that Russia presents as national interests in the Arctic were identified, and based on this, a plan to strengthen cooperation in the Arctic between Korea and Russia was sought.

keywords: Siberia; Arctic policy; NSR; Arctic security; Arctic resource

5-6 *Engineering; Telecommunications*

VHF/UHF Open-Sleeve Dipole Antenna Array for Airborne Ice Sounding and Imaging Radar

Won, Hoyun., Hong, Yang-Ki., Li, Linfeng., Awasthi, Abhishek., Nickerson, Natalie., Bryant, Briana., Choi, Minyeong., Yan, Stephen., Taylor, Drew., O'Neill, Charles. and **Lee, Joohan.**

Ieee Antennas and Wireless Propagation Letters. 2021. 20(6): 883-887.

doi: 10.1109/lawp.2021.3066288.

This paper presents a simple, lightweight, and ultrawideband, VHF/UHF open-sleeve dipole antenna array for airborne ice measuring radar. The proposed antenna array achieves a wide bandwidth of 300 MHz via mutual coupling from neighboring excited elements. A hollow aluminum tube is used for both dipole and parasitic elements to minimize the antenna's weight. The simulation results show that to achieve a bandwidth of 300 MHz with a peak realized gain up to 12 dBi in the frequency range from 170 to 470 MHz, the length of the dipole (L_{dip}) and parasitic elements (L_{para}) of elements 1 and 4 of the 4-element antenna array need to be 670 mm and 200 mm, respectively. At the same time, elements 2 and 3 require a L_{dip} of 640 mm and L_{para} of 180 mm. Based on these dimensions, a 4-element antenna array is fabricated and tested. The measured antenna performance results show a good agreement with the simulated results.

Keyword Index

A

B

C

D

E

F

G

H

I

J

K

L

M

N

O

P

Q

R

S

T

Author Index

K

L

M

N

O

P

R

S

T

Y

Compiled by Library of Korea Polar Research Institute

KOPRI ABSTRACTS contains journal articles written by KOPRI researchers and other researchers funded by KOPRI. The following KOPRI authors can be seen as highlighted in bold text.
The ***KOPRI ABSTRACTS*** are published once a year and distributed world wide by KOPRI since launching in 2014.

KOPRI
Korea Polar Research Institute
igloo Library

**26 Songdomirae-ro, Yeonsu-gu,
Incheon, 21990, Korea
www.kopri.re.kr**

ISSN 2289-0734